



*Interaction of rotationally cold molecules
with external fields*

*Interacción de moléculas
rotacionalmente frías con campos externos*

Tesis Doctoral
por
JUAN JOSÉ OMISTE ROMERO

Programa de doctorado en Física y Matemáticas, FisyMat

Departamento de Física Atómica, Molecular y Nuclear
Universidad de Granada
2013

Editor: Editorial de la Universidad de Granada
Autor: Juan José Omiste Romero
D.L.: GR 359-2014
ISBN: 978-84-9028-764-4

Tesis Doctoral dirigida por
DRA. ROSARIO GONZÁLEZ FÉREZ

Dña. Rosario González Férrez, Doctora en Ciencias Físicas y Profesora Titular del Departamento de Física Atómica, Molecular y Nuclear de la Universidad de Granada

MANIFIESTA:

Que la presente Memoria titulada *Interacción de moléculas rotacionalmente frías con campos externos*, presentada por Don Juan José Omiste Romero para optar al Grado de Doctor en Física, ha sido realizada bajo mi dirección en el Departamento de Física Atómica, Molecular y Nuclear de la Universidad de Granada y el Instituto Carlos I de Física Teórica y Computacional de la Universidad de Granada.

Granada, 14 de Junio de 2013

Fdo.: Rosario González Férrez

Memoria presentada por Don Juan José Omiste Romero para optar al Grado de Doctor en Física por la Universidad de Granada.

Fdo.: Juan José Omiste Romero

Compromiso de respeto de los derechos de autor

El doctorando D. Juan José Omiste Romero y la directora de tesis Dra. Rosario González Férrez garantizamos, al firmar esta tesis doctoral, que el trabajo ha sido realizado por el doctorando bajo la dirección de la directora de tesis y hasta donde nuestro conocimiento alcanza, en la realización del trabajo, se han respetado los derechos de otros autores a ser citados, cuando se han utilizado sus resultados o publicaciones.

Granada, 14 de Junio de 2013

Directora de la Tesis

Doctorando

Fdo. Rosario González Férrez

Fdo. Juan José Omiste Romero

Título de Doctor con Mención Internacional

Con el fin de obtener la Mención Internacional en el Título de Doctor, se han cumplido, en lo que atañe a esta Tesis Doctoral y a su Defensa, los siguientes requisitos:

1. Esta Memoria ha sido escrita en inglés, con la introducción y las conclusiones además en español.
2. Esta Tesis ha sido evaluada por dos investigadores externos pertenecientes a centros no españoles.
3. Uno de los miembros del tribunal proviene de una universidad europea no española.
4. Una parte de la defensa de la Tesis se ha realizado en inglés.
5. Una parte de esta Tesis Doctoral se ha realizado en Alemania, en el Zentrum für Optische Quantentechnologie de la Universidad de Hamburgo, Alemania.

A mi familia
A mi abuelo Antonio
A mi padrino Paco

Agradecimientos

En primer lugar querría dar las gracias a Rosario, por su perseverancia, confianza y apoyo durante todos estos años. Gracias por todo lo que me has enseñado sobre la constancia, esfuerzo y orgullo por el trabajo bien hecho. También a Jesús por todas las oportunidades que me ha brindado y todo lo que ha hecho por mí desde que empecé a colaborar con él cuando todavía estaba en la carrera. Y con ellos, agradezco a todos mi compañeros del grupo y del departamento.

I would also like to thank Peter Schmelcher for the time I spent in Hamburg working at his group and to Jochen Küpper for the great collaboration we have since I started my PhD.

A todos mis compañeros de la becariera, de la facultad y con ellos a todos mis amigos de Granada. Por tantas *fruitful discussions*, aunque la mayoría no fueran de física, por los ratos en comedores, jugando squash, padel, tenis, voley playa, salseando, en el paintball, de barbacoas, de cervezas y por muchas cosas más.

A todos mis compañeros del Colegio Mayor Gárnata y especialmente a todos con los que tengo una gran amistad. Gracias por tantos buenos e irrepetibles momentos, de barbacoas, de tantas y tantas fiestas, de largas tardes de estudio, de excursiones y de largas charlas hasta bien entrada la madrugada. A mis amigos de Motril, que me seguís apreciando aunque no os vea tanto como quisiera y me haya convertido en todo un *sanitex*, gracias por estos años de buena amistad. Gracias a todos por vuestro apoyo en los momentos difíciles.

A todos los que de una u otra forma me han motivado a dedicarme a las matemáticas y la física. En primer lugar, a mi padre, que desde pequeño me hizo ver las matemáticas siempre por casa, aunque a mi hermano no le hiciera demasiada gracia. A mi tío Fernando, que nunca se cansaba de dibujarme *circuitillos* llenos de resistencias ni de ayudarme cuando empezaba a programar. Tampoco puedo olvidar a don Manuel Perdonés, que no hizo más que lo que define al buen maestro: motivarme, ya fuera resolviendo límites imposibles o programando un tetris en QBasis. Por último, a mis profesores Antonio Alonso y Antonio López, por todo su esfuerzo para prepararnos a mis compañeros de faena y a mí para las olimpiadas de química y matemáticas. En especial a Antonio López, que supo transmitirme como nadie su pasión por las matemáticas.

A mi familia, en especial a mis padres y a mi hermano Antonio. Sé que cualquier cosa que escriba será poco para expresar todo lo que os tengo que agradecer. Muchas gracias por vuestro constante apoyo y ánimo.

Contents

1	Introduction	1
2	Introducción	9
3	Hamiltonian of molecules in the presence of external fields	17
3.1	The Hamiltonian of the Field-Free Rotor	18
3.1.1	Linear rotor	18
3.1.2	Symmetric top rotor	18
3.1.3	Asymmetric top rotor	19
3.2	The interaction with a homogenous static electric field	20
3.3	The interaction with a non resonant laser field	21
3.4	Symmetries and representations	23
4	Numerical methods	29
4.1	The time-independent Schrödinger equation	29
4.1.1	The Linear Variational Method	29
4.1.2	Numerical diagonalization of the Hamiltonian matrix	30
4.2	The time-dependent Schrödinger equation	30
4.2.1	Short Iterative Lanczos propagation method	30
4.2.2	Split-operator procedure	32
4.3	Projection of the wavefunction on the screen	35
5	Publications	41
6	Submitted publications and preprint	87
7	Conclusions and outlook	121
8	Conclusiones y perspectivas futuras	125
9	Author's publications	129
A	The Molecular and the Laboratory Fixed Frames: the Euler Angles	131
B	Wigner matrix elements	135
C	Hamiltonian matrix elements	137
	Bibliography	140

Chapter 1

Introduction

The study of molecules exposed to external fields represents, in spite of its substantial history, a very active, fruitful and promising research area. The great developments in the laser and optical technologies together with the possibility of producing strong and stable electric fields have stimulated further studies on the control of the molecular dynamics. The manipulation of the rotational degrees of freedom by external fields enables the alignment and/or the orientation of the molecule. The alignment refers to the angular confinement of the molecular fixed axes along the laboratory fixed frame axes, and the orientation adds a well-defined direction to this concept. The experimental as well as theoretical efforts undertaken in this research area are motivated by the broad range of intriguing perspectives and possible applications of these systems. One of the first applications was the stereodynamic control of chemical reactions, which allows to perform a deeper study of their inherent quantum features, opening new doors to a better efficiency of this process [1–3]. For instance, the experimental studies of the reactions $\text{K} + \text{CH}_3\text{I}$ [4] and $\text{Rb} + \text{CH}_3\text{I}$ [5–7] showed that the reactivity is largely enhanced if the I-end of CH_3I is oriented to the alkali atom. This control of the molecular motion has allowed the investigations of electronic and structural properties of the molecules, such as spectroscopy [8, 9], electron diffraction [10], photoelectron angular distribution [11–13], high harmonic generation [14, 15] and diffractive imaging of gas-phase molecules [16, 17], towards recording the molecular movie [18]. The high control of both the translational [19] and rotational degrees of freedom [20–22] of complex molecules has also been achieved, direct quantum effects in the stereodynamics of molecular reactions have been observed in ultracold alkali dimers [23].

The first attempt on orienting molecules by means of external fields were carried out experimentally using the electrostatic field of an hexapole [24–27]. Since the force induced in the molecule by this field is proportional to its orientation, this technique makes possible the separation of molecules in different rotational states. In the 90's, Loesch and Remscheid proposed the orientation of molecules by means of strong dc fields [28]. This brute force technique is based on the adiabatic transformation of field-free rotational states into pendular states, i. e., a coherent superposition of field-free rotational states. These pendular states appear for strong electric fields when the molecule is oriented along the field direction and the rotational motion becomes a librating one. For the first time, $^1\Sigma$ diatomic molecules were successfully oriented [29, 30]. This procedure has also been used to measure molecular properties, such as the permanent dipole moment of the electronic ground state [31] and excited states using pendular spectroscopy [32] or steric effects in chemical reactions [28]. Its main disadvantage is that it only works properly for rotationally cold molecules with large permanent dipole moment subject to strong external electric fields.

This brute force technique can be also used to achieve alignment in polar molecules, since orientation entails it. However, it is not suitable for nonpolar molecules because a permanent

dipole moment is needed. Friedrich and Herschbach explored the possibility of exploiting the interaction of a strong nonresonant laser field with the induced dipole moment of the molecules to align and trap them [33, 34]. The first experimental verification came from Kim and Felker [35] using Raman spectroscopy in naphthalene trimers in strong laser fields. Seideman developed further this idea for asymmetric molecules exposed to long and short linearly and elliptically polarized laser pulses [36–40]. The 1D alignment is achieved by a linearly polarized laser field [41], when the most polarizable axis (MPA) of the molecule is aligned along the laser polarization axis. In contrast, in the 3D alignment, each of the molecular axes are aligned along a laboratory axis and requires the use of an elliptically polarized laser field [42]. Let us also mention that it has also been studied the possibility of aligning molecules by using moderate and strong magnetic fields [43, 44].

In the strong laser field regime, the level structure is characterized by pendular pairs of quasidegenerate aligned states of opposite parity [45]. By using semiclassical methods, it has been proven that the energy gap between these two quasidegenerate states is proportional to $\exp(-\gamma\sqrt{I})$, with γ being a constant depending on the doublet and I the laser intensity. A major breakthrough to achieve a strong orientation came with the proposal of using a weak electric field to couple the levels in this tunneling doublet and fully hybridize them [46, 47]. In such a way, two strongly oriented states, but in opposite directions, are created. This prediction was done within an adiabatic picture assuming that the switching-on time of the laser pulse is larger than the molecular rotational period. This theoretical study has been generalized to symmetric top molecules in tilted dc and nonresonant laser fields [48].

The feasibility of this method was proven experimentally, but the degree of orientation observed was less than expected theoretically [49, 50]. The main reason for such a weak orientation is due to the thermal distribution of the molecular beam. Thus, the combination of oriented and antioriented states with similar thermal weights gives rise to a small orientation for the molecular beam. A major breakthrough in the experimental capabilities came in 2009, by using an inhomogeneous electric field a molecular beam of selected quantum states of iodobenzene was produced. As a consequence, an unprecedented degree of orientation was measured [20, 51]. In this experimental setup, the beam of quantum-state-selected molecules travels towards the detector. These molecules are now in the presence of the weak homogeneous electric field of the velocity map imaging spectrometer, and a nanosecond laser pulse is switched on. As an additional degree of freedom, they are able to change the angle between the laser polarization axis and the electric field direction. In such a way, they create either oriented or aligned molecular beams. To measure the degree of orientation and alignment a probe laser pulse is overlapped in time and space with the alignment laser. This probe laser produces a Coulomb explosion of the molecules, and the ionic fragments are accelerated towards the detector. Within the recoil approximation, the 2D images provided by these Coulomb-exploded fragments represent a 2D projection of the 3D wavefunction, and, therefore, allow them to measure the orientation and alignment of the molecule. These experiments were performed under the assumption that the alignment and orientation of these molecules were adiabatic, because the full width at half maximum (i. e. FWHM) of the laser pulse (\sim ns) is larger than the rotational period of these systems. For the alignment experiments, several theoretical studies were in agreement with the measurements [19, 36, 42]. However, there were a lack of theoretical investigations about the impact of combined dc and ac fields on asymmetric top molecules, which could be used to interpret the experimental measurements.

Aim of this Thesis

The aim of this thesis is to theoretically investigate the impact of external fields on polar molecules. We now describe in more detail this goal following the temporal development of our work through this thesis.

We start by studying an asymmetric top molecule in combined electric and linearly polarized laser fields using the rigid rotor approximation. We assume that the dc field is static, and take the temporal envelope of the laser pulse as constant and equal to one. We have analyzed the energies, the orientation and alignment as the parameters of the fields are varied, i. e., laser intensity, dc field strength and angle between both. We have also provided a detailed description of the symmetries of the rigid rotor Hamiltonian for all the possible field configurations and each irreducible representation has been treated independently.

This knowledge has allowed us to perform a theoretical investigation of the experiment described above, with the aim of reproducing their measurements for the alignment and mixed-field orientation of asymmetric tops. Based on the adiabatic hypothesis, we have solved the time-independent Schrödinger for the experimental field configurations, and computed the directional properties of the quantum states forming the molecular beam. Our theoretical results were able to reproduce the experimental measurements for adiabatic alignment but not for the mixed-field orientation. This disagreement shows that the adiabatic hypothesis to describe the mixed-field orientation is not correct. We have partially solved this problem by proposing a diabatic model to classify the adiabatic or diabatic character of the numerous avoided crossing from the field-dressed spectrum.

Our study for the mixed-field orientation of asymmetric molecules indicate that an alternative description of this process is needed. We have carried out a time-dependent analysis for polar linear molecules. The time-dependent Schrödinger equation for a linear molecule in mixed-fields has been solved by taking into account the temporal profile of both fields. This theoretical study has allowed us to realized that under ns laser pulses the weak dc field orientation is not, in general, adiabatic. As a consequence, a time-dependent description of the mixed-field orientation process is required to explain the experimental results. We have identified the sources of nonadiabatic effects, and the experimental conditions needed to achieve an adiabatic molecular dynamics.

Our next goal was to generalize this time-dependent treatment of the mixed-field orientation to the more complicated asymmetric top molecules. A computational code has been developed to solve the time-dependent Schrödinger equation of an asymmetric top in an arbitrary field configuration. However, due to the complexity of the field-dressed dynamics, so far we have focused on the parallel fields case. Using benzonitrile as prototype example, we have found that in addition to the pendular doublets formation, the avoided crossing among adiabatic states is an important source of nonadiabatic effects.

Finally, we have considered an asymmetric top molecule whose dipole moment is not parallel to any molecular axis of symmetry, and investigated the impact of combined electric and nonresonant elliptically polarized laser field. Our first approach has been to describe this system within the adiabatic approximation. We have provided the first theoretical analysis of the mixed-field orientation for this kind of molecules. In particular, we have shown that the 3D orientation is obtained by using a weak static dc field and an elliptically polarized laser field. Furthermore, our results show that the 3D orientation becomes possible if a linearly polarized laser field is combined with a strong dc field. These findings open new doors to the

experiments with this kind of molecules.

We describe now the structure of this dissertation. We start in **Chapter 3** by describing the Hamiltonian of rigid solid molecules in the presence of a homogenous static electric and an off-resonance laser fields under the Born-Oppenheimer approximation. For all the field configurations, we provide a detailed study of the symmetries and the corresponding irreducible representations.

Our work rely on solving the time-dependent as well as time-independent Schrödinger equations of these molecular systems. The computational techniques employed in this thesis are presented in **Chapter 4**. We start describing the linear variational method that transforms the time-independent Schrödinger equation, which is a second order differential equation in several variables, in a matrix eigenvalue problem. Next, we provide the more important features of the short iterative Lanczos propagation and the split-operator methods used to solve the time-dependent Schrödinger equations of asymmetric tops and linear molecules, respectively. In the mixed-field experiments, the orientation and alignment are measured by the detection on a CCD camera of the molecular ions created in the Coulomb explosion [51]. The images recorded on the screen represent 2D projections of the 3D wavefunction of the molecule just before the Coulomb explosion. Using these 2D images, they measure the degree of alignment and the orientation ratio. At the end of **Chapter 4**, we describe the theoretical procedure to obtain the 2D projections of the field-dressed wavefunctions and the experimental quantities that are measured.

The results are collected in **Chapter 5** and **Chapter 6**, which correspond to the published and unpublished results, respectively. In the three publications [52–54] which contains theoretical and experimental results, we are fully responsible of the theoretical parts.

The publications are contained in **Chapter 5** are the following:

1. **J. J. Omiste**, R. González-Férez and P. Schmelcher, *Rotational spectrum of asymmetric top molecules in combined static and laser fields*, Journal of Chemical Physics **135**, 064310 (2011) [55]

In this work, we perform a theoretical description of asymmetric top molecules in tilted nonresonant linearly polarized laser and an electric field within the rigid rotor approximation. We provide a systematic study of the symmetries, and each irreducible representation is treated independently, so that we can distinguish between avoided and real crossings in the field-dressed spectrum. We focus on investigating the energy shifts, the orientation, alignment and hybridization of the angular motion for several field configurations. For the ground state, we propose a novel 3D orientation technique based on applying a strong electric field perpendicular to a linearly polarized laser. This field configuration gives rise to the orientation of the dipole moment along the dc field axis, and the alignment of less polarizable molecular axis along the ac field axis.

2. **J. J. Omiste**, M. Gärttner, P. Schmelcher, R. González-Férez, L. Holmegaard, J. H. Nielsen, H. Stapelfeldt and J. Küpper, *Theoretical description of adiabatic laser alignment and mixed-field orientation: the need for a non-adiabatic model*, Physical Chemistry Chemical Physics **13**, 18815-18824 (2011) [52]

In this publication, we provide the first theoretical description of the mixed-field experiments on asymmetric top molecules, in particular, for benzonitrile (BN). Since the

time scale associated to the laser field was longer than the molecular rotational period, this process was widely accepted as adiabatic. Based on this hypothesis, we solve the time-independent Schrödinger equation and compute the orientation and alignment of the molecular beam including all states populated in the experiment. For perpendicular fields, our theoretical results are in very good agreement with the alignment measurements. In contrast, our adiabatic description could not reproduce the degree of orientation achieved in the experiments. This discrepancy indicates, for the first time, that the mixed-field orientation could not be an adiabatic process. The field-dressed spectrum is characterized by a large amount of avoided crossings. Our theoretical results show that not all of them are crossed adiabatically. Thus, we propose a diabatic model to classify the character of the avoided crossings in titled fields: those between states with the same field-free magnetic quantum number M are passed adiabatically; whereas those between states with different M are crossed diabatically. The degree of orientation obtained by means of this diabatic model shows a better agreement with the experimental measurements.

3. J. H. Nielsen, H. Stapelfeldt, J. Küpper, B. Friedrich, **J. J. Omiste** and R. González-Férez, *Making the best of mixed-field orientation of polar molecules: A recipe for achieving adiabatic dynamics in an electrostatic field combined with laser pulses*, Physical Review Letters **108**, 193001 (2012) [53]

In this work, we have experimentally and theoretically studied the mixed-field orientation of rotational-state-selected OCS molecules. The molecular beam is nearly pure in the rotational-ground state ($\sim 92\%$). We provide the first time-dependent description of the mixed-field orientation experiments by solving the time-dependent Schrödinger equation. We have shown that for the prototypical field configuration used in current mixed-field orientation experiments, the molecular field dynamics is, in general, nonadiabatic, and a time-dependent description of these systems is mandatory. We have identified two main sources of nonadiabatic effects. First, when the pendular doublets are formed as the laser intensity is increased, the two quasidegenerate states are strongly coupled, which leads to a transfer of population from the oriented one to the antioriented and vice-versa. Second, for tilted fields, the states from the same field-free J -manifold are strongly coupled and are driven apart at weak laser intensities, which gives rise to a population redistribution among them. Moreover, this time-dependent treatment allows us to investigate under which experimental conditions the mixed-field orientation would be an adiabatic process.

4. **J. J. Omiste** and R. González-Férez, *Nonadiabatic effects in long-pulse mixed-field orientation of a linear polar molecule*, Physical Review A **86**, 043437 (2012) [56]

In this publication, we carry out a theoretical analysis of the rotational dynamics of a linear molecule in combined dc and nonresonant laser fields. For several rotational states, their field-dressed dynamics is analyzed in detail for experimentally accessible static field strengths and laser pulses. We provide results for their directional cosines and compared them to the predictions of the adiabatic theory. In addition, we investigate several field regimes identifying the sources of nonadiabatic effects and provide the field parameters under which the adiabatic dynamics would be achieved.

The rest of the results of this thesis are collected in the three preprints, two of them have been submitted for publication, presented in **Chapter 6**. These works are the following:

5. **J. J. Omiste**, and R. González-Férez, *Rotational dynamics of an asymmetric top molecule in parallel electric and nonresonant laser fields*, arXiv:1306.1429v1 (2013) [57]

Here, we present the first time-dependent study of the impact of a dc field and a nonresonant linearly polarized laser pulse on an asymmetric top molecule. Using benzonitrile as prototype example, we perform a detailed analysis of the field-dressed dynamics for several experimentally accessible field configurations. Due to the complexity of the rotational dynamics, we focus on parallel fields. Our calculations show that the loss of adiabaticity is caused by two effects: i) the formation of the pendular doublets, and ii) the avoided crossings among neighboring adiabatic levels. Both phenomena give rise to a strong coupling between the involved states and the corresponding redistribution of population. The proximity between the avoided crossings and the doublets formation prevents us from using a two-state model to analyze these avoided crossings. Unlike the case of the doublet formation, we show that these avoided crossings cannot be tuned by varying the electric field strength. Thus, for these molecules, the adiabatic mixed-field orientation requires the use of laser pulses with longer temporal widths, i. e., longer FWHM.

6. J. L. Hansen, **J. J. Omiste**, J. H. Nielsen, D. Pentlehner, J. Küpper, R. González-Férez and H. Stapelfeld, *Mixed-field orientation of non-symmetric molecules*, preprint (2013) [54]

In this work, we consider the 6-chloropyridazine-3-carbonitrile ($C_4N_2H_2ClCN$) or CPC molecule, being its permanent dipole moment non parallel to the any axis of inertia. For this system, we present a theoretical and experimental study of its 3D alignment and orientation in mixed-fields. The alignment pulses have either linear or elliptical polarizations. In our theoretical calculations, we use the adiabatic approximation and solve the time-independent Schrödinger equation for the experimental field configurations. We find that for a weak dc field and a linearly polarized laser field, only the dipole moment component along the most-polarizable axis of the molecule is relevant for the orientation. Our calculations also show that the perpendicular component becomes relevant if strong electric fields are used. Our theoretical study confirms that an elliptically polarized laser and a tilted weak static electric fields are sufficient to obtain a 3D orientation.

7. **J. J. Omiste**, and R. González-Férez, *Mixed-field orientation of a thermal ensemble of polar molecule*, arXiv:1306.1251v1 (2013) [58]

In this work, we have investigated the orientation of a thermal sample of linear molecules for several field configurations. To do so, we solve the time-dependent Schrödinger equation for many states. Our calculations reveal that to achieve a significant orientation, either the rotational temperature is reduced or stronger dc fields of a few kV/cm are used. We also find that using a ns-Gaussian pulse, these avoided crossings are not passed diabatically.

Finally, some mathematical tools are collected in the Appendix. In **Appendix A** we summarize the key points of the transformation between the laboratory and the molecular

fixed frames by means of the Euler angles. The main properties of the Wigner matrix elements are collected in **Appendix B** and the matrix elements of the Hamiltonian are written in terms of the 3J Symbols in **Appendix C**.

Chapter 2

Introducción

El estudio de las moléculas expuestas a campos externos constituye actualmente un área de investigación muy activa, fructífera y prometedora, a pesar de la gran cantidad de resultados ya publicados en la literatura. Los avances alcanzados en la tecnología láser y en óptica unidos a la posibilidad de producir campos eléctricos estables e intensos han dado lugar a nuevas investigaciones sobre la manipulación y control de la dinámica molecular por medio de campos externos. En presencia de campos externos se obtiene la alineación y/o la orientación de la molécula. La alineación se refiere al confinamiento de los ejes del sistema de referencia fijo en la molécula a lo largo del sistema de referencia del laboratorio; en la orientación además el momento dipolar eléctrico de la molécula tiene una dirección bien definida. Los esfuerzos tanto teóricos como experimentales llevados a cabo en este área de investigación están motivados por la gran cantidad de nuevas e interesantes aplicaciones que estos sistemas presentan. Una de las primeras aplicaciones fue el control estereodinámico de las reacciones químicas, que permite realizar un estudio detallado de sus inherentes propiedades cuánticas y aumentar la eficiencia [1–3]. Por ejemplo, los estudios experimentales de las reacciones $K+CH_3I$ [4] y $Rb+CH_3I$ [5–7] mostraron que la reactividad mejora de forma significativa si el átomo de I del CH_3I está orientado hacia el átomo alcalino. La manipulación del grado de libertad rotacional ha permitido llevar a cabo investigaciones sobre las propiedades electrónicas y estructurales de las moléculas, como la espectroscopía [8, 9], difracción electrónica [10], distribución angular de los fotoelectrones [11–13], generación de armónicos altos [14, 15] y la toma de imágenes difractivas de moléculas en fase gaseosa [16, 17], con el objetivo final de rodar la película molecular [18]. Se ha conseguido un gran control tanto de los grados de libertad traslacionales [19] como rotacionales [20–22] de moléculas complejas, y se han observado efectos cuánticos de forma directa en la estereodinámica de reacciones moleculares en dímeros alcalinos ultrafríos [23].

En el primer experimento para orientar moléculas se utilizó el campo electrostático de un hexapolo [24–27]. La fuerza inducida en la molécula por este campo es proporcional a su orientación, por lo que este método permite la separación de las moléculas según sus estados rotacionales. En los años 90, Loesch y Remscheid propusieron la orientación de moléculas por medio de campos eléctricos intensos [28]. Esta técnica de *fuerza bruta* está basada en la transformación adiabática de los estados rotacionales en ausencia de campo en estados pendulares, que son una superposición coherente de autoestados rotacionales a campo cero. Estos estados pendulares aparecen para campos eléctricos muy intensos cuando la molécula está orientada y su movimiento rotacional se convierte en oscilatorio. Por primera vez, moléculas diatómicas $^1\Sigma$ fueron orientadas satisfactoriamente usando esta técnica [29, 30]. Este procedimiento ha permitido medir propiedades moleculares tales como el momento dipolar permanente del estado fundamental electrónico y de estados excitados usando espectroscopía pendular [31, 32] o efectos direccionales en reacciones químicas [28]. Su principal desventaja es que para orientar

de forma eficiente las moléculas, han de ser rotacionalmente frías con un momento dipolar alto y los campos eléctricos intensos.

Al orientar una molécula polar también se alinea. Sin embargo, la técnica de fuerza bruta no es apropiada para sistemas no polares ya que no tienen momento dipolar permanente. Friedrich y Herschbach exploraron la posibilidad de explotar la interacción entre la polarizabilidad de la molécula y un campo láser intenso no resonante para alinearla y atraparla [33,34]. La primera realización experimental la llevan a cabo Kim y Felker [35] usando espectroscopía Raman en trómeros de naftalina en campos láser intensos. Seideman amplió este estudio para moléculas asimétricas expuestas a pulsos láser largos y cortos de diferentes polarizaciones [36–40]. La alineación 1D se alcanza con campos láser linealmente polarizados [41], cuando el eje de mayor polarizabilidad (MPA) de la molécula se alinea a lo largo del eje de polarización del láser. Por el contrario, en la alineación 3D cada eje de la molécula se alinea a lo largo de un eje del laboratorio y requiere del uso de un campo láser elípticamente polarizado [42]. Además se ha investigado la posibilidad de alinear moléculas por medio de campos magnéticos moderados e intensos [43,44].

En el régimen de campo láser muy intenso, el espectro está caracterizado por pares o dobletes pendulares formados por dos estados alineados de paridad opuesta y energéticamente casi degenerados [45]. Usando métodos semiclásicos se ha probado que la separación de energía entre estos dos estados es proporcional a $\exp(-\gamma\sqrt{I})$, siendo γ una constante que depende del doblete e I la intensidad del láser. Basados en la proximidad energética entre ambos niveles, se propuso usar un campo eléctrico débil para acoplarlos e hibridarlos. De este modo se obtiene una orientación alta evitando emplear campos eléctricos fuertes como en el método de fuerza bruta [46,47]. Así, se crean dos estados muy orientados pero en direcciones contrarias. Esta predicción fue hecha en el marco adiabático, asumiendo que el tiempo de encendido del pulso láser es mucho mayor que el periodo rotacional de la molécula. Este estudio teórico fue generalizado para moléculas simétricas en un campo eléctrico y uno láser no resonante [48].

La viabilidad de esta propuesta teórica se pone de manifiesto experimentalmente casi de forma inmediata, pero se obtiene un grado de orientación muy inferior al esperado teóricamente [49,50]. Este hecho se explica por la distribución térmica que presenta el haz molecular usado en el experimento. De modo que la combinación de estados orientados y antiorientados con pesos térmicos similares da lugar a una orientación muy débil. En 2009 se lleva a cabo un avance experimental decisivo al crear un haz molecular de estados cuánticos seleccionados de iodobenceno usando un campo eléctrico inhomogéneo alcanzando así una orientación sin precedentes. [20, 51]. En este experimento, el haz de moléculas de estados cuánticos seleccionados viaja hacia el detector, y se expone al campo eléctrico homogéneo débil de un *velocity map imaging spectrometer* y a un pulso láser de nanosegundos. En el experimento se puede controlar el ángulo formado entre la polarización del láser y la dirección del campo eléctrico, y así crear tanto moléculas orientadas como alineadas. Para medir el grado de orientación y alineación se superpone temporal y espacialmente un pulso láser de sondeo con el láser de alineación. Este láser de sondeo produce una explosión de Coulomb de las moléculas, y los fragmentos iónicos son acelerados hacia el detector. En la aproximación de retroceso, las imágenes 2D de estos fragmentos de la explosión de Coulomb representan una proyección 2D de la función de onda 3D, y, por lo tanto, permiten medir la orientación y alineación molecular. Estos experimentos fueron realizados suponiendo que la alineación y la orientación eran procesos adiabáticos, porque la anchura temporal del pulso láser (\sim ns) era mayor que el periodo rotacional de estos sistemas. Varios estudios teóricos han reproducido los exper-

imentos de alineación y las correspondientes medidas [19, 36, 42]. Sin embargo, hasta ahora no se había llevado a cabo ningún análisis teórico sobre el impacto de una combinación de campos eléctrico y láser en moléculas asimétricas, que permitiese interpretar las observaciones experimentales.

Objetivo de esta Tesis

El objetivo de esta tesis es llevar a cabo un estudio teórico de la dinámica rotacional de moléculas polares en presencia de campos externos. Describimos a continuación este objetivo con mayor detalle y siguiendo el desarrollo temporal del trabajo realizado a lo largo de esta tesis doctoral.

Se ha comenzado estudiando una molécula asimétrica sometida a un campo eléctrico y uno láser linealmente polarizado usando la aproximación de rotor rígido. Para ello, hemos asumido que el campo eléctrico es estático, y para el pulso láser se ha tomado la envolvente temporal como constante e igual a uno. Hemos analizado las energías de los estados, su orientación y alineación al variar la intensidades del láser y del campo eléctrico y el ángulo entre ambos. También hemos realizado una descripción detallada de las simetrías del Hamiltoniano del rotor rígido para todas las posibles configuraciones de los campos. Numéricamente, cada representación irreducible ha sido tratada de forma independiente.

Basados en este estudio, se ha llevado a cabo una investigación teórica del experimento descrito anteriormente. Nuestro objetivo es interpretar y reproducir las medidas experimentales para la alineación y la orientación de moléculas asimétricas. Usando la aproximación adiabática, hemos resuelto la ecuación de Schrödinger independiente del tiempo para las configuraciones de campos usadas en el experimento, y calculado las propiedades direccionales de los estados cuánticos que forman el haz molecular. Nuestros resultados teóricos han reproducido las medidas experimentales para la alineación adiabática, pero no para la orientación. Este desacuerdo demuestra que la hipótesis adiabática no es correcta para describir la orientación en una combinación de campos. Se ha resuelto parcialmente este problema proponiendo un modelo diabático para clasificar el carácter adiabático o diabático de los numerosos cruces evitados que aparecen en el espectro molecular. De este modo, se ha obtenido un mejor acuerdo entre los resultados teóricos y experimentales.

Este estudio sobre la orientación de moléculas asimétricas en campos eléctrico y láser indica que es necesaria una descripción alternativa de este proceso. Así, se ha llevado a cabo un análisis de la dinámica rotacional de moléculas lineales polares expuestas a una combinación de campos electromagnéticos. Para ello, se ha resuelto la ecuación de Schrödinger dependiente del tiempo teniendo en cuenta el perfil temporal de ambos campos. Este estudio ha permitido probar que con pulsos láseres en el rango de los ns, la orientación usando un campo eléctrico débil no es, en general, adiabática y que se requiere una descripción dependiente del tiempo de este sistema para explicar las observaciones experimentales. Además, se han identificado los fenómenos físicos que inducen a la no adiabaticidad y las condiciones experimentales necesarias para alcanzar una dinámica rotacional adiabática.

Nuestro siguiente objetivo ha sido generalizar esta descripción de la dinámica rotacional en campos externos a sistemas moleculares más complejos como son las moléculas asimétricas. Se ha desarrollado la teoría necesaria y el correspondiente código computacional para resolver la ecuación de Schrödinger dependiente del tiempo de un rotor asimétrico en una combinación

arbitraria de campos. Sin embargo, debido a la complejidad de la dinámica rotacional, en esta tesis solo hemos analizado en detalle el caso de campos paralelos. Usando el benzonitrilo como prototipo, hemos encontrado que además de la formación de dobletes, los cruces evitados entre estados adiabáticos dominan la evolución temporal de una función de onda. Debido a la diferencia entre los tiempos característicos asociados a cada uno de estos fenómenos las condiciones de adiabaticidad son más difíciles de reproducir experimentalmente.

Finalmente, hemos considerado una molécula asimétrica cuyo momento dipolar no es paralelo a ningún eje molecular de simetría en presencia de un campo eléctrico y uno láser no resonante. Este es el primer estudio teórico sobre el impacto de campos externos en este tipo de moléculas. Llevamos a cabo esta descripción dentro de las aproximaciones adiabática y de sólido rígido. En concreto, hemos mostrado que la orientación 3D se obtiene usando un campo eléctrico estático débil y un campo láser elípticamente polarizado. Además, nuestros resultados muestran que la orientación 3D es posible si un láser linealmente polarizado se combina con un campo eléctrico intenso.

A continuación detallamos cual es la estructura de esta tesis doctoral.

En el **Capítulo 3** describimos el Hamiltoniano rotacional de estos sistemas dentro de la aproximación de rotor rígido en presencia de un campo eléctrico homogéneo y estático y láser fuera de resonancia. Para todas las posibles configuraciones de campos, se muestra un estudio detallado de las simetrías del Hamiltoniano rotacional y de sus correspondientes representaciones irreducibles.

Para llevar a cabo nuestros objetivos, hemos de resolver las ecuaciones de Schrödinger dependiente e independiente del tiempo para estos sistemas moleculares. Las técnicas computacionales empleadas en esta tesis se presentan en el **Capítulo 4**. Empezamos describiendo el método variacional lineal que transforma la ecuación de Schrödinger independiente del tiempo en un problema matricial de autovalores. A continuación, se detallan las características más importantes de la técnica de propagación en iteraciones cortas de Lanczos y el método del operador de división usados para resolver la ecuación de Schrödinger dependiente del tiempo para los rotores asimétricos y lineales, respectivamente. En los experimentos en campos eléctricos y de láser, la orientación y la alineación se miden detectando en una cámara CCD los iones moleculares creados en la explosión de Coulomb [20,51]. Las imágenes recogidas en la pantalla son proyecciones 2D de la función de onda 3D de la molécula justo antes de la explosión de Coulomb y a partir de ellas se obtienen los grados de alineación y orientación. Al final del **Capítulo 4**, describimos el procedimiento teórico para obtener las proyecciones 2D de las funciones de onda y las cantidades experimentales que son medidas.

Los resultados se recogen en el **Capítulo 5** y el **Capítulo 6**, que corresponden a los resultados publicados y no publicados, respectivamente. En las tres publicaciones [52–54], que incluyen resultados teóricos y experimentales, hemos llevado a cabo todo el trabajo teórico.

Las publicaciones contenidas en el **Capítulo 5** son las siguientes:

1. **J. J. Omiste**, R. González-Férez and P. Schmelcher, *Rotational spectrum of asymmetric top molecules in combined static and laser fields*, *Journal of Chemical Physics* **135**, 064310 (2011) [55]

En este trabajo hemos realizado una descripción teórica de las moléculas asimétricas en un campo láser no resonante linealmente polarizado y uno eléctrico dentro de la aproximación de rotor rígido. Hemos considerado que la dirección de ambos campos

forma un ángulo arbitrario. Se ha presentado un estudio sistemático de las simetrías, esto nos ha permitido tratar numéricamente cada representación irreducible de forma independiente y distinguir en el espectro los cruces evitados de los reales. Este trabajo se ha centrado en la investigación los desplazamientos de energía de los niveles, su orientación, alineación e hibridación del movimiento angular para varias configuraciones de los campos. Para el estado fundamental, proponemos una nueva técnica para obtener orientación 3D basada en aplicar un campo eléctrico intenso perpendicular al láser linealmente polarizado. Esta configuración de campos da lugar a la orientación del momento dipolar a lo largo del campo eléctrico, y a la alineación del eje molecular menos polarizable a lo largo del eje del campo láser.

2. **J. J. Omiste**, M. Gärttner, P. Schmelcher, R. González-Férez, L. Holmegaard, J. H. Nielsen, H. Stapelfeldt and J. Küpper, *Theoretical description of adiabatic laser alignment and mixed-field orientation: the need for a non-adiabatic model*, Physical Chemistry Chemical Physics **13**, 18815-18824 (2011) [52]

En esta publicación se ha llevado a cabo la primera descripción teórica de los experimentos de orientación y alineación de una molécula asimétrica, en concreto el benzonitrilo, en un campo eléctrico y uno láser [52]. Como la anchura temporal del pulso láser es mayor que el período rotacional molecular, este proceso se consideraba como adiabático en la comunidad experimental. Basados en esta hipótesis, se ha resuelto la ecuación de Schrödinger independiente del tiempo. Para el haz de moléculas del experimento, hemos calculado la orientación y alineación. Nuestros resultados teóricos reproducen las medidas experimentales del grado de alineación para campos perpendiculares, pero no el de orientación cuando los campos están inclinados. Esta discrepancia indica, por primera vez, que la orientación en una combinación de campos eléctrico y láser no puede ser un proceso adiabático. El espectro en presencia de campos está caracterizado por una gran cantidad de cruces evitados. Nuestros resultados teóricos muestran que no todos ellos son cruzados adiabáticamente. Por consiguiente, hemos propuesto un modelo diabático para clasificar el carácter de los cruces evitados en campos inclinados: aquellos que involucran estados con el mismo número cuántico magnético M en ausencia de campos son cruzados adiabáticamente; mientras que aquellos entre estados con diferente M son cruzados diabáticamente. El grado de orientación obtenido por medio del modelo diabático muestra un mejor acuerdo con las medidas experimentales.

3. J. H. Nielsen, H. Stapelfeldt, J. Küpper, B. Friedrich, **J. J. Omiste** and R. González-Férez, *Making the best of mixed-field orientation of polar molecules: A recipe for achieving adiabatic dynamics in an electrostatic field combined with laser pulses*, Physical Review Letters **108**, 193001 (2012) [53]

En este trabajo hemos estudiado experimental y teóricamente la orientación de la molécula de OCS en una combinación de campos eléctrico y láser. El haz molecular está formado por un 92% de moléculas en el estado rotacional fundamental. Se ha llevado a cabo la primera descripción de este sistema resolviendo la ecuación de Schrödinger dependiente del tiempo. Hemos encontrado que para la configuración de campos usada en los experimentos actuales, la dinámica molecular es, en general, no adiabática, y es necesario realizar una descripción dependiente del tiempo. Hemos identificado los dos principales fenómenos físicos que dan lugar a efectos no adiabáticos. Primero, cuando

se forman dobletes pendulares al aumentar la intensidad del láser, los dos estados casi degenerados están acoplados fuertemente, y esto conlleva una transferencia de población del orientado al antiorientado y viceversa. Segundo, para campos inclinados, los estados con el mismo momento angular J en ausencia de campos ahora están acoplados; a bajas intensidades se separan energéticamente dando lugar a una redistribución de la población entre ellos. Este trabajo nos ha permitido investigar bajo qué condiciones experimentales la dinámica rotacional sería un proceso adiabático.

4. **J. J. Omiste** and R. González-Férez, *Nonadiabatic effects in long-pulse mixed-field orientation of a linear polar molecule*, Physical Review A **86**, 043437 (2012) [56]

En esta publicación hemos llevado a cabo un análisis teórico de la dinámica rotacional de una molécula lineal en un campo eléctrico y uno láser no resonante. Para varios estados, su dinámica rotacional ha sido analizada en detalle para intensidades de ambos campos accesibles experimentalmente. Los resultados para orientación se han comparado con las predicciones de la teoría adiabática para varios regímenes de los campos. Se han identificado los fenómenos no adiabáticos que aparecen para campos paralelos e inclinados. Este estudio nos ha permitido predecir la configuración experimental que daría lugar a una dinámica adiabática.

El resto de los resultados de esta tesis doctoral se recogen en tres preprints, dos de ellos han sido enviados para su publicación, que se han incluido en el **Capítulo 6**. Estos trabajos son los siguientes:

5. **J. J. Omiste**, and R. González-Férez, *Rotational dynamics of an asymmetric top molecule in parallel electric and non-resonant laser fields*, arXiv:1306.1429v1 (2013) [57]

Aquí hemos llevado a cabo el primer estudio dependiente del tiempo del impacto de un campo eléctrico y uno láser no resonante linealmente polarizado en una molécula asimétrica. Usando el benzonitrilo como prototipo, realizamos un análisis detallado de la dinámica para varias configuraciones que son experimentalmente accesibles. Debido a la complejidad de este sistema, nos hemos centrado en el análisis de la dinámica en campos paralelos. Nuestros cálculos muestran que la pérdida de adiabaticidad es causada por dos efectos: i) la formación de los dobletes pendulares, y ii) los cruces evitados entre niveles adiabáticos vecinos. Ambos fenómenos dan lugar a un fuerte acoplamiento entre los estados involucrados y a una redistribución de población. La cercanía entre los cruces evitados y la formación de dobletes impide usar la aproximación de Landau-Zener para clasificar estos cruces evitados. A diferencia de la formación de dobletes, aumentar el campo eléctrico no asegura que la dinámica a través de los cruces evitados sea adiabática. Así, para estas moléculas, la orientación adiabática requiere de pulsos láser con anchuras temporales más largas.

6. J. L. Hansen, **J. J. Omiste**, J. H. Nielsen, D. Pentlehner, J. Küpper, R. González-Férez and H. Stapelfeld, *Mixed-field orientation of non-symmetric molecules*, preprint (2013) [54]

En este trabajo consideramos la molécula 6-cloropiridacina-3-carbonitrilo ($C_4N_2H_2ClCN$) o CPC cuyo momento dipolar permanente no es paralelo a ningún eje de inercia. Para

este sistema, presentamos un estudio teórico y experimental de su alineación y orientación 3D en una combinación campos eléctricos y láseres de polarización tanto lineal como elíptica. En nuestros cálculos teóricos usamos la aproximación adiabática y resolvemos la ecuación de Schrödinger independiente del tiempo para configuraciones experimentales de campos electromagnéticos. Encontramos que para un campo eléctrico débil y un campo láser linealmente polarizado, sólo la componente del momento dipolar a lo largo del eje más polarizable de la molécula es relevante para la orientación; y que la componente perpendicular contribuye en este proceso si se usan campos eléctricos intensos. Este estudio teórico confirma que un láser elípticamente polarizado y un campo eléctrico estático débil inclinado son suficientes para obtener orientación 3D.

7. **J. J. Omiste**, and R. González-Férez, *Mixed-field orientation of a thermal ensemble of polar molecule*, arXiv:1306.1251v1 (2013) [58]

En este trabajo, hemos investigado la orientación de un haz de moléculas lineales con distribución térmica para varias configuraciones de los campos externos. Para ello, se ha resuelto la ecuación de Schrödinger dependiente del tiempo para muchos estados rotacionales. Nuestros cálculos ponen claramente de manifiesto que para alcanzar una orientación significativa es necesario bien reducir la temperatura rotacional o usar campos eléctricos con intensidades de varios kV/cm. Además, mostramos que usando un pulso gaussiano de 20 nanosegundos, los cruces evitados no se pueden cruzar de forma adiabática.

Finalmente, se recogen algunas herramientas matemáticas usadas en esta tesis doctoral en los Apéndices. En el **Appendix A** resumimos los puntos clave de la transformación entre los sistemas de referencia fijo en el laboratorio y en la molécula por medio de los ángulos de Euler. Las principales propiedades de los elementos de las matrices de Wigner se muestran en el **Appendix B** y los elementos de matriz del Hamiltoniano se escriben en términos de los Símbolos 3J en el **Appendix C**.

Chapter 3

Hamiltonian of molecules in the presence of external fields

We study a polar linear or asymmetric top molecule exposed to a combination of an homogeneous static electric field and a nonresonant laser field. The field strengths are considered so that they have a notable impact on the rotational dynamics of the molecule, but affect weakly the electronic and vibrational structures, which are treated by first order perturbation theory. We work within the Born-Oppenheimer approximation, and further assume that the rotational and vibrational dynamics can be adiabatically separated. Then, these molecular systems are described within the rigid rotor approximation. In addition, we neglect relativistic, fine and hyperfine interactions, as well as the couplings with different electronic states. To describe the location of the molecule we use the laboratory (X, Y, Z) and molecule fixed

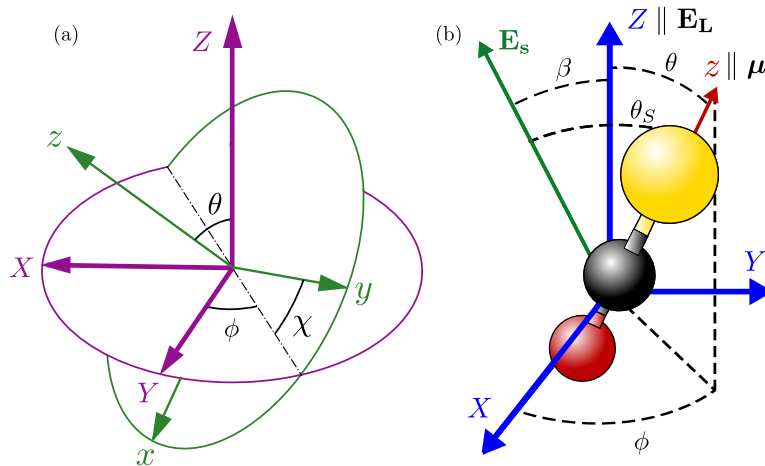


Figure 3.1: Relation of the Laboratory and Molecular fixed frame by means of the Euler angles (a) and field configuration with a linear molecule in the Laboratory fixed frame with the Euler angles (b).

frames (x, y, z) , LFF and MFF, respectively. The LFF is chosen so that the major polarization axis of the laser field is parallel the Z axis, and the homogenous electric field forms an angle β with this axis and defines the XZ plane, see right panel of Fig. 3.1. The axes of the MFF, (x, y, z) , correspond to the principal axes of inertia of the molecule. These two frames are related by the Euler angles $\Omega = (\phi, \theta, \chi)$ [59], which are shown of Fig. 3.1(a). The main properties of the transformation between the LFF and the MFF are collected in Appendix A.

The Hamiltonian of a rigid rotor molecule in this field configuration is given by

$$H = H_r + H_S + H_L, \quad (3.1)$$

where H_r is the field-free Hamiltonian, and H_S and H_L stand for the interactions with the electric and laser fields, respectively. In the following sections, we analyze in detail the contribution of each of these terms.

3.1 The Hamiltonian of the Field-Free Rotor

Let us start with the description of the field-free Hamiltonians for three different molecules: linear, symmetric and asymmetric top rotors.

3.1.1 Linear rotor

In absence of fields, the rigid rotor Hamiltonian for a linear rotor reads as

$$H_r = B\vec{J}^2, \quad (3.2)$$

with $B = \frac{\hbar^2}{2I}$ being the rotational constant, where I is the moment of inertia, and \vec{J} stands for the angular momentum operator. The eigenfunctions of the Hamiltonian are the spherical harmonics, $Y_{JM}(\theta, \phi)$, with J being the rotational quantum number and M the magnetic quantum number, that is, the eigenvalue of the projection of \vec{J} on the Z axis, J_Z . The eigenenergies of the Hamiltonian (3.2) are $E_J = BJ(J+1)$ and have $2J+1$ degeneracy.

3.1.2 Symmetric top rotor

A symmetric top rotor is characterized by only two rotational constants A and B_z , i. e., $B_x = B_y = A$. The field-free Hamiltonian of this system reads

$$H_{rsy} = AJ_x^2 + AJ_y^2 + B_z J_z^2 = A\vec{J}^2 + C J_z^2, \quad (3.3)$$

where J_x, J_y and J_z are the projection of the operator \vec{J} on the x, y and z axes of the MFF, respectively, and $C = B_z - B_x = B_z - A$. It is easy to proof that [59]

$$[H_{rsy}, \vec{J}^2] = [H_{rsy}, J_z] = [H_{rsy}, J_Z] = 0. \quad (3.4)$$

Thus, the projection of \vec{J} on the z and Z axes, K and M , respectively, are good quantum numbers. Consequently, the set of operators $\{H_{rsy}, J^2, J_z, J_Z\}$ are enough to identify an eigenstate of the field-free symmetric rigid rotor Hamiltonian. The corresponding wavefunctions are [59]

$$\langle \Omega | JKM \rangle = \psi_{J,K,M}(\phi, \theta, \chi) = (-1)^{M-K} \sqrt{\frac{2J+1}{8\pi^2}} D_{-M, -K}^J(\phi, \theta, \chi), \quad (3.5)$$

$$= \sqrt{\frac{2J+1}{8\pi^2}} D_{M, K}^{\dagger J}(\phi, \theta, \chi), \quad (3.6)$$

where $\Omega = (\phi, \theta, \chi)$ $D_{M, K}^J(\phi, \theta, \chi)$ are the Wigner matrix elements [59], with $K, M = -J, \dots, J$. Their main properties are collected in Appendix B. The energy corresponding to the eigen-

state $\psi_{J,K,M}(\phi, \theta, \chi)$ is $E_{J,K,M} = AJ(J+1) + CK^2$ having a degeneracy of $2(2J+1)$ for $|K| \neq 0$ and $2J+1$ for $K=0$.

Depending on the rotational constants, we can distinguish two types of symmetric rotors. For $C > 0$, the rotor is called *prolate*, and for fixed J , its energy levels increase with K . Whereas for $C < 0$, the rotor is *oblate*, and the energy of the states decrease for increasing K for a fixed J .

3.1.3 Asymmetric top rotor

The asymmetric top rotor is characterized by three different rotational constants. Note that, from now on, we fix the molecular fixed frame so that $B_z > B_y > B_x$. The asymmetry degree of the molecule is estimated by the Ray parameter $\kappa = \frac{2B_y - B_z - B_x}{B_z - B_x}$. The two extreme values $\kappa = -1$ ($B_y = B_x$) and $+1$ ($B_y = B_z$) correspond to prolate and oblate symmetric rotors, respectively.

The field-free rigid rotor Hamiltonian is given by

$$H_r = B_x J_x^2 + B_y J_y^2 + B_z J_z^2 = A \vec{J}^2 + B (J_+^2 + J_-^2) + C J_z^2, \quad (3.7)$$

with

$$\begin{aligned} A &= \frac{B_x + B_y}{2}, \\ B &= \frac{B_x - B_y}{4}, \\ C &= \frac{2B_z - B_x - B_y}{2}. \end{aligned}$$

The Hamiltonian of the field-free asymmetric rigid rotor H_r in equation (3.7) does not commute with J_z , hence K is no longer a good quantum number, whereas J and M still are. For arbitrary J , the Schrödinger equation can not be solved analytically. However, the eigenfunctions of the field-free asymmetric rigid rotor are written as linear combinations of the field-free wavefunctions of the symmetric rigid rotor

$$|JM\eta\rangle = \sum_{K=-J}^J c_{K,\eta} |JKM\rangle, \quad (3.8)$$

where the coefficients $c_{K,\eta}$ are real and η labels the different states with the same J and M . Unless accidental degeneracy, the energy levels are degenerate $2J+1$. In Fig. 3.2, we show the energy levels in the two limiting cases of prolate and oblate symmetric molecules. By changing adiabatically B in the rotational Hamiltonian H_r we can link one to one the states in these two limiting spectra.

Using this, we label the field-free asymmetric rotor eigenfunctions by $J_{K_a K_c} M$ [60], where K_a and K_c are the values of K for the prolate and oblate limiting cases, respectively, as shown in Fig. 3.2. This notation gives us useful information about the symmetry of the wavefunction. For instance, the parity of a given state $J_{K_a K_c} M$ under two fold rotations around the prolate or oblate axes is given by the parity of K_a and K_c , respectively.

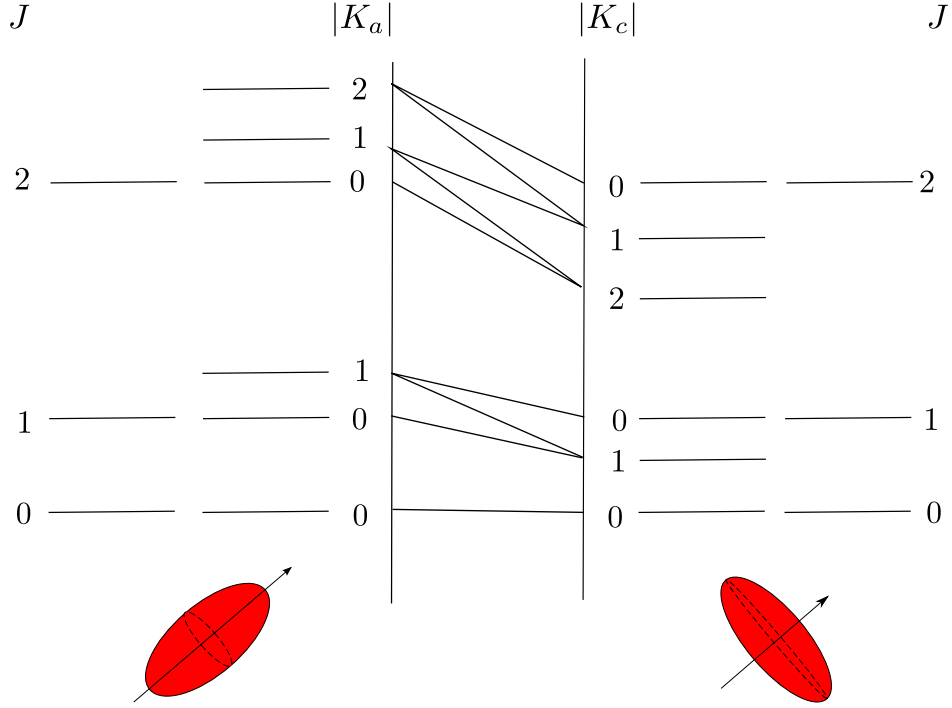


Figure 3.2: Labeling of the field-free levels of the asymmetric rotor.

3.2 The interaction with a homogenous static electric field

A homogenous static electric field, \vec{E}_S , interacts with the permanent electric dipole moment of the molecule, $\vec{\mu}$, its polarizability α , the hyperpolarizability and higher order terms. For the regime of electrostatic field strengths considered in this thesis, we assume that only the coupling due to $\vec{\mu}$ is significant and neglect higher orders. Thus, the Stark interaction is written as

$$H_S = -\vec{E}_S \cdot \vec{\mu}. \quad (3.9)$$

If we consider a permanent dipole moment $\vec{\mu}$ contained in the molecular plane xz the Stark Hamiltonian yields

$$\begin{aligned} H_S &= -E_S (\mu_z \cos \theta_{S_z} + \mu_x \cos \theta_{S_x}) \\ &= -E_S \cos \beta (\mu_z \cos \theta - \mu_x \sin \theta \cos \chi) + \\ &\quad -E_S \sin \beta [\mu_z \sin \theta \cos \phi + \mu_x (\cos \phi \cos \theta \cos \chi - \sin \phi \sin \chi)], \end{aligned} \quad (3.10)$$

where μ_z and μ_x are the projections of the permanent dipole moment along the z and x axes. The angles θ_{S_z} and θ_{S_x} are the angles formed by the z and x axes with the electric field, respectively. The expression (3.10) can be rewritten as a linear combination of Wigner matrix

elements

$$\begin{aligned}
H_S &= -E_S \mu_z \left(\cos \beta D_{00}^1(\Omega) + \sin \beta \sqrt{\frac{1}{2}} \left(D_{-10}^1(\Omega) - D_{10}^1(\Omega) \right) \right) + \\
&\quad -E_S \mu_x \left(\frac{\cos \beta}{\sqrt{2}} \left(D_{0-1}^1(\Omega) - D_{01}^1(\Omega) \right) + \right. \\
&\quad \left. + \frac{\sin \beta}{2} \left(D_{-1-1}^1(\Omega) + D_{11}^1(\Omega) - D_{1-1}^1(\Omega) - D_{-11}^1(\Omega) \right) \right), \quad (3.11)
\end{aligned}$$

where the term $D_{M''K''}^1(\Omega)$ couples two Wigner matrix elements fulfilling $|\Delta J| \leq 1$, $\Delta K = K''$ and $\Delta M = M''$. For instance, if $\beta = 0$, the component μ_z couples functions with $|\Delta K| = |\Delta M| = 0$ and $|\Delta J| \leq 1$, whereas μ_x couples states with $|\Delta J| \leq 1$, $|\Delta K| = 1$ and $\Delta M = 1$. For $\beta \neq \pi/2$ both components couples states with $|\Delta M| = 1$, as well.

For linear and some asymmetric molecules, $\vec{\mu}$ is parallel to the z axis of the MFF. In this case, the interaction term (3.9) is reduced to

$$\begin{aligned}
H_S &= -E_S \mu (\cos \beta \cos \theta + \sin \beta \sin \theta \cos \phi) \\
&= -E_S \mu \left(\cos \beta D_{00}^1(\Omega) + \sin \beta \sqrt{\frac{1}{2}} \left(D_{-10}^1(\Omega) - D_{10}^1(\Omega) \right) \right). \quad (3.12)
\end{aligned}$$

Note that for a linear molecule, $\Omega = (\theta, \phi)$.

3.3 The interaction with a non resonant laser field

As in the case of the dc field, the electric field of the non resonant laser field interacts with the permanent dipole moment, the polarizability and higher order terms. Here, we work in the intensity regime of the laser field, where the couplings due to $\vec{\mu}$ and α can not be neglected. This interaction is given by [40, 61]

$$\begin{aligned}
H_L &= \vec{\mu} \cdot \vec{E}_L(t) + \frac{1}{4} \sum_{\rho\rho'} E_\rho(t) \alpha_{\rho\rho'} E_{\rho'}^*(t), \quad (3.13) \\
&= \vec{\mu} \vec{E}_L(t) + \sum_{\rho} E_\rho(t) \mu_\rho^{ind}(t), \quad \mu_\rho^{ind} = \sum_{\rho'} E_{\rho'}(t) \alpha_{\rho\rho'} E_{\rho'}^*(t),
\end{aligned}$$

where $\vec{E}_L(t)$ and $E_\rho(t)$ are the electric field associated to the laser and its components referred to the $\rho = X, Y$ or Z axes of the LFF. $\alpha_{\rho,\rho'}$ is the polarizability tensor of the molecule referred to the LFF, with $\rho, \rho' = X, Y$ or Z . $\vec{\mu}^{ind}$ is the induced dipole moment produced by the laser field in the molecule. The polarizability tensor in the LFF and the MFF are related as follows

$$\alpha_{\rho\rho'} = \sum_{kk'} \langle \rho | k \rangle \alpha_{kk'} \langle k | \rho' \rangle,$$

with $k, k' = x, y$ and z axes.

In this thesis, we consider a non resonant laser field linearly polarized along the Z axis and an elliptically polarized one along the Z and X axes. The associated electric field components

along the Z and X directions are $E_{L,Z}(t) = E_{0Z}(t) \cos(2\pi\nu t)$ and $E_{L,X}(t) = E_{0X}(t) \cos(2\pi\nu t + \pi/2)$ [48], ν being its frequency, $E_{0Z}(t)$ and $E_{0X}(t)$ the envelope of the electric field of the Z and X components. We are considering the most general case, in which these electric field strengths $E_{0X}(t)$ and $E_{0Z}(t)$ depend on time. We assume that ν^{-1} is much shorter than the pulse duration and the rotational period. This allows us to average over these rapid oscillations in one period and, as a consequence, the coupling of this field with the permanent dipole moment $\vec{E}_L \cdot \vec{\mu}$ vanishes [62, 63]. The time averaged electric field in a cycle is $\langle E_{L,Z}(t) \rangle = \frac{2I_{ZZ}(t)}{c\epsilon}$, where $I_{ZZ}(t)$ is the intensity of the laser in the Z component, c the speed of light and ϵ_0 is the dielectric constant in the vacuum. Hence, the interaction of the non resonant laser field with the polarizability is [64]

$$H_L(t) = -\frac{I_{ZZ}(t)}{2c\epsilon_0} (\alpha^{zx} \cos^2 \theta_{Zz} + \alpha^{yx} \cos^2 \theta_{Zy}) + \\ -\frac{I_{XX}(t)}{2c\epsilon_0} (\alpha^{zx} \cos^2 \theta_{Xz} + \alpha^{yx} \cos^2 \theta_{Xy}), \quad (3.14)$$

where $\alpha^{ji} = \alpha_{jj} - \alpha_{ii}$ [61], with $i, j = x, y$ and z . The angle θ_{Pq} is the angle formed by the LFF P axis and the MFF q axis. Their cosines are written in terms of the Euler angles as

$$\cos \theta_{Zz} = \cos \theta, \quad (3.15)$$

$$\cos \theta_{Zy} = \sin \chi \sin \theta, \quad (3.16)$$

$$\cos \theta_{Xz} = \cos \phi \sin \theta, \quad (3.17)$$

$$\cos \theta_{Xy} = -\sin \phi \cos \chi - \cos \phi \cos \theta \sin \chi. \quad (3.18)$$

The Hamiltonian (3.14) in terms of the Wigner matrix elements reads

$$H_L(t) = -\frac{I_{ZZ}(t)}{2c\epsilon_0} \left(\frac{\alpha^{zx} + \alpha^{yx}}{3} D_{00}^2(\Omega) - \frac{\alpha^{yx}}{\sqrt{6}} (D_{02}^2(\Omega) + D_{0-2}^2(\Omega)) + \frac{\alpha^{zx} + \alpha^{yx}}{3} D_{00}^0 \right) + \\ -\frac{I_{XX}(t)}{2c\epsilon_0} \left(\frac{\alpha^{zx}}{\sqrt{6}} (D_{2,0}^2(\Omega) + D_{-2,0}^2(\Omega)) - \frac{\alpha^{zx}}{3} D_{00}^2(\Omega) + \frac{\alpha^{zx} + \alpha^{yx}}{3} D_{00}^0 + \right. \\ \left. + \frac{\alpha^{yx}}{2\sqrt{6}} (D_{02}^2(\Omega) + D_{0-2}^2(\Omega) - D_{20}^2(\Omega) - D_{-20}^2(\Omega)) + \right. \\ \left. - \frac{\alpha^{yx}}{4} (D_{22}^2(\Omega) + D_{2-2}^2(\Omega) + D_{-22}^2(\Omega) + D_{-2-2}^2(\Omega)) \right). \quad (3.19)$$

The interaction term H_L mixes basis elements with $|\Delta J| \leq 2$. Depending on the field configuration, $\Delta K = 0, \pm 2$ and $\Delta M = 0, \pm 2$ can also be mixed.

For a linearly polarized laser field, that is $I_{XX} = 0$, the interaction term H_L in expression

(3.14) becomes

$$\begin{aligned}
H_L(t) &= -\frac{I(t)}{2c\epsilon_0} (\alpha^{zx} \cos^2 \theta_{Zz} + \alpha^{yx} \cos^2 \theta_{Zy}) \\
&= -\frac{I(t)}{2c\epsilon_0} \left(\frac{\alpha^{zx} + \alpha^{yx}}{3} D_{00}^2(\Omega) - \frac{\alpha^{yx}}{\sqrt{6}} (D_{02}^2(\Omega) + D_{0-2}^2(\Omega)) \right. \\
&\quad \left. + \frac{\alpha^{zx} + \alpha^{yx}}{3} D_{00}^0(\Omega) \right), \tag{3.20}
\end{aligned}$$

where $I(t) = I_{ZZ}(t)$ is the intensity of the laser field at a time t . For this particular case, the Hamiltonian does not couple states with $\Delta M \neq 0$.

For a linear rotor and a linearly polarized laser field, the coupling with the laser is simplified since χ does not play a role, thus, $H_L(t)$ yields

$$H_L(t) = -\frac{I(t)}{2c\epsilon_0} (\Delta\alpha \cos^2 \theta_{Zz} + \alpha_{\perp}), \tag{3.21}$$

where $\Delta\alpha = \alpha_{\parallel} - \alpha_{\perp}$, with α_{\parallel} and α_{\perp} being the components of the polarizability parallel and perpendicular to the internuclear axis, respectively. Then, the field-free states with $|\Delta J| = 0, 2$ and $\Delta M = 0$ are coupled.

3.4 Symmetries and representations

One of the aim of this thesis is to compare our theoretical results with the experimental ones for alignment and mixed-field orientation of molecular beams, which are formed by asymmetric or linear top molecules, such as benzonitrile and OCS, respectively. The experimental group provides us the rotational states and their relative populations within the molecular beam. To describe the experimental results, we should uniquely identify these states when the dc field strengths or laser intensity are varied. Note that the labels of an eigenstate obtained by adiabatic following depend on the real and avoided crossings along the path through field parameter space, i. e., β , E_S or I_0 [48]. An important feature of the field-dressed spectrum of a molecule in external fields is the large amount of genuine and avoided crossings occurring between adjacent states as one of the field parameters is varied. The avoided crossings appear between levels of the same symmetry and some of them are characterized by a strong mixing of the involved field-dressed states. For a correct description of the experimental results, these avoided crossings should be distinguished from the genuine ones taking place between levels of different symmetry. Thus, an exhaustive analysis of the symmetries of the Hamiltonian in a rigid rotor in external fields and its irreducible representations is mandatory in order to properly identify the field-dressed states.

The number of representations and their features are determined by the symmetry group of the Hamiltonian in a field configuration [65]. First, we start with the description of the symmetries for asymmetric top molecules. Note that the symmetries of a linear rotor are a particular case of the symmetries of an asymmetric top.

The field-free asymmetric rotor belongs to the group of spatial rotations $SO(3)$, which ensures that J and M are good quantum numbers, and the point group D_2 , whose operations

Operation	Transformations		
	ϕ	θ	χ
E	$\phi \rightarrow \phi$	$\theta \rightarrow \theta$	$\chi \rightarrow \chi$
C_2^z	$\phi \rightarrow \phi$	$\theta \rightarrow \theta$	$\chi \rightarrow \chi - \pi$
C_2^y	$\phi \rightarrow \phi - \pi$	$\theta \rightarrow \pi - \theta$	$\chi \rightarrow \pi - \chi$
C_2^x	$\phi \rightarrow \phi - \pi$	$\theta \rightarrow \pi - \theta$	$\chi \rightarrow -\chi$

Table 3.1: Action of the symmetry operations of the D_2 group on the Euler angles.

are the identity E and the twofold rotations around the x, y and z axes of the MFF, C_2^x, C_2^y and C_2^z , respectively. The action of the symmetry operations on the Euler angles are collected in Table 3.1. We can construct the Wang states, which form a basis of a given representation of D_2 , as the following linear combinations [59]

$$|JKMs\rangle = \frac{1}{\sqrt{2}} \left(|JKM\rangle + (-1)^s |JK - M\rangle \right) \quad \text{if } K \neq 0, \quad (3.22)$$

$$|J0M0\rangle = |J0M\rangle \quad \text{if } K = 0, \quad (3.23)$$

with $s = 0, 1$. Using the properties of the Wigner matrix elements in Appendix B, we find that [59]

$$\begin{aligned} C_2^z |JKMs\rangle &= (-1)^K |JKMs\rangle, \\ C_2^y |JKMs\rangle &= (-1)^{J+K+s} |JKMs\rangle, \\ C_2^x |JKMs\rangle &= (-1)^{J+s} |JKMs\rangle, \end{aligned}$$

where the prefactor characterizes each irreducible representation.

If we include a static electric field, \vec{E}_S , and consider a molecule with $\vec{\mu}$ parallel to its z axis, the symmetry group is formed by $\{E, C^{Es}(\delta), C_2^z\}$, where $C^{Es}(\delta)$ are the arbitrary rotations around \vec{E}_S . If \vec{E}_S is parallel to the Z axis, then the arbitrary rotations around \vec{E}_S , $C^Z(\delta)$, ensure that M is a good quantum number. Note that the reflection on any plane which contains \vec{E}_S are symmetry operations, as well. The action of the symmetry operators in the Euler angles is collected in Table 3.2. Since C_2^z is still a symmetry operation, the parity of K is conserved. If $M \neq 0$, there are 4 representations for each $|M|$, depending on the parity of K and the sign of M . The existence of infinite planes of symmetry implies that, for the same $|M| \neq 0$, the states in the irreducible representations are doubly degenerated. However, if $M = 0$ there are 4 irreducible representations which are not degenerated, and their basis sets are characterized by the parity of K and $K + s$.

In the presence of only a linearly polarized laser field along the Z axis, the symmetry operations which form the group are those from D_2 , $C^Z(\delta)$ and the inversion I . This leads to 8 irreducible representations for each value of M , defined by the parity under the twofold rotations in the MFF and the inversion operation. If $|M| \neq 0$, the states are degenerate as in the case of a static electric field.

If we apply an additional static field tilted an angle $\beta \neq 0, \pi/2$ with the polarization axis of the laser, the symmetry group is reduced to $\{E, C_2^z, \sigma_{XZ}\}$, where σ_{XZ} is the reflection on the

Operation	Transformations		
	ϕ	θ	χ
$C^Z(\delta)$	$\phi \rightarrow \phi + \delta$	$\theta \rightarrow \theta$	$\chi \rightarrow \chi$
C_2^X	$\phi \rightarrow 2\pi - \phi$	$\theta \rightarrow \pi - \theta$	$\chi \rightarrow \chi + \pi$
σ_{XZ}	$\phi \rightarrow 2\pi - \phi$	$\theta \rightarrow \theta$	$\chi \rightarrow 2\pi - \chi$
C_2^Z	$\phi \rightarrow \phi + \pi$	$\theta \rightarrow \theta$	$\chi \rightarrow \chi$

Table 3.2: Action of the symmetry operations in tilted fields in the Euler angles

plane which contains the fields, that is, the XZ plane. In Table 3.2 we provide the application of σ_{XZ} on the Euler angles. In this case, there are four irreducible representations, depending on the parity under the rotations around the z -axis of the MFF and the parity under the reflection on the plane containing the fields. We can construct the generalized Wang states, $|JKMq\rangle^\sigma$ as follows

$$\begin{aligned} |JKMq\rangle^\sigma &= \frac{1}{\sqrt{2}} \left(|JKM\rangle + (-1)^q |J-K-M\rangle \right) \quad \text{for } M \text{ and/or } K \neq 0, \\ |J000\rangle^\sigma &= |J00\rangle \quad \text{otherwise,} \end{aligned} \quad (3.24)$$

with $q = 0, 1$. Applying σ_{XZ} and using the properties of the Wigner matrix elements (see Appendix B), it yields

$$\sigma_{XZ} |JKMq\rangle^\sigma = (-1)^{M+K+q} |JKMq\rangle^\sigma.$$

Hence, the generalized Wang states with the same parity of $M + K + q$ and K form the basis of one of these irreducible representations.

Now, if $\beta = \pi/2$, the Hamiltonian is invariant under the operations $\{E, C_2^z, \sigma_{XZ}, C_2^X\}$, being C_2^X a twofold rotation around the X axis. The action of C_2^X on the functions $|JKM\rangle$ is

$$C_2^X |JKM\rangle = (-1)^J |JK-M\rangle.$$

Analogously to the case of the operator σ_{XZ} , we can construct the eigenstates of C_2^X , $|JKMp\rangle^X$, as

$$\begin{aligned} |JKMp\rangle^X &= \frac{1}{\sqrt{2}} \left(|JKM\rangle + (-1)^p |JK-M\rangle \right) \quad \text{for } M \neq 0, \\ |JK00\rangle^X &= |JK0\rangle \quad \text{otherwise,} \end{aligned} \quad (3.25)$$

with $p = 0, 1$. These states fulfill

$$C_2^X |JKMp\rangle^X = (-1)^{J+p} |JKMp\rangle^X.$$

In this perpendicular configuration, the wavefunctions have to be simultaneously eigenstates of σ_{XZ} and C_2^X . Imposing the conditions (3.24) and (3.25) we define the states $|JKMqp\rangle_{\pi/2}$,

that are written in terms of $|JKM\rangle$ as

$$\begin{aligned}
|JKMqp\rangle_{\pi/2} &= \frac{1}{2} \left(|JKM\rangle + (-1)^q |J-K-M\rangle + (-1)^p |JK-M\rangle + \right. \\
&\quad \left. + (-1)^{q+p} |J-KM\rangle \right) \quad \text{if } M \text{ and } K \neq 0, \\
|J0M0p\rangle_{\pi/2} &= \frac{1}{\sqrt{2}} \left(|J0M\rangle + (-1)^p |J0-M\rangle \right) \quad \text{if } M \neq 0, \\
|JK0q0\rangle_{\pi/2} &= \frac{1}{\sqrt{2}} \left(|JK\rangle + (-1)^q |J-K0\rangle \right) \quad \text{if } K \neq 0, \\
|J0000\rangle_{\pi/2} &= |J00\rangle \quad \text{otherwise,}
\end{aligned} \tag{3.26}$$

and they satisfy

$$\begin{aligned}
\sigma_{XZ} |JKMqp\rangle^\sigma &= (-1)^{M+K+q} |JKMqp\rangle^\sigma, \\
C_2^X |JKMqp\rangle_{\pi/2} &= (-1)^{J+p} |JKMqp\rangle_{\pi/2}.
\end{aligned}$$

From these expressions, we see that there are 8 irreducible representations for this field configuration, which are labeled by the parity under the operators C_2^z , σ_{XZ} and C_2^X , given by $(-1)^K$, $(-1)^{M+K+q}$ and $(-1)^{J+p}$, respectively.

In the case of an elliptically polarized laser field along the Z and X directions, the minimal set of symmetry operations is $\{E, C_2^x, C_2^y, C_2^z, I, C_2^Z\}$. Compared to the linearly polarized case, we have lost the symmetry under arbitrary rotations around the Z axis, and therefore, M is not a good quantum number. However, C_2^Z ensures that the parity of M is still conserved. Including a static electric field parallel to the Z axis, the symmetry operations are reduced to $\{E, \sigma_{XZ}, C_2^z, C_2^Z\}$. Thus, there are 8 non degenerate irreducible representations labeled by the parity under σ_{XZ} , C_2^z and C_2^Z . The basis set elements are the states $|JKMq\rangle^\sigma$, with the same parity of K and M . The case of $\beta = \pi/2$, that is, \vec{E}_s parallel to the X -axis, is analogous to this one, but the symmetry operations are $\{E, \sigma_{XZ}, C_2^z, C_2^X\}$. There are 8 non degenerate irreducible representations, and the basis is formed by the states $|JKMqp\rangle_{\pi/2}$ with the same parity of K , $M + K + q$ and $J + p$. For the field configuration with $0 < \beta < \pi/2$, the group of symmetry operation is $\{E, C_2^z, \sigma_{XZ}\}$, which is the same as in the linearly polarized laser field case.

In this thesis we have also studied molecules with $\vec{\mu}$ contained in the plane xz . In this case, C_2^z is not a symmetry operation and the parity of K is not conserved. The symmetry groups described above for a molecule with $\vec{\mu}$ parallel to the MFF z -axis are the same for this system, except that C_2^z is not any longer a symmetry operator. As a consequence, for a certain field configuration, the number of irreducible representations is reduced by one half compared to the analogous case for $\vec{\mu} = \mu_z \hat{z}$.

For the linear rotor, the symmetry operations are reduced to those in the LFF. In the case of only a static field with $\beta = 0$, the symmetry group is formed by $\{E, C^Z(\delta)\}$. There are two irreducible representations for a given $|M|$, which are degenerated if $|M| \neq 0$. If we have an additional linearly polarized laser field and $\beta \neq 0$ the symmetry group is $\{E, \sigma^{XZ}\}$, leading to two irreducible representations. Since K is not defined for a linear rotor, the basis set

elements are special cases of the expression (3.24), but in terms of the spherical harmonics

$$\begin{aligned} Y_{JMq}^\sigma(\Omega) &= \frac{1}{\sqrt{2}} \left(Y_{JM}(\Omega) + (-1)^q Y_{JM}(\Omega) \right) \quad \text{for } M \neq 0, \\ Y_{J00}^\sigma(\Omega) &= Y_{J0}(\Omega) \quad \text{otherwise,} \end{aligned} \quad (3.27)$$

with $q = 0, 1$. The action of σ_{XZ} on these functions is

$$\sigma_{XZ} Y_{JMq}^\sigma(\Omega) = (-1)^{M+q} Y_{JMq}^\sigma(\Omega).$$

For perpendicular fields, the symmetry group is formed by $\{E, \sigma^{XZ}, C_2^X\}$, thus, there are 4 representations. The states $Y_{JMq}^\sigma(\Omega)$ are eigenfunctions of C_2^X , since

$$C_2^X Y_{JMq}^\sigma(\Omega) = (-1)^{J+q} Y_{JMq}^\sigma(\Omega).$$

As we have seen, the states of a certain irreducible representation have the same behaviour under the action of the symmetry operations. As a consequence, the Hamiltonian is not able to couple states belonging to different irreducible representations, allowing us to treat them independently. This is a great advantage, since the size of the basis set used to solve both the time-dependent and time-independent Schrödinger equation can be reduced, and with it, the number of operations and the storage, and the computational efficiency is enhanced.

Chapter 4

Numerical methods

4.1 The time-independent Schrödinger equation

In this section we present a method to solve the time-independent Schrödinger equation $H|\psi_n\rangle = E_n|\psi_n\rangle$, where H is the Hamiltonian, E_n and $|\psi_n\rangle$ are an eigenvalue and an eigenfunction, respectively. To do so, we expand the wavefunction in terms of the functions of a certain basis set. Then, the time-independent Schrödinger equation, which is a second order differential equation in several variables, is transformed in a matrix eigenvalue problem.

4.1.1 The Linear Variational Method

The *Ritz variational method* or *linear variational principle* [66, 67] allows us to search for upper bounds of the eigenvalues E_n . If we consider the basis $\{\phi_k\}_{k=1}^{\infty}$, the wavefunction is given by the following expansion

$$|\psi\rangle = \sum_{i=1}^N c_i |\phi_i\rangle, \quad (4.1)$$

where N is the number of elements of the basis set and c_i is the coefficient of $|\phi_i\rangle$. For computational reasons, we have cut the infinite series to a finite one including N elements of the basis.

The upper bounds of E_n are obtained by minimizing the expectation value of the Hamiltonian, $\langle\psi|H|\psi\rangle$. We impose that $\langle\psi|\psi\rangle = 1$ and use the Lagrange multiplier in the expression

$$\langle\psi|H|\psi\rangle - \lambda \langle\psi|\psi\rangle = 0, \quad (4.2)$$

where λ is a real constant. Using the expansion of the wavefunction, it yields

$$\sum_{i,j=1}^N c_i^* c_j \langle\phi_i|H|\phi_j\rangle - \lambda \sum_{i=1}^N |c_i|^2 = 0. \quad (4.3)$$

Let us assume that $c_i = c_i^*$. Taking derivatives with respect to c_i in this expression, we obtain

$$\sum_{j=1}^N c_j \langle\phi_i|H|\phi_j\rangle = \lambda c_i, \quad (4.4)$$

which is a matrix eigenvalue problem, and λ are upper bounds of E_n . By increasing the basis set size, we ensure that our numerical results are converged and independent of N .

4.1.2 Numerical diagonalization of the Hamiltonian matrix

To diagonalize the Hamiltonian matrix, we employ the restarted Lanczos procedure [68] implemented in the Arnoldi Package (ARPACK) [69, 70]. The convergence of this method is faster for the highest eigenvalues of the corresponding matrix [71]. To take advantage of this feature, we diagonalize $(H - \lambda' \mathbb{1})^{-1}$ where λ' is a real number and $\mathbb{1}$ is the identity matrix. Then, by properly choosing the value of λ' , we focus on an energy window of the Hamiltonian. This parameter λ' is changed several times, so that the range of energy in which we are interested is fully covered.

4.2 The time-dependent Schrödinger equation

For the time-dependent Schrödinger equation,

$$i\hbar \frac{\partial}{\partial t} |\psi(t)\rangle = H(t) |\psi(t)\rangle, \quad (4.5)$$

a solution is given by

$$|\psi(t + \Delta t)\rangle = U(\Delta t) |\psi(t)\rangle = \exp\left(-\frac{i}{\hbar} \int_t^{t+\Delta t} H(t') dt'\right) |\psi(t)\rangle, \quad (4.6)$$

where Δt is a small time step. For sufficiently small Δt , we can assume that the Hamiltonian is almost constant in this time interval $(t, t + \Delta t)$. Under this approximation, the solution reads

$$|\psi(t + \Delta t)\rangle = \exp\left(\frac{-i}{\hbar} H(t) \Delta t\right) |\psi(t)\rangle.$$

Several computational techniques have been developed to tackle the calculation of the action of the propagator in the wavefunction. They differ in the numerical method used to approximate the evolution operator. In this thesis, for linear molecules, we use the *Split-operator procedure* [72] and the *short iterative Lanczos* propagation method [73, 74] for the more complicated asymmetric top molecules. The basis set size and the number of time steps are increased until convergence is achieved.

4.2.1 Short Iterative Lanczos propagation method

The time-dependent Schrödinger equation (4.5) can be solved by expanding the wavefunction in a basis set as in subsection 4.1.1, but now allowing the coefficients to depend on time, $c_i = c_i(t)$,

$$|\Psi(t)\rangle = \sum_{i=1}^N c_i(t) |\phi_i\rangle. \quad (4.7)$$

Introducing this expression in equation (4.5) and left projecting on the basis elements, we find that the solution is given by the following system of first order differential equations

$$i\hbar \frac{\partial \vec{c}(t)}{\partial t} = \tilde{H}(t) \vec{c}(t), \quad (4.8)$$

where $\vec{c}(t)$ is the vector is formed by the coefficients $\{c_i(t)\}_{i=1}^N$, and the Hamiltonian matrix restricted to the basis set is $\tilde{H}_{i,j}(t) = \langle \phi_i | H(t) | \phi_j \rangle$. An approximation to the solution is

$$\vec{c}(t + \Delta t) = \exp\left(-\frac{i}{\hbar}\tilde{H}(t)\Delta t\right)\vec{c}(t). \quad (4.9)$$

where again we have taken small enough Δt so that $\tilde{H}(t)$ could be considered constant in the corresponding time interval. The next step consist on replacing the exponential by

$$\vec{c}(t + \Delta t) \approx \sum_{j=0}^{p-1} \frac{1}{j!} \left(\frac{-i\Delta t}{\hbar}\right)^j \tilde{H}^j \vec{c}(t). \quad (4.10)$$

where the infinite sum is cut and only the first p terms have been included. In this expansion, the contribution of the j -th term decreases as j is increased. For large values of N and p , obtaining $\vec{c}(t + \Delta t)$ requires a high computational effort, due to the large number of matrix-matrix and matrix-vector multiplications needed. The *short iteraterative Lanczos ethod* (SIL) solves this problem by reducing significantly the number of operations in this procedure. The Lanczos method consists on building systematically a basis of p orthogonal N dimensional vectors $\{\vec{a}_j\}_{j=0}^{p-1}$ in which the Hamiltonian \tilde{H} becomes a tridiagonal matrix. This basis generates a Krylov subspace, defined by the set of linearly independent vectors $\{\tilde{H}^j \vec{a}_0\}_{j=0}^{p-1}$. To ensure that these vectors are linearly independent, \vec{a}_0 must be a linear combination of at least p exact eigenfunctions of \tilde{H} . The procedure to obtain \vec{a}_j , with $j = 0, \dots, p-1$ is as follows [71]

$$\tilde{H}\vec{a}_0 = \alpha_0\vec{a}_0 + \beta_0\vec{a}_1 \quad (4.11)$$

$$\tilde{H}\vec{a}_j = \beta_{j-1}\vec{a}_{j-1} + \alpha_j\vec{a}_j + \beta_j\vec{a}_{j+1}, \quad (j > 0) \quad (4.12)$$

where

$$\alpha_j \equiv \vec{a}_j^\dagger \tilde{H} \vec{a}_j, \quad (4.13)$$

$$\beta_j \equiv \vec{a}_{j-1}^\dagger \tilde{H} \vec{a}_j. \quad (4.14)$$

The matrix $A_{N \times p}$ transforms the basis $\{\phi_j\}_{j=1}^N$ to $\{\vec{a}_k\}_{k=0}^{p-1}$ and it is built with the p first vectors of the Krylov space given by [75]

$$A_{N \times p} \equiv [\vec{a}_0 \vec{a}_1 \vec{a}_2 \dots \vec{a}_{p-1}], \quad (4.15)$$

and H_p reads

$$H_p \equiv \begin{pmatrix} \alpha_0 & \beta_0 & 0 & \dots & 0 & 0 \\ \beta_0 & \alpha_1 & \beta_1 & \dots & 0 & 0 \\ 0 & \beta_1 & \alpha_2 & \dots & 0 & 0 \\ \vdots & \vdots & \vdots & \ddots & \vdots & \vdots \\ 0 & 0 & 0 & \dots & \alpha_{p-2} & \beta_{p-2} \\ 0 & 0 & 0 & \dots & \beta_{p-2} & \alpha_{p-1} \end{pmatrix}. \quad (4.16)$$

Then, the time-dependent Schrödinger equation in the basis $\{\vec{a}_k\}_{k=0}^{p-1}$ is equivalent to

$$\frac{\partial \vec{d}(t)}{\partial t} = -\frac{i}{\hbar} H_p \vec{d}(t), \quad (4.17)$$

where $\vec{d}(t)$ is the vector form by the p coefficients of $\{\vec{a}_k\}_{k=0}^{p-1}$. As a initial condition, we choose $\psi(t = t_0)$ to be \vec{a}_0 , where t_0 is the initial time, then it holds

$$\vec{d}(0) = \begin{pmatrix} 1 \\ 0 \\ 0 \\ \vdots \end{pmatrix}.$$

An approximated solution of equation (4.17) for small Δt is

$$\vec{d}(t + \Delta t) = \exp\left(-\frac{i}{\hbar} H_p \Delta t\right) \vec{d}(t), \quad (4.18)$$

which is solved by diagonalizing the tridiagonal matrix H_p . Finally, we write $\vec{d}(t)$ in the basis $\{|\phi_k\rangle\}$. Since this method involves a truncated basis, we can control the error at each time step by imposing that the component of the last reduced vector \vec{a}_{p-1} to satisfy [75]

$$|d_{p-1}(t)|^2 \leq \epsilon. \quad (4.19)$$

To ensure the convergence of our calculations we have fixed $\epsilon \leq 10^{-10}$. This time integration has been performed by using the subroutine `silstep.f` of the *Multiconfiguration Time-Dependent Hartree method* implemented in MCTDH package [74].

4.2.2 Split-operator procedure

The split-operator procedure scheme consists on approximating the propagator in expression (4.6) by [72, 73]

$$\begin{aligned} U(\Delta t) &= \exp\left(-\frac{i}{2\hbar} H_{int} \Delta t\right) \times \exp\left(-\frac{i}{\hbar} H_r \Delta t\right) \times \exp\left(-\frac{i}{2\hbar} H_{int} \Delta t\right) \\ &+ O[(\Delta t)^3]. \end{aligned} \quad (4.20)$$

where $H = H_r + H_{int}$, H_r and H_{int} are the rotational and interaction terms of the Hamiltonian, respectively. The main advantage of this method is that the operators $\exp\left(-\frac{i}{2\hbar} H_{int} \Delta t\right)$ and $\exp\left(-\frac{i}{\hbar} H_r \Delta t\right)$ are treated independently. In the next section we describe a tool to evaluate the time propagator based on the *Finite Basis Representation* (FBR) and the *Discrete Variable Representation* (DVR).

Discrete Variable Representation

We consider a finite basis set on \mathbb{R} , $\{\phi_n(r)\}$, which is complete square integrable, being $\phi'_n(r)$ and $r\phi_n(r)$ square integrable, as well. The *Finite Basis Representation* (FBR) consists on representing a wavefunction by its projection on the basis functions $\{\phi_n(r)\}$. We assume that $\{\phi_n(r)\}$ satisfies the Gaussian quadrature

$$\int_{\mathcal{I}} \omega(r)f(r)dr = \sum_{\alpha=0}^{N-1} \omega_{\alpha}f(r_{\alpha}), \quad (4.21)$$

where $f(r)$ is a polynomial of degree lower or equal to $2N - 1$, $\omega(r)$ is the weight function corresponding to this family of orthogonal polynomials $\{\phi_n(r)\}$ on the interval \mathcal{I} and ω_{α} are the weights at the grid points r_{α} . Then, the following expressions are exact

$$\langle \phi_j | \phi_k \rangle = \sum_{\alpha=0}^{N-1} \omega_{\alpha} \phi_j(r_{\alpha})^* \phi_k(r_{\alpha}) = \delta_{jk}, \quad (4.22)$$

$$\langle \phi_j | r | \phi_k \rangle = \sum_{\alpha=0}^{N-1} \omega_{\alpha} r \phi_j(r_{\alpha})^* \phi_k(r_{\alpha}) = \widehat{X}_{jk}^{FBR}, \quad (4.23)$$

with \widehat{X}_{jk}^{FBR} being the position operator matrix. Diagonalizing the position matrix \widehat{X} , we obtain

$$\left(\mathbf{U}^{\dagger} \widehat{X} \mathbf{U} \right)_{\alpha\beta} = r_{\alpha} \delta_{\alpha\beta}, \quad (4.24)$$

with \mathbf{U} being a unitary matrix, which satisfies

$$\chi_{\alpha}(r) = \sum_{n=0}^{N-1} \phi_n(r) \mathbf{U}_{n,\alpha}. \quad (4.25)$$

These functions $\chi_{\alpha}(r)$ are the eigenvectors of \widehat{X} and form a basis, and fulfill that $\langle \chi_{\alpha} | \chi_{\beta} \rangle = \delta_{\alpha\beta}$ and $\langle \chi_{\alpha} | r | \chi_{\beta} \rangle = r_{\alpha} \delta_{\alpha\beta}$. \mathbf{U} allows us to transform to the Discrete Variable Representations, DVR, in which the wavefunction is represented by its value in the set of grid points $\{r_{\alpha}\}$.

r_{α} are the grid points of the quadrature and it can be proved that $\omega_{\alpha}^{1/2} = \frac{\mathbf{U}_{k\alpha}^*}{\phi_k(r_{\alpha})}$ for any k [72, 76]. By using (4.24) we obtain that the potential expressed in the DVR, V^{DVR} , is diagonal

$$V_{\alpha\beta}^{DVR} = V(r_{\alpha}) \delta_{\alpha\beta}. \quad (4.26)$$

This is a great advantage, because we can easily deal with the exponential of the interaction term in the propagator (4.20). The coefficients of the wavefunction $\psi(r)$ in the DVR reads $\langle \chi_{\alpha} | \psi \rangle = \omega_{\alpha}^{1/2} \psi(r_{\alpha})$ for $\alpha = 0, \dots, N - 1$. Hence, the wavefunction can be written in the DVR as

$$\psi^{DVR} = (\sqrt{\omega_0} \psi(r_0, t), \dots, \sqrt{\omega_{N-1}} \psi(r_{N-1}, t)). \quad (4.27)$$

Whereas, in the FBR, the wavefunction $\psi(r)$ is represented by its coefficients in the basis

$$\psi^{FBR} = (c_0, \dots, c_{N-1}). \quad (4.28)$$

As we said above, both representations are related by the unitary transformation \mathbb{U} , i. e., it holds

$$\psi^{FBR} = \mathbb{U}\psi^{DVR},$$

that is,

$$c_j = \sum_{k=0}^{N-1} \mathbb{U}_{j,k} \sqrt{\omega_k} \psi(r_k),$$

and similarly,

$$\psi^{DVR} = \mathbb{U}^\dagger \psi^{FBR},$$

which is equivalent to

$$\sqrt{\omega_k} \psi(r_k) = \sum_{j=0}^{N-1} \mathbb{U}_{j,k}^\dagger c_j.$$

For a linear rotor in external fields, we use the Legendre polynomials to treat the angular variable θ . The FBR of the wavefunction in terms of the Legendre polynomials $P_j(\cos\theta)$ reads

$$\psi(\theta, t) = \sum_{j=0}^{N-1} c_j(t) P_j(\cos\theta). \quad (4.29)$$

According to the definition (4.25), the unitary transformation from DVR to FBR is

$$\mathbb{U}_{j,k} = \sqrt{\omega_k} P_j(\cos\theta_k), \quad (4.30)$$

where θ_k are the nodes of the $P_N(\cos\theta)$ polynomial and ω_k are the weights of the associated Gaussian quadrature. In the DVR, the matrix representation of the interaction is diagonal, and, consequently, its exponential. However, the matrix elements of the field-free Hamiltonian, $B\vec{J}^2$, are not diagonal and are more complicated to obtain. To do so, we use the unitary transformation between the DVR and the FBR, we compute it in the FBR and then transform it back. The procedure is as follows

$$\begin{aligned} \left\{ \exp(-iB\vec{J}^2\Delta t) \psi \right\}^{DVR} &= \mathbb{U}^\dagger \left\{ \exp(-iB\vec{J}^2\Delta t) \right\}^{FBR} \psi^{FBR} \\ &= \mathbb{U}^\dagger \left(\left\{ \exp(-iBj(j+1)\Delta t) c_j \right\}_{j=0}^{N-1} \right). \end{aligned}$$

For a given grid point θ_k , we expand the matrix \mathbb{U} on the right hand side

$$\exp(-iB\vec{J}^2\Delta t) \sqrt{\omega_k} \psi(\theta_k, t) = \sum_{j=0}^{N-1} \mathbb{U}_{j,k}^\dagger \exp(-iBj(j+1)\Delta t) c_j = \sum_{k'=0}^{N-1} \mathbb{T}_{k,k'} \psi(\theta_{k'}, t),$$

where

$$\mathbb{T}_{k,k'} = \sum_{j=0}^{N-1} \mathbb{U}_{j,k}^\dagger \exp[-iBj(j+1)\Delta t] \mathbb{U}_{j,k'}.$$

In general, the field-dressed Hamiltonian does not show cylindrical symmetry and also depends on ϕ [74]. In this case, we can not use a DVR based in a Gaussian quadrature.

Instead, we choose the exponential DVR based on the functions $\exp(i\phi)$. The grid points ϕ_k are taken equidistant between 0 and 2π , and their weight is $\frac{2\pi}{2N+1}$. Note that we have chosen $2N+1$ grid points in ϕ , to have the same accuracy as in the θ coordinate.

The transformation between the grid points (θ_l, ϕ_k) and the finite basis set $\{Y_{jm}(\theta, \phi)\}$ is given by

$$\mathbb{U}_{jmlk} = \sqrt{\frac{2\pi\omega_l}{2N+1}} Y_{jm}^*(\theta_l, \phi_k).$$

This leads to

$$\exp[-iB\vec{J}^2]^{DVR} \sqrt{\omega_l} \sqrt{\frac{2\pi}{2N+1}} \psi(\theta_l, \phi_k, t) = \sum_{l'=0}^{N-1} \sum_{k'=0}^{2N} \mathbb{T}_{l,k,l',k'} \sqrt{\omega_{l'}} \sqrt{\frac{2\pi}{2N+1}} \psi(\theta_{l'}, \phi_{k'}, t),$$

where

$$\mathbb{T}_{l,k,l',k'} = \sum_{j=0}^{N-1} \sum_{m=-j}^j \mathbb{U}_{j,m,l,k}^\dagger \exp[-iBj(j+1)\Delta t] \mathbb{U}_{j,m,l',k'}.$$

4.3 Projection of the wavefunction on the screen

In the experimental setup, the molecular beam composed of several rotational states is traveling towards the detector. These molecules are exposed to a combination of a nonresonant linearly polarized YAG laser field and a static electric field in its direction of motion so that they are oriented or aligned depending on the field configuration. In the experiment, they measure the alignment or orientation by provoking a Coulomb explosion of the molecule with a probe laser pulse. When the Coulomb explosion takes place, one of the molecular radicals is cut off acquiring an additional velocity component in the direction of the electric dipole moment [20, 51–53]. Note that we are assuming the axial recoil approximation. Therefore, depending on the orientation of the molecule in the moment of the Coulomb explosion, the ionic-fragment is detected on the screen at a certain point. These molecular ions are collected and detected in a CCD camera, and these images provide a 2D projection of the 3D field-dressed wavefunction. To reproduce these results, for each populated rotational state, we compute the 3D wavefunction using the experimental field configuration, and make the 2D projection of this wavefunction. In addition, our theoretical description should also include the alignment selectiveness of the probe laser (depending on its polarization), and the distribution of the ion recoil velocities. We take into account that the measurements are influenced by a volume effect due to the spatial shape of both, the YAG and probe laser. We do not consider that the efficiency of the Coulomb explosion could depend nonlinearly on the intensity of the probe pulse.

In this section, we describe how to obtain theoretically these 2D experimental images, i. e., the projections onto the detector screen of the three dimensional molecular wavefunction.

The experiment defines a new reference frame, the screen fixed frame (x_s, y_s, z_s) , its $y_s z_s$ -plane contains the detector screen where the ions are collected, and the electrostatic field is parallel to its x_s -axis. The direction of the linear polarization of YAG laser is contained on the $x_s z_s$ -plane and forms an angle β with the x_s -axis. This new frame is obtained by rotating the LFF an angle $\alpha = \pi/2 - \beta$ around the Y -axis.

We consider that the molecule is in certain state characterized by its wavefunction $\Psi_\gamma(\theta, \phi, \chi)$. Then, the probability for the molecule to have the orientation (θ, ϕ, χ) with respect to the LFF is given by the probability density distribution $|\Psi_\gamma(\theta, \phi, \chi)|^2 \sin \theta d\theta d\phi d\chi$. Since the direction of the molecular dipole moment is independent on the angle χ , the probability for the molecular z -axis to be oriented according to (θ, ϕ) is given by the following integral

$$\rho_\gamma(\theta, \phi) = \int_0^{2\pi} |\Psi_\gamma(\theta, \phi, \chi)|^2 d\chi. \quad (4.31)$$

The angular distribution $\rho_\gamma(\theta, \phi)d\Omega$ provides an estimation of the amount of ions ejected into the solid angle $d\Omega = \sin \theta d\theta d\phi$. It is related to a spatial distribution on the 2D screen by $\bar{\rho}_\gamma(y, z)dydz = \rho_\gamma(\theta(y, z), \phi(y, z))|\mathcal{J}| \sin(\theta(y, z)) dy dz$, with \mathcal{J} being the Jacobian of the transformation between the coordinates (θ, ϕ) and (y, z) . This transformation is

$$\begin{aligned} y_s &= a \sin \theta \sin \phi \\ z_s &= a(\cos \theta \sin \beta + \sin \theta \cos \phi \cos \beta), \end{aligned} \quad (4.32)$$

where $a = vt_f$, and t_f is the flight time needed by the ion to reach the screen. Note that with the definition (4.32) for the y_s -coordinate, any point (y_s, z_s) on the screen corresponds to two different orientations (θ, ϕ) and $(\theta, \pi - \phi)$. A unique (invertible) transformation is obtained by restricting ϕ to the interval $[-\pi/2, \pi/2]$. Thus, the total probability on the screen is the sum of the probabilities computed with eq. (4.32), and an analogous transformation where ϕ is changed by $\pi - \phi$. The Jacobian is

$$\left| \frac{\partial(\theta, \phi)}{\partial(y, z)} \right| = \frac{1}{a \sin \theta \sqrt{a^2 - y_s^2 - z_s^2}}. \quad (4.33)$$

Thus, it yields

$$\bar{\rho}_\gamma(y, z) = \frac{\rho_\gamma(\theta(y, z), \phi(y, z))}{a \sqrt{a^2 - y_s^2 - z_s^2}} \quad (4.34)$$

for the 2D screen spatial distribution. This expression is limited to the disk $y_s^2 + z_s^2 \leq a^2$, and diverges on the margin $y_s^2 + z_s^2 = a^2$.

The next factor to include in our description is the detection selectivity of the probe laser, which depends on the polarization of this field. When the probe laser is linearly polarized perpendicular to the screen, i.e., parallel to the x_s -axis and to the static electric field, the detection efficiency is proportional to $\cos^2 \alpha_l$ where α_l is the angle between the molecular z -axis and the polarization of the probe beam [77]. Note that for a multiphoton ionization the factor is $\cos^{n+1} \alpha_l$, we are considering that the process is dominated by a single ionization with $n = 1$. Using the relation $\cos^2 \alpha_l = 1 - y_s^2/a^2 - z_s^2/a^2$, we arrive at the following expression for the distribution of the ions on the 2D screen:

$$\bar{\rho}_\gamma^l(y_s, z_s) = \rho_\gamma(\theta(y_s, z_s), \phi(y_s, z_s)) \frac{\sqrt{1 - y_s^2/a^2 - z_s^2/a^2}}{a^2}. \quad (4.35)$$

For a probe laser linearly polarized parallel to the z_s -axis, i.e., on the vertical of the screen, the detection efficiency is proportional to $\cos^2 \alpha_m$ where α_m is the angle between the molecular

z -axis and the z_s -axis, and it yields

$$\overline{\rho^p}_\gamma(y, z) = \rho_\gamma(\theta(y_s, z_s), \phi(y_s, z_s)) \frac{z_s^2/a^2}{a^2 \sqrt{1 - y_s^2/a^2 - z_s^2/a^2}}. \quad (4.36)$$

For a circularly polarized probe pulse, the detection efficiency factor is proportional to $\cos^2 \alpha_c$, with α_c being the angle between the molecular z -axis and the $x_s z_s$ -plane containing the probe laser polarization. For tilted fields ($\beta \neq \pi/2$), such a circular polarization ensures that any molecule will be ionized and detected with the same probability independently of β . Using that $\cos^2 \alpha_c = 1 - y_s^2/a^2$, it yields for the 2D-screen probability density

$$\overline{\rho^c}_\gamma(y_s, z_s) = \rho_\gamma(\theta(y_s, z_s), \phi(y_s, z_s)) \frac{1 - y_s^2/a^2}{a^2 \sqrt{1 - y_s^2/a^2 - z_s^2/a^2}}. \quad (4.37)$$

The singularity that arises from the Jacobian determinant has not been canceled, and $\overline{\rho^c}_\gamma(y_s, z_s)$ and $\overline{\rho^p}_\gamma(y_s, z_s)$ are divergent at the margin $y_s^2 + z_s^2 = a^2$. This singularity is only removed when the ion velocity distribution is implemented.

These expressions (4.35), (4.36), and (4.37) are valid for the corresponding polarizations of the probe laser, even if the YAG pulse and a static electric field are not present.

So far we have assumed that all ions acquire the same recoil velocity in the dissociation process. Experimentally, however, they follow a certain distribution $D(a)$, which has only nonzero values at positive velocities. The screen image is obtained by averaging over all these velocities with their corresponding weights as

$$P_\gamma(y_s, z_s) = \int_0^\infty \overline{\rho}_\gamma(y_s, z_s; a) D(a) da.$$

In $\overline{\rho}_\gamma(y_s, z_s; a)$, see eq. (4.35)-(4.37), we have made explicit its dependence on ion-velocity, which is the same for the all molecules. For clarity, we have dropped the polarization index l, p and c in $\overline{\rho}_\gamma(y_s, z_s; a)$. As an example, the experimental velocity distribution $D(a)$ for the ejected ions CN^+ in the Coulomb explosion of benzonitrile is shown in Fig. 4.1. The second and third peak are associated with the two ionization channels of the CN -radical, whereas the first one is caused by other ions not related with the orientation of the molecule. Thus, we are not taking into account this peak, and a combination of two Gaussian functions has been fitted the second and third ones removing the background, see Fig. 4.1. Note that neglecting the contribution of this first peak will be a source of discrepancy with the experiment [77]. Since a is not the velocity itself but just a distance proportional to the velocity, we have rescaled the abscissa such that the maximum of $D(a)$ is at $a = 1$.

Numerically, it is very costly to compute $\overline{\rho}_\gamma(y_s, z_s; a) P^{\text{lin/circ}}(y_s, z_s; a)$ for every value of a appearing in this integral. Since a is a scaling factor, which causes a stretching of the screen image, the integration in eq. (4.38) can be simplified by: i) calculating $\overline{\rho}_\gamma(y, z; a = 1)$ on a certain grid and reusing it; ii) using polar coordinates in the 2D-screen, i.e., $r = \sqrt{y^2 + z^2}$ and $\theta_{2D} = \arctan(z/y)$; and iii) performing the integral with the change of variables $u = r/a$. Following these steps, we can write that

$$P_\gamma(y, z) = \int_0^\infty \frac{1}{r} \overline{\rho}_\gamma(u, \theta_{2D}) D(r/u) du. \quad (4.38)$$

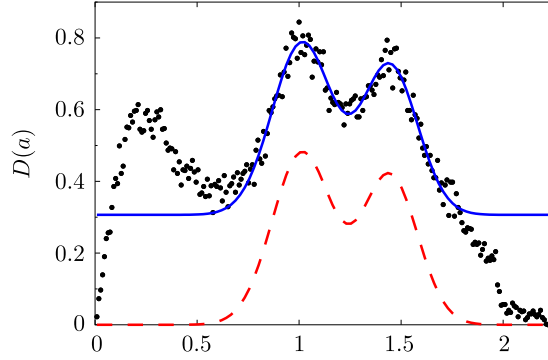


Figure 4.1: Experimental recoil velocity distribution rescaled to have a maximum for $a = 1$ (blue points), fitted functions using two Gaussians (solid line) and two Gaussians without background (dashed line).

The advantage of this expression is that $\bar{\rho}_\gamma(u, \theta_{2D}) = \bar{\rho}_\gamma(r/a, \theta_{2D})$ is only needed on an appropriate grid in u and θ_{2D} to calculate $P_\gamma(y, z)$ for any point (y, z) . In contrast, $D(r/u)$ depends on r , i.e., on (y, z) , but this is no problem if the functional form of $D(a)$ is known and if we use the experimental data they can easily be interpolated. In the experiment, the molecular beam is not formed only by a state but by an ensemble of molecules in different quantum states. A certain level $\gamma = J_{K_a K_c} M$ has a relative weight $W_\gamma = W_{J_{K_a K_c} M}$ within the molecular beam. These weights have been computed by simulating the trajectories through the beam line, which includes all mechanical apertures of the experimental setup, for individual molecules in a given rotational quantum states [51]. By including into the 2D-screen probability distribution the population of the individual states that are probed, we arrive at

$$P_T(y_s, z_s) = \int_0^\infty \frac{1}{r} \bar{\rho}_T(u, \theta_{2D}) D(r/u) du, \quad (4.39)$$

with

$$\bar{\rho}_T(u, \theta_{2D}) = \sum_\gamma W_\gamma \bar{\rho}_\gamma(u, \theta_{2D}), \quad (4.40)$$

where the sum runs over all populated states.

Experimental measures

The alignment of a molecule is quantified by the expectation value $\langle \cos^2 \theta \rangle_\gamma$, the closer it is to 1, the larger is the alignment. However, $\langle \cos^2 \theta \rangle_T = \sum_\gamma W_\gamma \langle \cos^2 \theta \rangle_\gamma$ cannot be experimentally measured. Instead, in the experiment the alignment is determined by the expectation value $\langle \cos^2 \theta_{2D} \rangle_T = \sum_\gamma W_\gamma \langle \cos^2 \theta_{2D} \rangle_\gamma$, where $\theta_{2D} = \arctan(z_s/y_s)$ is the angle between the z_s -axis of the screen plane and the projection of the ion recoil velocity vector onto the detector plane.

When the linear polarization of the YAG laser is not perpendicular to the static electric field ($\beta \neq \pi/2$), the up/down symmetry of the 2D-images is lost, and an asymmetric distribution appears showing a certain degree of orientation. The molecular orientation is normally analyzed in terms of $\langle \cos \theta \rangle_\gamma$, which can not be experimentally measured. For each 2D-image, this up/down asymmetry is experimentally quantified by the amount of ions in the upper part of the screen plane, N_{up} , compared to the total number of detected ions N_{tot} . This

orientation measure is computationally given by the ratio N_{up}/N_{tot} , with

$$N_{up} = \int_{-\infty}^{\infty} \int_{z_s \geq 0} P_T(y_s, z_s) dy_s dz_s, \quad (4.41)$$

and

$$N_{tot} = \int_{-\infty}^{\infty} \int_{-\infty}^{\infty} P_T(y_s, z_s) dy_s dz_s.$$

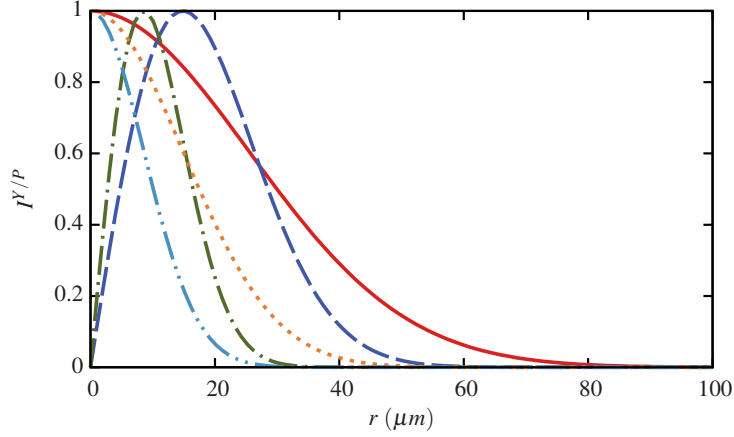


Figure 4.2: Profile of the YAG (solid line), probe (dotted line) and cubic probe (double-dotted dashed line) together with the dissociation probability of the probe laser with linear (dashed line) and cubic (dashed-dotted line) selectivity as a function of the distance to the center of the beam.

Volume effect

Finally, to compare our numerical results with the experimental data, we consider that not all the molecules experience the same laser intensities, because the molecular beam has a finite size, and the YAG and probe pulses have a certain spatial distributions. We take into account that each molecule in the beam feels a different intensity of the YAG depending on its position, and that the probability for a molecule to be dissociated is determined by the intensity of probe laser. Including the volume effect diminishes both, the measured orientation and alignment, since weaker values of the laser intensities must be considered, as well. We assume that the size of the molecular beam is larger than the beam waist of the YAG and probe lasers, and that the molecules are uniformly distributed within the beam.

For both lasers, we assume a Gaussian profile

$$I^{Y/P}(y_s, z_s) = I^{Y/P} \exp(-(y_s^2 + z_s^2)/\omega_{Y/P}^2),$$

with a beam waist of $\omega_Y = 36 \mu\text{m}$ and $\omega_P = 21 \mu\text{m}$ for the YAG and probe pulses, respectively, and that they are symmetric under rotations around the propagation direction. Numerically, we compute the orientation or alignment for different YAG intensities I , and using the YAG beam profile we derive it as a function of spatial position $r^2 = z_s^2 + y_s^2$. Thus, taking the

volume effect into account, it yields

$$f_V = \frac{\delta}{\omega_P^2} \int_0^\infty f(I(r)) r e^{-\delta r^2 / \omega_P^2} dr \quad (4.42)$$

where $f(r)$ is either the orientation ratio N_{up}/N_{tot} or the alignment $\langle \cos^2 \theta_{2D} \rangle_T$, and δ is the selectivity of the laser. In Fig. 4.2, we show the influence of each laser. Each point of the beam feels a different intensity of the YAG. The probability to probe a molecule in that position is proportional to the selectivity used. For $\delta = 3$, the measurements correspond to molecules exposed to higher intensities than for $\delta = 1$. If the spatial width of the molecular beam is comparable to the spatial width of the lasers ω_Y and ω_P , we should include another term accounting for the spatial distribution of the molecular density in the expression (4.42).

Chapter 5

Publications

In this chapter, we present the publications which constitute this thesis

1. *Authors:* **J. J. Omiste**, R. González-Férez and P. Schmelcher
Title: Rotational spectrum of asymmetric top molecules in combined static and laser fields
Journal: Journal of Chemical Physics
Volume: 135
Pages: 064310
Year: 2011
2. *Authors:* **J. J. Omiste**, M. Gärttner, P. Schmelcher, R. González-Férez, L. Holmegaard, J. H. Nielsen, H. Stapelfeldt and J. Küpper
Title: Theoretical description of adiabatic laser alignment and mixed-field orientation: the need for a non-adiabatic model,
Journal: Physical Chemistry Chemical Physics
Volume: 13
Pages: 18815-18824
Year: 2011
3. *Authors:* J. H. Nielsen, H. Stapelfeldt, J. Küpper, B. Friedrich, **J. J. Omiste** and R. González-Férez
Title: Making the best of mixed-field orientation of polar molecules: A recipe for achieving adiabatic dynamics in an electrostatic field combined with laser pulses
Journal: Physical Review Letters
Volume: 108
Pages: 193001
Year: 2012
4. *Authors:* **J. J. Omiste** and R. González-Férez
Title: Nonadiabatic effects in long-pulse mixed-field orientation of a linear polar molecule
Journal: Physical Review A
Volume: 86
Pages: 043437
Year: 2012

Rotational spectrum of asymmetric top molecules in combined static and laser fields

J. J. Omiste,^{1,a)} R. González-Férez,¹ and P. Schmelcher²

¹*Instituto Carlos I de Física Teórica y Computacional, and Departamento de Física Atómica, Molecular y Nuclear, Universidad de Granada, 18071 Granada, Spain*

²*Zentrum für Optische Quantentechnologien, Luruper Chaussee 149, Universität Hamburg, 22761 Hamburg, Germany*

(Received 7 June 2011; accepted 25 July 2011; published online 12 August 2011)

We examine the impact of the combination of a static electric field and a non-resonant linearly polarized laser field on an asymmetric top molecule. Within the rigid rotor approximation, we analyze the symmetries of the Hamiltonian for all possible field configurations. For each irreducible representation, the Schrödinger equation is solved by a basis set expansion in terms of a linear combination of symmetric top eigenfunctions respecting the corresponding symmetries, which allows us to distinguish avoided crossings from genuine ones. Using the fluorobenzene and pyridazine molecules as prototypes, the rotational spectra and properties are analyzed for experimentally accessible static field strengths and laser intensities. Results for energy shifts, orientation, alignment, and hybridization of the angular motion are presented as the field parameters are varied. We demonstrate that a proper selection of the fields gives rise to a constrained rotational motion in three Euler angles, the wave function being oriented along the electrostatic field direction, and aligned in other two angles.

© 2011 American Institute of Physics. [doi:10.1063/1.3624774]

I. INTRODUCTION

The manipulation of large molecules by using external fields represents, in spite of its long history, a very active and promising research area. Indeed, major efforts have been undertaken to create samples of oriented and/or aligned molecules, and a large variety of experimental techniques have been developed, such as, the brute force orientation,¹ hexapole focusing,²⁻⁴ a train of laser pulses,^{5,6} or a combination of a laser pulse and a weak static electric field.⁷⁻⁹ The control and manipulation of the directional features of molecules, i.e., of their rotational degree of freedom, optimize the information content on experimental measurements performed in the laboratory frame. Indeed, the availability of asymmetric top molecules in oriented and/or aligned pendular states allows for a wealth of interesting applications in areas as diverse as spectroscopy,^{10,11} photoelectron angular distributions,^{12,13} stereodynamic control of chemical reactions,¹⁴⁻¹⁷ dissociation of molecules,¹⁸⁻²¹ electron diffraction,²² or high-harmonic generation.^{23,24}

The experimental achievements have been accompanied by theoretical efforts to understand and explain the intriguing physical phenomena appearing in asymmetric top molecules exposed to external fields. Regarding the impact of radiative fields on these molecules, the corresponding theoretical studies have been especially fruitful in explaining a vast amount of experimental results, such as, the rotational revival structure following the irradiation by an intense picosecond laser pulses,²⁵ the three-dimensional alignment by elliptically polarized laser fields,²⁶⁻²⁸ or the use of long and short laser

pulses to control the rotation.^{29,30} Analogously, the motivation of the theoretical works considering an electrostatic field was either to interpret some experimental results,¹⁰ or to confirm the feasibility of other experiments, e.g., the Stark deceleration of polyatomic asymmetric molecules.³¹ The molecular orientation due to the interaction with a static electric field has been investigated for asymmetric top molecules with their permanent dipole moment μ parallel to a principal axis of inertia, and for the non-parallel case.^{4,32,33} In the strong electrostatic field regime, an analytical study of the energy-level representation has shown that the asymmetric top pendular states are well described by a two-dimensional (2D) anisotropic harmonic oscillator,³⁴ and it has been used to reproduce spectroscopic results in the pendular regime for static fields up to 200 kV cm⁻¹.¹¹

A detailed analysis of the rotational spectrum of symmetric top molecules exposed to combined electrostatic and non-resonant radiative fields was recently performed by Härtelt and Friedrich.³⁵ For tilted fields, only the projection of the total angular momentum \mathbf{J} onto the body fixed frame z -axis K remains as good quantum number, and a 2D description of the rotational spectrum of the molecule is required. The corresponding dynamics is very complicated, indeed, in the presence of a static electric field; it has been shown that the molecular spectrum presents classical and quantum monodromy.³⁶ They provide correlation diagrams between the field-free states and the pendular levels of the intense laser field³⁷ as well as the strong electrostatic field regime. For a selection of states, they investigate the energy shifts and directional properties (orientation and alignment) for parallel and perpendicular fields. In these systems, the coupling of both field interactions could provoke an enhancement of the orientation giving rise to an oriented and antioriented pair of levels.

^{a)} Author to whom correspondence should be addressed. Electronic mail: omiste@ugr.es.

For an oblate system, this phenomenon appears in the tunneling doublets created by the interaction of the molecular polarizability with the linear polarized laser field (this effect was already analyzed for linear molecules^{38–40}), whereas for a prolate molecule, it appears among exactly degenerate doublets of indefinite parity appearing in the strong laser field regime.

A classical theoretical analysis of asymmetric top molecules exposed to a combination of static and laser fields has been performed recently.⁴¹ However, the quantum analog has not yet been addressed in the literature, to the best of our knowledge. Recently, the authors have developed a diabatic model to describe the evolution of alignment and orientation of asymmetric top molecules in combined fields as the laser intensity is varied.⁴² The outcome of this theoretical study has been compared to the experimental data obtained for the benzonitrile molecule¹³ proving the importance of non-adiabatic processes in the field-dressed molecular dynamics. Thus, motivated by the current experimental interest on these asymmetric molecules^{7–9,12,13} and by the fact that the rotational dynamics of most polyatomic molecules can be described as asymmetric tops, we extend in the present work the previous study on symmetric tops³⁵ to these more complicated systems. We perform a theoretical investigation of an asymmetric top in the presence of combined electrostatic and non-resonant radiative fields within the rigid rotor description. The field-dressed rotational spectrum is significantly more complicated, and the more general case of non-collinear field requires a full 3D description. We will perform a detailed analysis of the symmetries of the Hamiltonian for all possible field configurations. In tilted fields, the reduction of the symmetries enhances the complexity of the spectrum, and a large amount of avoided crossing appears between states of the same symmetry. Hence, to simplify the analysis and interpretation of our results, the Schrödinger equation is numerically solved for each irreducible representation by expanding the wave function in a basis with the corresponding symmetry. As prototype examples, we consider (C_6H_5F) and pyridazine ($C_4H_4N_2$) molecules. These two systems have similar values of their polarizability tensors and dipole moments, but different inertia tensors and are, therefore, affected differently by the external fields. We explore their rotational spectrum as either the laser intensity, the electrostatic field strength, or the inclination angle between them is varied. Our focus is on the energy shifts, the directional properties, and the hybridization of the angular motion. Depending on the dominant interaction, a rich field-dressed dynamics is observed with levels achieving different degrees of orientation and/or alignment. The role played by the inclination angle is exemplary investigated via a set of states and in avoided crossings between two adjacent levels. Moreover, we show that due to the combination of both field interactions the rotational motion is restricted in the three Euler angles, being oriented along the static electric field direction and constrained in the XY plane of the laboratory frame, which is perpendicular to the laser polarization. This mechanism of orientation and 2D alignment is very sensitive to the field parameters and to the molecular properties.

The paper is organized as follows. In Sec. II, the rotational Hamiltonian is presented together with a comprehen-

sive consideration of its symmetries for the different field configurations. In Sec. III, we discuss the numerical results for two asymmetric molecules, fluorobenzene and pyridazine, as the field parameters are modified. In particular, we explore three different cases: (i) for fixed laser intensity and three inclination angles, we vary the electrostatic field strength, (ii) for fixed electrostatic field and three inclination angles, the laser intensity is enhanced, and (iii) for fixed laser intensity and electrostatic field strengths, the angle between them is continuously changed from 0 to $\pi/2$. The conclusions and outlook are provided in Sec. IV.

II. HAMILTONIAN OF AN ASYMMETRIC TOP MOLECULE IN THE PRESENCE OF THE FIELDS

We consider a polar and polarizable asymmetric top molecule exposed to a homogeneous static electric field and a non-resonant linearly polarized laser. Our study is restricted to the regime of field strengths that significantly affects the rotational dynamics of the molecule, whereas its impact on the electronic and vibrational structure can be described by first order perturbation theory. We work within the Born-Oppenheimer approximation, assuming that the rotational and vibrational dynamics can be adiabatically separated, and apply a rigid rotor description of the molecular systems. Furthermore, we neglect relativistic, fine, and hyperfine interactions as well as couplings of different electronic states. We are working with off-resonance conditions concerning the laser. Thus, the interaction of the field does not induce a coupling between the ground potential energy surface and an excited one as is, e.g., the case for light-induced conical intersections.^{43,44} There, it has been recently proven that when a diatomic molecule is placed inside a standing laser field (optical lattice), a periodic array of conical intersections is induced by the laser field, thereby leading to a strong coupling of the translational and rovibrational molecular motions and resulting energy exchange processes. In the laboratory fixed frame (LFF) (X, Y, Z), the Z -axis is chosen parallel to the polarization of the laser, and the direction of the homogeneous electric field is taken forming an angle β with this axis and contained in the XZ plane. The molecular or body fixed frame (MFF) (x, y, z) is defined so that the permanent electric dipole moment is parallel to the z -axis, and for the considered systems the smallest moment of inertia is parallel to the x -axis. The relation between both frames is given by the Euler angles $\Omega = (\phi, \theta, \chi)$,⁴⁵ which are shown together with the field configurations in Fig. 1. We only analyze molecules having the electric dipole moment parallel to one of the axis, and a diagonal polarizability tensor. Thus, the rigid rotor Hamiltonian reads

$$H = H_r + H_S + H_L, \quad (1)$$

where H_r is the field-free Hamiltonian, and H_S and H_L stand for the interactions with the static and the laser field, respectively.

In the absence of the fields, the rigid rotor Hamiltonian is given by

$$H_r = B_x J_x^2 + B_y J_y^2 + B_z J_z^2, \quad (2)$$

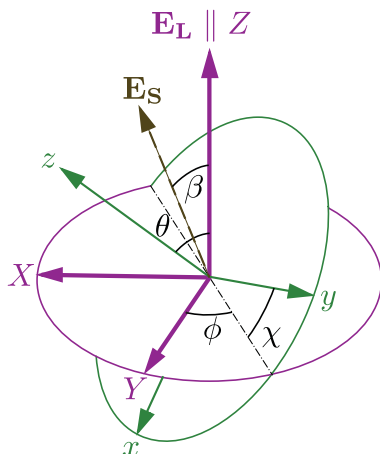


FIG. 1. Laboratory and molecular fixed coordinate frames and field configuration.

where the angular momentum operators refer to the MFF, with $B_i = \hbar^2/2I_{ii}$ being the rotational constant and I_{ii} the moment of inertia around the principal axis of inertia i , with $i = x$, y , and z . An estimation of the degree of asymmetry is provided by Ray's parameter, $\kappa = (2B_y - B_z - B_x)/(B_y - B_x)$, where the rotational constants of the considered system satisfy $B_z \geq B_y \geq B_x$. For a symmetric top ($B_x = B_y$), Ray's parameter takes the extreme values $\kappa = 1$ and -1 for the oblate and prolate cases, respectively.

For the regime of electrostatic field strengths \mathbf{E}_S considered here, we can neglect the interaction via the molecular polarizability, arriving at the following the Stark Hamiltonian:

$$H_S = -\mathbf{E}_S \cdot \boldsymbol{\mu} = -E_S \mu \cos \theta_S, \quad (3)$$

where θ_S is the angle between the permanent molecular electric dipole moment, $\boldsymbol{\mu} = \mu \hat{\mathbf{z}}$, and the static electric field with $\cos \theta_S = \cos \beta \cos \theta + \sin \beta \sin \theta \cos \phi$ and $0 \leq \beta \leq \pi/2$.

Here, we consider a non-resonant laser field linearly polarized along the Z -axis, $\mathbf{E}_L(t) = E_{\max} g(t) \cos(2\pi \nu t) \hat{\mathbf{Z}}$, with the frequency ν , the field strength E_{\max} , and $g(t)$ being the pulse envelope. We assume that ν^{-1} is much shorter than the pulse duration or the rotational period, so that we can average over the rapid oscillations, which causes the coupling of this field with the permanent dipole moment to vanish.^{46,47} In addition, we assume that the pulse duration is much longer than the rotational period of the molecular system, such that the states adiabatically follow the change of the field, and we restrict our analysis to the adiabatic limit $g(t) \rightarrow 1$. Hence, the interaction of the laser with the polarizability is the leading order term, and can be written as

$$H_L = -\frac{I}{2c\epsilon_0} (\alpha^{zx} \cos^2 \theta + \alpha^{yx} \sin^2 \theta \sin^2 \chi), \quad (4)$$

with $\alpha^{ji} = \alpha_{jj} - \alpha_{ii}$, and α_{ii} being the i th diagonal element of the polarizability tensor, with $i = x$, y , and z .⁴⁸ In this expression, we have used $\langle E_L^2 \rangle = I/c\epsilon_0$, c being the speed of light, ϵ_0 the dielectric constant, and expectation value $\langle E_L^2 \rangle$ indicates the time average. We remark that since the laser frequency is off-resonance, for the considered laser intensities,

TABLE I. Action of the symmetry operations on the Euler angles.

Operation	Transformations		
	ϕ	θ	χ
C_2^z	$\phi \rightarrow \phi$	$\theta \rightarrow \theta$	$\chi \rightarrow \chi - \pi$
C_2^y	$\phi \rightarrow \phi - \pi$	$\theta \rightarrow \pi - \theta$	$\chi \rightarrow -\chi$
C_2^x	$\phi \rightarrow \phi - \pi$	$\theta \rightarrow \pi - \theta$	$\chi \rightarrow \pi - \chi$
σ_{XZ}^a	$\phi \rightarrow 2\pi - \phi$	$\theta \rightarrow \theta$	$\chi \rightarrow 2\pi - \chi$
$C_X(\pi)$	$\phi \rightarrow 2\pi - \phi$	$\theta \rightarrow \pi - \theta$	$\chi \rightarrow \pi + \chi$
$C_{\perp Z}^a(\pi)$	$\phi \rightarrow 2\alpha - \phi$	$\theta \rightarrow \pi - \theta$	$\chi \rightarrow \chi + \pi$
$C_Z(\delta)$	$\phi \rightarrow \phi + \delta$	$\theta \rightarrow \theta$	$\chi \rightarrow \chi$

^aThe reflection cannot be represented only by a rotation and the operation $y \rightarrow -y$ should be performed as well.

the photoelectronic excitation is negligible and the dynamics takes place on the ground potential energy surface.

Our aim is to investigate the rotational spectrum of an asymmetric top molecule exposed to different field configurations. To do so, we solve the time-independent Schrödinger equation associated with the Hamiltonian (Eq. (1)), which even in the field-free case cannot be solved analytically. Let us start by analyzing how the symmetries of this Hamiltonian change when the angle between the fields varies.

A. Symmetries

A detailed analysis of the symmetries of an asymmetric top rotor in the field-free case and exposed to a static electric field has been performed in Ref. 34. Here, we extend this study to the field configurations investigated in this work.

The symmetries of the field-free Hamiltonian (Eq. (2)) are the spatial $SO(3)$ rotation group and a subgroup of this group relevant to the symmetries in the presence of the fields is the molecular point group $D_2 = \{E, C_2^x, C_2^y, C_2^z\}$, where E stands for the identity and C_2^i represents a rotation of π around the i -axis of the MFF, with $i = x$, y , and z . The action of these operators on the Euler angles are summarized in Table I. The D_2 -group has four irreducible representations. The Wang states, defined as

$$|JKMs\rangle^w = \frac{1}{\sqrt{2}} (|JKM\rangle + (-1)^s |J-KM\rangle), \quad K > 0,$$

$$|J0M0\rangle^w = |J0M\rangle, \quad K = 0,$$

with $s = 0$ and 1 , form the basis of these irreducible representations, characterized by the parity of $J + s$ and K . The action of the elements of the D_2 -group is $C_2^i |JKMs\rangle^w = (-1)^{\lambda_i} |JKMs\rangle^w$, with $i = x$, y , and z and $\lambda_x = J + K + s$, $\lambda_y = J + s$, and $\lambda_z = K$. The states $|JKM\rangle$ are the eigenfunctions of the field-free symmetric top rotor,

$$|JKM\rangle = (-1)^{M-K} \sqrt{\frac{2J+1}{8\pi^2}} D_{-M,-K}^J(\Omega), \quad (5)$$

with $D_{M,K}^J(\Omega)$ being the Wigner matrix elements,⁴⁵ J the total angular momentum, and K and M the projections of \mathbf{J} on the MFF z -axis and on the LFF Z -axis, respectively. To be self-contained, the definition and main properties of the Wigner matrix elements are presented in the Appendix.

For a field-free asymmetric top rotor, J and M are good quantum numbers, whereas, in contrast to a symmetric rotor, K is not well defined. For each M -value, there are four irreducible representations that depend on the parity of $J + s$ and K . The eigenstates are degenerate with respect to M , and for a certain M and J , the corresponding eigenfunctions are linear combinations of Wang states $|JKMs\rangle^w$ with different K values.

Since an external field defines a preferred direction in space, the symmetries of the corresponding Hamiltonian are reduced compared to the field-free case. As a consequence, the total angular momentum J is not a good quantum number, and only for certain field configurations M remains as a good quantum number.

In the presence of a non-resonant laser field linearly polarized along the Z -axis, the symmetry operations of the Hamiltonian are the D_2 point group, a rotation of an arbitrary angle δ around the Z -axis $C_Z(\delta)$, a rotation of π around an axis perpendicular to the Z -axis tilted at an angle α with respect to the X -axis $C_{\perp Z}^\alpha(\pi)$, and the reflection in any plane including the Z -axis (this reflection is equivalent to first applying a twofold rotation around any axis in the XY -plane followed by the action of the operator C_2^x or C_2^y ³⁴). Only M remains a good quantum number, and the levels with $\pm M$ are degenerate. Thus, we have eight irreducible representations for each $|M| > 0$, but due to the reflection at the plane, there is a twofold degeneracy and they can be effectively reduced to four representations being characterized by the parity of K and $J + s$, as in the field-free Hamiltonian. For $M = 0$, there are eight irreducible representations labeled by the parities of J , K , and s .

When an asymmetric top rotor is exposed to a static electric field (parallel to the Z -axis) or to both fields in the parallel configuration, i.e., $\beta = 0$, the symmetry operations are C_2^z from the D_2 point group, the rotation $C_Z(\delta)$, and the reflection in any plane including the Z -axis. In these two cases, M is still a good quantum number, and the states M and $-M$ are degenerate. For a certain $|M|$, the group has four irreducible representations characterized by the parity of K and the parity of s . Those representations with the same parity of K and $M > 0$ are degenerate in energy. The symmetric top eigenfunctions (Eq. (5)), with defined parity of K , form a basis of this irreducible representation. For the $M = 0$ case, these four representations are not energetically degenerate.

For non-parallel fields, M ceases to be a good quantum number. If the two fields are perpendicular, i.e., the electric field is parallel to the X -axis and $\beta = \pi/2$, the Hamiltonian commutes with only three symmetry operations: C_2^z , a rotation of π around the X -axis $C_X(\pi)$, and the reflection σ_{XZ} on the XZ -plane where the fields are contained, as well as their combinations. Using the field-free symmetric rotor wave functions, we can construct a basis for σ_{XZ} ,

$$|JKMq\rangle^\sigma = \frac{1}{\sqrt{2}}(|JKM\rangle + (-1)^q|J - K - M\rangle),$$

with M and/or $K \neq 0$, and

$$|J000\rangle^\sigma = |J00\rangle$$

with $M = K = 0$, where $q = 0$ and 1 , and $\sigma_{XZ}|JKMq\rangle^\sigma = (-1)^{M+K+q}|JKMq\rangle^\sigma$, and one for $C_X(\pi)$,

$$|JKMp\rangle^X = \frac{1}{\sqrt{2}}(|JKM\rangle + (-1)^p|JK - M\rangle),$$

with $M \neq 0$, and

$$|JK00\rangle^X = |JK0\rangle,$$

with $M = 0$, where $p = 0$ and 1 , and satisfying $C_X(\pi)|JKMp\rangle^X = (-1)^{J+p}|JKMp\rangle^X$. The group of all the symmetry operators, C_2^z , σ_{XZ} , and $C_X(\pi)$, has eight different irreducible representations according to the parity of $M + K + q$, $J + p$ and K . A basis of these irreducible representations is

$$|JKMqp\rangle_{\frac{\pi}{2}} = \frac{1}{2}(|JKM\rangle + (-1)^q|J - K - M\rangle + (-1)^p|JK - M\rangle + (-1)^{p+q}|J - KM\rangle),$$

with $M \neq 0$ and $K \neq 0$,

$$|JOM0p\rangle_{\frac{\pi}{2}} = \frac{1}{\sqrt{2}}(|JOM\rangle + (-1)^p|JO - M\rangle),$$

with $M \neq 0$ and $K = 0$,

$$|JK0q0\rangle_{\frac{\pi}{2}} = \frac{1}{\sqrt{2}}(|JK0\rangle + (-1)^q|J - K0\rangle),$$

with $M = 0$ and $K \neq 0$, and

$$|J0000\rangle_{\frac{\pi}{2}} = |J00\rangle,$$

with $K = M = 0$, where $q = 0$ and 1 , $p = 0$ and 1 , and the parity of $M + K + q$, K and $J + p$ are preserved.

Finally, when the fields form an angle $0 < \beta < \pi/2$, the Hamiltonian is invariant under the reflection σ_{XZ} and the rotation C_2^z . We have, therefore, four irreducible representations depending on the parity of $M + K + q$ and of K , and the corresponding basis is $\{|JKMq\rangle^\sigma\}$.

For an asymmetric top rotor exposed to any of these field configurations, the field-dressed spectrum exhibits many avoided crossings between energetically adjacent states of the same symmetry. When the spectrum is analyzed as the strength of one of these fields or the angle between them is varied, these avoided crossings should be distinguished from the real crossings taking place between levels of different symmetry. Hence, we solve the Schrödinger equation, by expanding the rotational wave function in a basis that respects the symmetries of the corresponding Hamiltonian. As a consequence, the coefficients of these expansions fulfill the properties of the basis vectors of the corresponding irreducible representation. For computational reasons, we have cut the (in principle) infinite series to a finite one, including only those functions with $J \leq J_{\max}$, and for a certain J , all $(2J + 1)$ -values of K , and, analogously, for M in the case $0 < \beta \leq \pi/2$. The size of the Hamiltonian matrix increases as J_{\max}^3 and J_{\max}^2 for the $0 < \beta \leq \pi/2$ and $\beta = 0$ configurations, respectively. In this study, we have used $J_{\max} = 24$, and the convergence is reached for the states analyzed here. Several matrix elements are presented in the Appendix.

The field-free states are labeled by the notation $J_{K_a, K_c} M$, where K_a and K_c are the values of K on the limiting

symmetric top rotor prolate and oblate cases, respectively.⁴⁹ For reasons of addressability, we use this notation for the field-dressed states, even if J and/or M are not good quantum numbers. Thus, $J_{K_a K_c} M$ refers to the level that is adiabatically connected as I , E_S , and/or β are modified with the field-free state $J_{K_a K_c} M$. The irreducible representation to which the states belong is also indicated. Analogous to a symmetric top molecule exposed to combined fields,³⁵ the final labels of the states depend on the path followed on the parameters to reach a certain field configuration, i.e., monodromy is observed. Since each interaction breaks different symmetries of the field-free Hamiltonian, the order in which the fields are turned on determines the evolution of the field-dressed states. The complexity of the spectrum is characterized by the amount of genuine and avoided crossings among the states, the symmetry of the two levels determine the type of crossing that they may suffer as one of the field parameters (E_S , I , or β) is varied, and, therefore, the corresponding labels may or not be interchanged.

III. RESULTS

In this section, we illustrate the impact of the external fields on two asymmetric top molecules: fluorobenzene (C_6H_5F) and pyridazine ($C_4H_4N_2$). Their data are summarized in Table II, according to Refs. 50–54 and their structure is shown in Fig. 2. They are characterized by a different degree of asymmetry: the fluorobenzene is intermediate-prolate with $\kappa = -0.5879$, and the pyridazine is near-oblate with $\kappa = 0.8824$. The permanent dipole moment of pyridazine is around 2.5 times larger than in fluorobenzene. The asymmetry of the polarizability tensor is very similar for both systems, for fluorobenzene, $\alpha^{zx} = 4.298 \text{ \AA}^3$ and $\alpha^{yx} = 3.848 \text{ \AA}^3$, whereas for pyridazine, $\alpha^{zx} = 4.51 \text{ \AA}^3$ and $\alpha^{yx} = 4.45 \text{ \AA}^3$. Since the rotational constants of pyridazine are larger than for fluorobenzene, for the same laser intensity, a weaker impact on the former should be expected. In the following, we carry out a study of the spectrum of these two systems, as the parameters that characterize the field configurations, E_S , I , or β , are modified. For the sake of simplicity, we analyze the energy, the orientation, the alignment, and hybridization of the states which belong to the representation with K and $M + K + q$, even (if $\beta \neq \pi/2$), and $J + p$, even (if $\beta = \pi/2$). Note that they represent well the main physical features observed in the overall spectrum, and similar behavior and properties are, therefore, obtained for the other representations.

TABLE II. Relevant data for fluorobenzene^{50–52} and pyridazine.^{53,54}

	Fluorobenzene	Pyridazine
B_x (MHz)	1716.916	3055.485
B_y (MHz)	2570.624	6048.613
B_z (MHz)	5663.72	6235.680
κ	-0.5879	0.8824
μ_z (D)	1.66	4.14
α_{xx} (\AA^3)	7.141	5.84
α_{yy} (\AA^3)	10.89	10.29
α_{zz} (\AA^3)	11.439	10.35

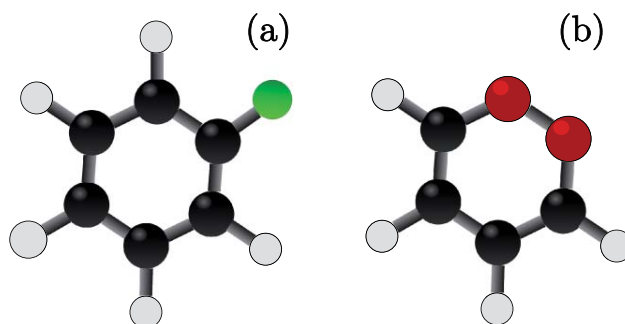


FIG. 2. Structure of the (a) fluorobenzene and (b) pyridazine molecules.

A. Impact of a linearly polarized laser field

The dynamics of the molecule in the presence of a linearly polarized laser field depends strongly on the anisotropy of the polarizability tensor. The interaction with the laser (Eq. (4)) exhibits several critical points. The minimum value $H_L = -I\alpha^{zx}/2\epsilon_0 c$ is reached for $\theta = 0$ or π and any value of χ . The interaction achieves three maxima at $\theta = \pi/2$ and $\chi = 0, \pi$, or 2π satisfying that $H_L = 0$, and two saddle points at $\theta = \pi/2$ and $\chi = \pi/2$ or $3\pi/2$ with $H_L = -I\alpha^{yx}/2\epsilon_0 c$. All of them are shown in Figs. 3(a) and 3(b), where H_L is plotted for $\chi = \pi/2$ and $0 \leq \theta \leq 2\pi$ and for $\theta = \pi/2$ and $0 \leq \chi \leq 2\pi$, respectively. The main difference between the two systems is that the values for H_L at the saddle point $\theta = \pi/2$ and $\chi = \pi/2$ is smaller for pyridazine compared to fluorobenzene, and the fact that the shape of H_L as a function of θ and for fixed χ is significantly flatter for the former. Taking into account that the rotational constants are much larger for pyridazine compared to fluorobenzene, we observe that for the same laser intensity I , the pyridazine wave function is more widespread with respect to θ and χ than for fluorobenzene. While the minima are responsible for the molecular alignment, the maxima or saddle points correspond to an “antialigned” wave function, that is, the dipole moment points perpendicular to the field direction.

To get a better physical insight into this interaction, we present its impact on the ground state energy, and the expectation values $\langle \cos^2 \theta \rangle$, $\langle \sin^2 \chi \rangle$, and $\langle K^2 \rangle$ in Figs. 4(a)–4(d), respectively. While, for both molecules, the energy as a function of I shows a similar decreasing behavior, their values being

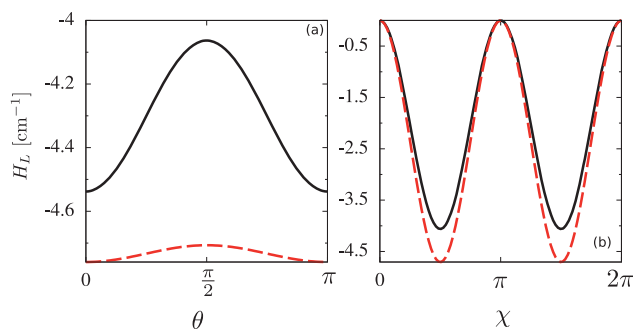


FIG. 3. Laser interaction term H_L , see Eq. (4), in units of cm^{-1} with $I = 10^{11} \text{ W cm}^{-2}$, for (a) $\chi = \pi/2$ and (b) $\theta = \pi/2$ (b) for fluorobenzene (solid) and pyridazine (dash).

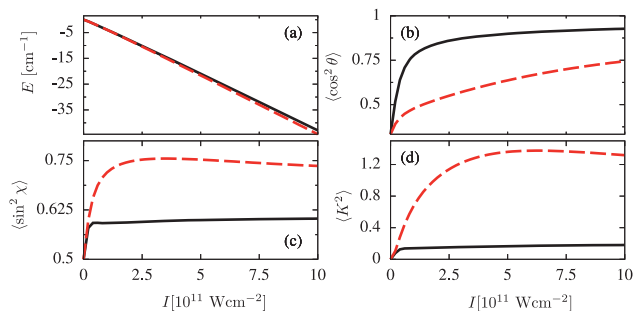


FIG. 4. (a) Ground state energy, (b) $\langle \cos^2 \theta \rangle$, (c) $\langle \sin^2 \chi \rangle$, and (d) $\langle K^2 \rangle$, as a function of the intensity of a linearly polarized laser field, for the fluorobenzene (solid) and pyridazine (dashed) molecules.

indistinguishable on the scale of Fig. 4(a), significant differences are observed for the other quantities. In the very strong laser field regime, the probability density of the fluorobenzene ground state tends to concentrate around the minima, and one should expect that $\langle \cos^2 \theta \rangle \rightarrow 1$ and $\langle \sin^2 \chi \rangle \rightarrow 0.5$ for very large intensities. This last relation holds because the χ -coordinate does not play any role in the absolute minima of H_L , and one concludes that the probability density should be uniformly distributed with respect to χ . Numerically we obtain that for the fluorobenzene ground state, $\langle \cos^2 \theta \rangle$ increases until 0.76 for $I = 10^{11} \text{ W cm}^{-2}$, smoothly increasing thereafter, and $\langle \sin^2 \chi \rangle$ reaches a plateau with a constant value 0.58 for $I \geq 4.2 \times 10^{10} \text{ W cm}^{-2}$. The barrier height of H_L as a function of θ for a certain value of χ , see Fig. 3(a), is around 9.2 times smaller for pyridazine than for fluorobenzene, and for the former, the rotational constants are larger, whereas the polarizability anisotropies α^{zx} and α^{yx} are of

the same order for both molecules. Hence, compared to fluorobenzene, the pyridazine ground state wave function should be spatially stronger delocalize with respect to θ , and, therefore, less aligned for the same laser intensity. We obtain here $\langle \cos^2 \theta \rangle = 0.49$ for $I = 10^{11} \text{ W cm}^{-2}$. As a consequence, the spreading of the wave function for χ is not observed in pyridazine: $\langle \sin^2 \chi \rangle$ shows a maximum of 0.75 for $I = 3 \times 10^{11} \text{ W cm}^{-2}$ and slightly decreases with further increasing I . For the field-free ground state, we have $\langle K^2 \rangle = 0$, and as I is increased, $\langle K^2 \rangle$ follows a similar evolution as $\langle \sin^2 \chi \rangle$. For fluorobenzene, $\langle K^2 \rangle$ achieves the value 0.14 for $I \approx 7.2 \times 10^{10} \text{ W cm}^{-2}$, followed by a plateau-like behavior around $\langle K^2 \rangle \approx 0.18$ for larger intensities for fluorobenzene, while it keeps an increasing trend up to 1.38 for $I = 5.9 \times 10^{11} \text{ W cm}^{-2}$ and decreasing smoothly afterwards for pyridazine. Let us emphasize that, for a field-free asymmetric rotor, K is not a good quantum number, and an eigenstate already shows a certain amount of K -mixing, but in the strong laser field regime, the second term of the laser interaction (Eq. (4)) should impact and enhance this K -mixing.

B. Constant static electric field and increasing laser intensity

In the presence of an additional static field, the interaction is given by $H_S + H_L$, see Eqs. (3) and (4), and the dynamics is significantly more complicated. The amount of extremal points of this potential and their character strongly depend on the field parameters as well as on the molecular polarizability and permanent dipole moment.

For fluorobenzene and pyridazine, we show in Figs. 5 and 6 the dependence of the energies (panels (a)–(c)),

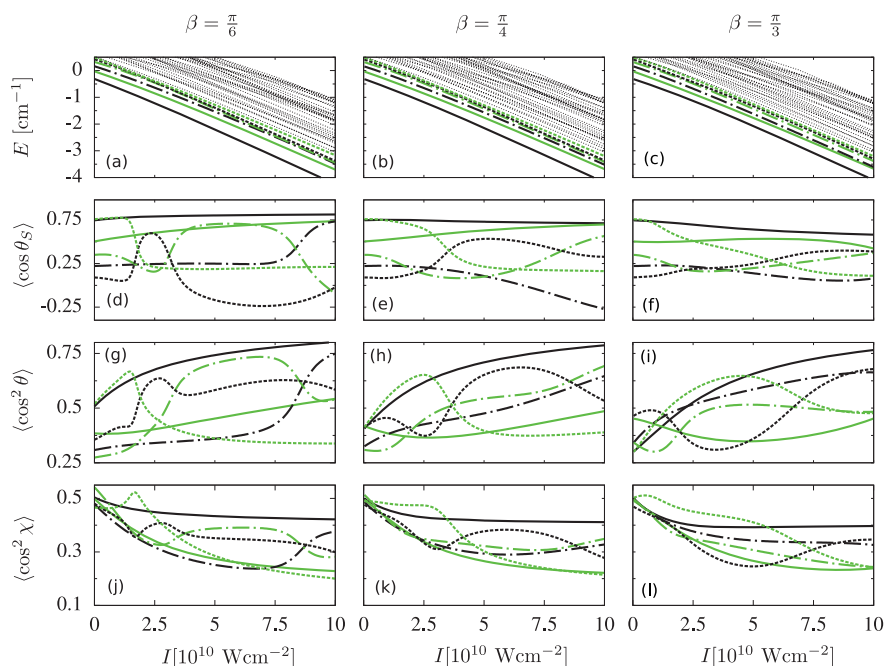


FIG. 5. (a)–(c) Energies and the expectation values, (d)–(f) $\langle \cos \theta_S \rangle$, (g)–(i) $\langle \cos^2 \theta \rangle$, and (j)–(l) $\langle \cos^2 \chi \rangle$ for a constant field $E_S = 20 \text{ kV cm}^{-1}$ as a function of the intensity of the laser field for $\beta = \pi/6$, $\pi/4$, and $\pi/3$ for the first states with both $M + q + K$ and K even for fluorobenzene. The states are $0_{00}0$ (solid black), $1_{01}1$ (solid green), $1_{01}0$ (dashed-dotted black), $2_{02}2$ (dashed-dotted green), $2_{02}1$ (dashed black), and $3_{03}2$ (dashed green). The spectrum (a, b, c) contains also highly excited states (very thin lines).

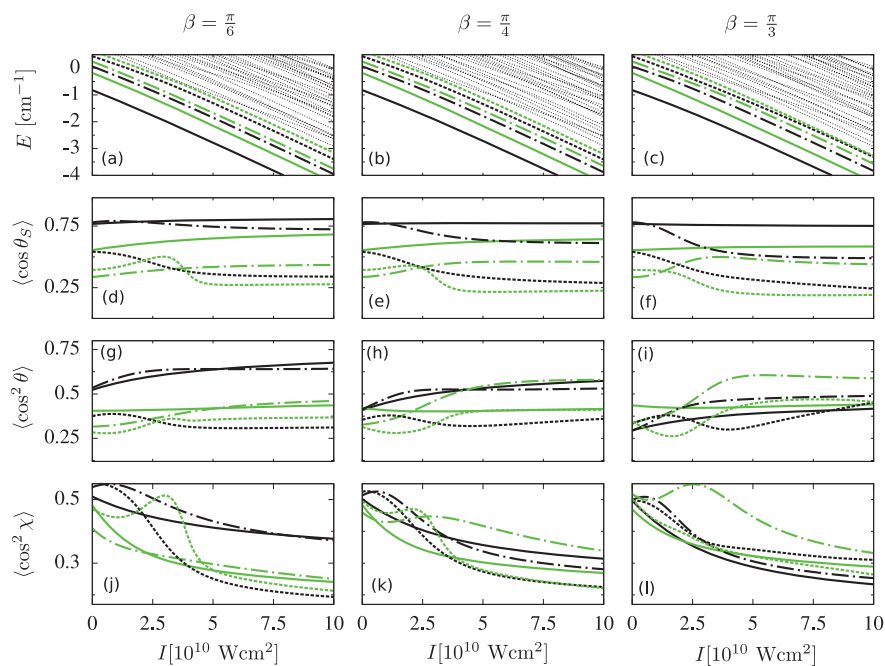


FIG. 6. (a)–(c) Energies and the expectation values, (d)–(f) $\langle \cos \theta_S \rangle$, (g)–(i) $\langle \cos^2 \theta \rangle$, and (j)–(l) $\langle \cos^2 \chi \rangle$ for a constant field $E_S = 20 \text{ kV cm}^{-1}$ as a function of the intensity of the laser field for $\beta = \pi/6$, $\pi/4$, and $\pi/3$ for the first states with both $M + q + K$ and K even for pyridazine. The states are $0_{00}0$ (solid black), $1_{01}1$ (solid green), $2_{02}2$ (dashed-dotted black), $1_{01}0$ (dash-dotted green), $2_{02}1$ (dashed black), and $2_{21}2$ (dashed green). The spectrum (a, b, c) contains also highly excited states (very thin lines).

expectation values $\langle \cos \theta_S \rangle$ (panels (d)–(f)), $\langle \cos^2 \theta \rangle$ (panels (g)–(i)), and $\langle \cos^2 \chi \rangle$ (panels (j)–(l)), as functions of the laser intensity for a constant electric field $E_S = 20 \text{ kV cm}^{-1}$, and $\beta = \pi/6$, $\pi/4$, and $\pi/3$, respectively. For the sake of simplicity and without losing generality, we restrict our analysis to the energetically lowest lying six states for the irreducible representations with both K and $M + K + q$ being even, which are the levels $J_{K_a, K_c} M = 0_{00}0$, $1_{01}0$, $1_{01}1$, $2_{02}1$, $2_{02}2$, and $3_{03}2$ for fluorobenzene, and $J_{K_a, K_c} M = 0_{00}0$, $1_{01}0$, $1_{01}1$, $2_{02}1$, $2_{02}2$, and $2_{21}2$ for pyridazine. To illustrate the complexity of the spectrum, we have included in the energy panels highly excited levels with the same symmetry (very thin lines). The adiabatic following has been done by increasing first the strength of the static electric field up to 20 kV cm^{-1} , the static field being tilted by an angle β with respect to the Z -axis. This is done for $I = 0$ and yields the labeling of the states in the presence of the static field. Thereafter, the laser intensity is increased. For both molecular systems, these levels are high-field-seekers, and their energies decrease as I is increased. For a given laser intensity, the lowering in energy (compared to the field-free value) increases with decreasing angle between both fields. Since all the states included in these figures possess the same symmetry, we encounter exclusively avoided crossings of energetically adjacent states. We have assumed that the avoided crossings are traversed adiabatically as I is increased (according to Landau-Zener transition theory), and consequently the character of the involved states is interchanged. These avoided crossings, which are not distinguishable on the energy scale panels (a)–(c) in Figs. 5 and 6, strongly affect the orientation and alignment features of these levels.

Let us start analyzing the results for fluorobenzene in Fig. 5. The orientation of the corresponding wave functions is illustrated by the expectation value $\langle \cos \theta_S \rangle$, with θ_S being the angle between the static electric field and the molecular fixed z -axis, which coincides with the direction of the permanent dipole moment. Only the states $0_{00}0$ and $3_{03}2$ present a significant orientation with respect to the static electric field direction that is reduced as β is increased. The ground state satisfies $\langle \cos \theta_S \rangle > 0.70$ for the three β values, and it has a plateau-like behavior, with a minor positive or negative slope as I is increased. The numerous avoided crossings have significant impact on the other levels, especially for $\beta = \pi/6$ and $\pi/4$, and the underlying states might evolve from a strongly oriented configuration into a weakly oriented or antioriented one. As an example, the state $3_{03}2$ after suffering for $I \approx 1.7 \times 10^{10} \text{ W cm}^{-2}$ an avoided crossing with the non-oriented $2_{02}1$ state loses its strong orientation. By further increasing I , the $2_{02}1$ level suffers another avoided crossing, which provokes a local maximum in $\langle \cos \theta_S \rangle$ for $I \approx 2.4 \times 10^{10} \text{ W cm}^{-2}$. Since for $\beta = \pi/3$ the width of all the avoided crossings is larger for all the levels, the orientation shows a smooth evolution as I is varied. A non-resonant linearly polarized laser field provokes the alignment of the wave function along the Z -axis, i.e., $\langle \cos^2 \theta \rangle$ tends to increase and ultimately approach the value 1 as I is increased (Figs. 5(g)–5(i)). This process competes now with the orientation due to the static field. Only the ground state alignment keeps an increasing trend as I is enhanced, and for the given three configurations, $\langle \cos^2 \theta \rangle > 0.75$ for $I = 10^{11} \text{ W cm}^{-2}$. An additional electric field at an angle $\beta = \pi/6$ or $\pi/4$ favors the alignment and $\langle \cos^2 \theta \rangle$ is larger than without static

field, see Fig. 4(b), whereas as the angle between the fields is augmented the values achieved for $\langle \cos^2 \theta \rangle$ come closer to those of Fig. 4(b). The level $1_{01}1$ does not achieve a large alignment, and for $\beta = \pi/4$, $\langle \cos^2 \theta \rangle$ exhibits a broad well that for $\beta = \pi/3$ is even wider since the coupling between the states changes. Around the avoided crossings, the wave function of the involved states alternate regions of significant alignment with other characterized by broad distribution as the laser intensity is varied, e.g., see the alignment of the states $3_{03}2$ and $2_{02}1$ for $I \approx 1.7 \times 10^{10}$ and 3.5×10^{10} W cm⁻² in Figs. 5(g) and 5(h), respectively. The impact of the avoided crossings is also noticeable for $\beta = \pi/3$. The behavior of $\langle \cos^2 \chi \rangle$ strongly depends on the considered level. Since the molecules exhibit a strong orientation with the electric field, the contribution in χ should be to increase the term $\langle \sin^2 \chi \rangle$ which will give rise to a decrease of the energy. For the states $0_{00}0$ and $1_{01}1$, $\langle \cos^2 \chi \rangle$ decreases as I is increased, and for both states there exists some region where $\langle \cos^2 \chi \rangle$ keeps a smooth behavior. For the other states, this expectation value is also affected by the presence of avoided crossings, and $\langle \cos^2 \chi \rangle$ alternates between increasing and decreasing behavior as a function of the laser intensity. Since the pyridazine possesses a larger permanent dipole moment than fluorobenzene, the impact of the static field is larger, and also dominates the dynamics, see Fig. 6. For the ground state and first excited one, $\langle \cos \theta_S \rangle$ is only weakly affected by the laser field, for the former $\langle \cos \theta_S \rangle \approx 0.75$ independently of I and β , while for the $1_{01}1$ level $\langle \cos \theta_S \rangle > 0.5$. The other levels present a right-way orientation, that can be converted from a strong to a mild one when an avoided crossing is encountered. Regarding the alignment, for most of the states, $\langle \cos^2 \theta \rangle$ shows a smooth behavior as I is enhanced for the three values of β . The impact of the avoided crossings on this expectation value is not very pronounced because most of the states show a weak alignment with a similar value of $\langle \cos^2 \theta \rangle$. Analogously

to fluorobenzene, the ground state has a larger alignment for $\beta = \pi/6$ and $\pi/4$ than in the absence of the static field, while for $\beta = \pi/3$ other states are found with larger alignment. For stronger fields, $\langle \cos^2 \chi \rangle$ monotonically decreases as I is enhanced for all the states, and the slope is more pronounced compared to fluorobenzene.

C. Constant laser intensity and increasing electric field strength

The pendular limit of an asymmetric top molecule in the presence of a strong electrostatic field was investigated by Kanya and Ohshima³⁴ using a power series expansion in μE_S . Their analytical expression for the energy, which neglects the contribution of terms in powers equal or smaller than $(\mu E_S)^{-1/2}$ (see Eq. (26) in Ref. 34) allowed us for a straightforward comparison to our numerical calculations. For $E_S = 100$ kV cm⁻¹, the energy and orientation cosines of the ground state agree within 0.05% and 0.025% for fluorobenzene and 0.04% and 0.019% for pyridazine, respectively. Note that for highly excited states, these relative errors increase.

For a constant laser field $I = 10^{10}$ W cm⁻², we now investigate the impact of increasing static field strength for three different configurations. Again, we consider the energetically lowest lying six states with the irreducible representation for K and $M + K + q$ being even. These levels have been adiabatically followed as the laser intensity is raised from $I = 0$ to 10^{10} W cm⁻² for $E_S = 0$; we label them, and finally the electrostatic field is turned on forming an angle β and its strength is increased. Thus, for both molecules, the levels are $0_{00}0$, $1_{01}0$, $1_{01}1$, $2_{02}0$, $2_{02}1$, and $2_{02}2$. For fluorobenzene and pyridazine, we present in Figs. 7 and 8, the evolution of the energies (panels (a)–(c)), $\langle \cos \theta_S \rangle$ (panels (d)–(f)), and $\langle \cos^2 \theta \rangle$ (panels (g)–(i)), as E_S is increased, for $I = 10^{10}$ W cm⁻², and $\beta = \pi/6$, $\pi/4$, and $\pi/3$, respectively. We remark that for such

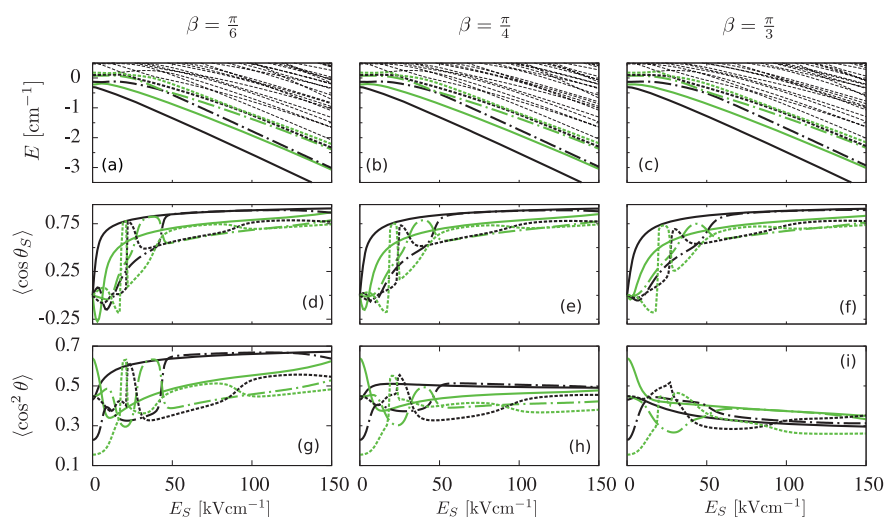


FIG. 7. (a)–(c) Energies and the expectation values, (d)–(f) $\langle \cos \theta_S \rangle$, and (g)–(i) $\langle \cos^2 \theta \rangle$ for a constant $I = 10^{10}$ W cm⁻² as a function of the strength of the static field for $\beta = \pi/6$, $\pi/4$, and $\pi/3$ for the energetically lowest states with both $M + q + K$ and K even for fluorobenzene. The states are $0_{00}0$ (solid black), $1_{01}0$ (solid green), $1_{01}1$ (dashed-dotted black), $2_{02}0$ (dashed-dotted green), $2_{02}1$ (dashed black), and $2_{02}2$ (dashed green). The spectrum (a, b, c) contains also highly excited states (very thin lines).

a weak laser intensity $I = 10^{10}$ W cm $^{-2}$, a static electric field of $E_S \geq 17.08$ and 7.26 kV cm $^{-1}$ for fluorobenzene and pyridazine, respectively, provides the larger contribution to the external field Hamiltonian $H_S + H_L$. If the interaction with the static field is dominant and much larger than the laser one, i.e., $E_S \mu \gg I \alpha^{ix} / 2 \epsilon_0 c$ with $i = y$ or z , the absolute minima of the potential $H_S + H_L$ are at (ϕ, β, χ) , with $\phi \rightarrow 0, 2\pi$ and $\chi \rightarrow \pi/2, 3\pi/2$. Thus, the wave function will be oriented toward the electric field direction with $\langle \cos^2 \theta \rangle \rightarrow \cos^2 \beta$ and $\langle \cos \theta_S \rangle \rightarrow 1$. However, these extremal points do not provoke any effect on the χ coordinate, because in the strong static field regime, the variation of $H_S + H_L$ as a function of χ represents a very shallow minimum and does not give rise to a localization of the wave function.

In the weak field regime, there are, for both molecules, several levels in addition to the ground state that are high-field seekers, and remaining levels are for low values of E_S low-field seekers. These levels present a mild wrong-way orientation with $\langle \cos \theta_S \rangle < 0$. Since in this regime the slope of the variation of the energy with E_S might be positive or negative, this favors the presence of sharp avoided crossings. As a consequence, the orientation of a pair of levels involved in an avoided crossings, i.e., $\langle \cos \theta_S \rangle$, suffers drastic variations over tiny ranges of the field strength. As the field strength is increased, we encounter the pendular regime: all the states are high-field-seekers, and they are strongly oriented along the static field direction. Indeed, for $E_S = 100$ kV cm $^{-1}$, we have that $\langle \cos \theta_S \rangle > 0.60$ and 0.70 for the considered fluorobenzene and pyridazine levels, respectively. In this regime, we still encounter avoided crossings but they are much wider. Due to the competition between both fields, these states do not achieve a significant alignment, see panels (g)–(i) in Fig. 7 and 8. We observe that $\langle \cos^2 \theta \rangle$ approaches $\cos^2 \beta$ in the strong field regime.

D. Orientation and 2-D alignment by means of perpendicular fields

External fields provide a tool to control the molecular dynamics: specifically it has been shown that an elliptically

polarized laser allows for *3D alignment* of asymmetric molecules, i.e., the system is aligned in all spatial directions.^{26,28,55,56} We show here that the combination of an electrostatic field with the linearly polarized laser gives rise to orientation in one direction and alignment in the other two. We hereby focus on the case $\beta = \pi/2$. In the strong static field regime, we have $\theta \rightarrow \pi/2$ and $\phi \rightarrow 0$, whereas, in order to decrease the energy the term $\sin^2 \chi$ in the laser Hamiltonian (Eq. (4)) should increase and approach one, i.e., $\chi \rightarrow \pi/2, 3\pi/2$. Then, the molecule will be fixed in space, and the wave function should be concentrated in the proximity of $\theta \sim \pi/2$, $\chi \sim \pi/2, 3\pi/2$, and $\phi \sim 0, 2\pi$. To demonstrate this behavior, we have computed the 1D probability density distribution in each one of the three Euler angles by integrating the square of the wave function in the other two angles. In Figs. 9(a)–9(c), these probability density distributions $\Theta(\theta) \sin \theta$, $\Phi(\phi)$, and $\Xi(\chi)$ are plotted as a function of θ , ϕ , and χ , respectively, for the ground state of pyridazine interacting with the orthogonal fields for different strengths. The probability density distributions for $E_S = 20$ kV cm $^{-1}$ and $I = 10^{11}$ W cm $^{-2}$ show the expected behavior, and this state presents a significant orientation along the X -axis of the LFF with $\langle \cos \theta_S \rangle = 0.749$ and $\langle \cos^2 \theta \rangle = 0.191$, whereas the alignment in the other two Euler angles is also pronounced and we get $\langle \cos^2 \chi \rangle = 0.143$ and $\langle \cos^2 \phi \rangle = 0.661$. A larger orientation is achieved if the static field strength is enhanced to $E_S = 50$ kV cm $^{-1}$ keeping the same laser intensity: $\langle \cos \theta_S \rangle = 0.849$ and $\langle \cos^2 \theta \rangle = 0.118$, for the distribution in χ and ϕ and we find $\langle \cos^2 \chi \rangle = 0.122$ and $\langle \cos^2 \phi \rangle = 0.723$, respectively. An opposite effect has the enhancement of the laser intensity to $I = 5 \times 10^{11}$ W cm $^{-2}$ and keeping $E_S = 20$ kV cm $^{-1}$. The orientation in θ is slightly reduced $\langle \cos \theta_S \rangle = 0.729$ and $\langle \cos^2 \theta \rangle = 0.222$, but $\langle \cos^2 \phi \rangle$ increases only to 0.682 , that is, the laser does not affect the azimuthal angle and in Fig. 9(b) the distribution $\Phi(\phi)$ is indistinguishable compared to the corresponding one for $E_S = 20$ kV cm $^{-1}$ and $I = 10^{11}$ W cm $^{-2}$. The alignment with respect to χ becomes stronger $\langle \cos^2 \chi \rangle = 0.075$. Of course, one should keep in mind that this effect is very sensitive to the fields strengths and their configuration, as well as the molecular

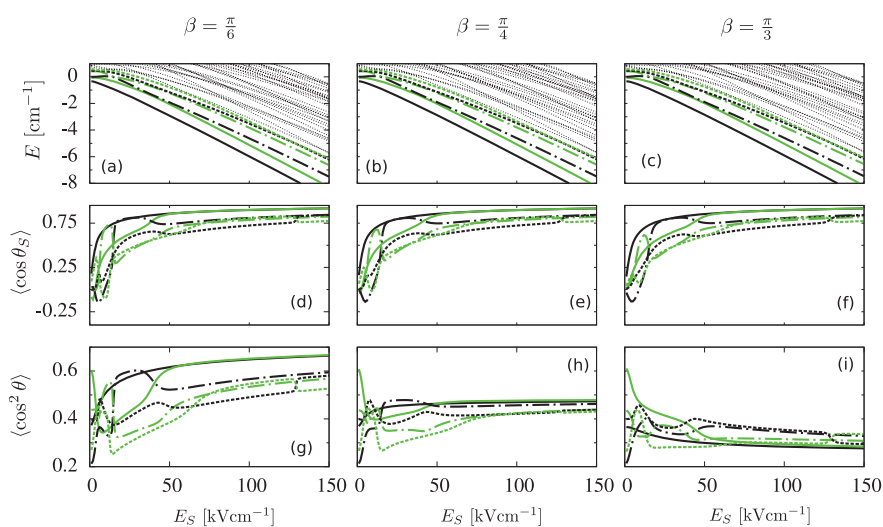


FIG. 8. Same as Fig. 7 but for pyridazine.

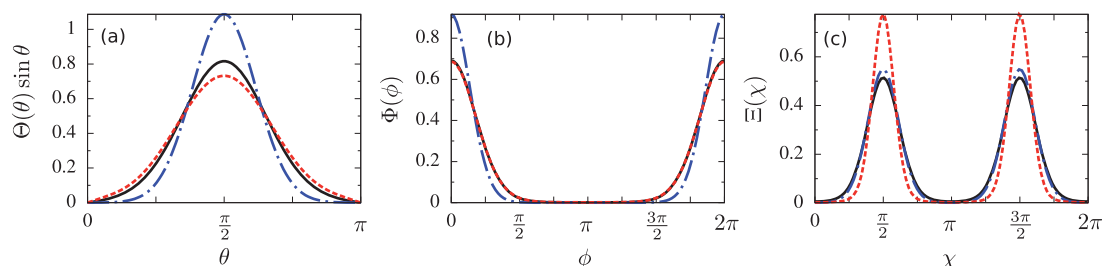


FIG. 9. One-dimensional probability density distribution in each Euler angle for the ground state of pyridazine for (a) $E_S = 20 \text{ kV cm}^{-1}$ and $I = 10^{11} \text{ W cm}^{-2}$ (solid), (b) $E_S = 50 \text{ kV cm}^{-1}$ and $I = 10^{11} \text{ W cm}^{-2}$ (dashed-dotted), and (c) $E_S = 20 \text{ kV cm}^{-1}$ and $I = 5 \times 10^{11} \text{ W cm}^{-2}$ (dashed).

parameters, i.e., the permanent dipole moment, polarizability anisotropies, and rotational constants. For fluorobenzene, a similar phenomenon could be found, but the wave function shows a slightly less pronounced orientation and alignment. If the fields are not perpendicular, the competition between both interactions will reduce the alignment achieved in the ϕ and χ angles.

E. Influence of the inclination of the fields

The inclination of the fields plays an essential role on their impact on the rotational dynamics of the system, and as already discussed, the symmetries are drastically modified as β is varied. Indeed, β is another parameter in the Hamiltonian that enriches the physical phenomena observed, and its variation can provoke the appearance of avoided crossings between energetically adjacent states of the same symmetry. For pyridazine, we represent in Figs. 10(a) the energy, 10(b) $\langle \cos \theta_S \rangle$, 10(c) $\langle \cos^2 \theta \rangle$, and 10(d) $\langle M^2 \rangle$, as a function of β with $E_S = 20 \text{ kV cm}^{-1}$ and $I = 10^{11} \text{ W cm}^{-2}$, for the previous set of states with K and $M + K + q$ even and following the same labeling as in Sec. III B. For these field strengths, the static electric field interaction dominates over the laser field interaction, similar to Fig. 8. In general, the energies show a smooth behavior as β is varied, and depending on the state, they exhibit an increasing or decreasing trend, see Fig. 10(a), e.g., the ground state energy increases from -5 cm^{-1} to -4.6 cm^{-1} for $\beta = 0$ to $\pi/2$, respectively. The energy gap between the first four states is large enough to prevent the presence of avoided crossings among them, the first avoided crossing being between the fourth and fifth excited states, $2_{02}1$ and $2_{21}2$, for $\beta \approx 1.096$ (close to $3\pi/8$). Regarding the orientation and alignment along the electric and laser fields directions, respectively, different behaviors are observed. The ground state keeps a significant and approximately constant orientation with $\langle \cos \theta_S \rangle > 0.75$ for any value of β ; as the electric field is rotated away from the Z-axis, the ground state probability density follows this field. In contrast to this, since the laser interaction is not dominant, its alignment is drastically reduced from $\langle \cos^2 \theta \rangle \approx 0.75$ to 0.22 when β increases from 0 to $\pi/2$. For any field configuration, the $1_{01}1$ level shows a moderate orientation and alignment with a plateau-like behavior for $\langle \cos \theta_S \rangle$ and $\langle \cos^2 \theta \rangle$. Compared to the ground state, the $2_{02}2$ level presents a similar orientation and alignment for $\beta = 0$, but a very different evolution of these features as β is varied, and for $\beta = \pi/2$, it keeps a moderate alignment and a weak

orientation. For parallel fields, M is a good quantum number, and a non-parallel configuration allows the interaction and mixing between states with different field-free M -value. This phenomenon is illustrated by means of the expectation value $\langle M^2 \rangle$ in Fig. 10(d). As the angle β is increased, the evolution of $\langle M^2 \rangle$ strongly depends on the character of the corresponding level. For the ground state, $\langle M^2 \rangle$ increases as β is enhanced, and for $\beta = \pi/2$, it reads $\langle M^2 \rangle = 0.746$. The $\langle M^2 \rangle$ value of the $1_{01}1$ level is close to 1 for $\beta \leq \pi/8$, but for larger values of β decreases to 0.6 for $\beta = \pi/2$. In contrast, for the other analyzed level with $M = 1$, $2_{02}1$, the interaction with states with larger M is dominant for $\beta > \pi/4$, and $\langle M^2 \rangle = 3$ for $\beta = \pi/2$. For the considered $M = 2$ levels, $2_{02}2$ and $2_{21}2$, the mixing with states with lower M is dominant, and $\langle M^2 \rangle$ is smaller than in the parallel configuration, e.g., for the $2_{02}2$ level and $\beta = \pi/2$, we have $\langle M^2 \rangle = 0.4063$.

With varying inclination angle β between both fields, the avoided crossings leave their fingerprints in the relevant observable. For pyridazine, the states $2_{02}0$ and $2_{02}1$ belong to different irreducible representations for $\beta = 0$ and $\pi/2$, and to the same one for $0 < \beta < \pi/2$. (Note that the labeling of the states has been done in the same way as in Fig. 8). For non-collinear fields, they suffer an avoided crossing which we have traced for $I = 10^{10} \text{ W cm}^{-2}$ and different values of β in Fig. 11. The results for the minimal energetical width $\Delta E = |E_{2_{02}0} - E_{2_{02}1}|$ and the electrostatic field strength at which this minimum appears are presented in Figs. 11(a) and 11(b), respectively, as the angle β is varied. For perpendicular fields,

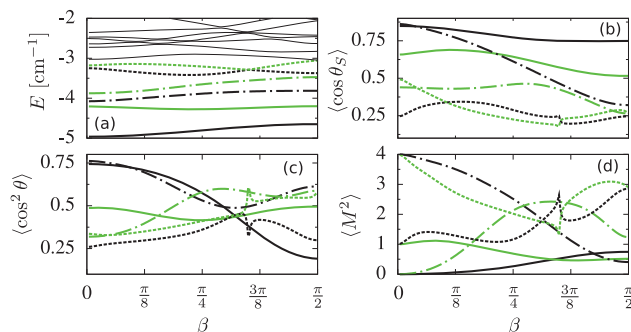


FIG. 10. (a) Energies and expectation values, (b) $\langle \cos \theta_S \rangle$, (c) $\langle \cos^2 \theta \rangle$, and (d) $\langle M^2 \rangle$ for pyridazine in the presence of a static field $E_S = 20 \text{ kV cm}^{-1}$ and a laser field $I = 10^{11} \text{ W cm}^{-2}$ as a function of β for the energetically lowest states with both $M + q + K$ and K even. The states are $0_{00}0$ (solid black), $1_{01}1$ (solid green), $2_{02}2$ (dashed-dotted black), $1_{01}0$ (dashed-dotted green), $2_{02}1$ (dashed black), and $2_{21}2$ (dashed green).

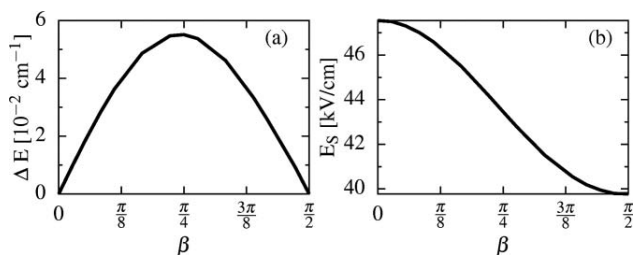


FIG. 11. Width ΔE (a) and electrostatic field strength E_S (b) at the avoided crossing taking place between the states 2_{020} and 2_{021} for pyridazine, for $I = 10^{10} \text{ W cm}^{-2}$ and different inclination angles β .

the levels suffer a real crossing and are accidentally degenerate $\Delta E = 0$ for $I = 10^{10} \text{ W cm}^{-2}$ and $E_S = 39.78 \text{ kV cm}^{-1}$, whereas for $\beta = 0$, they possess a different magnetic quantum number M and exhibit a symmetry-related crossing but now for $E_S = 47.55 \text{ kV cm}^{-1}$. As we see in panel (a), ΔE increases till it reaches the maximal value of $5.33 \times 10^{-2} \text{ cm}^{-1}$ for $\beta = \pi/4$, decreasing afterwards to 0 for $\beta = \pi/2$. The static field strength at which the avoided crossing takes places, see panel (b), decreases monotonously as β increases. Indeed, the variation of E_S with β is well matched by the following function $3.88 \cos(2.06\beta) + 43.67$, and it is reduced by 7.74 kV cm^{-1} when β goes from 0 to $\pi/2$.

IV. CONCLUSIONS

In this work, we have investigated the impact of a combination of an electrostatic and a non-resonant linearly polarized laser field on the rotational spectrum of asymmetric top molecules. This study has been performed in the framework of the Born-Oppenheimer approximation considering that the vibrational and electronic dynamics are not affected by the external fields. Our analysis is restricted to a rigid rotor description of molecules having their permanent dipole moment parallel to one axis of inertia, and the polarizability tensor is diagonal in the basis formed by the principal axis of inertia. We have analyzed the symmetries and irreducible representations of the Hamiltonian for the different field configurations. Numerically, each irreducible representation has been treated independently, by expanding the wave function in a basis respecting the corresponding symmetries. This procedure allows us to distinguish the avoided crossings from genuine ones involving states of the same and different symmetry, respectively. The presence of the avoided crossings in the field-dressed spectrum affects the directional properties of the molecule; they might significantly alter the spectroscopy as well as the steric dynamics of the system. The labeling of a certain state and the passage through the avoided crossing that it suffers depend on the way the symmetries are broken, i.e., on the temporal sequence followed to turn on the fields, which should be taken into account to determine the adiabaticity of a certain process.

The richness and variety of the resulting field-dressed rotational dynamics have been illustrated by analyzing the energetic shifts, as well as the orientation, alignment, and the hybridization of the angular motion. As prototype example, we have investigated the fluorobenzene and pyridazine

molecules. For three field configurations, the evolution of a certain set of states belonging to a certain symmetry has been analyzed with varying electrostatic field strength or laser intensity. Different types of behaviors were observed, depending on the dominant field interaction as well as on the considered molecular system, through its rotational constant, dipole moment, and polarizability tensor. Due to the competition between both interactions, the features of the rotational spectrum are significantly changed as the field parameters are modified. In the strong laser field regime, the presence of an intense electric field reduces the orientation of the ground state, especially as β is rotated from zero to larger values, and highly excited levels only present a very weak alignment. Whereas, if the electrostatic field is dominant, the states are oriented along its direction, and they only present a mild alignment along the Z -axis in the LFF. We have shown that a proper combination of non-collinear fields gives rise to a strong orientation along the static field direction together with a 2D-alignment on the other two axes of the molecule. In particular for $\beta = \pi/2$, the molecular plane is fixed onto the XY -plane of the LFF, and the orientation is along the X -axis. Finally, we have also investigated the role played by the inclination angle of the fields β , by analyzing the spectral properties of several states; the loss of the azimuthal symmetry has been quantified by the expectation value $\langle M^2 \rangle$, which is a conserved magnitude for parallel fields. An avoided crossing between two states has been traced as β is modified; the electrostatic field strength at which it takes places varies within a few kV cm^{-1} , and the corresponding energetical width will allow us to compute the adiabaticity of the crossing once the variation of the field strength is known. A natural extension to this work would be to consider other molecular systems, especially different conformers of the same molecule, looking for specific phenomena that might help to distinguish between the molecules.

ACKNOWLEDGMENTS

Financial support by the Spanish project FIS2008-02380 (MICINN) (Grant Nos. FQM-2445 and FQM-4643) (Junta de Andalucía) is gratefully appreciated. J.J.O. and R.G.F. belong to the Andalusian research group FQM-207. J.J.O. acknowledges the support of ME under the program FPU. We thank J. Küpper for fruitful discussions.

APPENDIX: WIGNER AND HAMILTONIAN MATRIX ELEMENTS

The field-free eigenstates of a symmetric top molecule, see Eq. (5), are proportional to the Wigner matrix elements, $D_{M,K}^J(\Omega)$, which are defined as

$$D_{M,K}^J(\Omega) = e^{-iM\phi} d_{M,K}^J(\theta) e^{-iK\chi}, \quad (\text{A1})$$

where $d_{M,K}^J(\theta)$ are the reduced Wigner matrix elements.⁴⁵ To evaluate the matrix elements of the Hamiltonian, we have used the following properties of the Wigner matrix: the complex conjugate,

$$D_{M,K}^{J\dagger}(\Omega) = (-1)^{M-K} D_{-M,-K}^J(\Omega), \quad (\text{A2})$$

the relation between the Wigner reduced matrix elements that reads

$$d_{m',m}^j(\theta) = (-1)^{m-m'} d_{m,m'}^j(\theta), \quad (\text{A3})$$

$$d_{m',m}^j(\theta) = (-1)^{m'-m} d_{-m',-m}^j(\theta), \quad (\text{A4})$$

$$d_{m',m}^j(\theta) = d_{m,m'}^j(-\theta), \quad (\text{A5})$$

and the integral of the triple product of Wigner matrices,

$$\int d\Omega D_{-K,-M}^J(\Omega) D_{K_1,M_1}^{J_1}(\Omega) D_{K_2,M_2}^{J_2}(\Omega) = 8\pi^2 \begin{pmatrix} J_1 & J_2 & J \\ M_1 & M_2 & -M \end{pmatrix} \begin{pmatrix} J_1 & J_2 & J \\ K_1 & K_2 & -K \end{pmatrix}, \quad (\text{A6})$$

where $\begin{pmatrix} j_1 & j_2 & j_3 \\ m_1 & m_2 & m_3 \end{pmatrix}$ are the $3J$ Symbols.

For completeness, we provide the non-zero matrix elements appearing in the evaluation of the full Hamiltonian. For the field-free Hamiltonian H_r (Eq. (2)), we have

$$\begin{aligned} \langle J'K'M'|H_r|JKM\rangle &= (AJ(J+1) + CK^2)\delta_{J',J}\delta_{K',K}\delta_{M',M} \\ &+ B\sqrt{J(J+1) - K(K+1)} \\ &\times \sqrt{J(J+1) - (K+1)(K+2)}\delta_{J',J}\delta_{|K'-K|,2}\delta_{M',M}, \end{aligned}$$

where A , B , and C are defined as $A = (B_x + B_y)/2$, $B = (B_x - B_y)/4$, and $C = (2B_z - B_x - B_y)/2$.⁵⁷ The Stark interaction H_S (Eq. (3)), rewritten in terms of Wigner matrix elements, is given by

$$\begin{aligned} H_S &= -\mu E_S \cos\theta_S = -\mu E_S h_S \\ &= -\mu E_S \left(\cos\beta D_{00}^1(\Omega) + \sin\beta \sqrt{\frac{1}{2}} (D_{-1,0}^1(\Omega) - D_{1,0}^1(\Omega)) \right). \end{aligned} \quad (\text{A7})$$

Thus, the non-zero matrix elements are

$$\begin{aligned} \langle JK M|h_S|JK M\rangle &= \frac{MK}{J(J+1)} \cos\beta, \\ \langle JK M+1|h_S|JK M\rangle &= \frac{K \sin\beta}{2J(J+1)} \sqrt{J(J+1) - M(M+1)}, \\ \langle J+1KM|h_S|JK M\rangle &= \cos\beta \sqrt{\frac{[(J+1)^2 - M^2][(J+1)^2 - K^2]}{(2J+3)(2J+1)(J+1)^2}}, \\ \langle J+1KM+1|h_S|JK M\rangle &= -\frac{\sin\beta \sqrt{[(J+1)^2 - K^2](J+M+1)(J+M+2)}}{2(J+1)\sqrt{(2J+3)(2J+1)}}, \\ \langle J+1KM-1|h_S|JK M\rangle &= -\langle J+1K-M+1|h_S|JK -M\rangle. \end{aligned}$$

The laser Hamiltonian H_L (Eq. (3)) takes now the form

$$\begin{aligned} H_L &= -\frac{I}{2\epsilon_0 c} h_L = -\frac{I}{2\epsilon_0 c} \left(\frac{\alpha^{zx} + \alpha^{zy}}{3} D_{00}^2(\Omega) \right. \\ &\left. - \frac{\alpha^{yx}}{\sqrt{6}} [D_{02}^2(\Omega) + D_{0-2}^2(\Omega)] + \frac{\alpha^{zx} + \alpha^{yx}}{3} \right). \end{aligned} \quad (\text{A8})$$

In this expression, we have omitted the terms which only introduce a shift in the energy. Performing the integrals corresponding to each term, we get

$$\begin{aligned} \langle JK M|h_L|JK M\rangle &= \left(\frac{\alpha^{zx} + \alpha^{zy}}{3} \right) \\ &\times \frac{[3M^2 - J(J+1)][3K^2 - J(J+1)]}{2J(J+1)(2J-1)(2J+3)} + \frac{\alpha^{zx} + \alpha^{yx}}{3}, \\ \langle J+1KM|h_L|JK M\rangle &= (\alpha^{zx} + \alpha^{zy}) \\ &\times \frac{MK\sqrt{[(J+1)^2 - M^2][(J+1)^2 - K^2]}}{J(J+1)(J+2)\sqrt{(2J+3)(2J+1)}}, \\ \langle J+2KM|h_L|JK M\rangle &= \left(\frac{\alpha^{zx} + \alpha^{zy}}{2} \right) \sqrt{[(J+2)^2 - K^2][(J+1)^2 - K^2]} \\ &\times \frac{\sqrt{[(J+2)^2 - M^2][(J+1)^2 - M^2]}}{(J+1)(J+2)(2J+3)\sqrt{(2J+1)(2J+5)}}, \end{aligned}$$

$$\begin{aligned} \langle JK M|h_L|JK + 2M\rangle &= -\alpha^{yx} [3M^2 - J(J+1)] \\ &\times \frac{\sqrt{[J^2 - (K+1)^2](J-K)(J+K+2)}}{2J(J+1)(2J+3)(2J-1)}, \\ \langle J+1KM|h_L|JK + 2M\rangle &= -\alpha^{yx} M \sqrt{[(J+1)^2 - M^2]} \\ &\times \frac{\sqrt{[(J-K)^2 - 1](J-K)(J+K+2)}}{2J(J+1)(J+2)\sqrt{(2J+1)(2J+3)}}, \end{aligned}$$

$$\begin{aligned} \langle J+2KM|h_L|JK + 2M\rangle &= -\alpha^{yx} \sqrt{[(J+2)^2 - M^2][(J+1)^2 - M^2]} \\ &\times \frac{\sqrt{[(J-K)^2 - 1](J-K)(J-K+2)}}{4(J+1)(J+2)(2J+3)\sqrt{(2J+1)(2J+5)}}, \end{aligned}$$

$$\langle J'K'M'|h_L|JK M\rangle = \langle J' - K' - M'|h_L|J - K - M\rangle.$$

¹H. J. Loesch and A. Remscheid, *J. Chem. Phys.* **93**, 4779 (1990).

²P. R. Brooks, *Science* **193**, 11 (1976).

³D. H. Parker and R. B. Bernstein, *Annu. Rev. Phys. Chem.* **40**, 561 (1989).

⁴T. D. Hain, R. M. Moision, and T. J. Curtiss, *J. Chem. Phys.* **111**, 6797 (1999).

⁵K. F. Lee, D. M. Villeneuve, P. B. Corkum, A. Stolow, and J. G. Underwood, *Phys. Rev. Lett.* **97**, 173001 (2006).

⁶M. D. Poulsen, T. Ejdrup, H. Stapelfeldt, E. Hamilton, and T. Seideman, *Phys. Rev. A* **73**, 033405 (2006).

⁷L. Holmegaard, J. H. Nielsen, I. Nevo, H. Stapelfeldt, F. Filsinger, J. Küpper, and G. Meijer, *Phys. Rev. Lett.* **102**, 023001 (2009).

⁸F. Filsinger, J. Küpper, G. Meijer, L. Holmegaard, J. H. Nielsen, I. Nevo, J. L. Hansen, and H. Stapelfeldt, *J. Chem. Phys.* **131**, 064309 (2009).

⁹I. Nevo, L. Holmegaard, J. Nielsen, J. L. Hansen, H. Stapelfeldt, F. Filsinger, G. Meijer, and J. Küpper, *Phys. Chem. Chem. Phys.* **11**, 9912 (2009).

¹⁰D. T. Moore, L. Oudejans, and R. E. Miller, *J. Chem. Phys.* **110**, 197 (1999).

¹¹R. Kanya and Y. Ohshima, *J. Chem. Phys.* **121**, 9489 (2004).

- ¹²L. Holmegaard, J. L. Hansen, L. Kalhøj, S. L. Kragh, H. Stapelfeldt, F. Filsinger, J. Küpper, G. Meijer, D. Dimitrovski, M. Abu-samha, C. P. J. Martiny, and L. Madsen, *Nat. Phys.* **6**, 428 (2010).
- ¹³J. L. Hansen, L. Holmegaard, L. Kalhøj, S. L. Kragh, H. Stapelfeldt, F. Filsinger, G. Meijer, J. Küpper, D. Dimitrovski, M. Abu-samha, C. P. J. Martiny, and L. B. Madsen, *Phys. Rev. A* **83**, 023406 (2011).
- ¹⁴V. Aquilanti, M. Bartolomei, F. Pirani, D. Cappelletti, and F. Vecchiocattivi, *Phys. Chem. Chem. Phys.* **7**, 291 (2005).
- ¹⁵P. R. Brooks and E. M. Jones, *J. Chem. Phys.* **45**, 3449 (1966).
- ¹⁶F. J. Aoiz, B. Friedrich, V. J. Herrero, V. S. Rábanos, and J. E. Verdasco, *Chem. Phys. Lett.* **289**, 132 (1998).
- ¹⁷R. Zare, *Science* **20**, 1875 (1998).
- ¹⁸M. Wu, R. J. Bemish, and R. E. Miller, *J. Chem. Phys.* **101**, 9447 (1994).
- ¹⁹R. Baumfalk, N. H. Nahler, and U. Buck, *J. Chem. Phys.* **114**, 4755 (2001).
- ²⁰A. J. van den Brom, T. P. Rakitzis, and M. H. M. Janssen, *J. Chem. Phys.* **121**, 11645 (2004).
- ²¹M. L. Lipciuc, A. J. van den Brom, L. Dinu, and M. H. M. Janssen, *Rev. Sci. Instrum.* **76**, 123103 (2005).
- ²²P. Reckenthaeler, M. Centurion, W. Fuß, S. A. Trushin, F. Krausz, and E. E. Fill, *Phys. Rev. Lett.* **102**, 213001 (2009).
- ²³J. Levesque, Y. Mairesse, N. Dudovich, H. Pépin, J.-C. Kieffer, P. B. Corkum, and D. M. Villeneuve, *Phys. Rev. Lett.* **99**, 243001 (2007).
- ²⁴R. Velotta, N. Hay, M. B. Mason, M. Castillejo, and J. P. Marangos, *Phys. Rev. Lett.* **87**, 183901 (2001).
- ²⁵M. D. Poulsen, E. Péronne, H. Stapelfeldt, C. Z. Bisgaard, S. S. Viftrup, E. Hamilton, and T. Seideman, *J. Chem. Phys.* **121**, 783 (2004).
- ²⁶J. J. Larsen, K. Hald, N. Bjerre, H. Stapelfeldt, and T. Seideman, *Phys. Rev. Lett.* **85**, 2470 (2000).
- ²⁷M. Artamonov and T. Seideman, *J. Chem. Phys.* **128**, 154313 (2008).
- ²⁸M. Artamonov and T. Seideman, *Phys. Rev. A* **82**, 023413 (2010).
- ²⁹S. S. Viftrup, V. Kumarappan, S. Trippel, H. S.E. Hamilton, and T. Seideman, *Phys. Rev. Lett.* **99**, 143602 (2007).
- ³⁰S. S. Viftrup, V. Kumarappan, L. Holmegaard, C. Z. Bisgaard, H. Stapelfeldt, M. Artamonov, E. Hamilton, and T. Seideman, *Phys. Rev. A* **79**, 023404 (2009).
- ³¹A. Schwettman, J. Franklin, K. R. Overstreet, and J. P. Shaffer, *J. Chem. Phys.* **123**, 194305 (2005).
- ³²J. Bulthuis, J. Miller, and H. J. Loesch, *J. Phys. Chem. A* **101**, 7684 (1997).
- ³³W. Kong and J. Bulthuis, *J. Phys. Chem. A* **104**, 1055 (2000).
- ³⁴R. Kanya and Y. Ohshima, *Phys. Rev. A* **70**, 013403 (2004).
- ³⁵M. Härtelt and B. Friedrich, *J. Chem. Phys.* **128**, 224313 (2008).
- ³⁶I. N. Kozin and R. N. Roberts, *J. Chem. Phys.* **118**, 10523 (2003).
- ³⁷W. Kim and P. M. Felker, *J. Chem. Phys.* **108**, 6763 (1998).
- ³⁸B. Friedrich and D. Herschbach, *J. Phys. Chem. A* **103**, 10280 (1999).
- ³⁹B. Friedrich and D. R. Herschbach, *J. Chem. Phys.* **111**, 6157 (1999).
- ⁴⁰L. Cai, J. Marango, and B. Friedrich, *Phys. Rev. Lett.* **86**, 775 (2001).
- ⁴¹C. A. Arango and G. S. Ezra, *Int. J. Bifurcation Chaos Appl. Sci. Eng.* **18**, 1127 (2008).
- ⁴²J. J. Omiste, M. Gärtner, P. Schmelcher, R. González-Férez, L. Holmegaard, J. H. Nielsen, H. Stapelfeldt, and J. Küpper, *Phys. Chem. Chem. Phys.* (in press).
- ⁴³N. Moiseyev, M. Šindelka, and L. S. Cederbaum, *J. Phys. B* **41**, 221001 (2008).
- ⁴⁴M. Šindelka, N. Moiseyev, and L. S. Cederbaum, *J. Phys. B* **44**, 045603 (2011).
- ⁴⁵R. N. Zare, *Angular Momentum: Understanding Spatial Aspects in Chemistry and Physics* (Wiley, New York, 1988).
- ⁴⁶C. M. Dion, A. Keller, O. Atabek, and A. D. Bandrauk, *Phys. Rev. A* **59**, 1382 (1999).
- ⁴⁷N. E. Henriksen, *Chem. Phys. Lett.* **312**, 196 (1999).
- ⁴⁸T. Seideman and E. Hamilton, *Nonadiabatic Alignment by Intense Pulses: Concepts, Theory, and Directions*, Advances in Atomic, Molecular, and Optical Physics Vol. 52 (Academic, New York, 2005), p. 289.
- ⁴⁹G. W. King, R. M. Hainer, and P. C. Cross, *J. Chem. Phys.* **11**, 27 (1943).
- ⁵⁰B. Bak, D. Christensen, L. Hansen-Nygaard, and E. Tannenbaum, *J. Chem. Phys.* **26**, 134 (1957).
- ⁵¹K. J. Miller, *J. Am. Chem. Soc.* **112**, 8543 (1990).
- ⁵²D. G. de Kowalewski, P. Kökeritz, and H. Selen, *J. Chem. Phys.* **31**, 1438 (1959).
- ⁵³K. K. Innes, I. G. Ross, and W. R. Moomaw, *J. Mol. Spectrosc.* **132**, 492 (1988).
- ⁵⁴A. Hinchliffe and H. J. Soscùn M., *J. Mol. Struct.: THEOCHEM* **304**, 109 (1994).
- ⁵⁵H. Stapelfeldt and T. Seideman, *Rev. Mod. Phys.* **75**, 543 (2003).
- ⁵⁶A. Rouzée, S. Guérin, O. Faucher, and B. Lavorel, *Phys. Rev. A* **77**, 043412 (2008).
- ⁵⁷H. W. Kroto, *Molecular Rotation Spectra* (Dover, New York, 1992).

Cite this: *Phys. Chem. Chem. Phys.*, 2011, **13**, 18815–18824

www.rsc.org/pccp

PAPER

Theoretical description of adiabatic laser alignment and mixed-field orientation: the need for a non-adiabatic model

J. J. Omiste,^a M. Gärttner,^b P. Schmelcher,^c R. González-Férez,^{*a}
L. Holmegaard,^{de} J. H. Nielsen,^f H. Stapelfeldt^{dg} and J. Küpper^{ehi}

Received 15th April 2011, Accepted 1st June 2011

DOI: 10.1039/c1cp21195a

We present a theoretical study of recent laser-alignment and mixed-field-orientation experiments of asymmetric top molecules. In these experiments, pendular states were created using linearly polarized strong ac electric fields from pulsed lasers in combination with weak electrostatic fields. We compare the outcome of our calculations with experimental results obtained for the prototypical large molecule benzonitrile (C_7H_5N) [J. L. Hansen *et al.*, *Phys. Rev. A*, 2011, **83**, 023406.] and explore the directional properties of the molecular ensemble for several field configurations, *i.e.*, for various field strengths and angles between ac and dc fields. For perpendicular fields one obtains pure alignment, which is well reproduced by the simulations. For tilted fields, we show that a fully adiabatic description of the process does not reproduce the experimentally observed orientation, and it is mandatory to use a diabatic model for population transfer between rotational states. We develop such a model and compare its outcome to the experimental data confirming the importance of non-adiabatic processes in the field-dressed molecular dynamics.

1 Introduction

Controlling molecular motions has direct impact in a wide variety of molecular sciences, including stereo-chemistry,^{1–4} molecular-frame investigations of geometric and electronic properties, such as photoelectron angular distributions^{5–7} and high-harmonic generation,^{8,9} as well as for diffractive imaging of gas-phase molecules,^{10,11} aiming at recording the “molecular movie”.¹² Recently, there has been tremendous progress in the control of the translational¹³ and rotational^{14–17} motions of even complex molecules. For extremely well controlled ultracold alkali dimers, direct quantum effects on the stereodynamics of molecular reactions have recently been observed.¹⁸

Angular confinement of molecular ensembles is referred to as alignment—the confinement of molecule-fixed axes along laboratory-fixed axes—and orientation—adding a well-defined direction. Traditionally, these two levels of angular control have been separated: strong ac fields from pulsed lasers have been used to create alignment,¹⁴ whereas state-selection¹⁹ and brute-force orientation using strong dc electric fields^{20,21} have been used to create orientation (which typically also creates alignment). About a decade ago it was realized that strong simultaneous alignment and orientation could be created using combined ac and dc electric fields.^{22,23} This has been experimentally verified in a few cases.^{24–26} Adding methods to control the translational motion one can perform a quantum-state selection before the alignment and orientation experiment.^{13,27,28} This two-step approach has allowed the creation of unprecedented degrees of one-dimensional (1D) and three-dimensional (3D) alignment and orientation even for complex asymmetric top molecules.^{6,15,29–31}

Theoretical studies of the rotational spectra in the presence of combined electrostatic and non-resonant radiative fields have been restricted to linear and symmetric top molecules so far.^{22,23,32} Recently, some of us developed the theory for asymmetric top molecules in combined fields.³³ When the static and linearly polarized laser field directions are tilted with respect to one another, the symmetries of the corresponding Hamiltonian are significantly reduced. This is the most general field configuration, its theoretical treatment being most challenging. Since each external field interaction breaks different symmetries of the field-free Hamiltonian, the order in which the fields are

^a Instituto Carlos I de Física Teórica y Computacional and Departamento de Física Atómica, Molecular y Nuclear, Universidad de Granada, 18071 Granada, Spain.
E-mail: rogonzal@ugr.es

^b Max Planck Institut für Kernphysik, Saupfercheckweg 1, 69117 Heidelberg, Germany

^c Zentrum für Optische Quantentechnologien, Universität Hamburg, Luruper Chaussee 149, Hamburg, 22761, Germany

^d Department of Chemistry, University of Aarhus, 8000 Aarhus C, Denmark

^e Center for Free-Electron Laser Science, DESY, Notkestrasse 85, 22607 Hamburg, Germany

^f Department of Physics and Astronomy, University of Aarhus, 8000 Aarhus C, Denmark

^g Interdisciplinary Nanoscience Center (iNANO), University of Aarhus, 8000 Aarhus C, Denmark

^h Fritz-Haber-Institut der MPG, Faradayweg 4-6, 14195 Berlin, Germany

ⁱ University of Hamburg, Luruper Chaussee 149, 22761 Hamburg, Germany

turned on determines the evolution of the field-dressed rotational dynamics. The labels of the eigenstates at a certain field configuration obtained by adiabatic following depend on the path through parameter space, *i.e.*, monodromy is observed. For linear and symmetric top molecules exposed to external fields, the phenomena of classical and quantum monodromy have been encountered in the corresponding dressed spectra.^{34–36} The labeling procedure is also numerically very demanding due to the large amount of genuine and avoided crossings occurring between adjacent states as one of the field parameters is varied.

In the present work, we describe the recent experimental results obtained for the alignment and orientation of asymmetric top molecules in combined fields.^{6,15,29–31} In the framework of the rigid rotor approximation, we perform a full investigation of the field-dressed eigenstates for those field configurations considered in the experiment. The Schrödinger equation for the rotational/pendular states is solved separately for each irreducible representation by expanding the wave function in a basis with the correct symmetries. Our theoretical analysis also includes (i) a diabatic approximation to account for population transfer through the avoided crossings as the laser intensity is varied; (ii) the velocity distribution of the ions after the Coulomb explosion; and (iii) a volume effect model to describe the fact that not all the molecules feel the same laser intensity because the orienting and the detection laser pulses have finite spatial intensity profiles. The field-dressed eigenfunctions are weighted with the known relative state populations in the molecular beam.²⁹ Then, we compute the angular probability density functions for different field configurations and their velocity-mapping images (VMIs). The recently performed alignment and orientation experiment for benzonitrile (BN, C₇H₅N) molecules^{6,31} provides us with experimental data that are very well suited to present and discuss our theoretical model in a comparative study. We numerically compute the alignment and orientation for an ensemble of quantum-state selected benzonitrile molecules, and compare our results to the experimental data. For comparison with a cold thermal ensemble—without state selection—we also provide the corresponding results for a benzonitrile sample at 1 K. In particular, for perpendicular fields, we obtain good agreement between the computational and experimental results for the degree of alignment. For tilted fields, we show that a fully adiabatic description of the rotational/pendular dynamics cannot reproduce the experimental results for the mixed-field orientation of benzonitrile. When a diabatic model is implemented for the treatment of the avoided crossings, our theoretical study reproduces with reasonable accuracy the experimental degree of orientation. Hence, we demonstrate the impact of non-adiabatic processes on the field-dressed molecular dynamics. We have developed a general theoretical description of alignment and mixed-field orientation for asymmetric tops in long pulses of strong ac electric and weak dc fields.

The paper is organized as follows: in Section 2 the relevant experimental details are described. The theoretical model is presented in Section 3, which includes the discussion of the rigid rotor Hamiltonian and its symmetries, the diabatic model to treat the avoided crossings, the screen projection of the 3D probability densities and the experimental observables. The theoretical results for the alignment and orientation of a beam

of benzonitrile molecules are compared to the experimental data in Section 4. The conclusions and outlook are provided in Section 5.

2 Experimental details

A detailed description of the alignment and mixed-field orientation experiments is given elsewhere.^{6,29,31} Briefly, a pulsed, cold molecular beam of benzonitrile molecules seeded in helium is expanded from an Even–Lavie valve into vacuum. The molecular beam is skimmed before entering a 15 cm long electrostatic deflector 41 cm downstream from the nozzle. The deflector disperses the molecules in the beam according to their effective dipole moments, creating a vertically varying distribution of quantum states in the probe region 77 cm downstream from the nozzle. Alignment and orientation are induced by the dc electric field of the VMI spectrometer and by a strong Nd:YAG laser pulse (10 ns, 1064 nm) and probed using ion imaging of CN⁺ fragments following Coulomb explosion of benzonitrile with a strong ultrashort Ti:Sapphire laser pulse (30 fs, 800 nm, 5.4×10^{14} W cm⁻²). Alignment and orientation experiments were performed for the undeflected beam and for the quantum-state selected sample at a vertical height of 1.75 mm; see Fig. 2 in ref. 31 for details.

3 Theoretical model

An exact theoretical quantum description of the alignment and orientation experiments is very demanding, since it requires the solution of the corresponding time-dependent Schrödinger equation for each state populated in the molecular ensemble. Instead, we retreat to a quasi-static description parametric in the field strength and angles, and solve the time-independent Schrödinger equation for several field configurations. A diabatic model, based on the field-free symmetries, is used to account for the population transfer through the avoided crossings encountered as the YAG pulse intensity is varied.

3.1 The Hamiltonian

We consider a nonresonant laser field of intensity I and linearly polarized along the Z_L -axis of the laboratory fixed frame (LFF) (X_L, Y_L, Z_L) and a homogeneous electrostatic field of strength E_S contained in the $X_L Z_L$ -plane and forming an angle β with Z_L . The rigid rotor Hamiltonian of a polar asymmetric top molecule exposed to this field configuration is given by

$$H = J_{X_M}^2 B_{X_M} + J_{Y_M}^2 B_{Y_M} + J_{Z_M}^2 B_{Z_M} - E_S \mu \cos \theta_S - \frac{2\pi I}{c} (\alpha^{Z_M X_M} \cos^2 \theta + \alpha^{Y_M X_M} \sin^2 \theta \sin^2 \chi), \quad (1)$$

with B_{X_M} , B_{Y_M} , and B_{Z_M} being the rotational constants. The molecule or body fixed frame (MFF) (X_M, Y_M, Z_M) is defined so that the permanent electric dipole moment μ is parallel to the Z_M -axis. The LFF and the MFF are related by the Euler angles (ϕ, θ, χ) .³⁷ The polarizability tensor is diagonal in the MFF with components α_{ii} with $i = X_M, Y_M, Z_M$, and the interaction with the laser field depends on the polarizability anisotropies $\alpha^{ij} = \alpha_{jj} - \alpha_{ii}$, $i, j = X_M, Y_M, Z_M$. The angle

between the static electric field and the molecular Z_M -axis is θ_S with $\cos \theta_S = \cos \beta \cos \theta + \sin \beta \sin \theta \cos \phi$. This study is restricted to molecules with the permanent dipole moment parallel to one of the principal axes of inertia, as it is the case for benzonitrile.

Let us shortly summarize the approximations and assumptions made in the derivation of the Hamiltonian (1). We perform a non-relativistic description within the framework of the rigid rotor approximation, assuming that the electronic and vibrational structures are not affected by the external fields. In addition, we presuppose that the laser is non-resonant and that the inverse of the oscillation frequency is much larger than the rotational period of the molecular system and pulse duration. Thus, we can average over the rapid oscillations, so that the interaction of this field with the molecular dipole moment is zero, and only the interaction with the polarizability is left. Additionally, since the YAG laser pulse duration is much larger than the timescale of the rotational dynamics, we assume that the alignment and orientation processes are, in principle, adiabatic, and we take the time profile of the pulse as a constant equal to 1. The validity of this assumption will be discussed in detail through the paper. The spatial dependence of the laser intensity will also be taken into account by means of a volume effect model, see below.

The configuration of the fields determines the symmetries of the Hamiltonian (1). For the field-free case, they are given by the spatial group $SO(3)$ and the molecular point group D_2 —*i.e.*, the Fourgroup V —consisting of the identity and the two-fold rotations C_2^i around the MFF i -axis, with $i = X_M, Y_M$ and Z_M . The Schrödinger equation associated with the Hamiltonian (1) cannot be solved analytically, and only the total angular momentum, J , and its projection onto the Z_L -axis of the laboratory fixed frame, M , are good quantum numbers, whereas K , the projection of J onto the Z_M -axis of the molecular fixed frame, is not conserved. Since an external field defines a preferred direction in space, the symmetries of the corresponding Hamiltonian are reduced compared to the field-free case. Here we consider three field configurations. For a single static field parallel to the LFF- Z_L -axis, the symmetry operations are $C_2^{Z_M}$, any arbitrary rotation around the Z_L -axis and a reflection in any plane containing Z_L , thus, M is still conserved. For a certain $|M|$, there are 4 irreducible representations, and for $M \neq 0$ the states with M and $-M$ are degenerate. If the molecule is exposed to both fields, with the electric field being rotated away from the Z_L -axis, the azimuthal symmetry is lost and M ceases to be a good quantum number. In the perpendicular case, $\beta = 90^\circ$, the Hamiltonian (1) is invariant under $C_2^{Z_M}$, a rotation of π around the X_L -axis, and the reflection $\sigma_{X_L Z_L}$ ($X_L Z_L$ is the plane containing the fields); as a consequence there are 8 irreducible representations. For tilted fields with $\beta \neq 90^\circ$, two symmetries are left, $\sigma_{X_L Z_L}$ and $C_2^{Z_M}$, and the corresponding group has only 4 irreducible representations. For a detailed description and analysis of the symmetries for all possible situations, we refer the reader to the recent works.^{33,38}

The field-dressed eigenstates of an asymmetric top are characterized by the avoided crossings appearing between levels of the same symmetry as one of the parameters of the field

configuration, *i.e.*, E_S , I , or β , is varied. For non-collinear fields, the small amount of irreducible representations implies an eigenstate diagram with a high degree of complexity due to the large number of avoided crossings. Furthermore, a small degree of asymmetry on the inertia tensor facilitates the appearance of avoided crossings on the corresponding field-dressed states.³⁹ For the correct analysis of the computational results, these avoided crossings should be distinguished from genuine ones taking place between levels of different symmetries. Hence, the time-independent Schrödinger equation associated to the Hamiltonian (1) is solved for each irreducible representation by expanding the wave function in a basis that respects the corresponding symmetries.³³

The field-free states are identified by the quantum labels $J_{K_a K_c} M$, with J and M being good quantum numbers, and K_a and K_c the projections of J onto the Z_M -axis of the molecular fixed frame in the oblate and prolate limiting cases,⁴⁰ respectively. For reasons of addressability, we will denote the field dressed states by means of these field-free labels indicating if an adiabatic or diabatic picture has been used.

To illustrate the molecular dynamics in the state-selection process using the electric deflector, we plot the Stark energies and expectation value $\langle \cos \theta \rangle \equiv \langle J_{K_a K_c} M | \cos \theta | J_{K_a K_c} M \rangle$ of the populated states of benzonitrile in Fig. 1(a) and (b) as a function of the electrostatic field strength. This plot covers the range of electric field strengths present in the deflector. It includes 84 individual rotational states accounting for 98% of the population of the molecular ensemble. This level diagram shows a complex structure with both genuine and avoided crossings. In the weak electrostatic field regime, both high- and low-field seekers are encountered, whereas in the pendular limit,

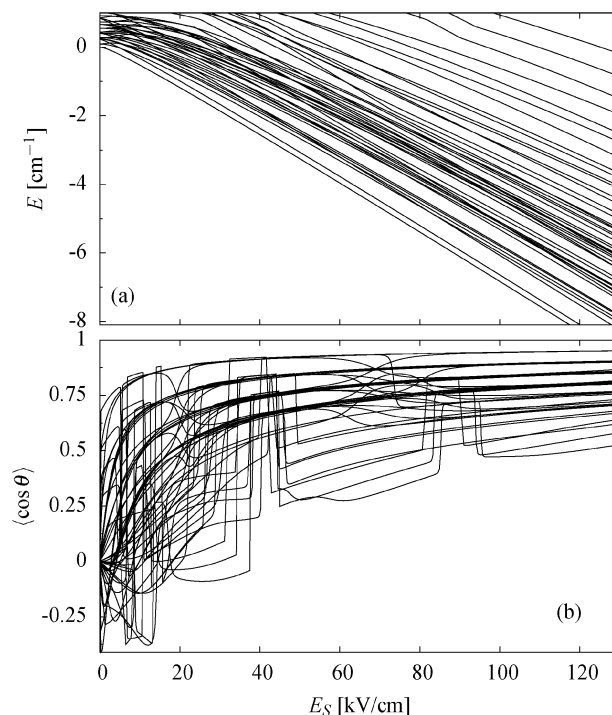


Fig. 1 (a) Energies and (b) expectation value $\langle \cos \theta \rangle$ as a function of the static field strength of the populated rotational states for benzonitrile.

and, in particular, in the regime of interest for the state selection experiment, all these levels are high-field-seekers. For $E_S > 50 \text{ kV cm}^{-1}$, most of these populated states present a significant orientation with $\langle \cos \theta \rangle > 0.5$, and 32% of them have a strong one with $\langle \cos \theta \rangle > 0.8$. The avoided crossings have a strong impact on the character of the involved states, and $\langle \cos \theta \rangle$ suffers large variations over tiny ranges of electrostatic field strengths, see Fig. 1(b). Note that the dc field applied in the orientation experiment, 286 V cm^{-1} , is very small on the scale of this figure.

3.2 The diabatic model

After entering the region of the extractor field, *i.e.*, the static electric field of the VMI spectrometer, the molecules are exposed to a laser field with increasing intensity (YAG laser pulse). As the laser intensity varies, a certain state may undergo several avoided crossings with levels of the same symmetry. The presence of these avoided crossings as well as their diabatic or adiabatic nature have a strong impact on the outcome of the experiment.

Several theoretical studies have analyzed in detail the character of such avoided crossings for molecules exposed to an electrostatic field by using different adiabaticity criteria.^{39,41–43} Their main and common conclusion is that the assumption of a fully adiabatic dynamics is incorrect as no general statement can be made about the character of the avoided crossings. These works suggest that an investigation of the character of the avoided crossings encountered as I is varied should be mandatory for a correct description of the experimental results. To do so, we use the following adiabatic passage criterion⁴⁴

$$\eta = \frac{\langle i | \frac{\partial H'}{\partial t} | j \rangle}{(E_i - E_j)^2} \ll 1, \quad (2)$$

where E_i and E_j are the eigenenergies for the states i and j and H' is the interaction term. Due to the large amount of avoided crossings in the laser field-dressed states, a systematic and detailed study of the adiabatic or diabatic character of all of them is unfeasible. Thus, we employ a simple diabatic model that provides an approximation to the dynamics, and determines the population transfer as the field parameters are varied. Note that some previous works have proposed different population transfer models based on symmetry considerations.^{41,42,45}

If the fields are not collinear and the polarization of the laser pulse is parallel to the Z_L -axis, the electrostatic field induces the coupling of states with different field-free values of the quantum number M . For the experimentally used electrostatic field strength, $E_S = 286 \text{ V cm}^{-1}$, the Stark interaction is much weaker than the laser field one. Thus, the hybridization of the quantum number M is so small that for a certain level $\langle M^2 \rangle$ remains almost unperturbed and equal to its field free value. Our diabatic model consists in assuming that (i) an avoided crossing between two levels with different field-free values of M is considered as being crossed diabatically; and (ii) crossings between levels with the same field-free value of M are passed adiabatically. To illustrate the validity of this diabatic model we have analyzed two exemplary avoided crossings of the field-dressed spectrum with $\beta = 45^\circ$ and $E_S = 286 \text{ V cm}^{-1}$ by means of the adiabatic passage parameter η in eqn (2).

In this case, the interaction term is given by $H' = -(2\pi I/c)(\alpha^{Z_M X_M} \cos^2 \theta + \alpha^{Y_M X_M} \sin^2 \theta \sin^2 \chi)$. For the time profile of the YAG pulse, we use $I(t) = I \exp(-t^2/(2\sigma^2))$ with $I = 5 \times 10^{11} \text{ W cm}^{-2}$ and $\sigma = 4.25 \text{ ns}$ (FWHM = 10 ns). Fig. 2(a), (d), (b), (e) and (c), (f) depict the energy, $\langle \cos^2 \theta \rangle$, and η as a function of I for the avoided crossings between the states $2_{02}0$ and $2_{02}1$, and $4_{04}4$ and $3_{21}1$, respectively. The levels $2_{02}0$ and $2_{02}1$ suffer an avoided crossing for $I \approx 3.5 \times 10^9 \text{ W cm}^{-2}$, with $\Delta E = 5.5 \times 10^{-4} \text{ cm}^{-1}$ and $\eta = 192$. Hence, we conclude that it is crossed diabatically. In contrast, for the avoided crossing among the states $4_{04}4$ and $3_{21}1$ occurring at $I \approx 3.82 \times 10^{10} \text{ W cm}^{-2}$, we obtain $\Delta E = 8.69 \times 10^{-2} \text{ cm}^{-1}$ and $\eta = 0.12$, which according to eqn (2) is an intermediate case—neither diabatic nor adiabatic. Using a fully adiabatic picture these two states are labeled $4_{04}4$ and $3_{21}1$, but using the diabatic model their labels are different since $\langle M^2 \rangle = 3.999$ and 4.007 , respectively, for $I = 3.6 \times 10^{10} \text{ W cm}^{-2}$, which explains the mixing between both levels. The criterion (2) or the Landau-Zener formula does not classify this avoided crossing as being diabatic or adiabatic, but within our approximation we consider it to be adiabatic.

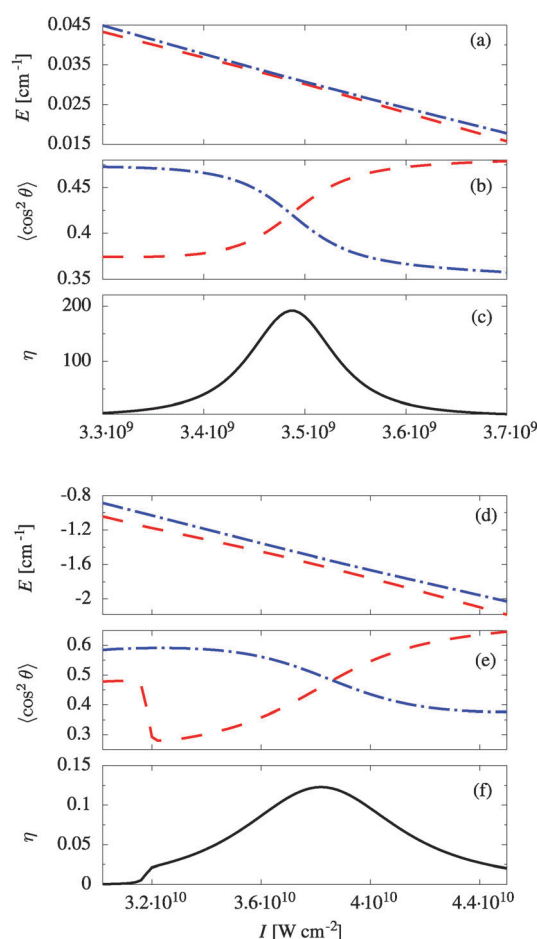


Fig. 2 Energy E ((a) and (d)), expectation value $\langle \cos^2 \theta \rangle$ ((b) and (e)), adiabatic passage criterion parameter (2) ((c) and (f)) for the levels $2_{02}0$ (dash-dotted line) and $2_{02}1$ (dashed line) states; and for the states $4_{04}4$ (dash-dotted line) and $3_{21}1$ (dashed line) states as a function of the YAG laser intensity, for $E_S = 286 \text{ V cm}^{-1}$ and $\beta = 45^\circ$. See the text for more details.

For tilted fields ($\beta \neq 90^\circ$), a certain avoided crossing may involve two states one being oriented and the other one antioriented. Hence, considering it as diabatic or adiabatic has significant consequences on the final result for orientation. Of course, our diabatic model is an approximation, since many avoided crossings are encountered that do not fall clearly into the class of adiabatic or diabatic crossings according to our adiabatic passage criterion. Generally, these cases would require solving the time-dependent Schrödinger equation including the time profile of the YAG pulse.

If the fields are perpendicular, the corresponding Hamiltonian (1) has 8 irreducible representations, and the amount of avoided crossings is significantly reduced compared to the $\beta \neq 90^\circ$ configuration. For the populated states of one irreducible representation, the expectation value $\langle \cos^2 \theta \rangle$ is plotted in Fig. 3 as a function of the laser intensity, for $E_S = 286 \text{ V cm}^{-1}$ and $\beta = 90^\circ$. The inset of this figure shows the energy levels in the strong-laser-field regime. For the laser intensities at which the experiment is performed, most of the populated levels are characterized by a pronounced alignment. In particular, we find $\langle \cos^2 \theta \rangle > 0.8$ for all these states and $I > 4.1 \times 10^{11} \text{ W cm}^{-2}$. Since, the character—regarding alignment—of two states that had previously suffered an avoided crossing is very similar, passing through it diabatically or adiabatically is not crucial for the final alignment result.

3.3 The projection of the probability density on the screen detector

When a molecule is multiply ionized using an intense ultrashort laser pulse, it dissociates due to Coulomb repulsion and the created ionic fragments are collected in a 2D space resolving detector. Within the axial recoil approximation the momentum of the CN^+ fragments created in this process is parallel to the C–CN bond direction before ionization. In order to calculate the screen image from the molecular wave functions we define a new reference frame (x, y, z) , containing the detector screen on its yz -plane. This frame is obtained by rotating the LFF by an angle $90^\circ - \beta$ about the Y_L -axis. Note that the electrostatic field is parallel to the x -axis, and the polarization vector of the linearly polarized YAG laser lies in the xz -plane, forming an angle β with the x -axis.

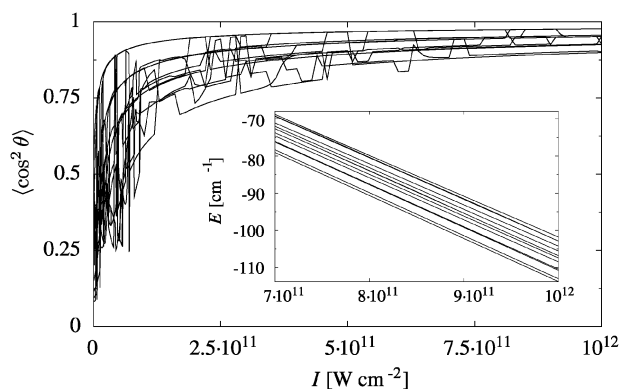


Fig. 3 Expectation value $\langle \cos^2 \theta \rangle$ and energies (inset panel) as a function of the YAG pulse intensity of the populated rotational states for benzonitrile, for $E_S = 286 \text{ V cm}^{-1}$ and $\beta = 90^\circ$. Only one irreducible representation is presented.

An asymmetric top molecule in a certain state, characterized by the wave function $\Psi_\gamma(\theta, \phi, \chi)$, with $\gamma = J_{K_a K_c} M$, is traveling towards a screen (velocity in the x -direction). Since the direction of the molecular dipole moment is independent of the angle χ , the probability for the molecular Z_M -axis to be oriented according to (θ, ϕ) is given by integrating in χ the absolute square of the wave function. The angular distribution $\rho_\gamma(\theta, \phi) d\Omega$ provides a measure of the amount of ions ejected into the solid angle $d\Omega = \sin \theta d\theta d\phi$. It is related to a spatial distribution on the 2D screen by $\rho_\gamma(y, z) dy dz = \rho_\gamma(\theta(y, z), \phi(y, z)) |J| \sin(\theta(y, z)) dy dz$, with J being the Jacobian of the transformation between the coordinates (θ, ϕ) and (y, z) . Assuming that all the ions have the same velocity, v in the absolute value, this transformation reads as

$$\begin{aligned} y &= a \sin \theta \sin \phi \\ z &= a (\cos \theta \sin \beta + \sin \theta \cos \phi \cos \beta), \end{aligned} \quad (3)$$

where $a = vt_f$, and t_f is the time of flight to reach the screen. Note that with the definition (3) for the y -coordinate, any point (y, z) corresponds to two different orientations (θ, ϕ) and $(\theta, 180^\circ - \phi)$. Thus, the screen image is the sum of two projection images, each obtained for a restricted range of ϕ .

An important ingredient that should be taken into account to obtain realistic screen images is the alignment selectivity of the probe laser. We approximate the effectivity of the dissociation process by the factor $\cos^2 \alpha$, with α being the angle between probe laser polarization and the C–CN bond direction.³⁰ Note that this approximation for modeling the probe selectivity as $\cos^2 \alpha$ is in accord with the experimental observations. Thus, the 2D screen spatial distribution is given by

$$\rho_\gamma^i(y, z) = \frac{\rho_\gamma(\theta(y, z), \phi(y, z))}{a \sqrt{a^2 - y^2 - z^2}} A_i(y, z) \quad (4)$$

where $A_i(y, z)$ is the mentioned alignment selectivity factor, and the index i indicates the probe pulse polarization. For a linearly polarized probe beam in the x -direction, we obtain $A_l(y, z) = 1 - y^2/a^2 - z^2/a^2$, and in the z -direction $A_p(y, z) = z/a$. For tilted fields ($\beta \neq 90^\circ$), a circularly polarized probe in the xz -plane ensures that any molecule is ionized and detected with the same probability independently of β , and it gives $A_c(y, z) = 1 - y^2/a^2$. The apparent singularity in eqn (4) at $y^2 + z^2 = a^2$ will disappear when we integrate over different ion recoil velocities.

So far we have assumed that all ions acquire the same recoil velocity. Experimentally, however, they follow a certain distribution $D(a)$, which is assumed to have only nonzero values at positive velocities. The screen image is obtained by averaging over all these velocities with their corresponding weights as

$$P_\gamma^i(y, z) = \int_0^\infty \rho_\gamma^i(y, z; a) D(a) da$$

with $i = l, p$ and c depending on the probe polarization. The experimental velocity distribution $D(a)$ for the CN^+ ions created in the Coulomb explosion of benzonitrile is shown in Fig. 4. The second and third peaks are the two Coulomb explosion channels relevant for determining the orientation of the C–CN axis. The two peaks are fitted to a combination of two Gaussian functions, after subtraction of the background, and used further on in the model. Since a is not the velocity but

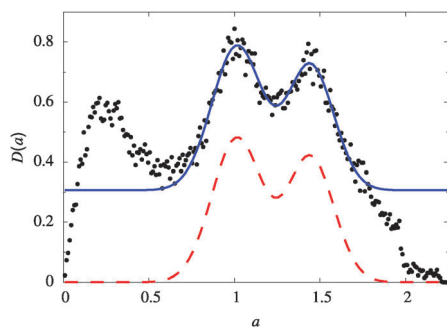


Fig. 4 Experimental recoil velocity distribution of CN^+ ions rescaled to have a maximum for $a = 1$ (points), fitted functions using two Gaussians (solid line) and two Gaussians without background (dashed line).

a distance proportional to it, we have rescaled the abscissa such that the maximum of $D(a)$ is at $a = 1$.

In the experiment, the molecular beam contains molecules in different quantum states. A certain level $\gamma = J_{K_a K_c} M$ has a relative weight $W_\gamma = W_{JK_a K_c M}$ within this ensemble, which is determined by classical trajectory simulations for all relevant rotational states using Monte Carlo sampling of the initial phase distributions.²⁹ Including the resulting populations in the laser interaction zone, the final 2D-screen probability distribution reads

$$P_T^i(y, z) = \sum_\gamma W_\gamma P_\gamma^i(x, y), \quad (5)$$

where the sum runs over all populated states and the index i indicates the polarization of the probe beam.

3.4 The experimental observables

The alignment of a molecule is quantified by the expectation value $\langle \cos^2 \theta \rangle_\gamma$, with $0 < \langle \cos^2 \theta \rangle < 1$, where larger values correspond to stronger alignment. While $\langle \langle \cos^2 \theta \rangle \rangle = \sum_\gamma W_\gamma \langle \cos^2 \theta \rangle_\gamma$ is not experimentally determined, the alignment is characterized through $\langle \langle \cos^2 \theta_{2D} \rangle \rangle = \sum_\gamma W_\gamma \langle \cos^2 \theta_{2D} \rangle_\gamma$, where $\theta_{2D} = \arctan(z/y)$ is the angle between the z -axis of the screen plane and the projection of the ion recoil velocity vector onto the detector plane. Let us remark that $\langle \cos^2 \theta_{2D} \rangle_\gamma$ is computed from the final 2D probability density in eqn (5), whereas $\langle \cos^2 \theta \rangle_\gamma$ from the 3D wave functions.

When the linear polarization of the YAG laser is not perpendicular to the static electric field ($\beta \neq 90^\circ$), the up/down symmetry of the 2D-images is lost, and an asymmetric distribution appears showing a certain degree of orientation. This up/down asymmetry is experimentally quantified by the ratio $N_{\text{up}}/N_{\text{tot}}$, with N_{up} being the amount of ions in the upper part of the screen plane, and N_{tot} the total number of detected ions. In our description, they are given by

$$N_{\text{up}} = \int_{-\infty}^{\infty} \int_{z \geq 0} P_T(y, z) dy dz, \quad (6)$$

and

$$N_{\text{tot}} = \int_{-\infty}^{\infty} \int_{-\infty}^{\infty} P_T(y, z) dy dz.$$

Note that due to the normalization we have that $N_{\text{tot}} = 1$.

Finally, to compare our numerical data with the experimental results, we take into account the finite spatial width of the YAG and probe pulses. Both laser beams have a Gaussian

profile with widths of $\omega_Y = 36 \mu\text{m}$ and $\omega_P = 21 \mu\text{m}$, respectively, and are overlapped in time and space. The YAG pulse ensures the alignment or orientation of the molecules, whereas the probe pulse is needed for detection purposes. The degree of alignment and the dissociation probability vary with the position of a molecule in the interaction volume. Thus, we integrate over the overlap region of the probe laser with the molecular beam considering the YAG-laser intensity. Hereby, we have assumed a linear behavior of the dissociation efficiency on the probe laser intensity. This is an approximation, as recent works on non-resonant strong field dissociation for other systems have proved a I^3 -dependence.⁴⁶ However, our calculations indicate that the orientation and alignment results are not very sensitive to a variation of this dependency. We have also assumed that the spatial profile of the molecular beam is much broader than that of the laser beams, hence, the variations of the density of molecules can be neglected.

4 Computational results

In this section, we apply the above described approach using benzonitrile as a prototype example. Recent experimental results for this molecule³¹ allow us to directly compare them to our numerical studies. The moments of inertia are given by $B_{X_M} = 1214 \text{ MHz}$, $B_{Y_M} = 1547 \text{ MHz}$, and $B_{Z_M} = 5655 \text{ MHz}$, the electric dipole moment is $\mu = 4.515 \text{ D}$, and the principal moments of polarizability are $\alpha_{X_M X_M} = 7.49 \text{ \AA}^3$, $\alpha_{Y_M Y_M} = 13.01 \text{ \AA}^3$, and $\alpha_{Z_M Z_M} = 18.64 \text{ \AA}^3$.^{31,47}

4.1 Alignment results

The experimental fields geometry consists of a weak static electric field perpendicular to the screen with strength $E_S = 286 \text{ V cm}^{-1}$ and a strong alignment laser linearly polarized along the Z_L -axis (z -axis). For the probe pulse we consider the three possible polarizations: (i) linearly polarized perpendicular to the screen; (ii) linearly polarized parallel to the screen; and (iii) circularly polarized in the xz -plane perpendicular to the screen. The computational results shown below include the recoil velocity distribution and the volume effect.

The theoretical results for the density distribution of the molecular beam on the screen are presented in Fig. 5(a)–(c) for $E_S = 286 \text{ V cm}^{-1}$ and for YAG pulse intensities $I = 5 \times 10^{10} \text{ W cm}^{-2}$, $10^{11} \text{ W cm}^{-2}$, and $7 \times 10^{11} \text{ W cm}^{-2}$, respectively. A strong confinement of the probability distribution is observed, the molecules are aligned with their Z_M -axis pointing along the polarization axis of the YAG laser. This 1D alignment becomes more pronounced as I is increased. The two ionization channels that characterize the velocity distribution for BN, *cf.* Fig. 4, appear as double maxima on the upper and lower humps of the 2D images. They become more prominent as I is increased, *i.e.*, for a YAG pulse with $I = 7 \times 10^{11} \text{ W cm}^{-2}$, while they are overlapping for lower intensities.

We quantify this alignment by the expectation values $\langle \langle \cos^2 \theta \rangle \rangle$, $\langle \langle \cos^2 \theta_{2D} \rangle \rangle^l$, $\langle \langle \cos^2 \theta_{2D} \rangle \rangle^p$, and $\langle \langle \cos^2 \theta_{2D} \rangle \rangle^c$, which are presented in Fig. 6 as a function of the YAG intensity I for the whole molecular beam. The indexes l , p and c indicate the probe pulse polarization: linearly-polarized perpendicular and linearly-polarized parallel to the static field and circularly-polarized, respectively. Without the presence of any aligning

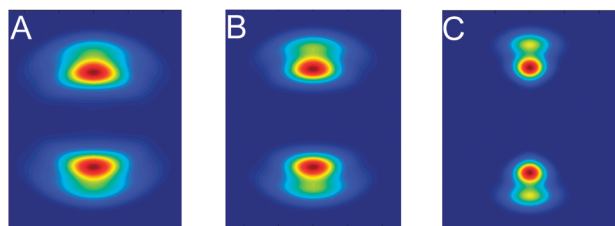


Fig. 5 The 2D projection of the density distribution of the benzonitrile molecular beam for (a) $I = 5 \times 10^{10} \text{ W cm}^{-2}$, (b) $10^{11} \text{ W cm}^{-2}$ and (c) $7 \times 10^{11} \text{ W cm}^{-2}$, $E_S = 286 \text{ V cm}^{-1}$ and $\beta = 90^\circ$. For direct comparison with recent experimental results, we refer to the BN^+ image in Fig. 3(c) in ref. 31 which was recorded under conditions similar to those used in the calculation of panel C.

or orienting fields the screen image is already biased by the “geometric alignment” of the probe pulse. An analytical calculation shows for a random isotropic distribution that $\langle \langle \cos^2 \theta \rangle \rangle = 1/3$, $\langle \langle \cos^2 \theta_{2D} \rangle \rangle^I = 0.5$, $\langle \langle \cos^2 \theta_{2D} \rangle \rangle^P = 3/4$, and $\langle \langle \cos^2 \theta_{2D} \rangle \rangle^C = 5/8$. This mild confinement obtained when the probe pulse is circularly polarized or linearly polarized parallel to the screen is due to the enhanced ionization probability for molecules having the C_2 axis (*i.e.*, the C–CN axis) parallel to the laser polarization.⁴⁸ If the molecules are exposed only to the weak electric field, $E_S = 286 \text{ V cm}^{-1}$, these field-free values are only slightly perturbed $\langle \langle \cos^2 \theta \rangle \rangle \approx 0.34$, $\langle \langle \cos^2 \theta_{2D} \rangle \rangle^I = 0.51$, $\langle \langle \cos^2 \theta_{2D} \rangle \rangle^P = 0.7496$, and $\langle \langle \cos^2 \theta_{2D} \rangle \rangle^C = 0.6319$.³⁰

These four expectation values qualitatively all show a similar evolution as the YAG pulse intensity is varied: a steep increase followed by a plateau-like behavior which indicates a saturation of the degree of alignment. This dependence of the alignment on the YAG pulse intensity nicely reproduces the experimental behavior observed for a molecular beam of iodobenzene (IB).^{15,29} Note that the differences due to the polarizations of the probe pulse are noticeable for low intensities, whereas for strong alignment fields they all converge to the same asymptotic limit. For $I = 7 \times 10^{11} \text{ W cm}^{-2}$, we obtain $\langle \langle \cos^2 \theta \rangle \rangle = 0.946$, $\langle \langle \cos^2 \theta_{2D} \rangle \rangle^I = 0.972$, $\langle \langle \cos^2 \theta_{2D} \rangle \rangle^P = 0.973$, and $\langle \langle \cos^2 \theta_{2D} \rangle \rangle^C = 0.974$. The value obtained experimentally, 0.89, for $\langle \langle \cos \theta_{2D} \rangle \rangle^P$ ³¹ is somewhat lower which we ascribe to contaminant ions, like

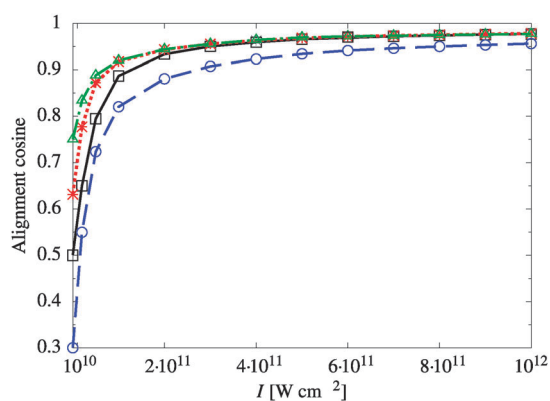


Fig. 6 Alignment cosines for the molecular beam of benzonitrile as a function of the YAG pulse intensity, $E_S = 286 \text{ V cm}^{-1}$ and $\beta = 90^\circ$: $\langle \langle \cos^2 \theta \rangle \rangle$ (circles and dashed line), $\langle \langle \cos^2 \theta_{2D} \rangle \rangle^I$ (squared and solid line), $\langle \langle \cos^2 \theta_{2D} \rangle \rangle^C$ (asterisks and dotted line), and $\langle \langle \cos^2 \theta_{2D} \rangle \rangle^P$ (triangles and dash-dotted line).

C_2H_2^+ (with the same mass-to-charge ratio as CN^+) in the images. Ions like C_2H_2^+ do not have a strong angular confinement and therefore reduced the apparent degree of alignment in the image. For IB, a molecule which is expected to attain an alignment degree similar to that of BN because of a similar polarizability tensor, the recoil ion used, I^+ , is more clean since there are no contaminant ions at the mass of 127. As a result, the observed degree of alignment is as high as 0.97 for $\langle \langle \cos \theta_{2D} \rangle \rangle^I$,²⁹ in good agreement with the theoretical predictions.

For completeness, we have also considered a thermal sample of BN at 1 K and $I = 7 \times 10^{11} \text{ W cm}^{-2}$, obtaining $\langle \langle \cos^2 \theta_{2D} \rangle \rangle^I = 0.961$, which agrees well with the experimental value for IB.⁴⁹

4.2 Orientation results

The polarization axis of the YAG-laser is now rotated about the Y_L -axis, and forms an angle β ($\beta \neq 90^\circ$) with the weak electrostatic field perpendicular to the screen, $E_S = 286 \text{ V cm}^{-1}$. The orientation ratio $N_{\text{up}}/N_{\text{tot}}$ (eqn (6)) is derived for a circularly polarized probe pulse, including the velocity distribution and the volume effect and using the diabatic model described above.

The theoretical results for the projected density distribution of the molecular beam are presented in Fig. 7(a) and (b) for two intensities and $\beta = 135^\circ$. As a consequence of the rotation of the YAG polarization axis, the up/down symmetries of the wave functions are lost. The 1D orientation becomes more pronounced as I is increased. For $\beta = 135^\circ$, the projection of CN^+ ions onto the 2D detector overlaps the two Coulomb explosion channels to an extent that they cannot be discerned.

The theoretical results for the orientation $N_{\text{up}}/N_{\text{tot}}$ are presented in Fig. 8 as a function of the tilt angle β and for three intensities. The main feature of the $N_{\text{up}}/N_{\text{tot}}$ is that it is almost independent of the alignment laser intensity and of β . For these three intensities, all the populated states are within the pendular regime. Thus, if the volume effect was neglected, the ratio $N_{\text{up}}/N_{\text{tot}}$ would be independent of I for this pendular regime of laser intensities. By taking into account the spatial distribution of the probe and YAG beams, the molecules show

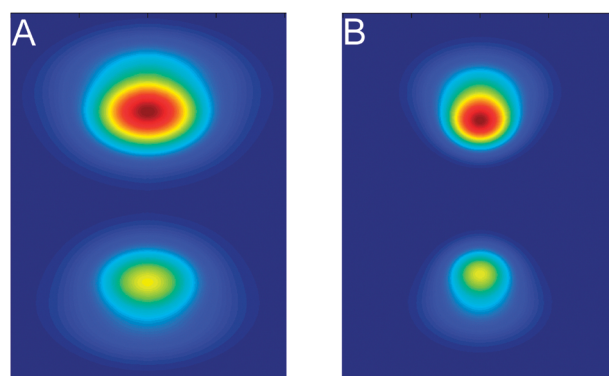


Fig. 7 The 2D projection of the density distribution of the benzonitrile molecular beam for (a) $I = 10^{11}$, and (b) $7 \times 10^{11} \text{ W cm}^{-2}$, $E_S = 286 \text{ V cm}^{-1}$ and $\beta = 135^\circ$. For a direct comparison of panel B to an experimental image recorded under similar conditions of the laser parameters and rotational state distribution, we refer to the BN^+ image in Fig. 3(f) in ref. 31.

the smallest orientation for $I = 10^{11} \text{ W cm}^{-2}$. This is explained by the larger contribution of lower intensities, for which the molecules are not yet in the pendular regime, to the volume effect integral for $I = 10^{11} \text{ W cm}^{-2}$, and as a consequence $N_{\text{up}}/N_{\text{tot}}$ is reduced. For $I = 5 \times 10^{11}$ and $7 \times 10^{11} \text{ W cm}^{-2}$, the contribution of lower intensities is not strong enough to cause any noticeable difference. Note that for IB, it was also experimentally found that $N_{\text{up}}/N_{\text{tot}}$ is independent of the YAG pulse intensity.²⁹ For $\beta = 90^\circ$, the molecular beam does not show any orientation and it holds $N_{\text{up}}/N_{\text{tot}} = 0.5$. For a certain YAG pulse intensity, $N_{\text{up}}/N_{\text{tot}}$ quickly increases as β is increased from 90° and reaches a plateau-like behavior for the rest of the field configurations. For $\beta = 135^\circ$ and $I = 7 \times 10^{11} \text{ W cm}^{-2}$, we obtain $N_{\text{up}}/N_{\text{tot}} = 0.636$ which is smaller than the experimental result of 0.71.³¹ Thus, our theoretical model underestimates the orientation obtained in the experiment.

An important discrepancy between theoretical and experimental results is the variation of $N_{\text{up}}/N_{\text{tot}}$ for β close to 90° . For a molecular beam of IB,²⁹ it was experimentally shown that $N_{\text{up}}/N_{\text{tot}}$ smoothly increases (decreases) as β is increased (decreased) from 90° , reaching for $\beta \lesssim 60^\circ$ and $\beta \gtrsim 120^\circ$ the plateau. In contrast, the theoretical $N_{\text{up}}/N_{\text{tot}}$ sharply increases, and its β -independent value is already achieved for $\beta \gtrsim 91^\circ$. In the pendular regime, the strong laser interaction pairs states into quasi-degenerate doublets. The electrostatic field can induce a strong coupling between these levels giving rise to a large orientation if the energy gap is small enough. For certain intensities, some excited levels may not show such a narrow energy gap to obtain a significant orientation, but their relative weight within the molecular beam is so small that their contribution to the final result is not relevant. For a linear molecule in combined fields,⁵⁰ such a sharp rise was predicted for the expectation value $\langle \cos \theta \rangle$ as the static field strength is increased, *i.e.*, increasing or decreasing β from 90° in our case. From Fig. 2 of Friedrich and Herschbach²² this effect is obtained for the interaction with the laser field being 25 000 times larger than the one with the static field. We could perform a

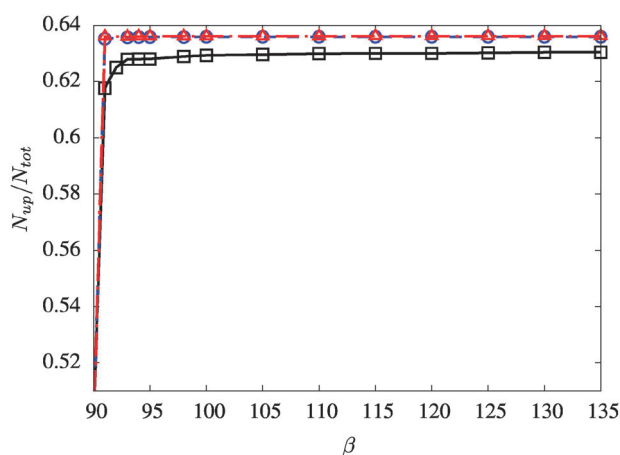


Fig. 8 The theoretical orientation ratio $N_{\text{up}}/N_{\text{tot}}$ as a function of the angle β for the molecular beam of benzonitrile, YAG pulses with $I = 10^{11}$ (squares and solid line), 5×10^{11} (circles and dashed line) and $7 \times 10^{11} \text{ W cm}^{-2}$ (triangles and dash-dotted line) and a static field with $E_S = 286 \text{ V cm}^{-1}$.

similar comparison and for BN, $I = 7 \times 10^{11} \text{ W cm}^{-2}$, $E_S = 286 \text{ V cm}^{-1}$ and $\beta = 95^\circ$, the interaction of the YAG pulse, $2\pi I \alpha^{Z_M X_M} / c$, is 43 600 times larger than the coupling with the static field, $\mu E_S \cos \beta$.

Let us remark that our diabatic model for the population transfer is equivalent to considering a field configuration with a linearly polarized YAG pulse being parallel to an electrostatic field with strength $E_S \cos \beta$. This field geometry is neglecting the component of the electric field $E_S \sin \beta$ perpendicular to the YAG polarization, which is responsible for breaking the azimuthal symmetry and causing M to stop being a good quantum number. This approximation can be done because the interaction due to the static field is sufficiently weak. We have performed the full calculation considering the simplified case of parallel fields, the static one with strength $E_S = 286 \cos 135^\circ \text{ V cm}^{-1}$ and $I = 7 \times 10^{11} \text{ W cm}^{-2}$, obtaining for the orientation the value $N_{\text{up}}/N_{\text{tot}} = 0.636$.

To illustrate the necessity of the diabatic model, we build up the molecular ensemble by successively adding states according to their weights. Thus, our initial ensemble contains only the ground state, and for the second one, we add the second and third most populated levels. The relative weights of the states within these molecular beams are the same as in the full molecular ensemble. Fig. 9 presents the orientation $N_{\text{up}}/N_{\text{tot}}$ as a function of the percentage of states included in the ensemble for $I = 7 \times 10^{11} \text{ W cm}^{-2}$ and $\beta = 135^\circ$. The ratio $N_{\text{up}}/N_{\text{tot}}$ has been computed with the diabatic model for the population transfer and a fully adiabatic picture, *i.e.*, all avoided crossings are assumed to be passed adiabatically. The first three populated states, $0_{00}0$, $1_{01}1$ and $1_{01}-1$, are perfectly oriented: $N_{\text{up}}/N_{\text{tot}} = 1$. For the sets including the levels adding 20% of the total population, the diabatic and adiabatic results agree because these states do not suffer any avoided crossings. As highly excited levels are added to the molecular beam, the difference between both calculations becomes more evident due to the presence of the diabatic avoided crossings. They both show a zig-zag decreasing trend as the population is increased. The ratio $N_{\text{up}}/N_{\text{tot}}$ computed

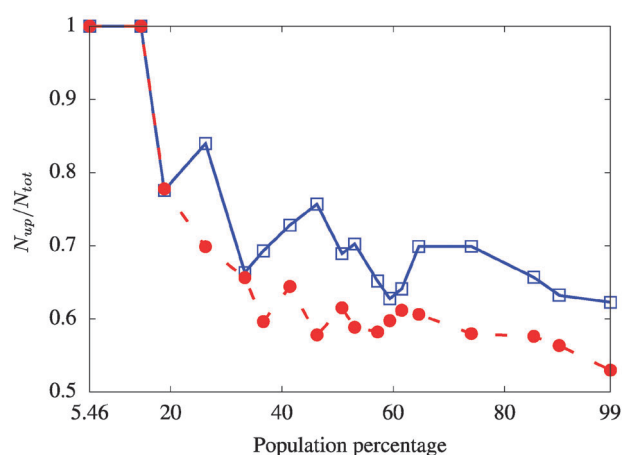


Fig. 9 The theoretical orientation ratio $N_{\text{up}}/N_{\text{tot}}$ as a function of the population of the molecular beam of benzonitrile, for the field configuration $I = 7 \times 10^{11} \text{ W cm}^{-2}$, $E_S = 286 \text{ V cm}^{-1}$, and $\beta = 135^\circ$, computed with the diabatic model for the population transfer (squares and solid line) and a fully adiabatic picture (circles and dashed line).

under the adiabaticity assumption is smaller than the diabatic result as more states are added. Taking into account all states populated in the molecular beam, the adiabatic model does not yield any appreciable amount of orientation: we obtain $N_{\text{up}}/N_{\text{tot}} = 0.53$ which strongly underestimates the experimental result. In addition we have observed that the adiabatic orientation ratio $N_{\text{up}}/N_{\text{tot}}$ is no longer β -independent. This confirms that non-adiabatic crossings play a crucial role in understanding the strong orientation observed in the experiment.

Finally, it is worth noting for the field configuration $I = 7 \times 10^{11} \text{ W cm}^{-2}$ and $\beta = 135^\circ$ that a thermal sample of BN at 1 K shows a weak degree of orientation with $N_{\text{up}}/N_{\text{tot}} = 0.563$.

5 Summary and conclusions

We have presented a theoretical model to investigate the degree of alignment and orientation of a beam of asymmetric top molecules exposed to combined electrostatic and non-resonant linearly polarized laser fields. Our analysis combines the field-dressed wave functions with the experimental distribution of the populated quantum states. As a first step, we solve the three-dimensional Schrödinger equation within the rigid rotor approximation. For a certain field geometry, we treat each irreducible representation independently, by expanding the wave function in a basis that respects the corresponding symmetries. Since the dc electric field strength is very weak, we consider M as being almost conserved, and a diabatic model is introduced to approximate the population transfer through the avoided crossings as the YAG pulse intensity is increased. The 2D projection of a wave function is derived by using the detection selectivity factors of the probe pulse, the velocity distribution of the detected ions, and a volume effect average.

This theoretical model has been checked by comparing the numerical and experimental results for benzonitrile. The molecular beam has been simulated using the population of each quantum state numerically obtained from deflection profiles.²⁹ For several field configurations, we have performed a detailed study of the directional properties of the molecular mixture. In particular, we have explored the degrees of alignment and orientation as the YAG pulse intensity and the angle between both fields are varied. For perpendicular fields, a good agreement between the computational and experimental results is obtained. Let us remark that we do not take into account the background of unwanted ions which contaminate the velocity mapping images for BN and reduce the experimental degree of alignment.³¹ Hence, a better agreement could be achieved for other systems with cleaner Coulomb explosion imaging channels, like IB.

Regarding the orientation results, we have shown that the assumption of a fully adiabatic dynamics is incorrect for the prototypical experiment and predicts a non-oriented molecular beam—which is not in agreement with the experimental results. Indeed, we have proven that the degree of orientation does not adiabatically follow the time envelope of the YAG laser with a FWHM = 10 ns in the experiment. By employing a simple diabatic model, the experimental results for orientation

could be reproduced reasonably well. Based on the comparison with the experimental measures, the important impact of the diabaticity on the field-dressed molecular dynamics is hereby demonstrated. However, note that our model does not produce the smooth β -dependence of $N_{\text{up}}/N_{\text{tot}}$ that was experimentally obtained for IB.²⁹

This theoretical model is based on several approximations that may be the source of discrepancies with the experimental results. The molecules are exposed to an alignment laser pulse with a certain time profile, but we are performing a time-independent description of the field-dressed rotational dynamics. We compensate this deficiency by using a simple partially diabatic approach to model the population transfer. However, a general statement on the character of the avoided crossings cannot be made, and some of them could not be classified clearly by our adiabaticity criterion. The semiclassical calculations of the molecular trajectories through the deflector have been derived using a fully adiabatic picture, whereas it has been theoretically shown that such an approximation may be incorrect.³⁹ These assumptions for both processes might not be fully satisfied. A full time-dependent description of the process would properly treat the avoided crossing, but it is computationally very challenging. Possible distortion effects due to the strong laser pulse are also not taken into account. Furthermore, we are working within the axial recoil approximation neglecting the interactions between the ionic fragments on their way to the detector. Analogously, collisions and interactions between the molecules within the molecular beam⁵¹ were not considered. The geometric alignment due to the strong-field ionization has been assumed to be a single-photon absorption, but it is a multiphoton process.⁴⁶ The nuclear hyperfine structure has been neglected. Whereas it can be of the same order of magnitude as the interaction with the weak static field (*i.e.*, for IB⁵²), this is clearly not the case for BN.⁴⁷

Certainly, it would be interesting to perform a comparison of these computational results with experimental data obtained for other molecular species either with a smaller number of populated states or with a cleaner imaging signal. A rather natural extension of the present work would be to go beyond any of the approximations described above. A more sensitive criterion for the avoided crossing treatment, a time-dependent description, or the inclusion of the hyperfine interaction should improve these theoretical results.

Acknowledgements

We acknowledge support by Frank Filsinger for the trajectory simulations providing the populations of individual quantum states. We thank Gerard Meijer for continuous interest and support of this project and Marko Härtelt and Bretislav Friedrich for helpful discussions. Financial support by the Spanish project FIS2008-02380 (MICINN) as well as the Grants FQM-2445 and FQM-4643 (Junta de Andalucía) is gratefully appreciated. J.J.O. acknowledges the support of ME under the program FPU. R.G.F. and J.J.O. belong to the Andalusian research group FQM-207. M.G. acknowledges financial support by the German Studies Foundation (Studienstiftung des deutschen Volkes).

References

- 1 P. R. Brooks and E. M. Jones, *J. Chem. Phys.*, 1966, **45**, 3449.
- 2 S. Stolte, *Ber. Bunsen-Ges. Phys. Chem.*, 1982, **86**, 413.
- 3 R. Zare, *Science*, 1998, **20**, 1875.
- 4 V. Aquilanti, M. Bartolomei, F. Pirani, D. Cappelletti and F. Vecchiocattivi, *Phys. Chem. Chem. Phys.*, 2005, **7**, 291.
- 5 A. Landers, T. Weber, I. Ali, A. Cassimi, M. Hattass, O. Jagutzki, A. Nauert, T. Osipov, A. Staudte, M. Prior, H. Schmidt-Böcking, C. Cocke and R. Dörner, *Phys. Rev. Lett.*, 2001, **87**, 013002.
- 6 L. Holmegaard, J. L. Hansen, L. Kalhøj, S. L. Kragh, H. Stapelfeldt, F. Filsinger, J. Küpper, G. Meijer, D. Dimitrovski, M. Abu-samha, C. P. J. Martiny and L. B. Madsen, *Nat. Phys.*, 2010, **6**, 428.
- 7 C. Z. Bisgaard, O. J. Clarkin, G. R. Wu, A. M. D. Lee, O. Gessner, C. C. Hayden and A. Stolow, *Science*, 2009, **323**, 1464.
- 8 J. Levesque, Y. Mairesse, N. Dudovich, H. Pèpin, J.-C. Kieffer, P. B. Corkum and D. M. Villeneuve, *Phys. Rev. Lett.*, 2007, **99**, 243001.
- 9 R. Velotta, N. Hay, M. B. Mason, M. Castillejo and J. P. Marangos, *Phys. Rev. Lett.*, 2001, **87**, 183901.
- 10 J. C. H. Spence and R. B. Doak, *Phys. Rev. Lett.*, 2004, **92**, 198102.
- 11 F. Filsinger, G. Meijer, H. Stapelfeldt, H. Chapman and J. Küpper, *Phys. Chem. Chem. Phys.*, 2011, **13**, 2076.
- 12 R. J. D. Miller, R. Ernstorfer, M. Harb, M. Gao, C. T. Hebeisen, H. Jean-Ruel, C. Lu, G. Moriena and G. Sciaini, *Acta Crystallogr., Sect. A: Fundam. Crystallogr.*, 2010, **66**, 137.
- 13 S. Y. T. van de Meerakker, H. L. Bethlem and G. Meijer, *Nat. Phys.*, 2008, **4**, 595.
- 14 H. Stapelfeldt and T. Seideman, *Rev. Mod. Phys.*, 2003, **75**, 543.
- 15 L. Holmegaard, J. H. Nielsen, I. Nevo, H. Stapelfeldt, F. Filsinger, J. Küpper and G. Meijer, *Phys. Rev. Lett.*, 2009, **102**, 023001.
- 16 O. Ghafur, A. Rouzée, A. Gijsbertsen, W. K. Siu, S. Stolte and M. J. J. Vrakking, *Nat. Phys.*, 2009, **5**, 289.
- 17 A. Rouzée, A. Gijsbertsen, O. Ghafur, O. M. Shir, T. Bäck, S. Stolte and M. J. J. Vrakking, *New J. Phys.*, 2009, **11**, 105040.
- 18 M. H. G. de Miranda, A. Chotia, B. Neyenhuis, D. Wang, G. Quémener, S. Ospelkaus, J. L. Bohn, J. Ye and D. S. Jin, *Nat. Phys.*, 2011, **7**, 502.
- 19 J. Reuss, *Atomic and molecular beam methods*, Oxford University Press, New York, NY, USA, 1988, vol. 1, ch. 11, p. 276.
- 20 H. J. Loesch and A. Remscheid, *J. Chem. Phys.*, 1990, **93**, 4779.
- 21 B. Friedrich and D. R. Herschbach, *Z. Phys. D: At., Mol. Clusters*, 1991, **18**, 153.
- 22 B. Friedrich and D. R. Herschbach, *J. Chem. Phys.*, 1999, **111**, 6157.
- 23 B. Friedrich and D. R. Herschbach, *J. Phys. Chem. A*, 1999, **103**, 10280.
- 24 R. Baumfalk, N. H. Nahler and U. Buck, *J. Chem. Phys.*, 2001, **114**, 4755.
- 25 H. Sakai, S. Minemoto, H. Nanjo, H. Tanji and T. Suzuki, *Phys. Rev. Lett.*, 2003, **90**, 083001.
- 26 H. Tanji, S. Minemoto and H. Sakai, *Phys. Rev. A*, 2005, **72**, 063401.
- 27 M. Schnell and G. Meijer, *Angew. Chem., Int. Ed.*, 2009, **48**, 6010.
- 28 J. Küpper, F. Filsinger and G. Meijer, *Faraday Discuss.*, 2009, **142**, 155.
- 29 F. Filsinger, J. Küpper, G. Meijer, L. Holmegaard, J. H. Nielsen, I. Nevo, J. L. Hansen and H. Stapelfeldt, *J. Chem. Phys.*, 2009, **131**, 064309.
- 30 I. Nevo, L. Holmegaard, J. H. Nielsen, J. L. Hansen, H. Stapelfeldt, F. Filsinger, G. Meijer and J. Küpper, *Phys. Chem. Chem. Phys.*, 2009, **11**, 9912.
- 31 J. L. Hansen, L. Holmegaard, L. Kalhøj, S. L. Kragh, H. Stapelfeldt, F. Filsinger, G. Meijer, J. Küpper, D. Dimitrovski, M. Abu-samha, C. P. J. Martiny and L. B. Madsen, *Phys. Rev. A*, 2011, **83**, 023406.
- 32 M. Härtelt and B. Friedrich, *J. Chem. Phys.*, 2008, **128**, 224313.
- 33 J. J. Omiste, R. González-Férez and P. Schmelcher, arXiv:1106.1586v1.
- 34 C. A. Arango and G. S. Ezra, *Int. J. Bifurcation Chaos Appl. Sci. Eng.*, 2008, **18**, 1127.
- 35 C. A. Arango, W. W. Kennerly and G. S. Ezra, *J. Chem. Phys.*, 2005, **122**, 184303.
- 36 I. N. Kozin and R. N. Roberts, *J. Chem. Phys.*, 2003, **118**, 10523.
- 37 R. N. Zare, *Angular Momentum: Understanding Spatial Aspects in Chemistry and Physics*, John Wiley and Sons, New York, 1988.
- 38 R. Kanya and Y. Ohshima, *Phys. Rev. A*, 2004, **70**, 013403.
- 39 R. Escribano, B. Maté, F. Ortigoso and J. Ortigoso, *Phys. Rev. A*, 2000, **62**, 023407.
- 40 G. W. King, R. M. Hainer and P. C. Cross, *J. Chem. Phys.*, 1943, **11**, 27.
- 41 J. Bulthuis, J. Miller and H. J. Loesch, *J. Phys. Chem. A*, 1997, **101**, 7684.
- 42 W. Kong and J. Bulthuis, *J. Phys. Chem. A*, 2000, **104**, 1055.
- 43 A. Schwettman, J. Franklin, K. R. Overstreet and J. P. Shaffer, *J. Chem. Phys.*, 2005, **123**, 194305.
- 44 D. Bohm, *Quantum Theory*, Dover Publications, Inc., New York, 1989, ch. 20.
- 45 R. Kanya and Y. Ohshima, *J. Chem. Phys.*, 2004, **121**, 9489.
- 46 J. H. Nielsen, P. Simesen, C. Z. Bisgaard, H. Stapelfeldt, F. Filsinger, B. Friedrich, G. Meijer and J. Küpper, 2011, arXiv:1105.2413v1.
- 47 K. Wohlfart, M. Schnell, J.-U. Grabow and J. Küpper, *J. Mol. Spectrosc.*, 2008, **247**, 119.
- 48 J. J. Larsen, H. Sakai, C. P. Safvan, I. Wendt-Larsen and H. Stapelfeldt, *J. Chem. Phys.*, 1999, **111**, 7774.
- 49 V. Kumarappan, C. Z. Bisgaard, S. S. Viftrup, L. Holmegaard and H. Stapelfeldt, *J. Chem. Phys.*, 2006, **125**, 194309.
- 50 B. Friedrich and D. R. Herschbach, *Z. Phys. D: At., Mol. Clusters*, 1995, **36**, 221.
- 51 U. Erlekam, M. Frankowski, G. von Helden and G. Meijer, *Phys. Chem. Chem. Phys.*, 2007, **9**, 3786.
- 52 O. Dorosh, E. Białkowska-Jaworska, Z. Kisiel and L. Pszczłkowski, *J. Mol. Spectrosc.*, 2007, **246**, 228.

Nonadiabatic effects in long-pulse mixed-field orientation of a linear polar molecule

Juan J. Omiste* and Rosario González-Férez†

Instituto Carlos I de Física Teórica y Computacional, and Departamento de Física Atómica, Molecular y Nuclear, Universidad de Granada, 18071 Granada, Spain

(Received 6 July 2012; published 31 October 2012)

We present a theoretical study of the impact of an electrostatic field combined with nonresonant linearly polarized laser pulses on the rotational dynamics of linear molecules. Within the rigid rotor approximation, we solve the time-dependent Schrödinger equation for several field configurations. Using the carbonyl sulfide molecule as the prototype, the field-dressed dynamics is analyzed in detail for experimentally accessible static-field strengths and laser pulses. Results for directional cosines are presented and compared to the predictions of the adiabatic theory. We demonstrate that for the prototypical field configuration used in current mixed-field orientation experiments, the molecular field dynamics is, in general, nonadiabatic, and a time-dependent description of these systems is mandatory. We investigate several field regimes identifying the sources of nonadiabatic effects and provide the field parameters under which the adiabatic dynamics would be achieved.

DOI: [10.1103/PhysRevA.86.043437](https://doi.org/10.1103/PhysRevA.86.043437)

PACS number(s): 37.10.Vz, 33.80.-b, 33.57.+c, 42.50.Hz

I. INTRODUCTION

The creation of directional states of molecules represents an important tool to control and tailor the rotational degree of freedom. When a molecule is oriented the molecular fixed axes are confined along the laboratory fixed axes and its dipole moment is pointing in a particular direction. Experimentally, the availability of oriented molecules provides a wealth of interesting applications in a variety of molecular sciences, such as in chemical reaction dynamics [1–5], photoelectron angular distributions [6–8], and high-order harmonic generation [9,10].

Due to this broad interest, special efforts have been undertaken to create samples of oriented molecules and techniques based on the application of inhomogeneous [1,11] and homogeneous [12–16] electric fields as well as homogeneous magnetic fields [17] have been used. Friedrich and Herschbach proposed the use of combined weak electrostatic and strong nonresonant radiative fields to enhance the orientation of polar molecules [18,19]. This theoretical prediction was done within an adiabatic picture assuming that the switching-on time of the laser pulse is larger than the molecular rotational period [20]. For linear molecules, a linearly polarized laser field produces a double-well potential along the polarization direction. In the pendular limit, this double-well potential contains nearly degenerate pairs of states with opposite parity, forming tunneling doublets. If the molecules possess a permanent electric dipole moment, a strong pseudo-first-order Stark effect is induced by coupling the tunneling doublets with an additional electrostatic field. Due to this coupling, the two levels in a pendular doublet are efficiently oriented, but with their effective electric dipole moments pointing in opposite directions. As a consequence of this oriented and antioriented state pairing, the orientation is small in a molecular ensemble with the population thermally distributed. Therefore, the first experimental measures of the orientation of a molecular beam were indeed reduced to small values [21,22]. A significant improvement was gained by

using a quantum-state selected molecular beam, which allowed the creation of an unprecedented degree of orientation for complex asymmetric tops [23–25]. The first theoretical study of the mixed-field orientation experiment of asymmetric top molecules pointed out that a fully adiabatic description of the process does not reproduce the experimental observations [26].

Recently, we have experimentally and theoretically investigated the mixed-field orientation of the carbonyl sulfide (OCS) molecule [27]. Our analysis has proven that a time-dependent description of the mixed-field orientation process is required to explain the experimental results. We have shown how the nonadiabatic coupling of the levels forming quasidegenerate doublets as the laser intensity is increased gives rise to a reduction in the orientation and, therefore, to disagreement with the predictions of the adiabatic theory [18,19]. Herein, we provide a detailed theoretical analysis of the dynamics of a linear molecule exposed to an electrostatic field combined with a nonresonant laser pulse. In the framework of the rigid rotor approximation, we solve the time-dependent Schrödinger equation using experimental field configurations, i.e., a Gaussian laser pulse and a weak electrostatic field that is turned on at a constant speed. As the prototype example, we consider the OCS molecule. For several rotational states, we investigate the mixed-field orientation dynamics under different field configurations by varying either the laser peak intensity, the duration of the Gaussian pulse, the dc-field strength, or the angle between the two fields. Hence, we demonstrate that for some field configurations, the field-dressed dynamics is nonadiabatic and provide a detailed account of the sources of nonadiabaticity and the field regimes at which they appear. For parallel fields, the dynamics is characterized by the population transfer between adiabatic states when the pendular doublets are formed. Whereas for nonparallel fields, we encounter additional nonadiabatic effects when the states from the same J manifold, now having the same symmetry, are driven apart as the laser intensity is increased in the weak-field regime. For different field configurations, we identify and discuss the experimental conditions needed to achieve an adiabatic molecular dynamics.

The paper is organized as follows: In Sec. II we describe the Hamiltonian of the system and its symmetries for various

*omiste@ugr.es

†rogonzal@ugr.es

field configurations. The results for the energy, alignment, and orientation predicted by the adiabatic theory are analyzed in Sec. III. In Sec. IV, we focus on the molecular dynamics when the fields are parallel. In particular, we explore how the time-dependent orientation varies as the field parameters are modified and indicate the experimental conditions under which an adiabatic orientation would be achieved. A similar study is performed for tilted fields in Sec. V, where we show that the conditions for an adiabatic mixed-field orientation are more difficult to fulfill. In Sec. VI, we assume that, once the pulse is turned on, its peak intensity is kept constant and investigate the dynamics in this regime. In Sec. VII, we consider the ground state aligned by a cw laser and investigate the adiabaticity of the orientation dynamics when an electric field is applied. The conclusions are given in Sec. VIII.

II. THE HAMILTONIAN OF A LINEAR RIGID ROTOR IN EXTERNAL FIELDS

We consider a polar linear molecule exposed to a homogeneous static electric field and a nonresonant linearly polarized laser pulse. The field configuration is illustrated in Fig. 1: the polarization of the laser field $\mathbf{E}_L(t)$ lies along the Z axis of the laboratory fixed frame (LFF) (X, Y, Z) , and the dc field $\mathbf{E}_s(t)$ is contained in the XZ plane forming an angle β with the Z axis. The z axis of the molecule fixed frame (x, y, z) is defined by the permanent dipole moment $\boldsymbol{\mu}$ of the molecule. These two frames are related by the Euler angles $\Omega = (\theta, \phi)$ (cf. Fig. 1). The description of this system is done within the rigid rotor approximation, assuming that the vibrational and electronic dynamics are not affected by the fields. Thus, the rigid rotor Hamiltonian reads

$$H(t) = H_r + H_s(t) + H_L(t), \quad (1)$$

where H_r is the field-free Hamiltonian

$$H_r = B\mathbf{J}^2, \quad (2)$$

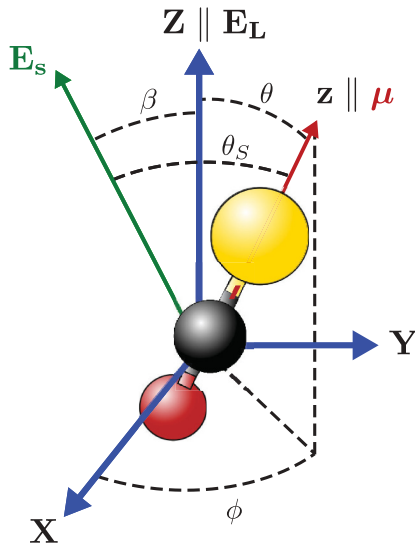


FIG. 1. (Color online) Laboratory fixed coordinate, Euler angles, schematic field configuration, and the OCS molecule.

with \mathbf{J} being the total angular momentum operator and B the rotational constant. $H_s(t)$ and $H_L(t)$ stand for the interactions with the static and laser fields, respectively.

The dipole coupling with the static field reads

$$H_s(t) = -\boldsymbol{\mu} \cdot \mathbf{E}_s(t) = -\mu E_s(t) \cos \theta_s, \quad (3)$$

with $\mathbf{E}_s(t) = E_s(t)(\sin \beta \hat{X} + \cos \beta \hat{Z})$ and $E_s(t)$ being the electrostatic-field strength. The angle between the dipole moment $\boldsymbol{\mu}$ and this field is θ_s (cf. Fig. 1), and $\cos \theta_s = \cos \beta \cos \theta + \sin \beta \sin \theta \cos \phi$.

The nonresonant laser-field molecule interaction can be written as [20]

$$H_L(t) = -\frac{I(t)}{2c\epsilon_0} \Delta\alpha \cos^2 \theta, \quad (4)$$

where $\Delta\alpha$ is the polarizability anisotropy, $I(t)$ is the intensity of the laser, c is the speed of light, and ϵ_0 is the dielectric constant. Note that we have neglected the term $-\alpha_{\perp} I(t)/2c\epsilon_0$, which represents only a shift in the energy.

In this work, the field configurations are chosen based on mixed-field orientation experiments [23,25,27]. Initially, the molecule is in field-free space, then the electrostatic field is switched on, and its strength is increased linearly with time. We ensure that this turning-on process is adiabatic, and once the maximum strength E_s is achieved, it is kept constant. For the laser pulse, we use a linearly polarized Gaussian pulse with a full width at half-maximum (FWHM) τ in the nanosecond range. The intensity is given by $I(t) = I_0 \exp(-t^2/2\sigma^2)$, where I_0 is the peak intensity, and σ is related to the FWHM $\tau = 2\sqrt{2 \ln 2} \sigma$. Numerically, the nonresonant laser field is turned on in such a way that the interaction due to this field is much weaker than coupling with the dc field.

The eigenstates of the field-free Hamiltonian, (2), are the spherical harmonics $Y_{JM}(\Omega)$, with J and M being the rotational and magnetic quantum numbers, respectively. Note that M is the projection of the total angular momentum \mathbf{J} on the LFF Z axis. The field-free Hamiltonian, (2), belongs to the $SO(3)$ group because the operator \mathbf{J}^2 remains unaltered under any rotation. In the presence of the external fields, the symmetries of the rotational Hamiltonian, (1), are significantly reduced. The operations describing the symmetries of the field-dressed Hamiltonian are listed in Table I. For a static field, the symmetry group is reduced to arbitrary rotations around the field axis and the identity $\{\mathcal{E}, \mathcal{C}_{E_s}(\delta)\}$. If only a linearly polarized laser field is applied, the Hamiltonian is invariant under arbitrary rotations around the Z axis and twofold rotations around any axis perpendicular to the Z axis, and the symmetry group is compound by $\{\mathcal{E}, \mathcal{C}_Z(\delta), \mathcal{C}_{\perp Z}(\pi)\}$. For parallel fields, the elements of the symmetry group are

TABLE I. Action of the symmetry operations on the Euler angles.

Operation	Transformation	
	ϕ	θ
\mathcal{E}	$\phi \rightarrow \phi$	$\theta \rightarrow \theta$
σ_{XZ}	$\phi \rightarrow 2\pi - \phi$	$\theta \rightarrow \theta$
$\mathcal{C}_X(\pi)$	$\phi \rightarrow 2\pi - \phi$	$\theta \rightarrow \pi - \theta$
$\mathcal{C}_{\perp Z}^{\alpha}(\pi)$	$\phi \rightarrow 2\alpha - \phi$	$\theta \rightarrow \pi - \theta$
$\mathcal{C}_Z(\delta)$	$\phi \rightarrow \phi + \delta$	$\theta \rightarrow \theta$

TABLE II. For the $\beta = 90^\circ$ and $\beta \neq 90^\circ$ field configurations, values of the parameters κ and ϵ for the wave functions with the correct symmetry for each irreducible representation.

$\beta \neq 90^\circ$		$\beta = 90^\circ$			
κ	σ_{XZ}	ϵ	$J + M$	σ_{XZ}	\mathcal{C}_X
M	Even	M	Even	Even	Even
$M + 1$	Odd	M	Odd	Even	Odd
		$M + 1$	Odd	Odd	Even
		$M + 1$	Even	Odd	Even

the identity \mathcal{E} , arbitrary rotations around the fields $\mathcal{C}_Z(\delta)$, and the reflection in any plane containing the fields. For a given $|M|$ value, the parity under the reflection on one of these planes defines two irreducible representations. Since the selection of this plane is not unique, states with $M \neq 0$ are doubly degenerated. Note that M remains as a good quantum number for these three field configurations with $\beta = 0^\circ$. For nonperpendicular and noncollinear fields, i.e., $\beta \neq 0^\circ$ and $\beta \neq 90^\circ$, the Hamiltonian is invariant under the identity \mathcal{E} and the reflection on the XZ plane containing the fields σ_{XZ} . This group $\{\mathcal{E}, \sigma_{XZ}\}$ has only two irreducible representations, characterized by the parity with respect to this reflection σ_{XZ} , and the functions belonging to the even and odd representations are $\Psi_{JM}^{e/o}(\Omega) = [Y_{JM}(\Omega) + (-1)^\kappa Y_{J-M}(\Omega)]/\sqrt{2}$, with κ given in Table II. If the fields are perpendicular, $\beta = 90^\circ$, the twofold rotation around the static field $\mathcal{C}_X(\pi)$ is also a symmetry operation. Thus, the symmetry group is formed by $\{\mathcal{E}, \sigma_{XZ}, \mathcal{C}_X(\pi)\}$ and has four irreducible representations labeled by the parity with respect to the transformations σ_{XZ} and $\mathcal{C}_X(\pi)$. The properly symmetrized functions for these four irreducible representations are $\Psi_{JM}^{e/o, e/o}(\Omega) = [Y_{JM}(\Omega) + (-1)^\epsilon Y_{J-M}(\Omega)]/\sqrt{2}$; the possible values of ϵ are listed in Table II.

The time-dependent Schrödinger equation associated with Hamiltonian (1) is solved by means of a second-order split-operator technique [28], combined with the discrete-variable and finite-basis representation methods for the angular coordinates [29–32]. For reasons of addressability, we label the time-dependent states $|J, M, l\rangle^0$ and $|J, M, l\rangle$ for $\beta = 0^\circ$ and $0^\circ < \beta < 90^\circ$, respectively, with $l = e$ and o indicating even or odd parity with respect to the XZ plane. The labels J and M refer to the field-free quantum number to which they are adiabatically connected. Note that the labeling of the states depends on the way the fields are turned on [33]. The time-dependent wave function depends on the time t , the peak intensity I_0 , the FWHM τ , the electrostatic-field strength E_s , and the angle β . For the sake of simplicity, we have not made these dependences explicit, but the field configuration is clearly indicated throughout the text.

To get better physical insight into the field-dressed dynamics, the time-dependent results are compared to those from the adiabatic theory. We take the adiabatic limit by using a constant electrostatic field E_s and constant laser intensity I in Hamiltonian (1). The corresponding time-independent Schrödinger equation is solved by expanding the wave function in a basis that respects the symmetries. The adiabatic states are labeled $|J, M, l\rangle_p^0$ and $|J, M, l\rangle_p$ for $\beta = 0^\circ$ and $0^\circ < \beta < 90^\circ$,

respectively, and we have not made their dependence on the field parameters explicit.

The field-dressed eigenfunctions of this time-independent Hamiltonian form a basis, which is used to analyze the time-dependent wave function $|\gamma\rangle$ by means of the expansion

$$|\gamma\rangle = \sum_{i=1}^N C_{\gamma_i}(t) |\gamma_i\rangle_p, \quad (5)$$

with $C_{\gamma_i}(t) = \langle \gamma | \gamma_i \rangle_p$, γ and γ_i including all the labels identifying these levels. For computational reasons, we have only considered the lowest-lying N adiabatic levels and always ensured that the contributions of highly excited states are negligible. Let us remark that for each time t , the expansion of the wave function is performed in a different adiabatic basis obtained by solving the time-independent Schrödinger equation using the static-field strength and laser intensity at time t , i.e., $E_s(t)$ and $I(t)$.

III. RESULTS IN THE ADIABATIC LIMIT

In this work, we use the OCS molecule (see Fig. 1) as a benchmark to illustrate our results. The rotational constant of OCS is $B = 0.20286 \text{ cm}^{-1}$, the permanent dipole moment $\mu = 0.71 \text{ D}$, and the polarizability anisotropy $\Delta\alpha = 4.04 \text{ \AA}^3$.

We start by analyzing the adiabatic limit. We restrict this study to the following eight states: $|0, 0, e\rangle_p^0$, $|1, 0, e\rangle_p^0$, $|1, 1, e\rangle_p^0$, $|2, 1, e\rangle_p^0$, $|2, 0, e\rangle_p^0$, $|3, 0, e\rangle_p^0$, $|2, 2, e\rangle_p^0$, and $|3, 2, e\rangle_p^0$. For $\beta = 0^\circ$, they adiabatically correspond to the states forming the four first doublets. Note that they well represent the main physical features observed in the overall molecular dynamics, and similar behavior and properties are, therefore, obtained for states in other irreducible representations.

For $E_s = 300 \text{ V/cm}$ and $\beta = 0^\circ$, the energies and the expectation values $\langle \cos^2 \theta \rangle$ and $\langle \cos \theta \rangle$ of these levels are plotted versus the laser intensity in Figs. 2(a)–2(c), respectively. The weak static field breaks the field-free degeneracy in the magnetic quantum number, and as the laser intensity is increased, these states become high-field seekers. In the strong-laser-field regime, once the pendular regime is reached, pairs of quasidegenerate states with the same symmetry are formed. The insets in Fig. 2(a) show how these doublets appear. The gap in energy in a doublet goes as $\Delta E \approx 2|\mu E_{sp} \langle i | \cos \theta | i \rangle_p|$, where $\mu_p \langle i | \cos \theta | i \rangle_p$ is the effective dipole moment of the state $|i\rangle_p$ in the doublet, which is of opposite sign for $|j\rangle_p$. Within a doublet, the two levels are characterized by the same hybridization of the angular motion ($\langle \mathbf{J}^2 \rangle$) and alignment ($\langle \cos^2 \theta \rangle$) [see Fig. 2(b)]. In contrast, they possess opposite orientations ($\langle \cos \theta \rangle$); one is oriented and the other antioriented [cf. Fig. 2(c)]. This opposite orientation is also illustrated in Fig. 2(d) by the polar plots of the square of their wave functions for $I = 10^{12} \text{ W/cm}^2$. The larger is the field-free rotational quantum number of the levels, i.e., their field-free energy, the stronger is the laser intensity needed to achieve a significant orientation. Indeed, the states in the third and fourth doublets are not aligned for $I \lesssim 2 \times 10^{11} \text{ W/cm}^2$ and, therefore, not oriented. Once the pendular regime is achieved, the orientation of these states $|\langle \cos \theta \rangle|$ approaches 1 as I is increased. If the laser field is sufficiently strong, this adiabatic orientation is

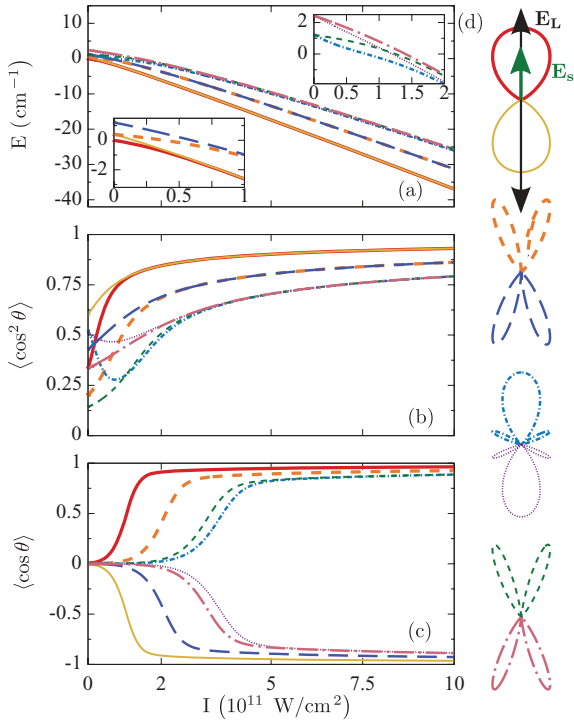


FIG. 2. (Color online) Adiabatic results for the (a) energy and expectation values, (b) $\langle \cos^2 \theta \rangle$, and (c) $\langle \cos \theta \rangle$ as a function I of the adiabatic states $|0,0,e\rangle_p^0$ [thick solid (red) line], $|1,0,e\rangle_p^0$ [thin solid (gold) line], $|1,1,e\rangle_p^0$ [thick short-dashed (orange) line], $|2,1,e\rangle_p^0$ [long-dashed (dark-blue) line], $|2,0,e\rangle_p^0$ [dot-short-dashed (blue) line], $|3,0,e\rangle_p^0$ [dotted (purple) line], $|2,2,e\rangle_p^0$ [thin short-dashed (green) line], and $|3,2,e\rangle_p^0$ [dot-long-dashed (pink) line]. Insets: Relevant energy and intensity ranges where the formation of the near-degenerate doublets occurs. (d) Polar plots of the square of their wave functions at $I = 10^{12}$ W/cm². $E_s = 300$ V/cm and $\beta = 0^\circ$ for all data.

independent of the dc-field strength and of the angle between the two fields.

IV. RESULTS FOR PARALLEL FIELDS

In this section, we investigate the rotational dynamics in a parallel configuration: a dc field of 300 V/cm and a Gaussian pulse with FWHM $\tau = 10$ ns and several peak intensities. Let us remark that recent experimental studies have demonstrated that the nonresonant ionization of OCS is negligible under alignment pulses similar to those analyzed in this work [34–36]. For the ground state $|0,0,e\rangle^0$, the expectation value $\langle \cos \theta \rangle$ is presented in Fig. 3(a) as a function of $I(t)$ up until the peak intensity I_0 is reached. For comparison, the adiabatic results are also shown.

Since the FWHM is 121 times larger than the rotational period, one would expect that the rotational dynamics follows the adiabatic limit. However, this is not the case, and there are significant discrepancies between the time-dependent and the adiabatic results. In contrast to what is predicted by the adiabatic theory, the final orientation decreases as the peak intensity of the laser pulse is increased. For $I_0 = 2 \times 10^{11}$ W/cm², $\langle \cos \theta \rangle$ initially resembles the adiabatic

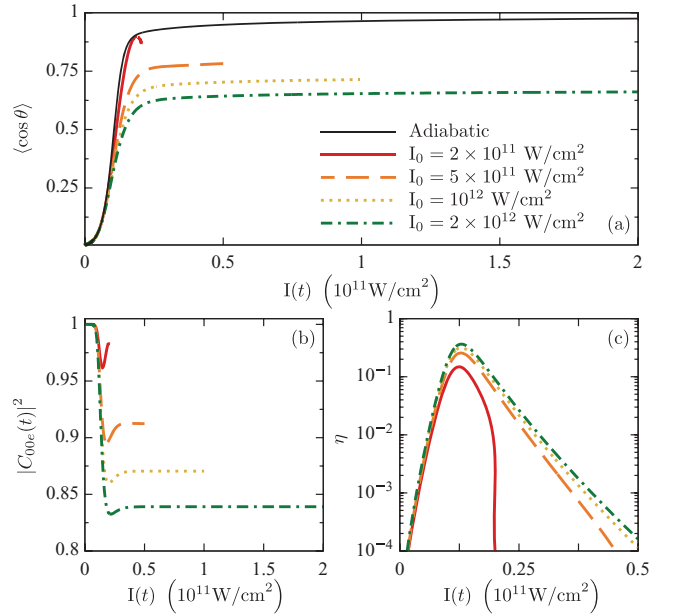


FIG. 3. (Color online) (a) For the ground state, time evolution of the expectation value $\langle \cos \theta \rangle$ as a function of $I(t)$ for Gaussian pulses of $\tau = 10$ ns and peak intensities $I_0 = 2 \times 10^{11}$ W/cm² [thick solid (red) line], $I_0 = 5 \times 10^{11}$ W/cm² [dashed (orange) line], $I_0 = 10^{12}$ W/cm² [dotted (gold) line], and $I_0 = 2 \times 10^{12}$ W/cm² [dot-dashed (green) line]. The adiabatic results for $\langle \cos \theta \rangle$ (thin solid line) are also included. (b) Squares of the projections of the time-dependent wave functions onto the adiabatic pendular state $|0,0,e\rangle_p^0$. (c) Adiabatic criteria η as a function of $I(t)$. The field configuration is $E_s = 300$ V/cm and $\beta = 0^\circ$.

behavior, but it achieves a maximum value $\langle \cos \theta \rangle = 0.899$ for $I(t) = 1.86 \times 10^{11}$ W/cm². For $I_0 = 5 \times 10^{11}$ W/cm², 10^{12} W/cm², and 2×10^{12} W/cm², the orientation shows a qualitatively similar but quantitatively different behavior: in the weak-laser-field regime, $\langle \cos \theta \rangle$ monotonically increases following the adiabatic limit, but for $I(t) \gtrsim 2 \times 10^{11}$ W/cm² it reaches a plateau behavior and the orientation is smaller than the adiabatic value. For instance, $\langle \cos \theta \rangle = 0.661$ for $I(0) = 2 \times 10^{12}$ W/cm², whereas the adiabatic value is $\langle \cos \theta \rangle = 0.975$.

The first physical insight into the nonadiabatic dynamics could be gained by analyzing the characteristic times of the molecule. When the states in a pendular doublet are quasidegenerated, the energy gap between them, $\Delta E \sim 2\mu E_s$, defines a time scale of this system [27]. Note that we have assumed $|\langle i | \cos \theta | i \rangle_p| = |\langle j | \cos \theta | j \rangle_p| \approx 1$, which holds in the strong-laser-field regime. For $E_s = 300$ V/cm and $\beta = 0^\circ$, the energy separation within the first doublet formed by $|0,0,e\rangle_p^0$ and $|1,0,e\rangle_p^0$ is $\Delta E = 6.97 \times 10^{-4}$ cm⁻¹, giving a time scale of 761.21 ps, which is larger than the rotational period, 82.2 ps. Thus, only pulses long enough compared to this pendular time would ensure an adiabatic orientation of the molecule.

Since the static-field strength is so weak, its impact on the rotational dynamics is very small, and before the pulse the levels could be considered as field-free rotor states. As the laser intensity increases, the states are hybridized

by the combined action of both fields, and the doublets of nearly degenerate states are formed in the strong-laser-field regime, as shown in Fig. 2(a). When the energy splitting of this pendular doublet approaches the coupling of the two sublevels due to the pseudo-first-order Stark interaction, these states can mix because they have the same symmetry for $\beta \neq 90^\circ$. As a consequence, there is a population transfer between the oriented and the antioriented states, which results in a decrease in the final orientation compared to the adiabatic limit. For this field configuration, the dynamics can be analyzed by means of the adiabatic states forming this pendular doublet, because their couplings to states in neighboring doublets are much smaller than the energy difference between them. Note that these adiabatic states are the eigenstates of the Hamiltonian at fixed time t .

Under a time-dependent interaction, i.e., in our case the interaction with the laser field $H_L(t)$, (4), the dynamics could be considered adiabatic if and only if the condition [37]

$$\eta = \frac{\hbar | \langle i | \frac{\partial H_L(t)}{\partial t} | j \rangle |}{|E_i - E_j|^2} \ll 1 \quad (6)$$

is fulfilled, with $|i\rangle_p$ and $|j\rangle_p$ being the eigenstates of the Hamiltonian in the adiabatic limit, and E_i and E_j their energies. According to this criterion, the probability of mixing, corresponding to the transfer of a population from one state of the doublet to the other, is determined by the rate of change of the laser-field interaction and the energy separation between the states. Thus, as the laser intensity is increased the population transfer between the two states in a doublet takes place because criterion (6) is not satisfied. To illustrate this phenomenon, we show the contribution of the adiabatic ground state $|C_{00e}(t)|^2$ to the time-dependent wave function of $|0,0,e\rangle^0$ [Fig. 3(b)] and the adiabatic parameter η when $\eta \geq 10^{-4}$ [Fig. 3(c)]. Note that $|C_{00e}(t)|^2 + |C_{10e}(t)|^2 = 1$. In these four cases, the dynamics is initially adiabatic, i.e., $|C_{00e}(t)|^2$ remains equal to 1 and $\eta \ll 1$. As $I(t)$ is increased, the energy splitting of the doublet decreases, and moreover, it becomes comparable to or even larger than the rate of turning-on of the pulse; thus, η is close to 1, and the population transfer takes place. This region where η is not negligible corresponds to the formation of the quasidegenerate doublet. Once the doublet is formed, $\Delta E = |E_i - E_j|$ reaches a small value and slowly decreases as $I(t)$ is enhanced, but the two states are oriented in opposite directions and their wave functions do not overlap. Therefore, the coupling due to the alignment laser is much smaller than ΔE , $\eta \ll 1$ and the population transfer no longer takes place, i.e., $|C_{00e}(t)|^2$ remains constant as $I(t)$ is enhanced. The larger is this population transfer, the smaller is the orientation compared to the adiabatic prediction. Since these adiabatic states contributing to the dynamics are quasidegenerated and have very close values of the alignment and hybridization of the angular motion, the lack of adiabaticity is not reflected in the time evolution of the energy, $\langle \cos^2 \theta \rangle$ or $\langle \mathbf{J}^2 \rangle$. For this field configuration, the molecular dynamics of excited states present features for $\langle \cos \theta \rangle$, $\langle \cos^2 \theta \rangle$, and $\langle \mathbf{J}^2 \rangle$ analogous to those presented for the ground state.

The adiabaticity of the field-dressed dynamics is determined by the rate of change of the laser-field interaction

compared to the largest time scale of the system. In the pendular regime, the energy splitting in a doublet goes as $\Delta E \sim 2\mu E_s$; then the population transfer decreases if E_s is increased. On the other hand, increasing the FWHM augments the time scale on which the pendular doublets are formed and facilitates the adaptation of the molecule to this field. That is, the mixed-field orientation will be more adiabatic when either longer pulses or stronger static electric fields are used. Let us remark that by the expression *the dynamics is more adiabatic*, we mean that, for a certain state, the weight of its corresponding adiabatic state in the time-dependent wave function is closer to 1 during the dynamics.

A. Influence of the peak intensity I_0

Here, we investigate the orientation at the maximum of the laser pulse, as done in most of the experiments [21,25,38]. The rate of change of the laser field and the adiabatic parameter, (6), depend linearly on I_0 . Then, for a Gaussian pulse with a fixed FWHM, the dynamics will be more diabatic if I_0 is increased. In this section, we consider the states $|0,0,e\rangle^0$, $|1,0,e\rangle^0$, $|1,1,e\rangle^0$, $|2,1,e\rangle^0$, $|2,0,e\rangle^0$, $|3,0,e\rangle^0$, $|2,2,e\rangle^0$, and $|3,2,e\rangle^0$. Their orientation at $t = 0$, i.e., $\langle \cos \theta \rangle$ for $I(0) = I_0$, is plotted as a function of I_0 in Figs. 4(a) and 4(b) for $E_s = 300$ V/cm and $E_s = 600$ V/cm, respectively. The fields are parallel, and the FWHM of these pulses is 10 ns.

For $E_s = 300$ V/cm, the orientation of the low-lying level in a doublet increases as I_0 is increased, reaching a maximum and smoothly decreasing thereafter. This is counterintuitive to what is expected in the adiabatic limit, namely, a larger orientation when the laser intensity is increased. The maximum in the orientation is achieved with an alignment pulse that already gives rise to a nonadiabatic dynamics. However, due to the coupling between the populated adiabatic states in the pendular pair ${}_p\langle i | \cos \theta | j \rangle_p$, the orientation is enhanced compared to what happens at the adiabatic limit. By further increasing I_0 , the population transferred between the two states is enhanced, but now the coupling between them is very small or even 0 due to their opposite orientation. As a consequence, the final orientation decreases as I_0 is increased. For a certain pendular doublet, the upper state is antioriented, and $\langle \cos \theta \rangle$ shows the opposite behavior as a function of I_0 . Regarding the third and fourth doublets, the states are not oriented or aligned for ac pulses with $I_0 \lesssim 2.4 \times 10^{11}$ W/cm². Compared to low-lying states, their orientation is smaller and the maximum of $\langle \cos \theta \rangle$ appears at higher peak intensities.

Upon increasing the static field strength to 600 V/cm the energy gap of the pendular pair is also increased, whereas the characteristic time scale of the system is reduced. Thus, for the same laser pulse, the dynamics is more adiabatic, i.e., population transfer is decreased, and the final orientation is increased [see Fig. 4(b)]. The orientation (antiorientation) of the pendular states also achieves a maximum (minimum), but it is so shallow that it is hardly appreciated on the scale of Fig. 4.

To illustrate the field-dressed dynamics, we plot in Fig. 5 the weights of the adiabatic states associated with the oriented levels in these pendular doublets. For the corresponding antioriented levels, the contributions of its associated adiabatic

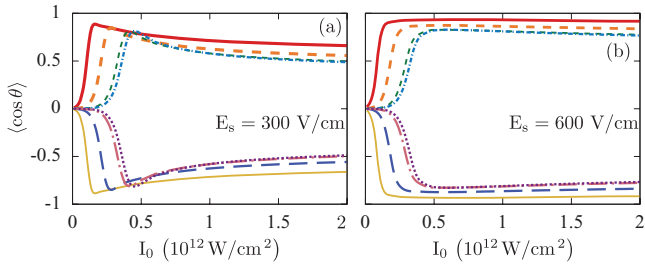


FIG. 4. (Color online) Expectation value $\langle \cos \theta \rangle$ at $t = 0$ as a function of the peak intensity I_0 for the states $|0,0,e^0$ [thick solid (red) line], $|1,0,e^0$ [thin solid (gold) line], $|1,1,e^0$ [thick short-dashed (orange) line], $|2,1,e^0$ [long-dashed (dark-blue) line], $|2,0,e^0$ [dot-short-dashed (blue) line], $|3,0,e^0$ [dotted (purple) line], $|2,2,e^0$ [thin short-dashed (green) line], and $|3,2,e^0$ [dot-long-dashed (pink) line], for $\beta = 0^\circ$ and (a) $E_s = 300$ V/cm and (b) $E_s = 600$ V/cm. The FWHM of the laser pulses is 10 ns.

state are identical to the one presented here, e.g., for the ground state, we present the contribution of the adiabatic ground state $|C_{00e}(0)|^2$, which is identical to the weight $|C_{10e}(0)|^2$ for $|1,0,e^0$. In an adiabatic molecular dynamics, these coefficients are equal to 1. Note that in the considered regime, only the two adiabatic states of the pendular doublet contribute to the dynamics. For all these levels, $|C_i(0)|^2$ decreases, i.e., the dynamics is less adiabatic, as I_0 is enhanced. Upon increasing E_s , ΔE is increased; thus, under the same Gaussian pulse the population transfer is reduced, i.e., $|C_i(0)|^2$ is closer to 1, and the range of peak intensities that can be considered adiabatic is increased.

B. Influence of the FWHM of the laser pulse

The duration of the Gaussian pulse plays an important role in the molecular dynamics. It has been shown that an alignment pulse of 10 ns is not enough to achieve an adiabatic mixed-field orientation for molecules such as OCS, benzonitrile, and iodobenzene [19,27,33,39]. The need to increase the rising time of the laser pulses to achieve the highest possible orientation has been pointed out [27,40,41]. By increasing the FWHM, the time needed to form the pendular doublets is also increased. For a given field configuration, at the point where

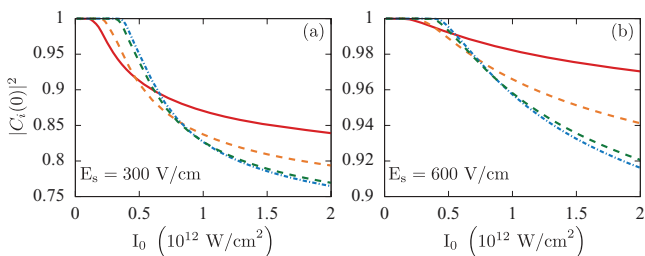


FIG. 5. (Color online) Projections of the time-dependent wave functions onto the corresponding adiabatic states as a function of the peak intensity I_0 for the states $|0,0,e^0$ [thick solid (red) line], $|1,1,e^0$ [thick short-dashed (orange) line], $|2,0,e^0$ [dot-short-dashed (blue) line], and $|2,2,e^0$ [thin short-dashed (green) line], for (a) $E_s = 300$ V/cm and (b) $E_s = 600$ V/cm. We use 10-ns laser pulses and $\beta = 0^\circ$.

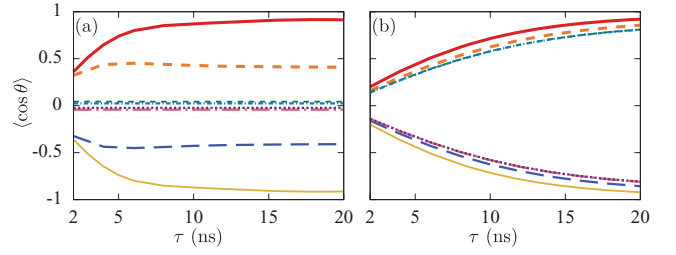


FIG. 6. (Color online) Expectation value $\langle \cos \theta \rangle$ at $t = 0$ as a function of τ for (a) $I_0 = 2 \times 10^{11}$ W/cm 2 and (b) $I_0 = 10^{12}$ W/cm 2 . The fields are parallel and $E_s = 300$ V/cm. The states and their labels are the same as in Fig. 4.

the pulse reaches a certain intensity the adiabatic parameter, (6), is reduced if τ is increased. Hence, the molecular dynamics becomes more adiabatic, and therefore, the population transfer to other pendular states is reduced. Here, we investigate how the directional properties of OCS depends on the laser-pulse FWHM. For the same set of states as in the previous section, Fig. 6 shows the orientation at $t = 0$ as a function of τ . The fields are parallel, and we consider the peak intensities $I_0 = 2 \times 10^{11}$ W/cm 2 and $I_0 = 10^{12}$ W/cm 2 and a dc field of $E_s = 300$ V/cm.

The degree of orientation of the two states in a given pendular pair shows the same behavior as a function of τ , but with their dipole moment pointing in opposite directions. In the first two doublets and with $I_0 = 2 \times 10^{11}$ W/cm 2 , $|\langle \cos \theta \rangle|$ increases with τ till it reaches a plateau-like behavior. The second pair satisfies that $|\langle \cos \theta \rangle| \approx 0.428$ for $\tau \gtrsim 10$ ns. Since the states in the third and fourth doublets have not achieved the pendular regime for $I_0 = 2 \times 10^{11}$ W/cm 2 , increasing the pulse duration does not have any impact on their orientation, and $\langle \cos \theta \rangle$ keeps a constant value close to 0 as τ is increased. For $I_0 = 10^{12}$ W/cm 2 , the degree of orientation of all the states increases and approaches the adiabatic limit as τ is enhanced. For the ground state and $\tau = 20$ ns, we obtain $\langle \cos \theta \rangle = 0.913$, which is very close to the adiabatic value $\langle \cos \theta \rangle = 0.964$.

These results show that for parallel fields, the mixed-field orientation dynamics of any state could be adiabatic if a sufficiently long pulse and sufficiently strong fields are used. For a 50-ns Gaussian pulse with $I_0 = 10^{12}$ W/cm 2 and $E_s = 300$ V/cm, the dynamics can be considered adiabatic for all these states, with $|C_i(0)|^2 \gtrsim 0.999$.

C. Influence of the electrostatic-field strength

Since the energy splitting in a pendular doublet is proportional to the static-field strength, the degree of adiabaticity in the molecular orientation should increase if E_s is enhanced, i.e., the characteristic time scale of the system is reduced. In Fig. 7 we present the final orientation at $t = 0$ of these eight states versus E_s . We have considered two laser pulses of $\tau = 10$ ns with peak intensities $I_0 = 2 \times 10^{11}$ W/cm 2 and 10^{12} W/cm 2 and $\beta = 0^\circ$.

For the lowest laser intensity, the orientation of the $|0,0,e^0$ and $|1,0,e^0$ states is constant and independent of the static field for $E_s \gtrsim 500$ V/cm with $|\langle \cos \theta \rangle| = 0.915$. The orientation of the levels $|1,1,e^0$ and $|2,1,e^0$ increases monotonically

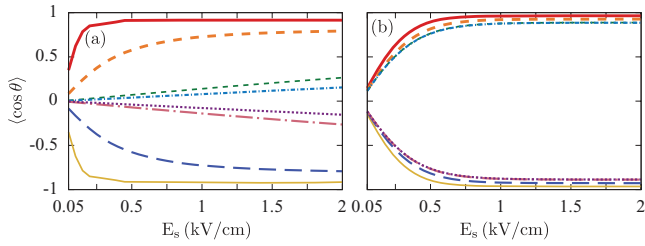


FIG. 7. (Color online) Expectation value $\langle \cos \theta \rangle$ at $t = 0$ as a function of E_s for (a) $I_0 = 2 \times 10^{11}$ W/cm² and (b) $I_0 = 10^{12}$ W/cm². We use a 10-ns laser pulse and $\beta = 0^\circ$. The states and their labels are the same as in Fig. 4.

as E_s is enhanced, and we obtain $|\langle \cos \theta \rangle| = 0.792$ for $E_s = 2$ kV/cm. This peak intensity is not high enough for the states in the third and fourth doublets to be in the pendular regime. Thus, these pairs are weakly oriented even if a strong dc field is used, e.g., for $E_s = 2$ kV/cm, $|\langle \cos \theta \rangle| = 0.265$ and 0.153 for the third and fourth doublets, respectively.

For the strong peak intensity, all the states are in the pendular regime, and their $|\langle \cos \theta \rangle|$ increases as E_s is increased, reaching a constant value for sufficiently strong static fields. Their orientation approaches the adiabatic limit, and for $E_s \gtrsim 1$ kV/cm, $|\langle \cos \theta \rangle| = 0.949$ for the states of the first doublet, and 99.91% of their population is in the corresponding adiabatic pendular state. For $E_s = 2$ kV/cm, the states in the fourth doublet satisfy $|\langle \cos \theta \rangle| = 0.885$, and 99.99% of their population is on the corresponding adiabatic level.

In conclusion, by combining sufficiently strong electrostatic fields with standard Gaussian pulses, i.e., with experimentally accessible peak intensities of 10^{12} W/cm² and a 10-ns FWHM, a significant orientation is obtained even for excited rotational levels. It is worth remarking that the fields have to be parallel; then, techniques such as the ion imaging method [25] could not be used to measure the degree of orientation, whereas techniques such as time of flight [21,38] are feasible.

V. RESULTS FOR NONPARALLEL FIELDS

Some experiments combine the ac electric field from a YAG pulse with the weak dc electric field present in the velocity-mapping image spectrometer and measure the degree of orientation by the ion imaging method [25]. For parallel fields, this technique does not work because all recoiling ions tend to collapse in the center of the detector. Then the mixed-field orientation experiments are performed with tilted fields. In this section, we investigate the rotational dynamics when the electrostatic field forms an angle $0^\circ < \beta < 90^\circ$ with the linearly polarized laser pulse. The azimuthal symmetry is lost, and the number of irreducible representations is reduced to 2 (see Sec. II). The states with different field-free magnetic quantum numbers are coupled by the electrostatic field.

The field-free wave function of the initial state is constructed as an eigenstate of the operators $\mathcal{C}_{E_s}(\pi)$ and σ_{XZ} (see Table I); i.e., $|J, M, e\rangle = R_Y(\beta)|J, M, e\rangle^0$, where $R_Y(\beta)$ is the rotation operator of an angle β around the LFF Y axis [42]. This ensures that this wave function has the correct symmetries

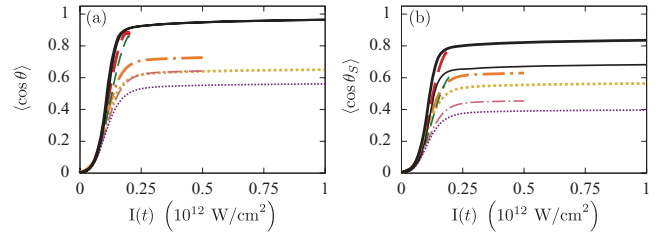


FIG. 8. (Color online) For the ground state, evolution of the expectation values (a) $\langle \cos \theta \rangle$ and (b) $\langle \cos \theta_s \rangle$ as a function of $I(t)$ of a 10-ns Gaussian pulse. The field configurations are $\beta = 30^\circ$ (thick line) and 45° (thin line) with peak intensities $I_0 = 2 \times 10^{11}$ W/cm² (dashed line), 5×10^{11} W/cm² (dot-dashed line), and 10^{12} W/cm² (dotted line). The static electric field is fixed at $E_s = 300$ V/cm. The adiabatic results (solid line) are also included.

and that its time evolution corresponds, in the adiabatic limit, to an eigenstate of the field-dressed Hamiltonian at any time.

Before the pulse is turned on, an important feature of the ground state is that its energy gap to the next state with the same symmetry is proportional to the rotational constant B , which is much larger than the coupling in the weak-laser-field regime. In this regime, it evolves as an isolated state, and its interaction to the neighboring levels can be considered negligible. Hence, analogously to the parallel-field configuration, the formation of the doublets in the pendular regime is the only source of nonadiabatic effects in its field-dressed dynamics. Note that the lowest lying level of the odd irreducible representation will show the same behavior.

For the ground state, the time evolutions of the expectation values $\langle \cos \theta \rangle$ and $\langle \cos \theta_s \rangle$ are presented as a function of $I(t)$ till the peak intensity is reached in Figs. 8(a) and 8(b). The Gaussian pulse has a 10-ns FWHM and peak intensities $I_0 = 2 \times 10^{11}$ W/cm², 5×10^{11} W/cm², and 10^{12} W/cm². We consider the inclination angles $\beta = 30^\circ$ and 45° and a dc field of $E_s = 300$ V/cm. For comparison, the adiabatic results are also included: $\langle \cos \theta \rangle$ is independent of β . For a certain laser pulse, increasing the inclination angle towards 90° implies a decrease in the energy splitting in the first doublet, $\Delta E \sim 2\mu E_s \cos \beta$, and, therefore, an increase in the adiabatic parameter, (6). Note that in the energy splitting we have not considered the component of the dc field along the LFF X axis. Compared to the $\beta = 0^\circ$ configuration, the dynamics can be considered less adiabatic if it is characterized by a larger population transfer to the other adiabatic state in this pendular pair. The final orientation is significantly decreased as β is increased, e.g., for $I_0 = 10^{12}$ W/cm², $\langle \cos \theta \rangle = 0.651$ and 0.561 , and the contribution of the adiabatic ground state is $|C_{00e}(0)|^2 = 0.837$ and 0.791 for $\beta = 30^\circ$ and 45° , respectively. For a certain angle β , the orientation achieved at $t = 0$ decreases as I_0 is increased (cf. Fig. 8). Since the molecular dynamics of the ground state is restricted to the two lower pendular adiabatic states, the time-dependent results for its energy and expectation values $\langle \cos^2 \theta \rangle$ and $\langle \mathbf{J}^2 \rangle$ resemble the adiabatic ones.

To illustrate the rotational dynamics of excited states, we show in Fig. 9(a) the orientation cosine $\langle \cos \theta \rangle$ as a function of $I(t)$ for $|1, 1, e\rangle$. The field configurations are the same as in Fig. 8. The adiabatic model predicts a sharp wrong-way

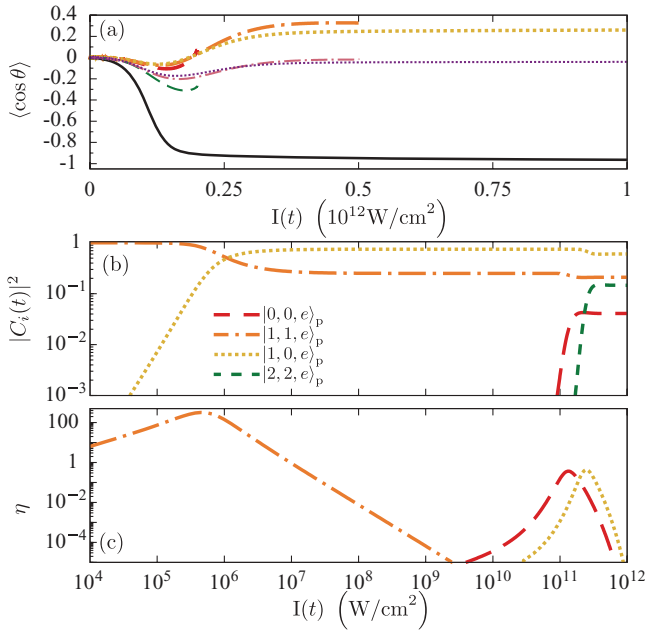


FIG. 9. (Color online) (a) For the $|1,1,e\rangle$ state, the expectation value $\langle \cos \theta \rangle$ as a function of $I(t)$ of a 10-ns Gaussian pulse. The field configurations are $\beta = 30^\circ$ (thick line) and 45° (thin line), with $I_0 = 2 \times 10^{11} \text{ W/cm}^2$ (dashed line), $I_0 = 5 \times 10^{11} \text{ W/cm}^2$ (dot-dashed line) and $I_0 = 10^{12} \text{ W/cm}^2$ (dotted line). The adiabatic results (solid line) are also included. For $I_0 = 10^{12} \text{ W/cm}^2$ and $\beta = 30^\circ$, (b) the squares of the projections of the time-dependent wave function on the adiabatic pendular states $|1,1,e\rangle_p$ (dot-dashed line), $|1,0,e\rangle_p$ (dotted line), $|0,0,e\rangle_p$ (long-dashed line), and $|2,2,e\rangle_p$ (short-dashed line) and (c) the adiabatic parameter between the pendular states $|1,1,e\rangle_p$ and $|1,0,e\rangle_p$ (dot-dashed line), $|1,1,e\rangle_p$ and $|0,0,e\rangle_p$ (dashed line), and $|1,0,e\rangle_p$ and $|2,2,e\rangle_p$ (dotted line). The dc field is fixed at $E_s = 300 \text{ V/cm}$.

orientation. In contrast, this state presents a weak or even 0 orientation, and in addition, a higher peak intensity does not imply a larger orientation. When the peak intensity is reached, this level shows a weak right-way orientation for $\beta = 30^\circ$: $\langle \cos \theta \rangle = 0.326$ and 0.259 , for $I_0 = 5 \times 10^{11} \text{ W/cm}^2$ and 10^{12} W/cm^2 , respectively. For $\beta = 45^\circ$ and peak intensities $I_0 = 5 \times 10^{11} \text{ W/cm}^2$ and 10^{12} W/cm^2 , due to the nonadiabatic dynamics, $|1,1,e\rangle$ is not oriented.

Let us analyze these results in detail. For highly excited states, the dynamics is more complicated. Apart from the doublet formation, there is another physical phenomenon at weak laser intensities which causes loss of adiabaticity. In the presence of only a weak static field, the M degeneracy of the states with the same field-free J is broken due to the quadratic Stark effect, i.e., the splitting goes as $\Delta E \sim E_s^2$. As the pulse is switched on, the energy gap between two states of this J manifold is much smaller than the rate of their coupling due to the laser field, i.e., η is larger than 1. For $\beta = 30^\circ$, the adiabatic parameter η between state $|1,1,e\rangle_p$ and state $|1,0,e\rangle_p$, both contributing to the dynamics of $|1,1,e\rangle$, is presented in Fig. 9(b), and it achieves large values for $I(t) \lesssim 5 \times 10^5 \text{ W/cm}^2$. As the states in this J manifold are driven apart by the laser field, the process is nonadiabatic and

there is a population transfer between them. The projections of the time-dependent wave function in terms of the adiabatic states $|0,0,e\rangle_p$, $|1,1,e\rangle_p$, $|1,0,e\rangle_p$, and $|2,2,e\rangle_p$ are presented in Fig. 9(d) for $\beta = 30^\circ$ and $I_0 = 10^{12} \text{ W/cm}^2$. Under these diabatic conditions, $|C_{11e}(t)|^2$ decreases as $I(t)$ is increased, whereas $|C_{10e}(t)|^2$ increases. Upon further increasing $I(t)$, the coupling between these states becomes very small or even 0 and their energy separation increases, so that η decreases and the population transfer is stopped. This process is so diabatic that the wave function does not change, but its projections on the adiabatic basis are modified because the basis varies with time. For instance, the field-free state is $|1,1,e\rangle = \cos \beta |1,1,e\rangle_p^0 + \sin \beta |1,0,e\rangle_p^0$, which belongs to the proper irreducible representation. After switching-on of the static field, its wave function can be approximated by the same expression because this field is very weak. Once the splitting of this J manifold is finished, i.e., for $I(t) \sim 5 \times 10^7 \text{ W/cm}^2$, the contributions of states $|1,1,e\rangle_p$ and $|1,0,e\rangle_p$ are approximately $\sin^2 \beta$ and $\cos^2 \beta$, respectively. Note that states $|J,M,e\rangle_p^0$ and $|J,M,e\rangle_p$ are not related adiabatically.

In contrast to the ground state, the wave function of any excited level has contributions from adiabatic states which correspond to different pendular doublets. As the laser intensity is increased, the molecular dynamics is affected by the formation of these pendular doublets. Thus, the final orientation could be significantly reduced compared to the parallel-field result. For instance, the time-dependent $|1,1,e\rangle$ state has contributions from the adiabatic levels $|1,1,e\rangle_p$ and $|1,0,e\rangle_p$, which correspond to the first and second pendular doublets, respectively. In Fig. 9(b) we show how the adiabatic parameters η between the pairs $|0,0,e\rangle_p - |1,1,e\rangle_p$ and $|1,0,e\rangle_p - |2,2,e\rangle_p$, which form the first and second doublets, respectively, achieve values close to 1. The final population of state $|1,1,e\rangle$ is $|C_{00e}(0)|^2 = 0.041$, $|C_{11e}(0)|^2 = 0.210$, $|C_{10e}(0)|^2 = 0.603$, and $|C_{22e}(0)|^2 = 0.146$, which gives rise to a small orientation. As a consequence of this population redistribution to other pendular doublets, features of the system such as the energy, alignment, and hybridization of the angular motion do not resemble the adiabatic results. In particular, since the levels on the second pendular doublet possess a smaller alignment, the adiabatic result is larger than the time-dependent one. For instance, for $\beta = 30^\circ$ and $I_0 = 10^{12} \text{ W/cm}^2$, once the time evolution is finished the alignment of this state $|1,1,e\rangle$ is $\langle \cos^2 \theta \rangle = 0.879$, compared to the $\langle \cos^2 \theta \rangle = 0.931$ obtained for the adiabatic level $|1,1,e\rangle_p$.

For $\beta = 45^\circ$, despite the fact that the $|1,1,e\rangle$ level is significantly aligned, $\langle \cos^2 \theta \rangle = 0.896$, it is not oriented with $\langle \cos \theta \rangle = -0.041$ for $I_0 = 10^{12} \text{ W/cm}^2$. This state does not gain any orientation if stronger peak intensities are used. This is a consequence of the population redistribution explained above. Indeed, this level can be considered a *dark state* for the mixed-field orientation dynamics. This physical phenomenon is not restricted to this state and field configuration. We show below that other levels also behave as dark states. It is worth noting that if, in a mixed-field orientation experiment, these dark states form part of the molecular beam, the degree of orientation will be diminished.

The population redistribution to other pendular doublets significantly affects the expectation value $\langle \cos \theta_s \rangle$. Terms which mix up adiabatic states with different magnetic quantum

numbers contribute to $\langle \cos \theta_s \rangle$. Since their wave functions could spatially overlap, their coupling matrix elements do not vanish, and $\langle \cos \theta_s \rangle$ oscillates as t is increased.

The phenomenon of population redistribution at weak laser intensities also occurs for highly excited rotational levels, and for them, more adiabatic states would be involved in it. Before the Gaussian pulse is turned on, the Stark separation of the states in a certain J manifold is increased if the electrostatic field strength is enhanced. Then the adiabatic parameter η is reduced, and the process of splitting of this J manifold becomes less diabatic. Indeed, for sufficiently strong dc fields, the dynamics would be adiabatic without population transfer between states with the same field-free J . For instance, the mixed-field dynamics of the $|1, 1, e\rangle$ level can be considered adiabatic in the weak-laser-field regime for $E_s \gtrsim 14$ kV/cm and $\beta = 30^\circ$.

Let us remark that the excited states could also suffer avoided crossings with adjacent levels having different field-free magnetic quantum numbers M as the pulse intensity is varied. The rotational dynamics in most of these crossings will be nonadiabatic [26].

A. Influence of the peak intensity I_0

Analogously to the parallel-field configuration, we investigate now the impact of the laser peak intensity on the orientation. To do so, we restrict this study to the following eight states: $|0, 0, e\rangle$, $|1, 0, e\rangle$, $|1, 1, e\rangle$, $|2, 0, e\rangle$, $|2, 1, e\rangle$, $|2, 2, e\rangle$, $|3, 0, e\rangle$, and $|3, 2, e\rangle$. Note that they are related to the ones analyzed in the parallel-field configuration, by a rotation of β around the LFF Y axis. Their orientation at $t = 0$, i.e., $\langle \cos \theta \rangle$ for $I(0) = I_0$, is plotted as a function of I_0 in Figs. 10(a) and 10(b) for $\beta = 30^\circ$, in Figs. 10(c) and 10(d) for $\beta = 45^\circ$, and in Figs. 10(e) and 10(f) for $\beta = 75^\circ$, with $E_s = 300$ and 600 V/cm, respectively. The FWHM of these Gaussian pulses is fixed at $\tau = 10$ ns.

Let us start analyzing the results for the ground state. For all field configurations, $\langle \cos \theta \rangle$ shows a qualitatively similar behavior as a function of the peak intensity: it initially increases, reaches a maximum, and decreases thereafter. At the peak intensity where the maximum of $\langle \cos \theta \rangle$ takes place, the dynamics of this state is nonadiabatic, but due to the coupling of the two states in the first pendular pair the orientation increases with respect to the adiabatic result. For a fixed peak intensity and electric field strength, $\langle \cos \theta \rangle$ decreases as β is increased towards 90° . For $\beta = 75^\circ$ and $I_0 = 2 \times 10^{11}$ W/cm², the ground state achieves a moderate maximal orientation, $\langle \cos \theta \rangle = 0.514$ and 0.796 for $E_s = 300$ and 600 V/cm, respectively.

The population transfer taking place at weak and strong laser intensities leaves its finger-prints in the dynamics of the excited states. Compared to the parallel-field results (cf. Fig. 4), their orientation is reduced for any inclination angle β and the pendular pairs are no longer formed by right- and wrong-way oriented states. Whereas for most of the field configurations, the ground state possesses the largest orientation, the levels $|1, 0, e\rangle$ or $|2, 1, 0\rangle$ could achieve a similar or even larger orientation, e.g., for $\beta = 45^\circ$ and 75° , $I_0 \approx 5 \times 10^{11}$ W/cm² and $E_s = 300$ V/cm. For $\beta = 30^\circ$ and $E_s = 600$ V/cm, the degree of orientation is moderate for

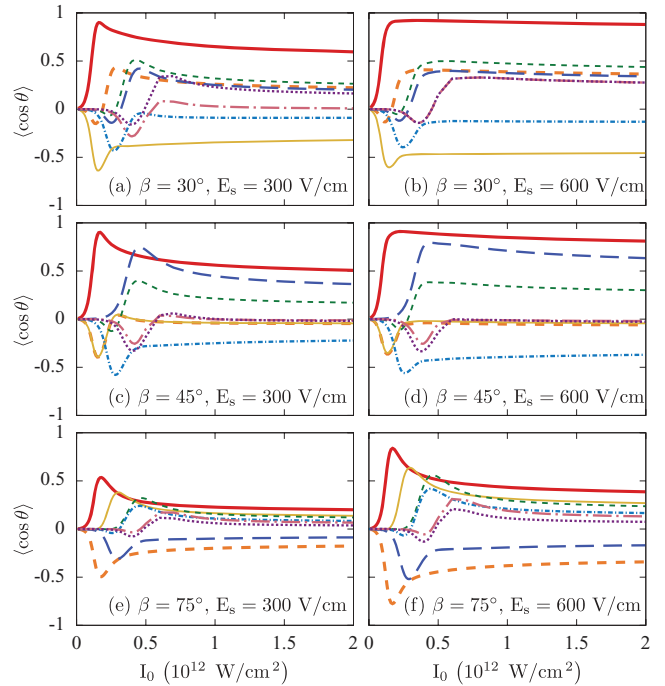


FIG. 10. (Color online) Expectation value $\langle \cos \theta \rangle$ at $t = 0$ as a function of the peak intensity I_0 for $|0, 0, e\rangle$ [thick solid (red) line], $|1, 0, e\rangle$ [thin solid (gold) line], $|1, 1, e\rangle$ [thick short-dashed (orange) line], $|2, 1, e\rangle$ [long-dashed (dark-blue) line], $|2, 0, e\rangle$ [dot-short-dashed (blue) line], $|3, 0, e\rangle$ [dotted (purple) line], $|2, 2, e\rangle$ [thin short-dashed (green) line], and $|3, 2, e\rangle$ [dot-long-dashed (pink) line]. The field configurations are (a), (b) $\beta = 30^\circ$, (c), (d) $\beta = 45^\circ$, and (e), (f) $\beta = 75^\circ$, with $E_s = 300$ and 600 V/cm, respectively. The FWHMs of the Gaussian pulses are fixed at 10 ns.

most of the states. Several dark states are found for $\beta = 45^\circ$: $|1, 1, e\rangle$, $|1, 0, e\rangle$, $|3, 0, e\rangle$, and $|3, 2, e\rangle$ [see Figs. 4(c) and 4(d)]. For instance, the levels $|1, 1, e\rangle$ and $|1, 0, e\rangle$ are strongly aligned with $\langle \cos^2 \theta \rangle = 0.927$ for $I_0 \gtrsim 2 \times 10^{12}$ W/cm² and $E_s = 600$ V/cm, whereas they are not oriented with $\langle \cos \theta \rangle \approx -0.059$ and -0.043 , respectively. For $\beta = 75^\circ$, when the peak intensity of the Gaussian pulse is reached most of the states present a weak orientation; only levels $|0, 0, e\rangle$ and $|1, 1, e\rangle$ have a large orientation for small values of I_0 .

These results indicate that with a 10 ns alignment pulse, strong dc fields and small inclination angles are required to reach a moderate orientation for excited states.

B. Influence of the FWHM of the laser pulse

For the same set of states as in the previous section, we analyze here how their directional properties depend on the FWHM of the Gaussian pulse. In Figs. 11(a) and 11(b) we show $\langle \cos \theta \rangle$ at $t = 0$ as a function of τ for $\beta = 30^\circ$ and 45° , respectively. The static electric field is fixed to $E_s = 300$ V/cm, and the peak intensity to $I_0 = 10^{12}$ W/cm².

The orientation of the ground state increases, approaching the adiabatic limit as τ is increased, and it reaches it with a 50-ns pulse. We encounter several excited states presenting a moderate or weak orientation, and their $|\langle \cos \theta \rangle|$ increases monotonically as τ is increased, e.g., for $\beta = 30^\circ$, the levels $|1, 0, e\rangle$, $|1, 1, e\rangle$, $|2, 0, e\rangle$, $|2, 1, e\rangle$, $|2, 2, e\rangle$, and $|3, 0, e\rangle$, and for

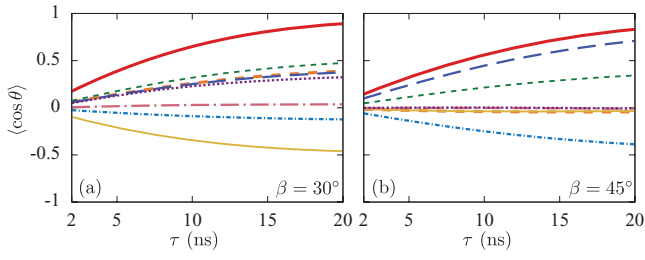


FIG. 11. (Color online) Expectation value $\langle \cos \theta \rangle$ at $t = 0$ as a function of τ . The field configurations are (a) $\beta = 30^\circ$ and (b) $\beta = 45^\circ$, with $I_0 = 10^{12}$ W/cm 2 and $E_s = 300$ V/cm. The states and their labels are the same as in Fig. 10.

$\beta = 45^\circ$, the levels $|2,0,e\rangle$, $|2,1,e\rangle$, and $|2,2,e\rangle$. For all of them, a 20-ns pulse is not enough to achieve the adiabatic regime. In contrast, other excited levels present a very small, almost-zero, orientation independently of the pulse duration. Some of these levels behave as dark states and are strongly aligned but not oriented independently of the pulse duration, e.g., the $|3,2,e\rangle$ state has $\langle \cos^2 \theta \rangle = 0.755$ and $|\langle \cos \theta \rangle| < 0.04$ for $\beta = 30^\circ$ and any value of τ . An analogous behavior is found for the levels $|1,0,e\rangle$, $|1,1,e\rangle$, $|3,0,e\rangle$, and $|3,2,e\rangle$ at $\beta = 45^\circ$. As described above, this phenomenon is due to the nonadiabatic dynamics at weak laser intensities when the levels of the J manifold are driven apart, and it takes place even for 50-ns pulses.

C. Influence of the electrostatic-field strength

In this section, we consider two inclination angles and investigate the impact of the electrostatic field on the mixed-field orientation dynamics of the same states. Figures 12(a) and 12(b) illustrate the behavior of $\langle \cos \theta \rangle$ at $t = 0$ as a function of E_s for $\beta = 30^\circ$ and 45° , respectively. The laser pulse has $\tau = 10$ ns and $I_0 = 10^{12}$ W/cm 2 .

The ground state presents the largest orientation, which increases as E_s is enhanced and is strongly oriented for sufficiently large fields, e.g., $\langle \cos \theta \rangle > 0.9$ for $E_s \geq 600$ V/cm and $\beta = 30^\circ$. Regarding the excited states, their orientation strongly depends on the inclination angle. For $\beta = 30^\circ$, $|\langle \cos \theta \rangle|$ increases monotonically till it reaches a plateau-like behavior, and they show a moderate orientation. Indeed, for $\beta = 30^\circ$, $I_0 = 10^{12}$ W/cm 2 , and $E_s = 2$ kV/cm, we obtain, at the maximum of the Gaussian pulse, $\langle \cos \theta \rangle = -0.402$ and 0.365 for states $|1,0,e\rangle$ and $|1,1,e\rangle$, respectively. For $\beta = 45^\circ$,

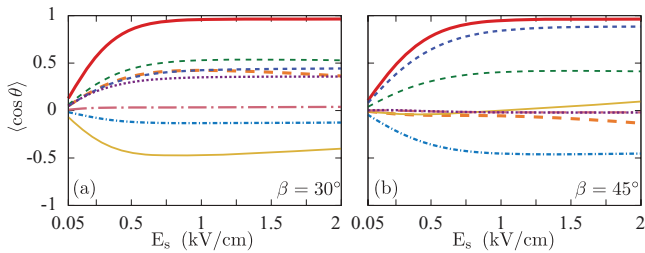


FIG. 12. (Color online) Expectation value of $\langle \cos \theta \rangle$ at $t = 0$ as a function of E_s for the field configurations $\tau = 10$ ns, $I_0 = 10^{12}$ W/cm 2 , and (a) $\beta = 30^\circ$ and (b) $\beta = 45^\circ$. Labeling of the states is as in Fig. 10.

the level $|2,1,e\rangle$ presents a large orientation: $\langle \cos \theta \rangle > 0.8$ for $E_s \gtrsim 800$ V/cm. There are some dark states for $\beta = 45^\circ$, which are not oriented even when dc fields of 2 kV/cm are used, e.g., $|3,0,e\rangle$ and $|3,2,e\rangle$.

For nonparallel fields, a strong dc field does not ensure a large orientation for excited rotational states. If the aim is a strongly oriented molecular ensemble, then this should be as pure as possible in the ground state.

In Hamiltonian (3), the term $-\mu E_s \sin \beta \sin \theta \cos \phi$ is responsible for the mixing of states with different field-free magnetic quantum numbers. In the weak-dc-field regime, the mixing between these states is so small that M can be considered conserved, and this term can be neglected. Upon increasing E_s , this coupling between levels with different field-free M values becomes important, and this should affect the molecular dynamics. Thus, the questions that remain open are, How important is the X component of the electrostatic field to the dynamics? and For which electric-field regime can we consider only its Z component, $\mathbf{E}_s = E_s \cos \beta \hat{Z}$?

As indicated above, even for tilted fields, the dynamics of the ground state can be described by a two-state model. Its energy separation to the next state with $M \neq 0$ is of the order of B and larger than the dc field coupling to these levels. Thus, for $E_s \lesssim 20$ kV/cm, the dynamics considering the dc field is equal to the one obtained when only its Z component is included.

For the excited states, the answer to these questions depends on how the initial wave function, before the fields are switched on, is constructed. The first option is to proceed as indicated at the beginning of this section; the field-free $\beta \neq 0^\circ$ and $\beta = 0^\circ$ wave functions are related by a rotation of β around the Y axis, $|J,M,e\rangle = R_Y(\beta)|J,M,e\rangle^0$. In this case, for the level $|1,1,e\rangle$, some differences in its orientation are observed for $E_s \gtrsim 1$ kV and $|\langle \cos \theta \rangle|$ is larger if the two components of \mathbf{E}_s are considered. These differences are increased as E_s is increased, e.g., for a 10-ns laser pulse with $I_0 = 1 \times 10^{12}$ W/cm 2 , $\beta = 45^\circ$, and $E_s = 5$ kV/cm, we obtain, at $t = 0$, $\langle \cos \theta \rangle = -0.629$, compared to $\langle \cos \theta \rangle = -0.019$ when only the Z component of \mathbf{E}_s is included. Upon increasing E_s this state will achieve an adiabatic dynamics only if both components of the static field are present. The second option is to construct the field-free $\beta \neq 0^\circ$ wave function equal to the field-free $\beta = 0^\circ$ one. In this case, the results resemble those of the parallel-field configuration taking into account $\cos \beta$ as the scaling factor for the static-field strength.

D. Influence of the inclination of the fields

The symmetries of the rotational Hamiltonian, (1) (see Sec. II), and therefore, the rotational dynamics strongly depend on the angle between the fields. In this section, we investigate in detail the impact of the inclination angle in the mixed-field orientation dynamics.

For the ground state $|0,0,e\rangle$, the orientation cosines $\langle \cos \theta \rangle$ and $\langle \cos \theta_s \rangle$ are plotted in Fig. 13, as a function of β , together with the adiabatic results. For a weak dc field and a strong laser field, the relation $\langle \cos \theta_s \rangle \approx \langle \cos \theta \rangle \cos \beta$ is satisfied within the adiabatic limit. In $\langle \cos \theta_s \rangle$ the term $\langle \sin \theta \cos \phi \rangle \sin \beta$ has been neglected, which can be done as long as the mixing between states with different field-free M values is very small. Upon increasing the electrostatic-field strength,

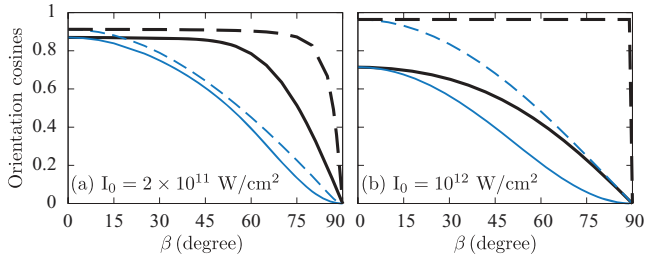


FIG. 13. (Color online) Expectation values $\langle \cos \theta \rangle$ (thick solid line) and $\langle \cos \theta_s \rangle$ (thin solid line) at $t = 0$ as a function of β for the ground state. The peak intensities are (a) $I_0 = 2 \times 10^{11}$ W/cm² and (b) $I_0 = 10^{12}$ W/cm². The adiabatic results for $\langle \cos \theta \rangle$ (thick dashed line) and $\langle \cos \theta_s \rangle$ (thin dashed line) are also presented. The FWHM of the laser pulse is fixed at $\tau = 10$ ns, and the dc field at $E_s = 300$ V/cm.

a regime would be encountered where this approximation no longer holds. An analogous relation is satisfied between the time-dependent orientation cosines of the ground state. For $I_0 = 2 \times 10^{11}$ W/cm², its orientation $\langle \cos \theta \rangle$ shows a plateau-like behavior till $\beta = 50^\circ$, which is very close to the adiabatic limit. Upon further increasing β , $\langle \cos \theta \rangle$ decreases and approaches 0. For $\beta = 90^\circ$, the states in a pendular doublet have different symmetries and are not coupled by the dc field, thus they might be strongly aligned but not oriented. For $I_0 = 10^{12}$ W/cm², $\langle \cos \theta \rangle$ monotonically decreases as β is increased towards 90° , and its value is always smaller than for $I_0 = 2 \times 10^{11}$ W/cm². For both laser fields, $\langle \cos \theta_s \rangle$ decreases as β is increased.

In Figs. 14(a)–14(d), we present the orientation cosine of the pairs $|0,0,e\rangle - |1,0,e\rangle$, $|1,1,e\rangle - |2,1,e\rangle$, $|2,2,e\rangle - |3,2,e\rangle$, and $|2,0,e\rangle - |3,0,e\rangle$, respectively, as a function of β . The static-field strength is $E_s = 300$ V/cm and we consider two Gaussian pulses of 10-ns FWHM and peak intensities $I_0 = 2 \times 10^{11}$ W/cm² and 10^{12} W/cm². Due to the complicated

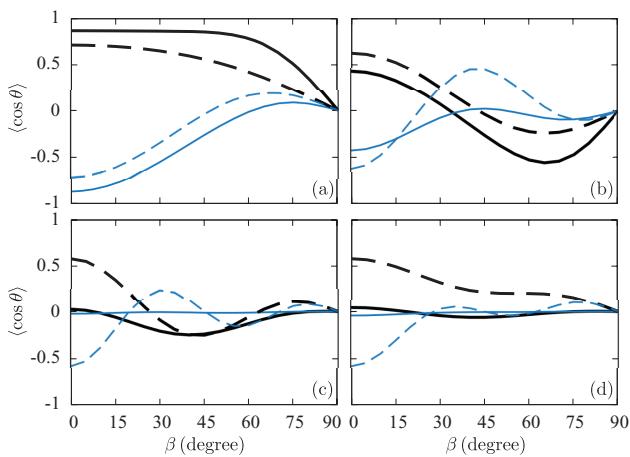


FIG. 14. (Color online) Expectation value $\langle \cos \theta \rangle$ at $t = 0$ as a function of β for the states (a) $|0,0,e\rangle$ (black line) and $|1,0,e\rangle$ (blue line), (b) $|1,1,e\rangle$ (black line) and $|2,1,e\rangle$ (blue line), (c) $|2,0,e\rangle$ (black line) and $|3,0,e\rangle$ (blue line), and (d) $|2,2,e\rangle$ (black line) and $|3,2,e\rangle$ (blue line). The field configuration is $E_s = 300$ V/cm, with $I_0 = 2 \times 10^{11}$ W/cm² (solid lines) and 10^{12} W/cm² (dashed lines). The FWHM of the laser pulse is fixed at $\tau = 10$ ns.

field-dressed dynamics of excited states for $0^\circ < \beta < 90^\circ$ with contributions from several pendular pairs, in $\langle \cos \theta_s \rangle$ the term $\langle \sin \theta \cos \phi \rangle$ cannot be neglected. Thus, the simple relation $\langle \cos \theta_s \rangle \approx \langle \cos \theta \rangle \cos \beta$ does not hold for these levels.

Based on the adiabatic theory, the ground state and the level $|1,0,e\rangle$ should present the same orientation but with opposite directions. However, this is only satisfied for $\beta = 0^\circ$. Due to the nonadiabatic effects at weak laser intensities, its $|\langle \cos \theta \rangle|$ is smaller than the corresponding value of $|0,0,e\rangle$ for $0 < \beta < 90^\circ$. For the second doublet [cf. Fig. 14(b)], $\langle \cos \theta \rangle$ oscillates as β is varied, and the orientation even changes its direction. Both states could present a moderate orientation at a certain value of β . The pendular regime is not achieved by the third and fourth pairs with a 10-ns laser pulse and $I_0 = 2 \times 10^{11}$ W/cm², and their orientation is either 0 or very small independent of β . For $I_0 = 10^{12}$ W/cm² and $\beta = 0^\circ$, these four states show a moderate orientation, which is reduced for any other angle and is small for $\beta \gtrsim 60^\circ$. At the strong peak intensity $I_0 = 10^{12}$ W/cm², in all pendular doublets one of the two levels presents the dark behavior with respect to the mixed-field orientation dynamics at a certain angle β .

These results show that if the molecular beam is rotationally cold, a small inclination angle will optimize the degree of orientation observed in the experiment.

VI. ROTATIONAL DYNAMICS ONCE THE LASER PULSE IS TURNED ON

Let us investigate the dynamics for $t > 0$ assuming that the laser peak intensity, reached at $t = 0$, and the dc-field strength are kept constant for $t > 0$; i.e., $I(t) = I_0$ and $E_s(t) = E_s$ for $t > 0$. At $t = 0$, the time-dependent wave function can be expressed in terms of the corresponding adiabatic basis. Since the Hamiltonian is time independent for $t > 0$, the contribution of each adiabatic state remains constant as t is increased. For a certain state $|\gamma\rangle$, the expectation value of an operator \hat{A} in this adiabatic basis reads as

$$\langle \hat{A} \rangle = \sum_j |C_{\gamma_j}(0)|^2 \langle \gamma_j | \hat{A} | \gamma_j \rangle_p + 2 \sum_{j < k} |C_{\gamma_j}(0)| |C_{\gamma_k}(0)| \times \langle \gamma_j | \hat{A} | \gamma_k \rangle_p \cos \left(\frac{\Delta E_{jk} t}{\hbar} + \delta_{jk} \right), \quad (7)$$

with $C_{\gamma_j}(0)$ being the weight at $t = 0$ of the adiabatic state $|\gamma_j\rangle_p$ to the wave function of $|\gamma\rangle$, ΔE_{jk} the energy splitting between the adiabatic levels $|\gamma_j\rangle_p$ and $|\gamma_k\rangle_p$, and δ_{jk} the phase difference of $C_{\gamma_j}(0)$ and $C_{\gamma_k}(0)$.

Based on the results presented above, the time-dependent wave function could have contributions from (i) only the adiabatic levels forming a pendular doublet or (ii) several adiabatic levels from at least two pendular doublets. All the states for $\beta = 0^\circ$ and the ground state for $0^\circ \leq \beta < 90^\circ$ could belong to the first case, whereas the second one refers to all excited states when $0^\circ < \beta < 90^\circ$, unless the static field is very strong.

Let us first analyze the case where the dynamics takes place within a pendular doublet. If the adiabatic states are not fully oriented, the coupling term in Eq. (7) is nonzero and this expectation value oscillates for $t > 0$ with a frequency equal to the energy splitting of the corresponding pendular doublet. For

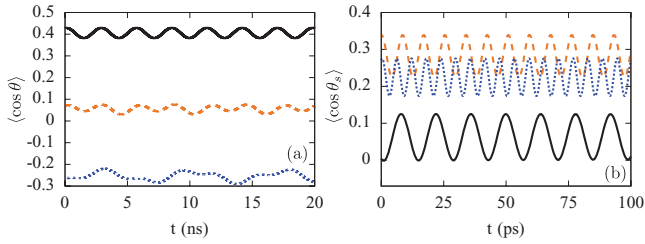


FIG. 15. (Color online) Orientation cosines once the peak intensity and dc-field strength are kept constant for $t > 0$. For state $|1, 1, e\rangle$, (a) the expectation value $\langle \cos \theta \rangle$ with $I_0 = 2 \times 10^{11}$ W/cm² and $\beta = 0^\circ$ (solid line), $\beta = 30^\circ$ (dashed line), and $\beta = 45^\circ$ (dotted line) and (b) the value $\langle \cos \theta_s \rangle$ with $\beta = 30^\circ$ and $I_0 = 2 \times 10^{11}$ W/cm² (solid line), $I_0 = 5 \times 10^{11}$ W/cm² (dashed line), and $I_0 = 10^{12}$ W/cm² (dotted line). The dc field is $E_s = 300$ V/cm.

the $|1, 1, e\rangle$ state, this behavior is shown for the time evolution of $\langle \cos \theta \rangle$ in Fig. 15(a), with $I_0 = 2 \times 10^{11}$ W/cm², $E_s = 300$ V/cm, and $\beta = 0^\circ$. An analogous behavior is obtained for the ground state and $0^\circ < \beta < 90^\circ$. Upon further increasing the peak intensity, the orientation of the adiabatic states increases, the coupling terms are reduced, approaching 0, and these regular oscillations will disappear.

When two pendular doublets participate in the dynamics, this oscillatory behavior becomes irregular, because the frequencies associated with the energy separations within each pendular doublet and between two of them do not form a commensurable set. As an example, we show in Fig. 15(a) these irregular oscillations of $\langle \cos \theta \rangle$ for $|1, 1, e\rangle$ with $\beta = 30^\circ$ and 45° , $E_s = 300$ V/cm, and $I_0 = 2 \times 10^{11}$ W/cm². Upon increasing I_0 , the dynamics of this state still has contributions from different pendular doublets, but the two states in a pendular pair are not populated. As a consequence, the coupling terms are reduced and the oscillation decreases or even disappears.

For $0^\circ < \beta < 90^\circ$, the time evolution of $\langle \cos \theta_s \rangle$ is dominated by the couplings of adiabatic levels from doublets with $|\Delta M| \approx 1$. This is illustrated in Fig. 15(b) for state $|1, 1, e\rangle$, with $I_0 = 2 \times 10^{11}$ W/cm², 5×10^{11} W/cm², and 10^{12} W/cm² and $\beta = 30^\circ$. Independently of I_0 , on this time scale $\langle \cos \theta_s \rangle$ oscillates, with the highest frequency given by the energy gap between the two pendular doublets involved, which is similar for the three peak intensities. On a larger time scale, the frequencies due to the states in a doublet will modulate the oscillations of $\langle \cos \theta_s \rangle$ in the weak-field regime.

VII. SWITCHING ON THE LASER PULSE FIRST: ORIENTATION OF THE ALIGNED PENDULAR STATES.

In previous sections, the field configuration was based on mixed-field orientation experiments [23,25,27]. Here, we investigate the molecular dynamics when the pendular pairs of aligned states are already formed and a dc electric field is turned on to orient them. Experimentally, the alignment could be induced by a nonresonant cw laser. We assume that this process is adiabatic [43,44]. For a sufficiently high intensity, these levels are strongly aligned but not oriented. Upon turning on the static field, these states have the same symmetry and

they should be oriented due to their interaction with this field. For this field configuration, we now check the validity of the adiabatic predictions [18,19] by comparing them to a time-dependent analysis.

If I_0 is large enough, the energy gap between the states in a pendular doublet is much smaller than the energy gap with the neighboring doublet. Thus, when the static field is switched on, the rotational dynamics of a certain pendular level can be approximated by a two-state model involving the two levels forming the corresponding pendular doublet [19]. At $t = 0$, $E_s(0) = 0$, and $I(0) = I_0$, the pendular states are $|\psi_l\rangle$, with $l = e$ and o indicating even or odd parity. Under this approximation, the levels $|\psi_r\rangle = (|\psi_e\rangle + |\psi_o\rangle)/\sqrt{2}$ and $|\psi_w\rangle = (|\psi_e\rangle - |\psi_o\rangle)/\sqrt{2}$ are right- and wrong-way oriented, respectively. The two-state-model Hamiltonian yields

$$H(t) = \begin{pmatrix} 0 & -\mu v_s t \langle \cos \theta_s \rangle_{eo} \\ -\mu v_s t \langle \cos \theta_s \rangle_{eo} & \Delta E \end{pmatrix},$$

where we have used $E_s(t) = v_s t$, with $v_s = E_s/T_0$ and T_0 being the switching-on speed and time, respectively. T_0 is chosen so that if the states are exposed only to this field, the turning-on process is adiabatic. We have taken $\langle \psi_e | H | \psi_e \rangle = 0$, $\langle \psi_o | H | \psi_o \rangle = \Delta E$, and $\langle \psi_e | H | \psi_o \rangle = \langle \psi_o | H | \psi_e \rangle = -\mu v_s t \langle \psi_e | \cos \theta_s | \psi_o \rangle = -\mu v_s t \langle \cos \theta_s \rangle_{eo}$. The time-dependent Schrödinger equation associated with this Hamiltonian admits a scaling factor. That is, when the dynamics is adiabatic using v_s for a pendular doublet with energy splitting ΔE for I_0 , then, for I'_0 and $\Delta E' = k \Delta E$, the dynamics is adiabatic for $v'_s = k^2 v_s$.

For the sake of simplicity, we focus on the ground state in a parallel-field configuration. For several switching-on speeds, Figs. 16(a) and 16(b) display the directional cosine and the population of the adiabatic ground state, respectively, as a function of $E_s(t)$, and $I_0 = 2 \times 10^{11}$ W/cm². Before the dc field is turned on, the alignment of the ground state is $\langle \cos^2 \theta \rangle = 0.845$, the energy separation within this pendular pair is $\Delta E \approx 5.36 \times 10^{-4}$ cm⁻¹, and there are 2.4 cm⁻¹ to the next pendular doublet. For $E_s = 1$ V/cm, the coupling term is $\mu \langle \cos \theta \rangle_{eo} E_s = 1.09 \times 10^{-5}$ cm⁻¹ with $\langle \cos \theta \rangle_{eo} = 0.915$. In an adiabatic picture, the energy gap ΔE cannot be neglected, and as $E_s(t)$ is increased the energy of the ground state does not increase linearly with E_s [19]. For

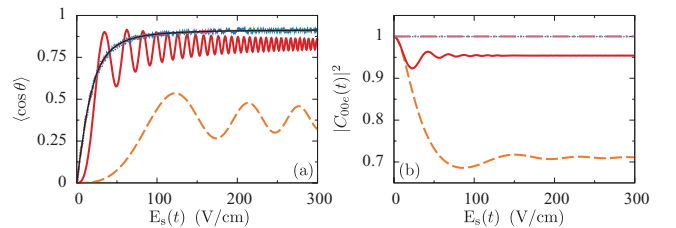


FIG. 16. (Color online) For the ground state, (a) expectation value $\langle \cos \theta \rangle$ and (b) weight of the adiabatic ground state on its time-dependent wave function as a function of $E_s(t)$, for turning-on speeds $v_s = 10^{10}$ Vcm⁻¹s⁻¹ [dashed (orange) line], $v_s = 10^9$ Vcm⁻¹s⁻¹ [solid (red) line], $v_s = 10^8$ Vcm⁻¹s⁻¹ [dotted (blue) line], and $v_s = 10^7$ Vcm⁻¹s⁻¹ [dot-dashed (pink) line], and adiabatic results (thin solid line). The fields are parallel and $I_0 = 2 \times 10^{11}$ W/cm².

$v_s = 10^{10}$ Vcm $^{-1}$ s $^{-1}$, with the adiabatic parameter $\eta \approx 1$, the rotational dynamics is nonadiabatic and there is a population transfer between the two states in this doublet. We note that for this process, the adiabatic parameter η is defined as in Eq. (6), but replacing the laser-field interaction $H_L(t)$, (4), with the dipole term $H_s(t)$, (3). The ground state presents a moderate orientation below the adiabatic limit due to the contributions of the adiabatic states $|0,0,e\rangle_p$ and $|1,0,e\rangle_p$; $|C_{00e}(t)|^2$ decreases until a minimum value, showing a smooth oscillation afterward [cf. Fig. 16(b)]. Due to the coupling term, $\langle \cos \theta \rangle$ oscillates as $E_s(t)$ is increased, and its frequency is equal to the energy separation between the adiabatic levels $|0,0,e\rangle_p$ and $|1,0,e\rangle_p$. A similar behavior is observed for 10^9 Vcm $^{-1}$ s $^{-1}$, but $\langle \cos \theta \rangle$ oscillates around a value closer to the adiabatic limit because the process is more adiabatic and $|C_{00e}(t)|^2 \approx 0.956$ for $E_s(t) \gtrsim 100$ V/cm. For $v_s = 10^8$ and 10^7 Vcm $^{-1}$ s $^{-1}$, the dynamics can be considered adiabatic, with $|C_{00e}(t)|^2 > 0.999$. However, for $v_s = 10^8$ Vcm $^{-1}$ s $^{-1}$, $\langle \cos \theta \rangle$ still shows small oscillations.

Upon increasing the laser intensity, the energy splitting of the levels in a pendular doublet is decreased, but their coupling due to the dc field is not significantly modified. Thus, the rotational dynamics becomes more diabatic, and larger turning-on times are needed to achieve the adiabatic limit. For $I_0 = 5 \times 10^{11}$ W/cm 2 , the ground state is separated by $\Delta E \approx 7.7 \times 10^{-7}$ cm $^{-1}$ from $|1,0,e\rangle_p$ and by 3.9 cm $^{-1}$ from the next pendular doublet. The coupling due to the dc field is 1.13×10^{-5} cm $^{-1}$ for $E_s = 1$ V/cm and with $\langle \cos \theta \rangle_{eo} = 0.948$. According to the scaling law of the time-dependent Schrödinger equation, this process would be adiabatic for $v_s \lesssim 20$ Vcm $^{-1}$ s $^{-1}$.

For $I_0 = 10^{12}$ W/cm 2 and the ground state, we find $\Delta E \approx 3.3 \times 10^{-10}$ cm $^{-1}$ and 5.7 cm $^{-1}$ to the second doublet, and $\mu \langle \cos \theta \rangle_{eo} E_s = 1.18 \times 10^{-5}$ cm $^{-1}$ for $E_s = 1$ V/cm and with $\langle \cos \theta \rangle_{eo} = 0.964$. Within an adiabatic framework, as E_s is increased the ground-state energy can be approximated by the pseudo-first-order Stark linear effect $|\mu E_s \langle 0,0,e | \cos \theta | 1,0,e \rangle_p|$ [19]. Note that ΔE is smaller than the dc-field coupling even for $E_s \approx 10^{-4}$ V/cm. Based on the scaling law of the two-state model Schrödinger equation, the dc field should be turned on very slowly, $v_s \lesssim 10^{-2}$ Vcm $^{-1}$ s $^{-1}$, to achieve the adiabatic limit. For higher turning-on speeds, the dynamics is so diabatic that the $|0,0,e\rangle$ wave function does not change, and its projections on the adiabatic states $|0,0,e\rangle_p$ and $|1,0,e\rangle_p$ are close to the field-free values even for $v_s \approx 10^5$ Vcm $^{-1}$ s $^{-1}$.

VIII. CONCLUSIONS

In this work, we have investigated the mixed-field orientation dynamics of linear molecules. The richness and variety of the field-dressed rotational dynamics have been illustrated by analyzing in detail the directional properties of several

low-lying states. In particular, we have explored the degree of orientation as the peak intensity and FWHM of the Gaussian pulse, the electrostatic field strength, and the angle between the two fields are varied.

By considering prototypical field configurations used in current mixed-field orientation experiments, we have proven that the assumption of a fully adiabatic dynamics is incorrect. For parallel fields, a nonadiabatic transfer of population takes place when the quasidegenerated pendular doublets are formed as the laser intensity is increased. As a consequence, the time-dependent results for the degree of orientation are smaller than the predictions of the adiabatic theory. Using current available experimental peak intensities, longer laser pulses or stronger static fields will increase the degree of orientation even for highly excited states. In particular, we have provided the field parameters under which the mixed-field orientation dynamics will be fully adiabatic. We have also shown that the field-dressed dynamics is more complicated if both fields are tilted. Apart from the nonadiabatic effects when the pendular doublets are formed, at weak laser intensities there is also population transfer due to the splitting of the states within a J manifold now having the same symmetry. For nonparallel fields, we have shown that the ground state is strongly oriented, whereas excited states might only present a moderate or weak orientation, and furthermore, some of them could behave as dark states in the mixed-field orientation dynamics. The requirements for an adiabatic dynamics are now more difficult to satisfy for excited levels than for the ground state. Again, we have indicated that the field configuration that will give rise to an adiabatic mixed-field orientation. If the peak intensity is kept constant after turning on the pulse, we have shown that the orientation of the states might oscillate with time due to the nonadiabatic dynamics. Finally, we have investigated the orientation dynamics of the adiabatically aligned ground state; the switching-on of the dc field has to be very slow to achieve a significant orientation.

Although our study is restricted to the OCS molecule, we stress that the above-observed physical phenomena are expected to occur in many other polar molecules. Indeed, the Hamiltonian can be rescaled, and the above results used to describe another polar linear molecule. In addition, due to the complexity of the rotational level structure of asymmetric tops, these nonadiabatic effects should have a negative impact in mixed-field orientation experiments [23,26].

ACKNOWLEDGMENTS

We would like to thank B. Friedrich, J. Küpper, J. H. Nielsen, P. Schmelcher, and H. Stapelfeldt for fruitful discussions. Financial support by Spanish project FIS2011-24540 (MICINN), Grants No. FQM-2445 and No. FQM-4643 (Junta de Andalucía), and Andalusian research group FQM-207 is gratefully appreciated. J.J.O. acknowledges the support of the M.E. under the FPU program.

[1] P. R. Brooks, *Science* **193**, 11 (1976).

[2] P. R. Brooks and E. M. Jones, *J. Chem. Phys.* **45**, 3449 (1966).

[3] H. J. Loesch and J. Möller, *J. Chem. Phys.* **97**, 9016 (1992).

[4] F. J. Aoiz, B. Friedrich, V. J. Herrero, V. S. Rábanos, and J. E. Verdasco, *Chem. Phys. Lett.* **289**, 132 (1998).

- [5] V. Aquilanti, M. Bartolomei, F. Pirani, D. Cappelletti, and F. Vecchiocattivi, *Phys. Chem. Chem. Phys.* **7**, 291 (2005).
- [6] C. Z. Bisgaard, O. J. Clarkin, G. Wu, A. M. D. Lee, O. Gessner, C. C. Hayden, and A. Stolow, *Science* **323**, 1464 (2009).
- [7] L. Holmegaard, J. L. Hansen, L. Kalhøj, S. L. Kragh, H. Stapelfeldt, F. Filsinger, J. Küpper, G. Meijer, D. Dimitrovski, M. Abu-samha *et al.*, *Nat. Phys.* **6**, 428 (2010).
- [8] J. L. Hansen, H. Stapelfeldt, D. Dimitrovski, M. Abu-samha, C. P. J. Martiny, and L. B. Madsen, *Phys. Rev. Lett.* **106**, 073001 (2011).
- [9] E. Frumker, C. T. Hebeisen, N. Kajumba, J. B. Bertrand, H. J. Wörner, M. Spanner, D. M. Villeneuve, A. Naumov, and P. B. Corkum, *Phys. Rev. Lett.* **109**, 113901 (2012).
- [10] P. M. Kraus, S. Vljakovic, A. Rupenyan, and H. J. Wörner (2012) [Phys. Rev. Lett. (to be published)].
- [11] S. Stolte, *Atomic and Molecular Beam Methods* (Oxford University Press, New York, 1988).
- [12] H. J. Loesch and A. Remscheid, *J. Chem. Phys.* **93**, 4779 (1990).
- [13] B. Friedrich and D. R. Herschbach, *Nature* **353**, 412 (1991).
- [14] B. Friedrich, D. P. Pullman, and D. R. Herschbach, *J. Phys. Chem.* **95**, 8118 (1991).
- [15] P. A. Block, E. J. Bohac, and R. E. Miller, *Phys. Rev. Lett.* **68**, 1303 (1992).
- [16] B. Friedrich, H. G. Rubahn, and N. Sathyamurthy, *Phys. Rev. Lett.* **69**, 2487 (1992).
- [17] A. Slenczka, B. Friedrich, and D. Herschbach, *Phys. Rev. Lett.* **72**, 1806 (1994).
- [18] B. Friedrich and D. R. Herschbach, *J. Chem. Phys.* **111**, 6157 (1999).
- [19] B. Friedrich and D. Herschbach, *J. Phys. Chem. A* **103**, 10280 (1999).
- [20] T. Seideman and E. Hamilton, *Adv. At. Mol. Opt. Phys.* **52**, 289 (2006).
- [21] H. Sakai, S. Minemoto, H. Nanjo, H. Tanji, and T. Suzuki, *Phys. Rev. Lett.* **90**, 083001 (2003).
- [22] U. Buck and M. Fárník, *Int. Rev. Phys. Chem.* **25**, 583 (2006).
- [23] L. Holmegaard, J. H. Nielsen, I. Nevo, H. Stapelfeldt, F. Filsinger, J. Küpper, and G. Meijer, *Phys. Rev. Lett.* **102**, 023001 (2009).
- [24] O. Ghafur, A. Rouzee, A. Gijsbertsen, W. K. Siu, S. Stolte, and M. J. J. Vrakking, *Nat. Phys.* **5**, 289 (2009).
- [25] F. Filsinger, J. Küpper, G. Meijer, L. Holmegaard, J. H. Nielsen, I. Nevo, J. L. Hansen, and H. Stapelfeldt, *J. Chem. Phys.* **131**, 064309 (2009).
- [26] J. J. Omiste, M. Gärttner, P. Schmelcher, R. González-Férez, L. Holmegaard, J. H. Nielsen, H. Stapelfeldt, and J. Küpper, *Phys. Chem. Chem. Phys.* **13**, 18815 (2011).
- [27] J. H. Nielsen, H. Stapelfeldt, J. Küpper, B. Friedrich, J. J. Omiste, and R. González-Férez, *Phys. Rev. Lett.* **108**, 193001 (2012).
- [28] M. D. Feit, J. A. Fleck, Jr., and A. Steiger, *J. Comput. Phys.* **47**, 412 (1982).
- [29] Z. Bačić and J. C. Light, *Annu. Rev. Phys. Chem.* **40**, 469 (1989).
- [30] G. C. Corey and D. Lemoine, *J. Chem. Phys.* **97**, 4115 (1992).
- [31] A. R. Offer and G. G. Balint-Kurti, *J. Chem. Phys.* **101**, 10416 (1994).
- [32] P. Sánchez-Moreno, R. González-Férez, and P. Schmelcher, *Phys. Rev. A* **76**, 053413 (2007).
- [33] M. Härtelt and B. Friedrich, *J. Chem. Phys.* **128**, 224313 (2008).
- [34] K. Oda, M. Hita, S. Minemoto, and H. Sakai, *Phys. Rev. Lett.* **104**, 213901 (2010).
- [35] D. Dimitrovski, M. Abu-samha, L. B. Madsen, F. Filsinger, G. Meijer, J. Küpper, L. Holmegaard, L. Kalhøj, J. H. Nielsen, and H. Stapelfeldt, *Phys. Rev. A* **83**, 023405 (2011).
- [36] J. L. Hansen, L. Holmegaard, J. H. Nielsen, H. Stapelfeldt, D. Dimitrovski, and L. B. Madsen, *J. Phys. B* **45**, 015101 (2012).
- [37] L. B. Ballentine, *Quantum Mechanics: A Modern Development* (World Scientific, Singapore, 1998).
- [38] B. Friedrich, N. H. Nahler, and U. Buck, *J. Mod. Opt.* **50**, 2677 (2003).
- [39] M. D. Poulsen, T. Ejdrup, H. Stapelfeldt, E. Hamilton, and T. Seideman, *Phys. Rev. A* **73**, 033405 (2006).
- [40] Y. Sugawara, A. Goban, S. Minemoto, and H. Sakai, *Phys. Rev. A* **77**, 031403(R) (2008).
- [41] M. Muramatsu, M. Hita, S. Minemoto, and H. Sakai, *Phys. Rev. A* **79**, 011403(R) (2009).
- [42] R. N. Zare, *Angular Momentum: Understanding Spatial Aspects in Chemistry and Physics* (John Wiley and Sons, New York, 1988).
- [43] J. Ortigoso, M. Rodríguez, M. Gupta, and B. Friedrich, *J. Chem. Phys.* **110**, 3870 (1999).
- [44] S. S. Viftrup, V. Kumarappan, S. Trippel, H. Stapelfeldt, E. Hamilton, and T. Seideman, *Phys. Rev. Lett.* **99**, 143602 (2007).

Making the Best of Mixed-Field Orientation of Polar Molecules: A Recipe for Achieving Adiabatic Dynamics in an Electrostatic Field Combined with Laser Pulses

Jens H. Nielsen,¹ Henrik Stapelfeldt,^{2,3,*} Jochen Küpper,^{4,5,6,†} Bretislav Friedrich,⁶
Juan J. Omiste,⁷ and Rosario González-Férez^{7,‡}

¹Department of Physics and Astronomy, Aarhus University, 8000 Aarhus C, Denmark

²Department of Chemistry, Aarhus University, 8000 Aarhus C, Denmark

³Interdisciplinary Nanoscience Center (iNANO), Aarhus University, 8000 Aarhus C, Denmark

⁴Center for Free-Electron Laser Science, DESY, 22607 Hamburg, Germany

⁵Department of Physics, University of Hamburg, 22761 Hamburg, Germany

⁶Fritz-Haber-Institut der Max-Planck-Gesellschaft, 14195 Berlin, Germany

⁷Instituto Carlos I de Física Teórica y Computacional and Departamento de Física Atómica, Molecular y Nuclear,
Universidad de Granada, 18071 Granada, Spain

(Received 20 January 2012; published 7 May 2012)

We have experimentally and theoretically investigated the mixed-field orientation of rotational-state-selected OCS molecules and achieved strong degrees of alignment and orientation. The applied moderately intense nanosecond laser pulses are long enough to adiabatically *align* molecules. However, in combination with a weak dc electric field, the same laser pulses result in nonadiabatic dynamics of the mixed-field *orientation*. These observations are fully explained by calculations employing both adiabatic and nonadiabatic (time-dependent) models.

DOI: 10.1103/PhysRevLett.108.193001

PACS numbers: 37.10.Vz, 33.15.-e, 33.80.-b, 42.50.Hz

Creating oriented samples of polar molecules, i.e., molecules with their dipole moment preferentially pointing towards one hemisphere rather than the opposite, has been a long-standing goal in molecular sciences. It was originally motivated by the crucial role played by orientation in chemical reaction dynamics [1]. More recently, its importance in novel applications such as (fs-time-resolved) photoelectron angular distributions [2–4], diffraction-from-within [5], or high-order harmonic generation [6] has been recognized.

Early methods exploited purely electrostatic fields. Using an electric multipole focuser, molecules in a single low-field-seeking quantum state can be selected due to their first-order Stark effect [7–9]. The degree of orientation is determined, and also limited, by the selected state. Alternatively, a strong homogeneous electric field can create so-called brute-force orientation [10,11]. This method requires very high electric field strengths and works best for rotationally cold molecules with large permanent dipole moments.

In 1999 a method based on the combined action of a moderately intense, nonresonant laser field and an electrostatic field was proposed [12]. For the case that the laser field is turned on significantly more slowly than the rotational period(s) of the molecule adiabatic behavior was assumed. The time-independent calculations showed that the degree of orientation could be nearly perfect under conditions present in many experimental setups. Furthermore, the degree of alignment, i.e., the confinement of the molecular axes to space-fixed axes, could also be very high. In addition, the method should be generally

applicable to a broad range of molecules and, therefore, promises the availability of strongly oriented and aligned molecules for various applications. Experiments performed in the first half of the 2000s showed the feasibility of the method but the degree of orientation observed was moderate [13,14]. A major reason for the weak orientation was that while the individual pendular states are strongly oriented, these states arise in pairs whose members are oriented oppositely with respect to one another. Consequently, the resulting overall degree of orientation, obtained as the weighted average over the populated quantum states, diminishes compared to what is expected for very cold or even single-state molecular ensembles. A significant improvement in the experimental capabilities was reported in 2009 when quantum-state selected molecules were employed as targets leading to strongly enhanced orientation [15–17]. However, it was already realized that an adiabatic description is not sufficient to reproduce the experimental observations [18].

In the present work, we seek the maximum of achievable orientation, as predicted by the original adiabatic description. Therefore, we prepare a nearly pure ($92^{+3}_{-5}\%$) rotational-ground-state ensemble of OCS molecules [19] and use a laser pulse that is sufficiently strong to ensure sharp alignment and that is turned on a 100 times slower than the rotational period of the molecules. Our experimental observations are, however, at odds, both qualitatively and quantitatively, with the predictions of the original theory [12]. Instead, the experimental findings, exploring the dependence of the orientation on both the laser intensity and on the static field strength, can be

rationalized by solving the time-dependent Schrödinger equation describing the mixed-field orientation. Our analysis directly shows the nonadiabatic coupling of the two sublevels of the near-degenerate doublets, created by the laser field, and allows us to predict the experimental conditions needed to ensure adiabatic dynamics.

The experimental setup has been described in detail before [17,19,20] and only a few important details will be pointed out, see Fig. 1(a). A pulsed molecular beam is formed by expanding a mixture of 1 mbar of OCS and 10 bar of neon into vacuum through a pulsed valve. The molecular beam is skimmed twice before entering a 15-cm-long electrostatic deflector. Here it is spatially dispersed in the vertical direction according to the effective dipole moments of the quantum states [17]. Hereafter, the molecules travel into a velocity map imaging (VMI) spectrometer where they are crossed by two pulsed laser beams. The first pulse ($\mathbf{E}_{\text{align}}$, $\lambda = 1064$ nm, $\tau_{\text{FWHM}} = 8$ ns, linearly polarized) provides the laser field for the mixed-field orientation whereas the weak static field, \mathbf{E}_{stat} , exploited for the orientation is (inherently) provided as part of the VMI spectrometer, which also defines its direction. The second pulse (probe, $\lambda = 800$ nm, $\tau_{\text{FWHM}} = 30$ fs, linearly polarized) is used to characterize the orientation and alignment by multiply ionizing the molecules, this is followed by Coulomb explosion and imaging of the recoiling S^+ fragments on a two-dimensional detector.

The strongest orientation is expected when $\mathbf{E}_{\text{align}}$ is parallel to \mathbf{E}_{stat} . This geometry is, however, not well suited for the ion imaging method to characterize the orientation because the experimental observable, the S^+ ions, will then be localized in the center of the detector. Consequently, all measurements are conducted with $\mathbf{E}_{\text{align}}$ rotated by an angle $\beta \neq 0$ with respect to \mathbf{E}_{stat} [see Fig. 1(a)]. Figures 1(b) and 1(c) show examples of S^+ ion images for $\beta = 45^\circ$ and 135° (equal to -45°). The S^+ ions from the Coulomb explosion channel $\text{S}^+ + \text{CO}^+$, appearing in the outermost part of the images, are highly directional and provide direct information about the alignment and orientation of the OCS molecules at the time of ionization.

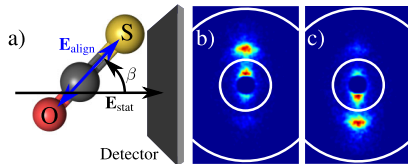


FIG. 1 (color online). (a) Schematic of the field configurations showing the polarization directions of the alignment and the probe pulses as well as the static field inside the VMI spectrometer and the definition of the angle β . (b), (c) S^+ ion images for $\beta = 45^\circ$ and 135° , respectively, and $E_{\text{stat}} = 571$ V/cm. The rings in the image depict the limits for S^+ ions from the $\text{S}^+ + \text{CO}^+$ channel used in the calculation of the degree of orientation.

The strong angular confinement of the S^+ ions shows that the OCS molecules are sharply one-dimensionally aligned along $\mathbf{E}_{\text{align}}$. In addition, a pronounced asymmetry of the S^+ ions emitted either along or opposite to \mathbf{E}_{stat} , with an excess of S^+ in the upper (lower) region for $\beta = 45^\circ$ (135°) is observed. This shows that the molecules are oriented with the S end preferentially pointing toward the detector screen—as expected and in agreement with previous studies [21]. To quantify the degree of orientation only ions from the $\text{S}^+ + \text{CO}^+$ channel are considered. We then specify the orientation by the ratio $N_{\text{up}}/N_{\text{tot}}$ of the number of these ions in the upper half of the image N_{up} compared to the total number of ions N_{tot} from this channel.

In the first set of measurements the degree of orientation is recorded as a function of the alignment pulse intensity, I_{align} , for two values of E_{stat} . The results are shown in Fig. 2. For low values of I_{align} the orientation ratio is almost the same for the two static fields but for $I_{\text{align}} > 2.5 \times 10^{11}$ W/cm 2 the results differ. For the strong static field the orientation reaches a maximum of approximately 0.8 at $I_{\text{align}} = 5 \times 10^{11}$ W/cm 2 and remains essentially constant out to 1.4×10^{12} W/cm 2 . In contrast, for the smaller static field the maximum orientation occurs already at $I_{\text{align}} = 3 \times 10^{11}$ W/cm 2 and the degree of orientation decreases as I_{align} is further increased, dropping to 0.70 at $I_{\text{align}} = 1.4 \times 10^{12}$ W/cm 2 . The calculated degree of mixed-field orientation using the adiabatic model for $\beta = 45^\circ$, as in the experiment, is shown in Fig. 2. Here, we have used rotational-state populations, in the coordinate system of the electric field in the deflector, with 92% in the $|\tilde{0}, \tilde{0}\rangle$ state, adiabatically corresponding to the field-free $J = M = 0$ state, 4% in the $|\tilde{1}, \tilde{1}\rangle$ state and 4% in the $|\tilde{1}, \tilde{-1}\rangle$ state [19]. These states are projected onto a coordinate system for the mixed-field orientation that is defined by $\mathbf{E}_{\text{align}}$. The properly symmetrized states are then $|0, 0, e\rangle$, $|1, 1, e\rangle$, and $|1, 1, o\rangle$, where e and o denote even and odd parity with respect to the plane defined by \mathbf{E}_{stat} and $\mathbf{E}_{\text{align}}$, respectively. The volume effect [18] is accounted for by using an experimentally determined cubic dependence on

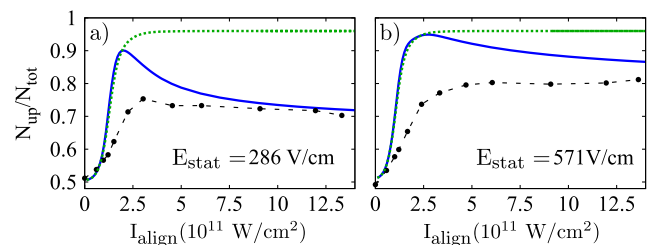


FIG. 2 (color online). Orientation ratio for $\beta = 45^\circ$ as a function of I_{align} , for the weak (a) and the strong (b) static field, showing the experimental results (black solid circles), the adiabatic calculations (green dotted line) and the time-dependent calculations (blue solid line).

the probe pulse intensity. These calculations predict that the orientation is independent of the applied static field. Following a rapid initial rise it reaches a value of 0.96 already at 4×10^{11} W/cm² and remains constant. Clearly, these predictions are at odds with the experimental findings: The simulated degree of orientation is much too strong and it does not reproduce the decrease of the orientation at intensities above 3×10^{11} W/cm², that is experimentally observed for the case of the smaller static field.

In the second set of measurements, shown in Fig. 3, the degree of orientation is recorded as a function of β for the weak and the strong static fields and for a fixed value of I_{align} of 9.1×10^{11} W/cm². For both static field strengths $N_{\text{up}}/N_{\text{tot}}$ decreases monotonically as β increases from 30° to 150°. At all β values the strong field leads to stronger orientation than the weak field. The $N_{\text{up}}/N_{\text{tot}}$ ratios calculated from the adiabatic model are essentially identical for the two static field strengths. The sharp rise (fall) of the curve to a value close to 0.96 (0.04) as β is increased (decreased) below (above) 90° shows that very strong orientation is reached already for a very modest static electric field along $\mathbf{E}_{\text{align}}$. This calculated behavior of the orientation differs qualitatively as well as quantitatively from the experimental results.

To obtain a better model of the mixed-field orientation process we solve the time-dependent Schrödinger equation using the experimental field configurations and rotational-state populations [22]. The results for $N_{\text{up}}/N_{\text{tot}}$ as a function of I_{align} are shown in Fig. 2. The predictions of stronger orientation for the strong static field and, in the weak static field case, the decreasing orientation at increasing intensity for $I_{\text{align}} > 3 \times 10^{11}$ W/cm² are in line with the experimental findings. Moreover, the smooth β dependence of the orientation, shown in Fig. 3, is fully captured by the time-dependent calculations. Quantitatively, the calculated values overestimate the degree of orientation. This could partly be due to temporal substructure in the experimentally applied laser pulses, which could induce more

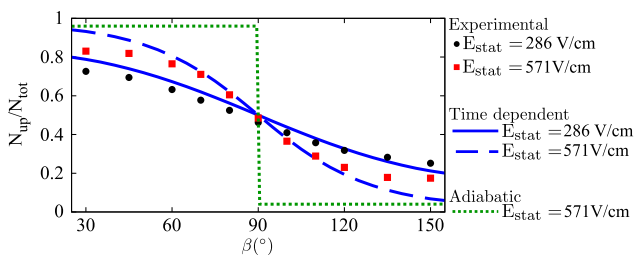


FIG. 3 (color online). The orientation ratio as a function of β for $I_{\text{align}} = 9.1 \times 10^{11}$ W/cm² for the experiment using $E_{\text{stat}} = 286$ V/cm (black circles) and $E_{\text{stat}} = 571$ V/cm (red squares), for the adiabatic calculations, which are identical for the two static fields (green dotted line), and for the time-dependent calculations using $E_{\text{stat}} = 286$ V/cm (blue dashed line) and $E_{\text{stat}} = 571$ V/cm (blue solid line).

nonadiabatic population transfer. Overall, these non-adiabatic-model calculations are in much better agreement with the experimental results than the adiabatically calculated ones.

The underlying physical picture for understanding the failure of the adiabatic model is obtained by considering the evolution of the states during the turn-on of the alignment pulse. Before the pulse, the rotational states are essentially described by field-free rotor states. As the laser field strength increases, the states are hybridized by the combined action of the laser and static fields. In Fig. 4(a) the formation of doublets of nearly degenerate pendular states in the strong laser-field regime is shown. For the laser and static fields used in the experiment the absolute ground state $|0, 0, e\rangle_p$ is right-way oriented; i.e., the permanent dipole moment is pointing along \mathbf{E}_{stat} . The upper level, $|1, 1, e\rangle_p$, of the lowest doublet is wrong-way oriented—see Fig. 4(b).

As the alignment field is turned on the states that eventually form the near-degenerate doublet are coming closer together. This is illustrated in Fig. 4(a) for the $|0, 0, e\rangle$, $|1, 1, e\rangle$ pair and the $|1, 0, e\rangle$, $|2, 2, e\rangle$ pair and it results from the ac Stark interaction. When the energy splitting within a pair approaches the coupling strength due to the dc Stark interaction between the two sublevels, the two states in

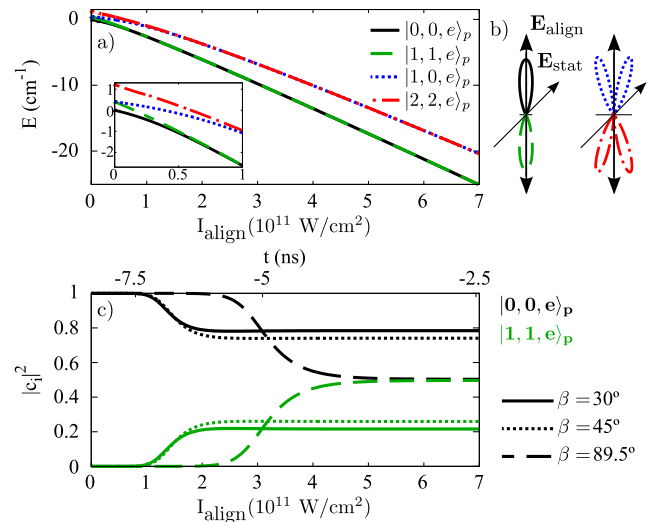


FIG. 4 (color online). (a) Energy of the four lowest lying rotational eigenstates as a function I_{align} (time). The inset shows the relevant energy and intensity ranges where the formation of the near-degenerate doublets occurs. (b) Polar plot representation of the wave functions for the four states shown in (a) at $I_{\text{align}} = 9 \times 10^{11}$ W/cm². The single-headed arrow shows the direction of the static field. (c) The squares of the coefficients for the projection of the time-dependent pendular wave function of the absolute ground state onto the adiabatic pendular state basis $|0, 0, e\rangle_p$ (black) and $|1, 1, e\rangle_p$ (green) as a function of I_{align} (time) for $\beta = 30^\circ$ (solid line), 45° (dotted line), and 89.5° (dashed line). $E_{\text{stat}} = 286$ V/cm for all data.

each pair can mix because they have the same symmetry, provided the laser and static fields are nonperpendicular. This will result in population transfer between the oriented and antioriented states. The probability for mixing, corresponding to a crossing from one state of the doublet to the other, is determined by the rate of the turn-on and the energy separation between the $|0, 0, e\rangle_p$ and $|1, 1, e\rangle_p$ states. If the splitting is small, which is the case for a weak static electric field, the two states will be strongly coupled. To ensure fully adiabatic transfer it is necessary to turn on the laser field on a time scale slower than the inverse of the energy splitting of the near-degenerate doublet. This time can be much longer than the rotational period of the molecule. For the lowest doublet formed in OCS with $E_{\text{stat}}=286\text{V/cm}$ and $I_{\text{align}}=9.1\times 10^{11}\text{W/cm}^2$ our calculations show that the alignment pulse must be 50 ns long to ensure adiabatic transfer. The 8 ns pulses used in the current experiments do not fulfill this adiabaticity criterion although they are a hundred times longer than the rotational period of OCS—the condition previously considered sufficient for adiabatic behavior.

The population transfer is illustrated in Fig. 4(c), where the decomposition of the time-dependent state, which starts as the rotational ground state, in terms of the pendular states, is shown during the time interval representing the turn-on of the alignment pulse for three β values. The field-free ground state is not transferred adiabatically to the pendular ground state: for $\beta=45^\circ$, the final state is decomposed into 74.06% $|0, 0, e\rangle_p$ and 25.94% $|1, 1, e\rangle_p$. Therefore, the resulting degree of orientation falls below that expected for a pure adiabatic transfer since the $|1, 1, e\rangle_p$ state is wrong-way oriented. Similarly, other field-free rotational states are mixed with different pendular states during the turn-on, for instance the initial state $|\tilde{1}, \tilde{1}\rangle$ ends up in a superposition of 13.00% $|0, 0, e\rangle_p$, 37.10% $|1, 1, e\rangle_p$, 35.64% $|1, 0, e\rangle_p$, and 14.26% $|2, 2, e\rangle_p$. For $\beta=89.5^\circ$, the electric field along the molecular axis is small, and the $|0, 0, e\rangle_p$ and $|1, 1, e\rangle_p$ states contribute with 50.32% and 49.68%, respectively, to the time evolution of $|\tilde{0}, \tilde{0}\rangle$, resulting in a vanishing orientation. By contrast, alignment is expected to remain strong since both the $|0, 0, e\rangle_p$ and $|1, 1, e\rangle_p$ states imply tight confinement of the molecular axis along the laser-field polarization, see Fig. 4(b). The experimental observations for perpendicular fields do indeed show no orientation but strong alignment [23].

In summary, the combined action of a moderately strong laser field and a weak electrostatic field remains an attractive approach for creating tightly oriented molecules, but to fully exploit the potential of the method it is necessary to redefine the meaning of adiabatic conditions. Unlike alignment, where adiabaticity is ensured by turning on the laser field slower than the rotational period of the pertinent molecule, adiabatic transfer in orientation necessitates that the laser field be turned on slower than the

inverse of the minimum spacing between the two pendular states in a doublet. This has repercussions for designing experimental parameters such that the degree of orientation be optimized. In the case of OCS, our calculations show that when $E_{\text{stat}}=286\text{V/cm}$ and $\beta=45^\circ$ adiabatic transfer of the $|\tilde{0}, \tilde{0}\rangle$ state to the $|0, 0, e\rangle_p$ state is obtained if a transform-limited laser pulse with a Gaussian pulse duration (full width half maximum) of 50 ns is used. In practice, such pulses are not easily supplied by lasers typically present in laboratories. Considering instead the 10 ns output from the widespread Nd:YAG lasers adiabatic transfer will occur for a static electric field of 2 kV/cm: The increased static field leads to a larger minimum spacing of the doublet and, thus, relaxes the requirement for the slowness of the laser-field turn-on. Such static fields are compatible with, for instance, VMI spectrometers. For a pulse durations of 500 ps, which would be relevant for using the stretched output from amplified Ti-sapphire lasers, a static field of 10 kV/cm is needed to ensure adiabatic conditions. Again this is compatible with electron or ion spectrometers [16].

We note that the lack of adiabatic behavior will also be influenced by avoided crossings between rotationally excited states at low laser intensities. For larger molecules, where the rotational level structure is quite complex, this effect is expected to be particularly important [18,24], but an increase of the static field strength should enhance the degree of orientation as already demonstrated experimentally for several asymmetric top rotors [2,15,17,20].

Financial support by the Spanish Project No. FIS2011-24540 (MICINN) as well as Grant No. FQM-4643 (Junta de Andalucía), the Lundbeck Foundation, the Carlsberg Foundation, and the Danish Council for Independent Research is gratefully appreciated. J.J.O. acknowledges the support of ME under the program FPU. R.G.F. and J.J.O. acknowledge support from the Andalusian research group Grant No. FQM-207.

*Corresponding author.

henriks@chem.au.dk

†Corresponding author.

jochen.kuepper@cfel.de

‡Corresponding author.

rogonzal@ugr.es

- [1] P. Brooks, *Science* **193**, 11 (1976).
- [2] L. Holmegaard *et al.*, *Nature Phys.* **6**, 428 (2010).
- [3] C. Z. Bisgaard, O. J. Clarkin, G. Wu, A. M. D. Lee, O. Geßner, C. C. Hayden, and A. Stolow, *Science* **323**, 1464 (2009).
- [4] J. L. Hansen, H. Stapelfeldt, D. Dimitrovski, M. Abusamha, C. P. J. Martiny, and L. B. Madsen, *Phys. Rev. Lett.* **106**, 073001 (2011).
- [5] A. Landers *et al.*, *Phys. Rev. Lett.* **87**, 013002 (2001).
- [6] H.-J. Wörner (private communication).

- [7] J. P. Gordon, H. J. Zeiger, and C. H. Townes, *Phys. Rev.* **99**, 1264 (1955).
- [8] J. Reuss, in *Atomic and Molecular Beam Methods*, edited by G. Scoles (Oxford University Press, New York, 1988), Vol. 1, Chap. 11, pp. 276–292.
- [9] T. P. Rakitzis, A. J. van den Brom, and M. H. M. Janssen, *Science* **303**, 1852 (2004).
- [10] H. J. Loesch and A. Remscheid, *J. Chem. Phys.* **93**, 4779 (1990).
- [11] B. Friedrich and D. R. Herschbach, *Nature (London)* **353**, 412 (1991).
- [12] B. Friedrich and D. Herschbach, *J. Chem. Phys.* **111**, 6157 (1999).
- [13] U. Buck and M. Fárník, *Int. Rev. Phys. Chem.* **25**, 583 (2006).
- [14] H. Sakai, S. Minemoto, H. Nanjo, H. Tanji, and T. Suzuki, *Phys. Rev. Lett.* **90**, 083001 (2003).
- [15] L. Holmegaard, J. H. Nielsen, I. Nevo, H. Stapelfeldt, F. Filsinger, J. Küpper, and G. Meijer, *Phys. Rev. Lett.* **102**, 023001 (2009).
- [16] O. Ghafur, A. Rouzée, A. Gijsbertsen, W. K. Siu, S. Stolte, and M. J. J. Vrakking, *Nature Phys.* **5**, 289 (2009).
- [17] F. Filsinger, J. Küpper, G. Meijer, L. Holmegaard, J. H. Nielsen, I. Nevo, J. L. Hansen, and H. Stapelfeldt, *J. Chem. Phys.* **131**, 064309 (2009).
- [18] J. J. Omiste, M. Gärttner, P. Schmelcher, R. González-Férez, L. Holmegaard, J. H. Nielsen, H. Stapelfeldt, and J. Küpper, *Phys. Chem. Chem. Phys.* **13**, 18 815 (2011).
- [19] J. H. Nielsen, P. Simesen, C. Z. Bisgaard, H. Stapelfeldt, F. Filsinger, B. Friedrich, G. Meijer, and J. Küpper, *Phys. Chem. Chem. Phys.* **13**, 18 971 (2011).
- [20] J. L. Hansen *et al.*, *Phys. Rev. A* **83**, 023406 (2011).
- [21] D. Dimitrovski, M. Abu-samha, L. B. Madsen, F. Filsinger, G. Meijer, J. Küpper, L. Holmegaard, L. Kalthøj, J. H. Nielsen, and H. Stapelfeldt, *Phys. Rev. A* **83**, 023405 (2011).
- [22] P. Sánchez-Moreno, R. González-Férez, and P. Schmelcher, *Phys. Rev. A* **76**, 053413 (2007).
- [23] L. Holmegaard, Ph.D. thesis, Aarhus University, 2010.
- [24] J. Bulthuis, J. Möller, and H. J. Loesch, *J. Phys. Chem. A* **101**, 7684 (1997).

Chapter 6

Submitted publications and preprint

In this chapter, we present the submitted publications which are also part of this thesis:

1. *Authors:* J. L. Hansen, **J. J. Omiste**, J. H. Nielsen, D. Pentlehner, J. Küpper, R. González-Férez and H. Stapelfeldt
Title: Mixed-field orientation of non-symmetric molecules
Year: 2013
2. *Authors:* **J. J. Omiste** and R. González-Férez
Title: Rotational dynamics of an asymmetric top molecule in parallel electric and non-resonant laser fields,
Citation: arXiv:1306.1429
Year: 2013
3. *Authors:* **J. J. Omiste** and R. González-Férez
Title: Mixed-field orientation of a thermal ensemble of linear polar molecules
Citation: arXiv:1306.1251
Year: 2013

Mixed-field orientation of non-symmetric molecules

Jonas L. Hansen,¹ Juan J. Omiste,² Jens H. Nielsen,³ Dominik Pentleher,³ Jochen Küpper,^{4,5,6} Rosario González-Férez,² and Henrik Stapelfeldt^{1,3}

¹*Interdisciplinary Nanoscience Center (iNANO), Aarhus University, 8000 Aarhus C, Denmark*

²*Instituto Carlos I de Física Teórica y Computacional and Departamento de Física Atómica, Molecular y Nuclear, Universidad de Granada, 18071 Granada, Spain*

³*Department of Chemistry, Aarhus University, 8000 Aarhus C, Denmark*

⁴*Center for Free-Electron Laser Science, DESY, 22607 Hamburg, Germany*

⁵*Department of Physics, University of Hamburg, 22761 Hamburg, Germany*

⁶*The Hamburg Center for Ultrafast Imaging, 22761 Hamburg, Germany*

(Dated: 27 May 2013)

The mixed-field orientation of an asymmetric-rotor molecule with non-parallel inertial, polarizability, and dipole moment axis systems is investigated experimentally and theoretically. We find that for the typical case of a strong ac field and a weak dc field solely the dipole moment component along the most-polarizable axis of the molecule is relevant for the orientation. Correspondingly, one- and three-dimensional orientation are induced by the combined action of a weak dc electric field and linearly- and elliptically-polarized laser fields, respectively. Simulations show that the second dipole moment component becomes relevant in strong dc electric fields combined with the laser field. This would create three-dimensionally oriented molecules in combined linearly-polarized laser fields and dc electric fields, inducing three-dimensional orientation in fully unsymmetric (bio)molecules.

PACS numbers: 37.20.+j, 33.15.-e

I. INTRODUCTION

The ability to control the rotational motion and to angularly confine molecules has various applications in molecular sciences. This includes studies of steric effects in chemical reactions, both, bimolecular and photoinduced, and the possibility to investigate molecules from their own point of view, the molecular frame. The latter mitigates the usual blurring of experimental observables caused by the random orientation of molecules in uncontrolled samples. Access to molecular frame measurements is crucial in several applications, notably in various modern schemes aiming at observing the (coupled) motion of nuclei and electrons during chemical reactions.¹⁻⁷

Methods based on the use of moderately intense, non-resonant, near-infrared laser pulses have proven particularly useful for controlling the alignment and, in conjunction with weak dc electric fields, orientation of a broad range of molecules.⁸ Alignment refers to the confinement of molecule-fixed axes along laboratory-fixed axes, and orientation refers to the molecular dipole moment (components) pointing in a particular direction. For a linear molecule, only a single axis needs to be confined in space to ensure complete rotational control. This can be achieved by a linearly polarized laser pulse, which will align the most polarizable axis (MPA), which coincides with the internuclear axis of the molecule. This is termed 1-dimensional (1D) alignment. Combined with a (weak) static electric field it can also control the head-versus-tail order of a polar molecule, i. e., induce 1D orientation.⁹⁻¹³

Complete rotational control of asymmetric top molecules requires the confinement of three molecular axes to laboratory frame fixed axes, resulting in 3D alignment. In the adiabatic limit, where the laser pulse

is turned on slower than the rotational periods of the molecule, it has been shown that an elliptically polarized laser pulse can induce 3D alignment.¹⁴⁻¹⁶ For polar molecules, where the permanent dipole moment (DPM) is parallel to the MPA it has also been shown that 3D orientation, i. e., 3D alignment and a unique direction of the DPM, can be achieved by combining the elliptically polarized laser pulse with a weak static electric field parallel to the major polarization axis.^{15,16} For most asymmetric top molecules, the DPM does, however, not coincide with the MPA. While 3D alignment is expected to work well for these less symmetric molecules, it remains to be explored if the combined action of a linearly or elliptically polarized laser pulse and a weak or strong static electric field can efficiently induce 3D orientation.

In the current work we investigate 3D alignment and orientation of asymmetric top molecules where the DPM is not parallel to the MPA. Our studies are motivated by the fact that many important biomolecules, e. g., amino acids, nucleic acids, peptides, and DNA strands, belong to this class of molecules. Controlling how they are turned in space would be of significant value in novel and emerging schemes for time-resolved molecular imaging.^{7,17,18} Following the conclusions from the current work, this three-dimensional control is indeed possible. Our studies focus on 6-chloropyridazine-3-carbonitrile (C₄N₂H₂ClCN, CPC). The molecule is chosen because the DPM is off-set by 57.1° from the MPA and because the atomic composition makes it possible to determine its 3-dimensional spatial orientation through Coulomb explosion imaging.

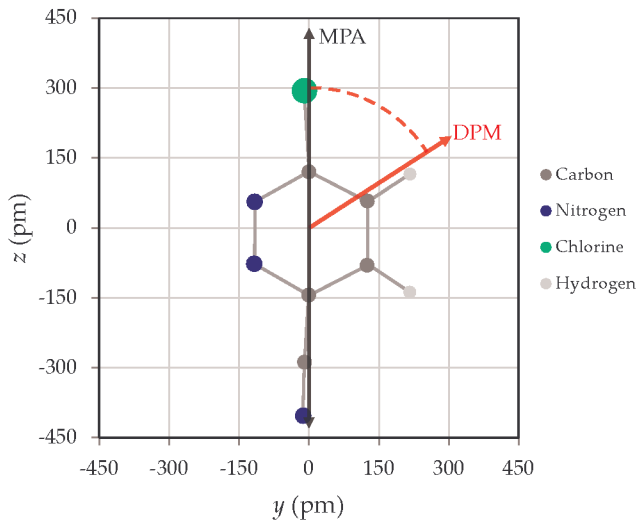


FIG. 1. Sketch of the molecular structure of 6-chloropyridazine-3-carbonitrile with the most polarizable axis (black doubleheaded arrow) and permanent dipole moment (red arrow). The coordinates of the individual atomic positions in CPC, from a geometry optimized quantum chemical calculation, show a slight shift of the chlorine and nitrile bond angles towards the nitrogens in the pyridazine ring. The x-axis is perpendicular to the figure plane.

II. MOLECULAR STRUCTURE AND ELECTRICAL PROPERTIES OF CPC

A sketch of the molecular structure of CPC and the position of the MPA and DPM vector are shown in Fig. 1 (a). The planar molecule consists of an aromatic pyridazine ring with a nitrile and a chlorine substituent. The N-N bond is shorter than the C-N and C-C bonds in the aromatic ring causing the bond angle of the substituents on the ring to bend slightly towards the pyridazine nitrogens, as can be seen from the energy optimized geometry of the molecule shown in Fig. 1 (b). Quantum chemical calculations¹⁹ determine the electric dipole moment of CPC to be 5.21 D with $\mu_x = 0$ D, $\mu_y = 4.37$ D, $\mu_z = 2.83$ D, i.e., in the molecular plane and at an angle of 57.1° with respect to the z axis. The static polarizability components of CPC are determined to be $\alpha_{xx} = 7.88 \text{ \AA}^3$, $\alpha_{yy} = 12.0 \text{ \AA}^3$ and $\alpha_{zz} = 22.3 \text{ \AA}^3$.

III. EXPERIMENTAL SETUP

Most aspects of the experimental setup have been described previously^{4,20,21} and only a few pertinent details will be given here. A few mbar of CPC (ChemFuture PharmaTech, > 97% chemical purity) was seeded in a helium carrier gas at a backing pressure of 90 bar and expanded into vacuum through a pulsed Even-Lavie valve²² heated to 170° . The expansion was skimmed twice before entering an electrostatic deflector, where the molecules

were deflected according to the effective dipole moment μ_{eff} of their specific rotational quantum state.²⁰

The quantum-state-dispersed molecular beam entered a velocity map imaging (VMI) spectrometer where it was crossed at 90° by two collinear laser beams. The laser beams were focused by a spherical lens ($f = 30$ cm) mounted on a motorized translation stage. This allowed for the height of the foci to be scanned with high precision. The molecules were aligned and oriented by the combined effect of pulses from one of the laser beams (YAG, $\lambda = 1064$ nm, $\tau_{\text{FWHM}} = 10$ ns, $\omega_0 = 34 \mu\text{m}$, $I_{\text{YAG}} = 8 \times 10^{11} \text{ W/cm}^2$, injection seeded) and the weak static electric field from the VMI spectrometer (E_s was varied between values of 286 V/cm, 571 V/cm, and 714 V/cm). The YAG beam was overlapped in space and time with pulses from a second laser (probe pulse: 800 nm, 30 fs, $24 \mu\text{m}$, $I_{\text{probe}} = 5 \times 10^{14} \text{ W/cm}^2$). These short pulses multiply ionized the molecules, which then fragmented into charged ions. These were projected onto a 2-dimensional particle detector in order to detect their recoil directions. For CPC molecules, Cl^+ ion momenta were recorded to determine the spatial orientation of the C-Cl bond axis with respect to the laboratory frame. The N^+ or H^+ fragment ion distributions were recorded to provide information about the orientation of the molecular plane in the laboratory frame. All experiments were conducted on deflected, state-selected molecular samples at a repetition rate of 20 Hz, limited by the YAG laser.

IV. THEORETICAL DESCRIPTION

We have theoretically investigated the rotational dynamics of the CPC molecule in combined static electric and non-resonant laser fields. Due to the complexity of this system, we retreated to a quasi-static description. We assumed that the interaction with the laser pulse can be described within the adiabatic limit. We applied a two-photon rotating-wave approach averaging over the rapid oscillations of the nonresonant field. In the framework of the rigid-rotor approximation, we solved the time-independent Schrödinger equation of the CPC molecule in a field configuration equivalent to the experimental one: a nonresonant laser field, elliptically polarized along the Y and Z -axes of the laboratory fixed frame (LFF) (X, Y, Z) and a homogeneous electrostatic field of strength E_s contained in the YZ -plane and at an angle β with respect to the Z axis. The relation between LFF and the molecular fixed frame (MFF) (x, y, z) is given by the Euler angles $\Omega = (\phi, \theta, \chi)$.²³ The Hamiltonian of this system is

$$H = J_x^2 B_x + J_y^2 B_y + J_z^2 B_z + H_s + H_l \quad (1)$$

with the rotational constant B_x , B_y and B_z and the interaction operators H_s and H_l with the dc and ac electric fields, respectively.

The Stark interaction reads

$$\begin{aligned} H_s &= -\mathbf{E}_s \cdot \boldsymbol{\mu} \\ &= -E_s \mu \cos \theta_{s\mu} \\ &= -E_s \mu_z \cos \theta_{sz} - E_s \mu_y \cos \theta_{sy} \end{aligned} \quad (2)$$

with μ being the absolute value of the electric dipole moment, and μ_z and μ_y its two components. The angles between the electric field and $\boldsymbol{\mu}$, and the MFF z and y -axes, $\theta_{s\mu}$, θ_{sz} and θ_{sy} , respectively, are given by the relations

$$\cos \theta_{sz} = \cos \beta \cos \theta + \sin \beta \sin \theta \sin \phi, \quad (3)$$

$$\begin{aligned} \cos \theta_{sy} &= \cos \beta \sin \theta \sin \chi \\ &\quad + \sin \beta (\cos \phi \cos \chi - \cos \theta \sin \phi \sin \chi) \end{aligned} \quad (4)$$

$$\cos \theta_{s\mu} = \cos(57.1^\circ) \cos \theta_{sz} + \sin(57.1^\circ) \cos \theta_{sy} \quad (5)$$

The interaction of the molecule with a nonresonant elliptically polarized laser field can be written as

$$\begin{aligned} H_l &= -\frac{I_{ZZ}}{2c\epsilon_0} (\alpha^{zx} \cos^2 \theta_{Zz} + \alpha^{yx} \cos^2 \theta_{Zy}) \\ &\quad - \frac{I_{YY}}{2c\epsilon_0} (\alpha^{yx} \cos^2 \theta_{Yy} + \alpha^{zx} \cos^2 \theta_{Yz}) \end{aligned} \quad (6)$$

where I_{YY} and I_{ZZ} are the intensities of the polarization components along the LFF Y and Z axes, respectively. The total intensity is $I_{YAG} = I_{YY} + I_{ZZ}$, and $I_{ZZ} = 3I_{YY}$ is used here. $\alpha^{ji} = \alpha_{jj} - \alpha_{ii}$, and α_{ii} are the i -th diagonal element of the polarizability tensor, with $i = x, y, z$. ϵ_0 the dielectric constant and c is the speed of light. θ_{Pq} are the angles between the LFF P -axis and the MFF q -axis, and they are related to the Euler angles as follows

$$\begin{aligned} \cos \theta_{Zz} &= \cos \theta, \\ \cos \theta_{Zy} &= \sin \theta \sin \chi, \\ \cos \theta_{Yz} &= \sin \phi \sin \theta, \\ \cos \theta_{Yy} &= \cos \phi \cos \chi - \cos \theta \sin \phi \sin \chi. \end{aligned}$$

If the laser field is linearly polarized, the interaction with this field is obtained by setting $I_{YY} = 0$ and $I_{YAG} = I_{ZZ}$ in Eq. 6.

Let us shortly summarize the symmetries of this system in the mixed-field configurations. In the field-free case, they are given by the spatial group $SO(3)$ and the molecular point group D_2 .^{24,25} The total angular momentum J and its projection M onto the Z -axis of the LFF are good quantum numbers. The projection of J onto the z -axis of the MFF (K) is not well defined. In the presence of a linearly polarized laser parallel to a dc electric field, i. e., $\beta = 180^\circ n$ ($n = 0, 1, 2, \dots$), the Hamiltonian Eq. 1 is invariant under the reflection on any plane containing the LFF Z -axis and arbitrary rotations around the Z -axis of the LFF, i. e., M is a good quantum number. Then, for every $|M| > 0$ there are 2 irreducible representations and the states with $M \neq 0$ are doubly degenerate. If the fields are perpendicular, i. e., $\beta = 90^\circ(2n + 1)$, the symmetry

operations are the reflection on the plane containing the fields and the 2-fold rotation around the dc field axis, i. e., the Y -axis of the LFF, and there are 4 irreducible representations. For $\beta \neq 180^\circ n, 90^\circ(2n + 1)$, the Hamiltonian is invariant under reflections in the plane containing the fields, and there are 2 irreducible representations. For an elliptically polarized laser field in the YZ plane and with the dc field parallel to the Z -axis, i. e., $\beta = 180^\circ n$, a π -rotation around the LFF Z -axis and the reflection on the YZ -plane, the laser polarization) are the symmetry operations and M is not a good quantum number, but its parity is. For the other two cases, $\beta = 90^\circ(2n + 1)$ and $\beta \neq 180^\circ n$, the system has the same symmetries as in the corresponding field configuration with a linearly polarized laser field.

The time-independent Schrödinger equation of the Hamiltonian Eq. 1 was solved by expanding the wave function in a basis set formed by linear combinations of field-free symmetric top rotor wave functions or Wigner functions.²³ Thus, for each field configuration, we constructed a basis that respects the symmetries of the corresponding irreducible representation.²⁵

V. EXPERIMENTAL RESULTS

A. Alignment

We start by showing that a linearly polarized YAG induces 1D alignment of the CPC molecules. For this purpose, the emission directions of Cl^+ ions are detected. The expected action of the YAG is that it aligns the MPA along its polarization axis and as such an experimental observable that provides direct and precise information about the spatial orientation of this axis would be ideal. Unlike in higher-symmetry molecules, e. g., iodobenzene,¹² no such observable exists. The emission direction of Cl^+ ions comes close, assuming axial recoil along the C-Cl bond axis, since the C-Cl axis is only offset by 3 degrees from the MPA. When only the linearly-polarized probe pulse is applied, polarized perpendicular to the detector, the Cl^+ image shown in Fig. 2(a) is circularly symmetric, as expected for randomly oriented molecules. When the YAG is included the Cl^+ ions tightly localize along its polarization axis parallel to the detector plane, see Fig. 2(b). These observations show that the C-Cl bond axes of the CPC molecules are aligned along the YAG polarization axis, i. e., that 1D alignment is induced. The degree of alignment is quantified by determining the average value of $\cos^2 \theta_{2D}$, $\langle \cos^2 \theta_{2D} \rangle$, where θ_{2D} is the angle between the YAG pulse polarization and the projection of a Cl^+ ion velocity vector on the detector screen. Only a confined radial range is used to determine $\langle \cos^2 \theta_{2D} \rangle$. This range at the outermost part of the images is marked by circles in Fig. 2(b). It corresponds to ions originating from a highly directional Coulomb explosion process. The derived values are plotted as a function of the YAG pulse intensity, I_{YAG} in Fig. 2(c).

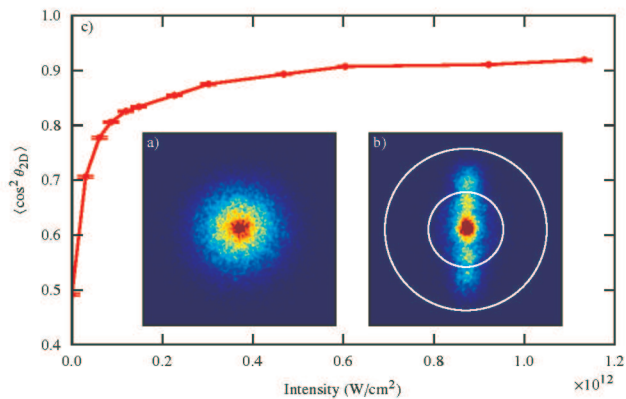


FIG. 2. Cl^+ images recorded (a) without and (b) with the YAG pulse, $I_{\text{YAG}} = 3 \times 10^{12} \text{ W/cm}^2$. (c) The degree of alignment $\langle \cos^2 \theta_{2D} \rangle$ as a function of I_{YAG} .

$\langle \cos^2 \theta_{2D} \rangle$ rises from 0.5, the value characterizing a sample of randomly oriented molecules, at $I_{\text{YAG}} = 0$ to 0.93 at the highest value of I_{YAG} . This behaviour is fully consistent with many previous studies of 1D adiabatic alignment.^{8,12} The $\langle \cos^2 \theta_{2D} \rangle$ values determined underestimate the true degree of alignment due to the offset between the C-Cl axis and MPA.

In order to investigate the effect on the molecular alignment when the YAG polarization is changed from linear to elliptical, an ellipticity ratio of 3:1 was applied, i.e., the intensity along the major polarization axis of the YAG is three times the intensity along the minor axis. For these measurements, N^+ and H^+ images, displayed in Fig. 3, are used to infer information about the molecular alignment. The images represent either a "side-view" when the major polarization axis is parallel to the detector, i.e., the molecules are watched from the side, or an "end-view" when the major polarization axis is perpendicular to the detector, i.e., the molecules are watched from the end.

For N^+ ions, the molecule is imaged in side-view. Fig. 3 (a1) shows the image obtained with the probe pulse by itself and serves a reference. In panel (a2) measurements including the linearly polarized YAG pulse are shown. The N^+ ions appear as two distinct areas at large radii along the vertical axis and as two pairs of wings protruding nearly horizontally from the horizontal centerline. Here, the 1D alignment of the molecules MPA along the vertical Z axis implies that the recoiling N^+ ions from the CN group will be ejected vertically, either up or down depending on the orientation of the molecule, and form the two distinct centerline regions of signal. This structure is similar to the Cl^+ ion structure (Fig. 2(b)) used for the determination of the 1D alignment discussed above. The wing structure is interpreted as N^+ ions originating from Coulomb explosion of the N atoms in the aromatic ring. Since the linearly polarized YAG pulse does not impose any constraint on the rota-

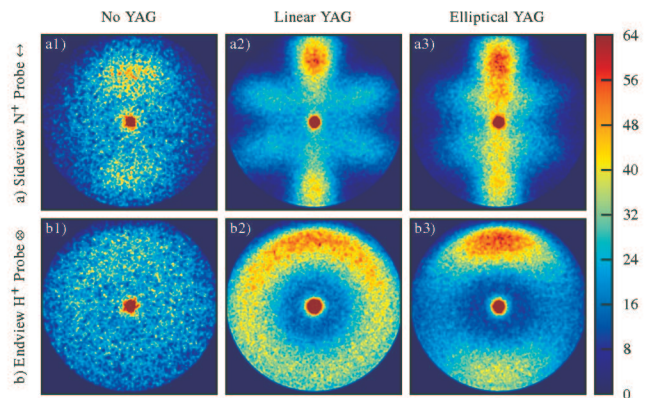


FIG. 3. a) N^+ and b) H^+ images demonstrating 1D and 3D alignment of CPC. The color scale is chosen such that the central low kinetic energy peak is saturated to enhance the visibility of the rest of the image.

tion of the ring the N^+ ions will be emitted in a double-torus-like pattern. Upon projection on the 2D detector plane this gives the wing-structure. Covariance analysis⁴ confirms that in the wing-structure the two N^+ ions from a single molecule are predominately produced on the same sides of the tori supporting this interpretation. When the YAG polarization is changed to elliptical the image in Fig. 3 (a3) is obtained. N^+ ions from the ring are confined close to the vertical axis, whereas the N^+ ion emission structure from the CN group is practically unchanged. This shows that the alignment of the MPA is not changed while the molecular plane is no longer free to rotate, but instead it is confined to the polarization plane. This demonstrates that the molecule is 3D aligned. The corresponding end-view images of H^+ in row (b) corroborate this interpretation: With a linearly polarized YAG pulse the H^+ ions emerge in the circularly symmetric pattern shown in panel (b2), corresponding to free rotation of the molecular plane around the YAG polarization axis. For an elliptically polarized YAG pulse, the H^+ ions are angularly localized around the vertical minor polarization axis, i.e., the molecular plane is confined to the polarization plane. The radial structures of panel (b2) and (b3) are the same, confirming that the long axes of the molecules remain aligned along the major polarization axis. Thus, the H^+ images confirm that the CPC molecules are 3D aligned by the elliptically polarized YAG pulse.

B. Orientation

Previous studies showed that 1D and 3D mixed-field orientation of quantum-state selected asymmetric top molecules can be efficiently produced in case the MPA and the permanent dipole moment of the molecule are parallel.^{12,16} Orientation was observed when the molecule was rotated away from the side-view geometry used in

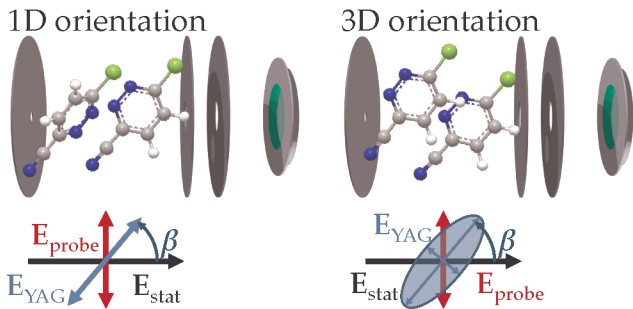


FIG. 4. Schematic illustration of the polarization state of the YAG and the probe pulse with respect to the static electric field and the detector plane used for 1D and 3D orientation. In the orientation experiments the polarization direction of the probe pulse is kept fixed to the plane of the detector, while β (the angle between the static field direction and the (major) polarization axis of the YAG pulse) is changed. For both schemes, the expected alignment and orientation can be visualized from the included molecular sketches.

pure alignment measurements; see Fig. 4 for a sketch of this experimental approach. In practice this was done by rotating the YAG pulse polarization to angles where $\beta \neq 90^\circ$. This provides a component of the static field along the dipole moment which mixes the pendular states of the tunneling doublet to form the corresponding oriented states. The experimental findings showed that the degree of orientation increased monotonically as β was rotated from 90° towards 0° or 180° . Later experiments and analysis have identified this behaviour as resulting from nonadiabatic dynamics in the mixed-field orientation.^{26–28} In the following we investigate if the 57.1° offset of the dipole moment from the MPA in CPC influences the efficiency of mixed-field orientation and if the degree of orientation peaks when the MPA or the permanent dipole moment is directed along the static field from the VMI spectrometer. The experimental observables used are the Cl^+ ion images which provide information about the orientation of the MPA.

Examples of Cl^+ ion images recorded for $\beta = 40^\circ$ (130°) are shown as insets in Fig. 5. For $\beta = 40^\circ$ (130°), more (less) ions are detected on the upper half of the detector than on the lower half. In analogy with previous studies we interpret these observations as orientation due to the combined effect of the YAG laser field and the static electric extraction field,¹² where the DPM z -component orients along the projection of the dc electric field onto the MPA. This implies that the partially negative nitrile end will be directed towards the repeller electrode (farthest away from the detector) where the potential is highest and the C-Cl bond towards the extractor electrode where the field is lowest – see Fig. 4. As a consequence, Cl^+ ions are expected to be ejected upwards (downwards) for $\beta = 40^\circ$ (130°). This is in agreement with the up-down asymmetry on the images.

The degree of orientation is quantified by dividing the number of ions detected on the upper half of the detector

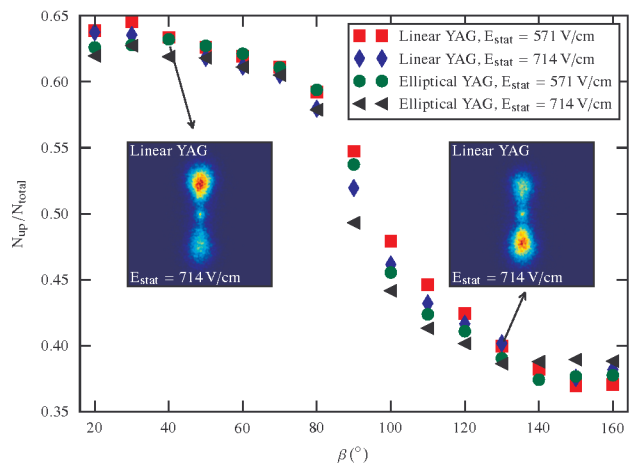


FIG. 5. Degree of orientation as a function of angle β between the static field and laser polarization for different field strengths. The values are determined from the distribution of Cl^+ ions. The insets show ion images at (left) $\beta = 40^\circ$ and (right) $\beta = 130^\circ$.

by the total amount of ions detected ($N_{\text{up}}/N_{\text{total}}$). This asymmetry parameter is plotted in Fig. 5 as a function of β . Measurements were carried out for both a linearly polarized and an elliptically polarized YAG pulse – in either case the measurements were performed at two values of the static electric field. The figure shows that for the linearly polarized and elliptically polarized data the degree of orientation increases gradually as the MPA is rotated towards the direction of the static electric field. No significant dependence on the static field strength is observed. This behaviour is similar to that observed for molecules where the MPA and the permanent dipole moment are parallel. The experimental findings are rationalized by our computational treatment – discussed in the next section.

VI. THEORETICAL RESULTS AND COMPARISON WITH OBSERVATIONS

Let us first consider the CPC molecule exposed to a static electric field parallel to the LFF Z -axis, i.e., $\beta = 0^\circ$. The μ_z (μ_y) term of the Stark effect interaction couples states with different parity under inversion along the molecular z (y) axis. As the dc field strength is increased, the electric dipole moment μ gets oriented along the electric field axis. The expectation values $\langle \cos \theta_{s\mu} \rangle$, $\langle \cos \theta_{sz} \rangle$ and $\langle \cos \theta_{sy} \rangle$, see Eq. 5, 3 and 4, measure the orientation of μ and of the molecular z and y axes, respectively. They are presented as a function of the dc field strength E_s in Fig. 6. For the rotational ground state and $E_s = 714 \text{ V/cm}$, we compute $\langle \cos \theta_{s\mu} \rangle = 0.327$, $\langle \cos \theta_{sz} \rangle = 0.384$, and $\langle \cos \theta_{sy} \rangle = 0.141$. In such a weak field the orientation of the y -axis, corresponding to the largest dipole moment com-

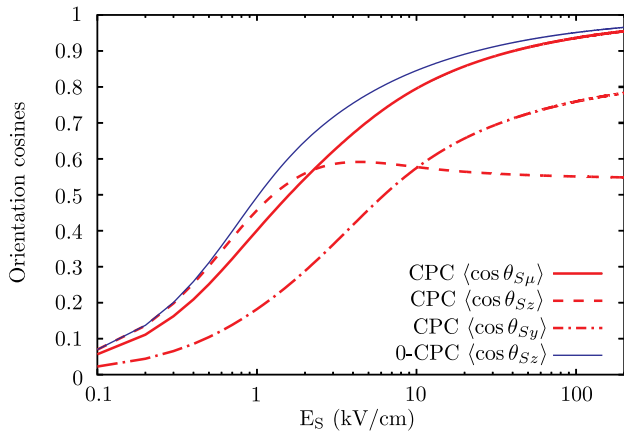


FIG. 6. Expectation values $\langle \cos \theta_{s\mu} \rangle$ (thick solid line), $\langle \cos \theta_{sz} \rangle$ (dashed line) and $\langle \cos \theta_{sy} \rangle$ (dot-dashed line) of CPC, and $\langle \cos \theta_{sz} \rangle$ (thin solid line) of 0-CPC as a function of the electric field strength E_s . The field configuration is $\beta = 0^\circ$ and $I_{\text{YAG}} = 0 \text{ W/cm}^2$.

ponent, is smaller than the orientation of the z axis, see Fig. 6, because the energy gap from the ground state to the first level with odd parity under inversion along the y -axis ($|J_{K_a K_c} M\rangle = |1_{11} 0\rangle$) is larger than to the first level with odd parity under the inversion along the z -axis ($|1_{01} 0\rangle$). When E_s is increased, the hybridization of the pendular levels increase, and this trend in the orientation is inverted; we encounter that $\langle \cos \theta_{sz} \rangle < \langle \cos \theta_{sy} \rangle$ for $E_s \gtrsim 10 \text{ kV/cm}$, see Fig. 6. In the strong-dc-field regime $\lim_{E_s \rightarrow \infty} \langle \cos \theta_{s\mu} \rangle = 1$, $\lim_{E_s \rightarrow \infty} \langle \cos \theta_{sz} \rangle = \cos(57.1^\circ) = 0.543$ and $\lim_{E_s \rightarrow \infty} \langle \cos \theta_{sy} \rangle = \cos(32.9^\circ) = 0.840$.

To investigate the influence of μ_y on the dc-field orientation, we have considered a molecule with the same rotational constants and polarizability as the CPC, but with $\mu_z = 2.83 \text{ D}$ and $\mu_y = 0 \text{ D}$. When this 0-CPC molecule is exposed to an electric field, only its z -axis gets oriented along the Z -axis. For weak dc fields, the ground states of the CPC and 0-CPC molecules show close values of $\langle \cos \theta_{sz} \rangle$, we find relative differences between 1% and 5% for $100 \text{ V/cm} \lesssim E_s \lesssim 700 \text{ V/cm}$. By increasing E_s , these relative differences increase and are larger than 10% for $E_s \gtrsim 1.2 \text{ kV/cm}$. The 0-CPC orients always better, i. e., its orientation cosine $\langle \cos \theta_{sz} \rangle$ is larger than the corresponding ones $\langle \cos \theta_{s\mu} \rangle$ and $\langle \cos \theta_{sz} \rangle$ of the CPC. Both molecules share the field-free energy level structure, but the μ_z and μ_y Stark interactions couple different states, which provoke a larger orientation for 0-CPC in despite of its smaller dipole moment. Only in the strong dc-field regime, when the pendular levels are strongly hybridized these two systems show a similar orientation. We obtain $\langle \cos \theta_{s\mu} \rangle = 0.955$ for the CPC ground state and $E_s = 200 \text{ kV/cm}$, and $\langle \cos \theta_{sz} \rangle = 0.966$ for the 0-CPC ground state.

We now consider the molecule in a linearly polarized strong laser field, when tunneling doublets of aligned states are formed.⁹ In an additional tilted weak electric field, the terms in μ_z and μ_y in Eq. 2 couple states in

TABLE I. Orientation and alignment of the ground state of the CPC molecule in a dc electric field and an linearly polarized YAG laser of $I_{\text{YAG}} = 8 \times 10^{11} \text{ W/cm}^2$ forming an angle of $\beta = 40^\circ$.

E_s [V/cm]	$\langle \cos^2 \theta_{Zz} \rangle$	$\langle \cos \theta_{Zz} \rangle$	$\langle \cos \theta_{Yy} \rangle$
571	0.985	0.993	0.126
714	0.985	0.993	0.156
5×10^3	0.985	0.993	0.638
5×10^4	0.985	0.992	0.893

the same doublet and between neighbouring doublets, respectively. For the experimentally employed field-strengths, the interaction due to the nonresonant laser field dominates. For $I_{\text{YAG}} = 8 \times 10^{11} \text{ W/cm}^2$, the energy splittings of the sublevels in the lowest two pendular doublets are smaller than 10^{-8} cm^{-1} , the energies of the two doublets differ by 0.20 cm^{-1} , and the MPA is strongly aligned along the Z -axis with $\langle \cos^2 \theta_{Zz} \rangle > 0.98$ for these four levels. For a weak dc field, the 0.20 cm^{-1} energy gap between two consecutive doublets is larger than the interaction due to this field: for $E_s = 714 \text{ V/cm}$, $E_s \mu_z = 3.4 \times 10^{-2} \text{ cm}^{-1}$ and $E_s \mu_y = 5.3 \times 10^{-2} \text{ cm}^{-1}$. Note that these quantities provide upper bounds to the dc field interactions because the angular dependence in Eq. 2 is set to 1, which holds only for fully oriented states. As a consequence, for weak dc fields, the coupling is only significant between states in the same doublet and the states become oriented or antioriented along the LFF Z -axis, but no orientation of the molecular y -axis is achieved. This can be illustrated by a comparison between the CPC and 0-CPC results in this field configuration. For $10 \text{ V/cm} \leq E_s$, these molecules present the same mixed-field orientation of the z -axis $\langle \cos \theta_{Zz} \rangle$ with relative differences smaller than 0.01%. At the experimental field regime, the mixed-field orientation of both systems is dominated by the Stark interaction due to μ_z , and the contribution of μ_y can be neglected. For the CPC ground state, the orientation and alignment are presented in Tab. I for $I_{\text{YAG}} = 8 \times 10^{11} \text{ W/cm}^2$ and $\beta = 40^\circ$. As E_s is increased (to values $E_s = 5 \text{ kV/cm}$ or $E_s = 50 \text{ kV/cm}$ in Tab. I), the coupling due to μ_y is enhanced and the molecular y -axis gets oriented along the laboratory Y -axis. In this strong electric field regime, the CPC molecule is 3D oriented. Thus, the difference between the CPC and 0-CPC systems appears only for strong dc fields when they are 3D and 1D oriented, respectively. However, even in this regime, they still have the same value of $\langle \cos \theta_{Zz} \rangle$.

If the dc field is parallel to the linearly polarized laser field, the MPA becomes oriented or antioriented along the LFF Z -axis but there are no constraints in the y -axis. If the dc field is perpendicular to the linearly polarized laser, due to symmetry no orientation along the LFF Z -axis exists. For a strong laser field, the MPA is aligned forming a small angle with the Z -axis, e. g., for the ground state, $\langle \cos^2 \theta_{Zz} \rangle = 0.985$ at

TABLE II. Orientation and alignment of the ground state of the CPC molecule in a dc electric field and an elliptically polarized YAG laser with $I_{\text{YAG}} = 8 \times 10^{11} \text{ W/cm}^2$ and $\beta = 40^\circ$.

E_s [V/cm]	$\langle \cos^2 \theta_{Zz} \rangle$	$\langle \cos \theta_{Zz} \rangle$	$\langle \cos^2 \theta_{Yy} \rangle$	$\langle \cos \theta_{Yy} \rangle$
571	0.981	0.990	0.914	0.938
714	0.981	0.990	0.914	0.954
5×10^3	0.981	0.990	0.915	0.955
5×10^4	0.981	0.990	0.917	0.957

$I_{\text{YAG}} = 8 \times 10^{11} \text{ W/cm}^2$. Thus, μ_y lies close to the plane perpendicular to the Z -axis which includes the dc field, and the molecular y -axis gets oriented along the Y -axis. For $I_{\text{YAG}} = 8 \times 10^{11} \text{ W/cm}^2$, $E_s = 714 \text{ V/cm}$, and $\beta = 90^\circ$, $\langle \cos \theta_{Yy} \rangle = 0.250$ for the ground state. Increasing the dc field strength, this orientation is enhanced, e. g., $\langle \cos \theta_{Yy} \rangle = 0.731$ for $E_s = 5 \text{ kV/cm}$, and the molecular plane is confined to the plane spanned by the laser field and the static field.

Let us now discuss the case of an elliptically polarized laser field. The molecule becomes 3D aligned with the most polarizable axis (the z -axis) confined along the Z -axis (the major polarization axis) and the second most polarizable axis confined along the minor polarization axis. Our calculation shows that $\langle \cos^2 \theta_{Zz} \rangle > \langle \cos^2 \theta_{Yy} \rangle$, e. g., $\langle \cos^2 \theta_{Zz} \rangle = 0.981$ and $\langle \cos^2 \theta_{Yy} \rangle = 0.913$ for $I_{\text{YAG}} = 8 \times 10^{11} \text{ W/cm}^2$. In this field configuration, the four lowest lying states with even parity under the reflection on the LFF ZY plane belong to 4 irreducible representations. These levels are quasidegenerate and form a quadruplet. For $I_{\text{YAG}} = 8 \times 10^{11} \text{ W/cm}^2$, the energy splittings within the two doublets are $7.83 \times 10^{-6} \text{ cm}^{-1}$ and $7.64 \times 10^{-6} \text{ cm}^{-1}$ and they are separated by $4.37 \times 10^{-5} \text{ cm}^{-1}$. In an additional electric field with $\beta \neq 0^\circ, 90^\circ$ these states all have the same symmetry and are Stark coupled. Now, both dc-field couplings, due to μ_z and μ_y , are significantly larger than the pendular-state-energy splittings. Thus, 3D orientation is feasible in the weak dc-field regime. This confinement of the molecular plane to the polarization one is illustrated in **Tab. II** for the ground state with $I_{\text{YAG}} = 8 \times 10^{11} \text{ W/cm}^2$ and $\beta = 40^\circ$. Let us mention that at least two non-zero components of $\boldsymbol{\mu}$ are required to achieve a 3D orientation. If the dc electric field forms an angle of $\beta = 0^\circ$ ($\beta = 90^\circ$) with the ac electric field, the CPC molecule is 3D aligned and 1D oriented, resulting, effectively, in 3D orientation:¹⁶ the molecular z (y) axis is oriented along the major (minor) polarization axis.

Analogous features are found for the excited rotational/pendular levels. The complexity of their field-dressed dynamics is significantly enhanced due to the large number of avoided crossings. These avoided crossings provoke abrupt changes on their directional properties, which play an important role on the mixed-field orientation of the molecular beam.²⁹

For the experimentally accessed regime of field

strengths, $\langle \cos \theta_{Zz} \rangle$ is independent of I_{YAG} and E_s , whereas $\langle \cos \theta_{Yy} \rangle$ increases until the strong dc field regime is reached and then is independent of both. Regarding the behaviour of the orientation cosines $\langle \cos \theta_{Zz} \rangle$ and $\langle \cos \theta_{Yy} \rangle$ versus β , three different regimes are observed: i) for weak alignment lasers, when the pendular doublets are not yet formed, or the energy splitting between two neighbouring doublets is larger than the dc-field interaction, $\langle \cos \theta_{Zz} \rangle$ or $\langle \cos \theta_{Yy} \rangle$ monotonically increase with β , respectively; ii) for stronger laser fields, these energy separations are significantly reduced, and the orientation is independent of β ; iii) if the dc-field interaction is much larger than the laser-field one, the orientation in both directions reaches a maximum at $\beta = 57.1^\circ$, because the effect of the static field becomes optimal at this field configuration. In particular, this time-independent description predicts an orientation of the MPA along the Z axis independent of β and E_s . Thus, the smooth behaviour of $N_{\text{up}}/N_{\text{total}}$ versus β in **Fig. 5** cannot be reproduced with this theoretical treatment. Indeed, the authors have recently demonstrated that only a time-dependent study can reproduce the intriguing physical phenomena taking place in the mixed-field orientation experiments.²⁷

For completeness, we have investigated the mixed-field orientation of thermal samples of CPC, in order to mimic the state-selection, assuming that the alignment and orientation processes are adiabatic.²⁹ For an elliptically polarized laser with $I_{\text{YAG}} = 8 \times 10^{11} \text{ W/cm}^2$, $E_s = 714 \text{ V/cm}$, and $\beta = 40^\circ$, the molecular sample at 1 K is strongly aligned but practically not oriented, consistent with experimental findings:³⁰ $\langle \cos^2 \theta_{2D} \rangle = 0.949$ ($\langle \cos^2 \theta_{Zz} \rangle = 0.931$, $\langle \cos^2 \theta_{Yy} \rangle = 0.680$), $\langle \cos \theta_{Zz} \rangle = 0.015$, $\langle \cos \theta_{Yy} \rangle = 0.021$ and $N_{\text{up}}/N_{\text{total}} = 0.51$. By reducing the temperature to 0.1 K, the alignment is slightly improved to $\langle \cos^2 \theta_{2D} \rangle = 0.980$ ($\langle \cos^2 \theta_{Zz} \rangle = 0.976$, $\langle \cos^2 \theta_{Yy} \rangle = 0.868$) and the orientation is strongly increased ($\langle \cos \theta_{Zz} \rangle = 0.36$, $\langle \cos \theta_{Yy} \rangle = 0.43$ and $N_{\text{up}}/N_{\text{total}} = 0.68$). This demonstrates that for our cold molecular beams ($\sim 1 \text{ K}$) the state-selection of low-energy rotational states is crucial for the creation of orientation.

VII. CONCLUSIONS

We have performed a combined experimental and theoretical investigation of mixed-field orientation of the 6-chloropyridazine-3-carbonitrile (CPC) molecule. Our studies are motivated by the fact that this molecule represents the large class of important species where the relevant molecular-frame coordinate systems, i. e., inertial frame, dipole moment, and polarizability, do not coincide. We show that the direct extension of weak-dc-field mixed-field orientation from molecules with parallel frames^{12,16,29} toward three-dimensional orientation is possible but does not agree with the simple picture in which the strong alignment of the most polarizable axis plus 1D spatial orientation of the dipole moment vector

along the dc field would completely lock the molecule in space.⁹ Instead, the detailed energy level structure of the pendular states has to be evaluated and it is shown that only one dipole component of CPC leads to strong enough Stark interactions to provide orientation. The other component correspond to Stark couplings of levels in different pendular doublets and they only become relevant under conditions similar to brute-force orientation of laser-field-free molecules. We demonstrate that 3D orientation of the unsymmetric CPC molecule is possible using elliptically polarized laser fields and a weak dc field. Moreover, our calculations predict that 3D orientation can be achieved using linearly polarized laser fields and strong dc fields arranged under an angle that corresponds to the angle between the most polarizable axis and the dipole moment.

Overall, it is clear that mixed-field orientation with appropriately polarized laser fields and weak dc fields is an effective tool for three-dimensional confinement of complex molecules. Even stronger control will be achievable in upcoming experiments combining strong dc electric fields and linearly-polarized laser fields. The degree of angular control demonstrated provides excellent prospects for the recording of molecular movies of complex molecules using ion-, electron-, or photon-imaging experiments.

VIII. ACKNOWLEDGEMENT

We are grateful to Frank Jensen for calculating the structure, dipole moment and polarizability components of CPC. This work has been supported by the excellence cluster “The Hamburg Center for Ultrafast Imaging – Structure, Dynamics and Control of Matter at the Atomic Scale” of the Deutsche Forschungsgemeinschaft. The work was supported by the Danish Council for Independent Research (Natural Sciences), The Lundbeck Foundation and the Carlsberg Foundation. Financial support by the Spanish project FIS2011-24540 (MICINN), the Grants P11-FQM-7276, FQM-2445 and FQM-4643 (Junta de Andalucía), and the Andalusian research group FQM-207 is gratefully appreciated. J.J.O. acknowledges the support of ME under the program FPU. Part of this work was done while R.G.F. was visitor at the Kavli Institute for Theoretical Physics, University of California at Santa Barbara within the program Fundamental Science and Applications of Ultracold Polar Molecules, she gratefully acknowledges partial financial support from the National Science Foundation grant no. NSF PHY11-25915.

¹C. Z. Bisgaard, O. J. Clarkin, G. Wu, A. M. D. Lee, O. Gessner, C. C. Hayden, and A. Stolow, *Science* **323**, 1464 (2009).

²F. Filsinger, G. Meijer, H. Stapelfeldt, H. Chapman, and J. Küpper, *Phys. Chem. Chem. Phys.* **13**, 2076 (2011).

³G. Sciaini and R. J. D. Miller, *Rep. Prog. Phys.* **74**, 096101 (2011).

⁴J. L. Hansen, J. H. Nielsen, C. B. Madsen, A. T. Lindhardt, M. P. Johansson, T. Skrydstrup, L. B. Madsen, and H. Stapelfeldt, *J. Chem. Phys.* **136**, 204310 (2012).

⁵C. J. Hensley, J. Yang, and M. Centurion, *Phys. Rev. Lett.* **109**, 133202 (2012).

⁶J. H. Ullrich, A. Rudenko, and R. Moshhammer, *Annu. Rev. Phys. Chem.* **63**, 635 (2012).

⁷A. Barty, J. Küpper, and H. N. Chapman, *Annu. Rev. Phys. Chem.* **64**, 415 (2013).

⁸H. Stapelfeldt and T. Seideman, *Reviews of Modern Physics* **75**, 543 (2003).

⁹B. Friedrich and D. Herschbach, *The Journal of Chemical Physics* **111**, 6157 (1999).

¹⁰H. Sakai, S. Minemoto, H. Nanjo, H. Tanji, and T. Suzuki, *Physical Review Letters* **90**, 083001 (2003).

¹¹U. Buck and M. Fárnfk, *International Reviews in Physical Chemistry* **25**, 583 (2006).

¹²L. Holmegaard, J. H. Nielsen, I. Nevo, H. Stapelfeldt, F. Filsinger, J. Küpper, and G. Meijer, *Physical Review Letters* **102**, 023001 (2009).

¹³O. Ghafur, A. Rouzee, A. Gijsbertsen, W. K. Siu, S. Stolte, and M. J. J. Vrakking, *Nature Physics* **5**, 289 (2009).

¹⁴J. J. Larsen, K. Hald, N. Bjerre, H. Stapelfeldt, and T. Seideman, *Physical Review Letters* **85**, 2470 (2000).

¹⁵H. Tanji, S. Minemoto, and H. Sakai, *Physical Review A* **72**, 063401 (2005).

¹⁶I. Nevo, L. Holmegaard, J. H. Nielsen, J. L. Hansen, H. Stapelfeldt, F. Filsinger, G. Meijer, and J. Küpper, *Physical Chemistry Chemical Physics* **11**, 9912 (2009).

¹⁷J. C. H. Spence and R. B. Doak, *Physical Review Letters* **92**, 198102 (2004).

¹⁸L. Holmegaard, J. L. Hansen, L. Kalhøj, S. Louise Kragh, H. Stapelfeldt, F. Filsinger, J. Kupper, G. Meijer, D. Dimitrovski, M. Abu-samha, C. P. J. Martiny, and L. Bojer Madsen, *Nature Physics* **6**, 428 (2010).

¹⁹Gaussian 2003³¹ B3LYP/aug-pc-1 calculations performed by Frank Jensen, Department of Chemistry, Aarhus University.

²⁰F. Filsinger, J. Küpper, G. Meijer, L. Holmegaard, J. H. Nielsen, I. Nevo, J. L. Hansen, and H. Stapelfeldt, *The Journal of Chemical Physics* **131**, 064309 (2009).

²¹J. H. Nielsen, P. Simesen, C. Z. Bisgaard, H. Stapelfeldt, F. Filsinger, B. Friedrich, G. Meijer, and J. Küpper, *Physical Chemistry Chemical Physics* **13**, 18971 (2011).

²²U. Even, J. Jortner, D. Noy, N. Lavie, and C. Cossart-Magos, *The Journal of Chemical Physics* **112**, 8068 (2000).

²³R. N. Zare, *Angular Momentum: Understanding Spatial Aspects in Chemistry and Physics* (WileyBlackwell, 1988).

²⁴R. Kanya and Y. Ohshima, *Physical Review A* **70**, 013403 (2004).

²⁵J. J. Omiste, R. González-Férez, and P. Schmelcher, *The Journal of Chemical Physics* **135**, 064310 (2011).

²⁶J. H. Nielsen, *Laser-Induced Alignment and Orientation of Quantum-State Selected Molecules and Molecules in Liquid Helium Droplets*, Ph.D. thesis, Aarhus University, Aarhus (2012).

²⁷J. H. Nielsen, H. Stapelfeldt, J. Küpper, B. Friedrich, J. J. Omiste, and R. González-Férez, *Physical Review Letters* **108**, 193001 (2012).

²⁸J. J. Omiste and R. González-Férez, *Physical Review A* **86**, 043437 (2012).

²⁹J. J. Omiste, M. Gärttner, P. Schmelcher, R. González-Férez, L. Holmegaard, J. H. Nielsen, H. Stapelfeldt, and J. Küpper, *Physical Chemistry Chemical Physics* **13**, 18815 (2011).

³⁰J. L. Hansen, *Imaging Molecular Frame Dynamics Using Spatially Oriented Molecules*, Ph.D. thesis, Aarhus University, Aarhus, Denmark (2012).

³¹M. J. Frisch, G. W. Trucks, H. B. Schlegel, G. E. Scuseria, M. A. Robb, J. R. Cheeseman, J. J. A. Montgomery, T. Vreven, K. N. Kudin, J. C. Burant, J. M. Millam, S. S. Iyengar, J. Tomasi, V. Barone, B. Mennucci, M. Cossi, G. Scalmani, N. Rega, G. A. Petersson, H. Nakatsuji, M. Hada, M. Ehara, K. Toyota, R. Fukuda, J. Hasegawa, M. Ishida, T. Nakajima, Y. Honda,

O. Kitao, H. Nakai, M. Klene, X. Li, J. E. Knox, H. P. Hratchian, J. B. Cross, V. Bakken, C. Adamo, J. Jaramillo, R. Gomperts, R. E. Stratmann, O. Yazyev, A. J. Austin, R. Cammi, C. Pomelli, J. W. Ochterski, P. Y. Ayala, K. Morokuma, G. A. Voth, P. Salvador, J. J. Dannenberg, V. G. Zakrzewski, S. Dapprich, A. D. Daniels, M. C. Strain, O. Farkas, D. K. Malick, A. D. Rabuck, K. Raghavachari, J. B. Foresman, J. V. Ortiz, Q. Cui,

A. G. Baboul, S. Clifford, J. Cioslowski, B. B. Stefanov, G. Liu, A. Liashenko, P. Piskorz, I. Komaromi, R. L. Martin, D. J. Fox, T. Keith, M. A. Al-Laham, C. Y. Peng, A. Nanayakkara, M. Challacombe, P. M. W. Gill, B. Johnson, W. Chen, M. W. Wong, C. Gonzalez, and J. A. Pople, "Gaussian 03, Gaussian, Inc., Wallingford CT," (2004).

Rotational dynamics of an asymmetric top molecule in parallel electric and non-resonant laser fields

J. J. Omiste* and R. González-Férez†

Instituto Carlos I de Física Teórica y Computacional, and Departamento de Física Atómica, Molecular y Nuclear, Universidad de Granada, 18071 Granada, Spain

(Dated: June 6, 2013)

We present a theoretical study of the rotational dynamics of asymmetry top molecules in parallel electric field and non-resonant linearly polarized laser pulses. The time-dependent Schrödinger equation is solved within the rigid rotor approximation. Using the benzonitrile molecule as prototype, we investigate the field-dressed dynamics for experimentally accessible field configurations and compare these results to the adiabatic predictions. We show that for an asymmetric top molecule in parallel fields, the formation of the pendular doublets and the avoided crossings between neighboring levels are the two main sources of non-adiabatic effects. We also provide the field parameters under which the adiabatic dynamics would be achieved.

I. INTRODUCTION

The availability of oriented molecules provides a wealth of intriguing applications in a variety of molecular sciences, such as in chemical reaction dynamics [1–5], photoelectron angular distributions [6–8], or high-order harmonic generation [9–11]. An oriented molecule is characterized by the confinement of the molecular fixed axes along the laboratory fixed axes and by its dipole moment pointing in a particular direction. Many experimental efforts have been undertaken to control the rotational degree of freedom, and in particular to orient polar molecules [1, 12–22].

Here, we focus on a theoretical study of the mixed-field orientation technique, which is based on the combination of weak dc and strong non-resonant radiative fields [19, 20]. Strongly oriented/antioriented states could be created by coupling the nearly degenerate pair of states with opposite parity forming a pendular doublet by means of a weak dc field. This theoretical prediction is based on an adiabatic picture in which the turn-on time of the laser pulse is larger than the molecular rotational period [23]. For asymmetric top molecules, a theoretical study based on a time-independent model of their mixed-field orientation pointed out that a fully adiabatic description of this process does not reproduce the experimental results [24]. We have recently found that a time-dependent description of the mixed-field orientation of linear molecules is required to explain the experimental observations [25, 26]. Two main sources of non-adiabatic effects were identified for linear molecules: i) the coupling of the levels forming quasidegenerate pendular doublets as the laser intensity is increased gives rise to a transfer of population between them; ii) the strongly coupled states from the same J manifold for tilted fields are driven apart as the laser intensity is increased in the weak-field regime, provoking a population redistribution among them. In

addition, for highly excited states, avoided crossing in the field-dressed spectrum could affect the rotational dynamics. A similar time-dependent study for polar asymmetric top molecules is desirable for a correct interpretation of the numerous mixed-field experiments with these systems [21, 27]. Compared to linear molecules, asymmetric tops possess a more dense level structure and, when the fields are turned on these level could be strongly coupled. Thus, a more complex rotational dynamics should be expected for asymmetric tops in combined dc and ac fields. Let us also mention that several theoretical and experimental studies have investigated the relevance of non-adiabatic phenomena on the manipulation of molecules in external fields [28–34]

In this work, we perform a theoretical investigation of the rotational dynamics of an asymmetric top in the presence of combined electric and non-resonant radiative fields within the rigid rotor description. Due to the complexity of the field-dressed spectrum, we restrict this study to parallel fields. The time-dependent Schrödinger equation is solved using experimental field configurations, i.e., a linearly polarized Gaussian laser pulse parallel to a weak electric field that is switched on at a constant speed. To simplify the interpretation of our results, each irreducible representation is treated independently by expanding the wave function in a basis with the proper symmetry. For several rotational states, we investigate the mixed-field dynamics under different field configurations and provide a detailed account of the sources of non-adiabaticity and the field regimes at which they appear. For these molecules, the field-dressed dynamics is characterized by the formation of the pendular doublets and the numerous avoided crossings of the field-dressed spectrum. In both cases, there is a population redistribution to neighboring adiabatic states when the laser intensity is enhanced, which could reduce the degree of orientation. We have proven that due the different time scales associated to each phenomenon, it might become experimentally harder to reach the adiabatic limit. Increasing the electric field strengths helps for the lowest-lying state in a certain irreducible representation; whereas for excited one a proper combination of dc field with the temporal

* omiste@ugr.es

† rogonzal@ugr.es

width of the pulse is needed to optimize the mixed-field orientation process.

The paper is organized as follows: In Sec. II we describe the Hamiltonian of the system, its symmetries and the numerical method used to solve the time-independent Schrödinger equation. In Sec. III we investigate the mixed-field dynamics of several rotational states as the laser intensity is increased, and identify the sources of non-adiabatic effects. We also explore the final orientation of these states as the field parameters are varied seeking for the adiabatic regime. The conclusions are given in Sec. IV.

II. THE HAMILTONIAN OF AN ASYMMETRIC TOP MOLECULE IN PARALLEL FIELDS

We consider a polar asymmetric top molecule in parallel homogeneous static electric field and non-resonant linearly polarized laser pulse. The polarization of the laser lies along the Z -axis of the laboratory fixed frame (LFF) (X, Y, Z) and the electric field is also parallel to this Z -axis. We only consider molecules with diagonal polarizability tensors, and the dipole moment parallel to the z -axis of the molecular fixed frame (MFF) (x, y, z) , and the smallest moment of inertia is parallel to the x -axis. The LFF and MFF are related by the Euler angles (θ, ϕ, χ) [35]. Within the rigid rotor approximation, the Hamiltonian reads

$$H(t) = H_R + H_s(t) + H_L(t), \quad (1)$$

where H_R stands for the field-free Hamiltonian

$$H_R = B_x J_x^2 + B_y J_y^2 + B_z J_z^2 \quad (2)$$

with J_k being the projection of the total angular momentum operator \mathbf{J} along the k -axis of the MFF with $k = x, y$ and z . The rotational constant along the MFF k -axis is $B_k = \frac{\hbar^2}{2I_{kk}}$ with I_{kk} the moment of inertia with respect to this axis k .

The interaction of the electric field $\mathbf{E}_s(t) = E_s(t)\hat{Z}$ with the permanent dipole moment, $\boldsymbol{\mu} = \mu\hat{z}$, reads

$$H_s(t) = -\boldsymbol{\mu} \cdot \mathbf{E}_s(t) = -\mu E_s(t) \cos \theta, \quad (3)$$

where $E_s(t)$ initially depends linearly on time, and once the maximum strength E_s is reached, it is kept constant. The turning on speed is chosen so that this process is adiabatic. Here, we work in the weak or moderate dc-field regime. Thus, we can neglect the coupling of this field with the molecular polarizability and higher order terms.

The interaction of the non-resonant laser field and the molecule can be written as [23]

$$H_L(t) = -\frac{I(t)}{2\epsilon_0 c} (\alpha^{zx} \cos^2 \theta + \alpha^{yx} \sin^2 \theta \sin^2 \chi), \quad (4)$$

where $\alpha^{km} = \alpha_{kk} - \alpha_{mm}$ are the polarizability anisotropies, being α_{kk} the polarizability along the molecular axis $k = x, y$ and z . ϵ_0 is the dielectric constant and c the speed of light. The intensity of the non-resonant laser pulse is $I(t)$. We analyze Gaussian pulses with intensity $I(t) = I_0 \exp\left(-\frac{t^2}{2\sigma^2}\right)$, I_0 is the peak intensity, which is reached at $t = 0$, and σ is related to full width half maximum (FWHM) as $\tau = 2\sqrt{2 \ln 2} \sigma$.

Based on current mixed-field orientation experiments, we assume a field-free molecule and turn on the electric field first. Once the maximum dc field strength is reached, the Gaussian pulse is switched on. Since the turning on of the dc field is adiabatic, here we investigate the non-adiabatic effects appearing in this second stage.

In this parallel field configuration, the symmetries of the rigid rotor Hamiltonian (1) are the identity, E , the two fold rotation around the MFF z -axis, arbitrary rotations around the LFF Z $C_Z(\delta)$, and the reflection in any plane containing the fields. Then, the projection of \mathbf{J} on the Z -axis M and the parity of its projection on the z -axis, i. e., the parity of K , are good quantum numbers. For $M \neq 0$, there are four irreducible representations and the symmetry of reflection on any plane containing the fields implies the well known degeneracy in $|M|$. For $M = 0$, the wave function can have even and odd parity under these reflections, giving rise to two irreducible representations for each parity of K .

To solve the time-dependent Schrödinger equation of the Hamiltonian (1), we employ the short iterative Lanczos algorithm for the time propagation [36], and a basis set representation for the angular coordinates. For each irreducible representation, we construct a basis using linear combinations of the field-free symmetric top eigenfunctions $|JKM\rangle$ [35] that respect the symmetries [37]. For reasons of addressability, we label the field-dressed wave function using the field-free notation $|J_{K_a, K_c} M\rangle_t$ where K_a and K_c are the values of K on the limiting symmetric top rotor prolate and oblate cases, respectively [38]. We have made explicit the dependence on time t of the wave function, but not on the field parameters I_0 , τ and E_s .

To have a better physical insight on the non-adiabatic effects of the field-dressed dynamics, the time-dependent wave function $|J_{K_a, K_c} M\rangle_t$ is expanded in the basis formed by the adiabatic basis at time t

$$|J_{K_a, K_c} M\rangle_t = \sum_{j=0}^N C_{\gamma_j}(t) |\gamma_j\rangle_p \quad (5)$$

with $C_{\gamma_j}(t) = {}_p\langle \gamma_j | J_{K_a, K_c} M \rangle_t$, and $|\gamma_j\rangle_p$ denotes the adiabatic states of Hamiltonian (1) taking the electric field strength and the laser intensities constant. Note that for each time step t , the time-independent Schrödinger equation is solved and an adiabatic basis is constructed. This pendular basis can be used to characterize as adiabatic or diabatic the time evolution of a

wave function. Thus, the rotational dynamics could be considered as fully adiabatic if the criterion

$$\eta = \frac{\hbar \left| \left\langle \gamma_i \left| \frac{\partial H_L(t)}{\partial t} \right| \gamma_j \right\rangle \right|}{|E_i - E_j|^2} \ll 1$$

is satisfied [39].

III. RESULTS

In this work, we use the benzonitrile molecule (BN) as prototype to illustrate our results. Its rotational constants are $B_x = 1214$ MHz, $B_y = 1547$ MHz and $B_z = 5655$ MHz, the permanent dipole moment $\mu = 4.515$ D and the polarizabilities are $\alpha_{xx} = 7.49$ Å³, $\alpha_{yy} = 13.01$ Å³ and $\alpha_{zz} = 18.64$ Å³ [40, 41]. For the sake of simplicity, we restrict this study to several rotational states of even parity with respect to the reflections on XZ -plane and under a π -rotation around the MFF z -axis. We stress that the observed physical phenomena also appear for levels within other irreducible representations. We consider experimentally accessible field configurations: a linearly polarized Gaussian pulse with the FWHM in the nanosecond range and peak intensities $10^{11} \text{ W/cm}^2 \leq I_0 \leq 10^{12} \text{ W/cm}^2$; and a weak dc field similar to the one present in a velocity-mapping image spectrometer of few hundreds V/cm.

In a mixed-field orientation experiment, the measurements are done once the laser pulse has reached the peak intensity, i. e., at $t = 0$ in our theoretical model. In this section, we first analyze the rotational dynamics as the laser intensity $I(t)$ is increased. This allows us to understand the different physical phenomena giving rise to a non-adiabatic dynamics. We also consider different experimentally accessible field configurations and investigate the orientation at $t = 0$ for several rotational states.

A. Field-dressed dynamics of the ground state of several irreducible representations

We start analyzing the mixed-field orientation of the ground states of the irreducible representations with $M = 0$ and 3, i. e., the levels $|0_{0,0}0\rangle$ and $|3_{0,3}3\rangle$. We have chosen these states because in mixed-field orientation experiment of BN they have a significant population in the quantum-state selected beam [21, 27], and the knowledge of their field-dressed dynamics is important for these experiments.

In Fig. 1(a) and Fig. 1(b) we present the orientation $\langle \cos \theta \rangle$ of the ground state $|0_{0,0}0\rangle_t$ as a function of the laser intensity $I(t)$ for $E_s = 300$ V/cm and $E_s = 600$ V/cm, respectively. The Gaussian pulses have $I_0 = 7 \times 10^{11} \text{ W/cm}^2$ and several FWHM. For comparison, the orientation of the adiabatic state $|0_{0,0}0\rangle_p$ is also

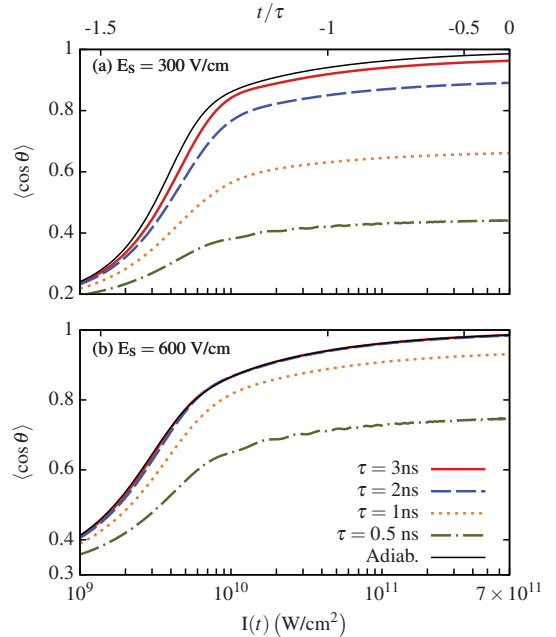


FIG. 1. (Color online) For the absolute ground state $|0_{0,0}0\rangle_t$, we present the expectation value $\langle \cos \theta \rangle$ versus the laser intensity $I(t)$ for (a) $E_s = 300$ V/cm and (b) $E_s = 600$ V/cm. The peak intensity is $I_0 = 7 \times 10^{11} \text{ W/cm}^2$ and the FWHM are $\tau = 3$ ns (red solid), $\tau = 2$ ns (blue long dashed), $\tau = 1$ ns (orange dotted) and $\tau = 0.5$ ns (green dashed-dotted).

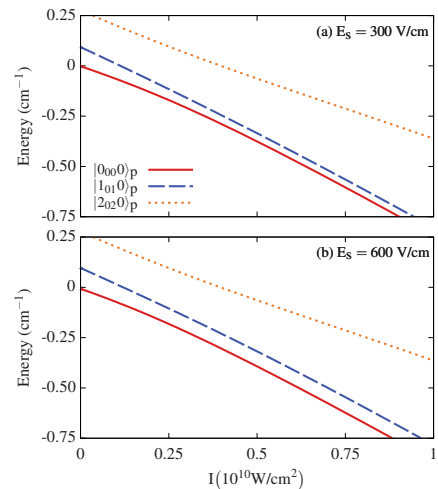


FIG. 2. (Color online) We present the formation of the pendular doublet between the states $|0_{0,0}0\rangle_p$ and $|1_{0,1}0\rangle_p$ in the adiabatic spectrum for dc field strengths (a) $E_s = 300$ V/cm and (b) $E_s = 600$ V/cm.

presented. For all these field-configurations, the orientation shows a qualitatively similar behavior: $\langle \cos \theta \rangle$ monotonically increases as $I(t)$ is increased, once the pendular limit is reached, the slope of $\langle \cos \theta \rangle$ versus $I(t)$ is reduced, and $\langle \cos \theta \rangle$ increases smoothly with a value smaller than the adiabatic limit. This reduction on the final orienta-

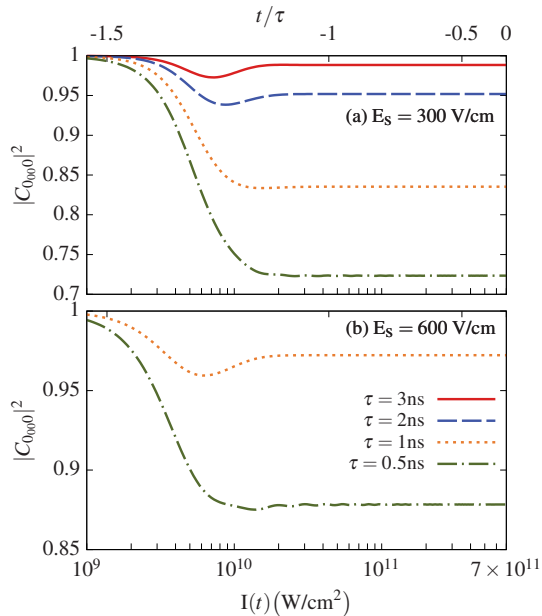


FIG. 3. (Color online) For the state $|0_{0,0}0\rangle_t$, we present the squares of the projection of the time-dependent wave function onto the adiabatic ground state $|0_{0,0}0\rangle_p$ versus the laser intensity $I(t)$ for dc field strengths (a) $E_s = 300$ V/cm and (b) $E_s = 600$ V/cm. The Gaussian pulse has $I_0 = 7 \times 10^{11}$ W/cm² and $\tau = 3$ ns (solid red), $\tau = 2$ ns (blue long dashed), $\tau = 1$ ns (orange dotted) and $\tau = 0.5$ ns (green dashed-dotted).

tion is due to the non-adiabatic effects. Analogously to the ground state of a linear molecule in combined electric and non-resonant laser fields, the loss of adiabaticity in the field-dress dynamics of $|0_{0,0}0\rangle_t$ is due to the formation of the quasidegenerate pendular doublets [26]. Thus, increasing the FWHM of the pulse will increase the orientation [25, 26, 42, 43]. In Fig. 2, we present how the pendular doublet between the adiabatic states $|0_{0,0}0\rangle_p$ and $|1_{0,1}0\rangle_p$ is formed. To illustrate this loss of adiabaticity of $|0_{0,0}0\rangle_t$ we show the population of the adiabatic ground state $|0_{0,0}0\rangle_p |C_{0_{0,0}0}(t)|^2$ in Fig. 3. Note that for the ground state, $|C_{0_{0,0}0}(t)|^2 + |C_{1_{0,1}0}(t)|^2 = 1$. For $E_s = 300$ V/cm, the rotational dynamics is adiabatic if the pulse has $\tau \geq 4$ ns, whereas for smaller values of τ the population transfer when the pendular doublet is formed could be very large. Using a 1 ns pulse, the population of the adiabatic ground state is $|C_{0_{0,0}0}(t)|^2 = 0.835$ at $t = 0$, and due to the contribution of the anti-oriented state $|1_{0,1}0\rangle_p$, the orientation at $t = 0$ of $|0_{0,0}0\rangle_0$ is reduced to $\langle \cos \theta \rangle = 0.661$. By increasing the dc field strength to $E_s = 600$ V/cm, the energy splitting of the pendular doublets is increased, and a Gaussian pulse of $\tau = 2$ ns already gives rise to an adiabatic dynamics for $|0_{0,0}0\rangle_t$. For a short pulse of 500 ps, the ground state is still strongly oriented with $\langle \cos \theta \rangle = 0.747$ and the contribution of the adiabatic ground state at $t = 0$ is $|C_{0_{0,0}0}(0)|^2 = 0.878$. For both dc fields and 500 ps, $\langle \cos \theta \rangle$ shows an oscilla-

tory behaviour as $I(t)$ is increased, which is due to the coupling between the two adiabatic states involved in the dynamics, i. e., the mixing term ${}_p \langle 0_{00}0 | \cos \theta | 1_{01}0 \rangle_p$.

The lowest-lying state in the irreducible representations with $M = 1$, $|1_{0,1}1\rangle_t$, is relatively well separated of neighboring levels with the same symmetry. Thus, its field-dressed dynamics shows analogous features as those discussed above for the $|0_{0,0}0\rangle_t$, and the formation of the pendular pair is the only effect provoking the loss of adiabaticity. Indeed, for $E_s = 300$ V/cm, a Gaussian pulse with $I_0 = 7 \times 10^{11}$ W/cm² and $\tau = 5$ ns gives rise to an adiabatic dynamics for this state.

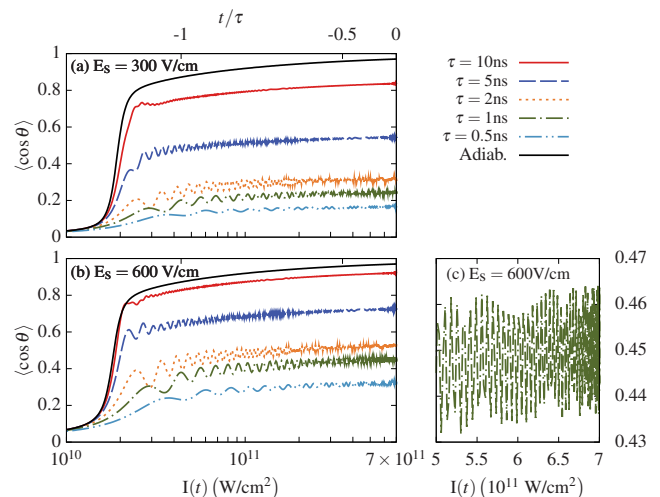


FIG. 4. (Color online) For the state $|3_{0,3}3\rangle_t$, we present the orientation cosine $\langle \cos \theta \rangle$ as a function of $I(t)$ for (a) $E_s = 300$ V/cm and (b) 600 V/cm. A detail of the oscillations of $\langle \cos \theta \rangle$ for 600 V/cm is shown in panel (c). The peak intensity of the pulses is $I_0 = 7 \times 10^{11}$ W/cm², and the FWHM are $\tau = 10$ ns (red solid line), $\tau = 5$ ns (dark blue long dashed line), $\tau = 2$ ns (orange dotted line), $\tau = 1$ ns (dark olive green dot-dashed line), $\tau = 0.5$ ns (light blue double-dot-dashed line). The adiabatic results are also shown (black solid line).

For higher values of M , the avoided crossings leave their fingerprints in the field-dressed dynamics of the corresponding ground state. As an example, we show in Fig. 4 the orientation cosine of $|3_{0,3}3\rangle_t$ for $E_s = 300$ V/cm and $E_s = 600$ V/cm, the adiabatic value of $\langle \cos \theta \rangle$ is also included. Comparing these results to those of the absolute ground state $|0_{0,0}0\rangle_t$ in Fig. 1, two main differences are encountered. First, $\langle \cos \theta \rangle$ initially increases as $I(t)$ is increased, and once the pendular doublet is formed $\langle \cos \theta \rangle$ oscillates around a mean value. Second, even the 10 ns Gaussian pulses do not to ensure an adiabatic dynamics for both dc field strengths. For instance, at $t = 0$ we obtain $\langle \cos \theta \rangle = 0.921$ for $E_s = 600$ V/cm and $\tau = 10$ ns, whereas the adiabatic value is $\langle \cos \theta \rangle = 0.970$. As the FWHM is increased, the amplitude of the oscillations of $\langle \cos \theta \rangle$ is reduced.

The oscillations in the evolution of $\langle \cos \theta \rangle$ can be explained due to the coupling between the adiabatic states

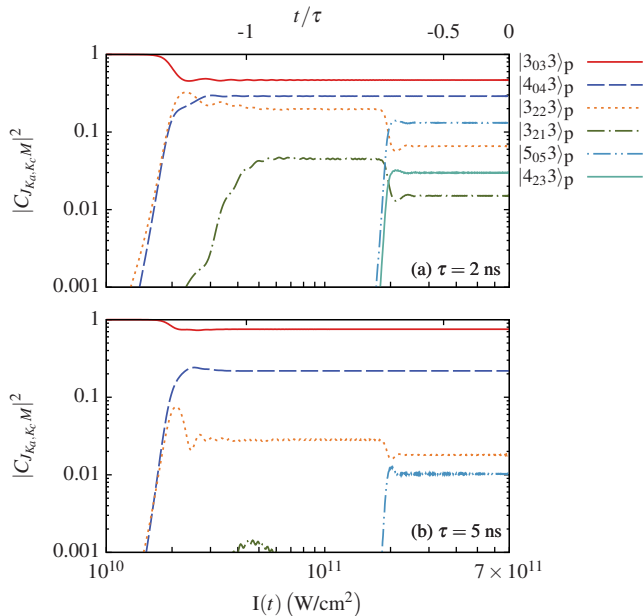


FIG. 5. (Color online) For the state $|3_{0,3}3\rangle_t$, we present the squares of the projections of the time dependent wave function onto the adiabatic states versus the laser intensity $I(t)$. The Gaussian pulse has $I_0 = 7 \times 10^{11} \text{ W/cm}^2$ and (a) $\tau = 5 \text{ ns}$ and (b) $\tau = 2 \text{ ns}$, and the dc field strength is $E_s = 300 \text{ V/cm}$.

contributing to the dynamics. The presence of avoided crossings in the spectrum provokes that adiabatic states from different pendular doublets are populated during the rotational dynamics of $|3_{0,3}3\rangle_t$. In Fig. 5(a) and Fig. 5(b), we plot the population of the pendular adiabatic states for $E_s = 300 \text{ V/cm}$, $I_0 = 7 \times 10^{11} \text{ W/cm}^2$ and $\tau = 2 \text{ ns}$ and 5 ns , respectively. We start analyzing in detail the results for $\tau = 2 \text{ ns}$. To rationalize the population redistribution taking place around $I(t) \approx 2 \times 10^{10} \text{ W/cm}^2$, see Fig. 5(a), we present a detail of the adiabatic level structure in Fig. 6(a). As the pendular doublet between the adiabatic levels $|3_{0,3}3\rangle_p$ and $|4_{0,4}3\rangle_p$ is formed, $|4_{0,4}3\rangle_p$ suffers an avoided crossing with $|3_{2,2}3\rangle_p$. For the states $|3_{0,3}3\rangle_p - |4_{0,4}3\rangle_p$ in the pendular doublet, the maximum value of adiabatic parameter is $\eta \approx 1.3$. The maximum of η for the state $|3_{2,2}3\rangle_p$ with $|3_{0,3}3\rangle_p$ and $|4_{0,4}3\rangle_p$ are $\eta \approx 0.44$ and 0.46 respectively. Thus, the two oriented states $|3_{0,3}3\rangle_p$ and $|3_{2,2}3\rangle_p$ are also coupled, even if their energy separation is larger. These values of η indicate that the dynamics in this region is not be adiabatic. Indeed, the population of these two states $|4_{0,4}3\rangle_p$ and $|3_{2,2}3\rangle_p$ simultaneously increases as the one of $|3_{0,3}3\rangle_p$ decreases. Once the pendular pair between $|3_{0,3}3\rangle_p$ and $|4_{0,4}3\rangle_p$ is formed their populations keep a constant behavior as $I(t)$ is increased. We observe the formation of the second pendular doublet in this irreducible representation for $I(t) \approx 3 \times 10^{10} \text{ W/cm}^2$: the population of the adiabatic states $|3_{2,2}3\rangle_p$ and $|3_{2,1}3\rangle_p$ decreases and increases, respectively. By further increas-

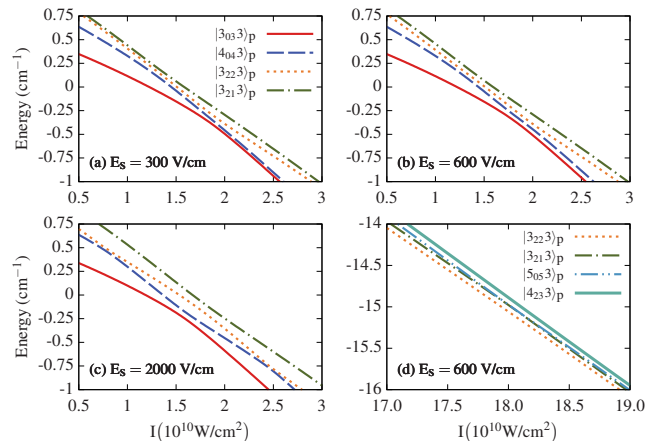


FIG. 6. (Color online) (a), (b) and (c) Adiabatic energy structure when the pendular doublets between the states $|3_{0,3}3\rangle_p$ and $|4_{0,4}3\rangle_p$ is formed for $E_s = 300 \text{ V/cm}$, $E_s = 600 \text{ V/cm}$ and $E_s = 2 \text{ kV/cm}$, respectively. (d) Avoided crossing between the adiabatic states $|3_{2,2}3\rangle_p$, $|3_{2,1}3\rangle_p$, $|5_{0,5}3\rangle_p$ and $|4_{2,3}3\rangle_p$.

ing $I(t)$ the states $|3_{2,2}3\rangle_p$ and $|3_{2,1}3\rangle_p$ suffer an avoided crossing with those from the third pendular doublet $|5_{0,5}3\rangle_p$ and $|4_{2,3}3\rangle_p$, see Fig. 6(d). Through this avoided crossing, there is a strong coupling between the oriented states $|3_{2,2}3\rangle_p$ and $|5_{0,5}3\rangle_p$ with the adiabatic parameter reaching the maximum value $\eta \approx 1.93$, and between the antioriented ones $|3_{2,1}3\rangle_p$ and $|4_{2,3}3\rangle_p$ with $\eta \approx 1.92$. In both cases the dynamics is not be adiabatic, and we observe in Fig. 5(a) how their populations are interchanged around $I(t) \approx 2 \times 10^{11} \text{ W/cm}^2$. The oscillations in $\langle \cos \theta \rangle$ are due to the coupling between all these adiabatic states that are populated. As the laser intensity is increased, these levels achieve the pendular regime and these crossed matrix elements between states in the same pendular pair, i. e., ${}_p \langle 3_{03}3 | \cos \theta | 4_{04}3 \rangle_p$, ${}_p \langle 3_{22}3 | \cos \theta | 3_{21}3 \rangle_p$ and ${}_p \langle 5_{05}3 | \cos \theta | 4_{23}3 \rangle_p$, approach zero. As t varies, the frequency of the oscillation is different because different pendular adiabatic states dominate the field-dressed dynamics, see Fig. 4(c). At $t = 0$, the field-dressed wave function of the state $|3_{0,3}3\rangle_0$ has significant contributions from 6 different adiabatic states, which gives rise to a weak orientation $\langle \cos \theta \rangle = 0.327$. For $\tau = 5 \text{ ns}$, the dynamics is more adiabatic. Thus, when the pendular doublets are formed the interchange of population is smaller than for a $\tau = 2 \text{ ns}$ pulse, see Fig. 5(b). The avoided crossings are still crossed diabatically. Indeed, the population of the states $|3_{2,1}3\rangle_p$ and $|4_{2,3}3\rangle_p$ is smaller than 0.001, and the field-dressed dynamics of $|3_{0,3}3\rangle_t$ is dominated by the adiabatic states $|3_{0,3}3\rangle_p$, $|4_{0,4}3\rangle_p$, $|3_{2,2}3\rangle_p$ and $|5_{0,5}3\rangle_p$. This explain that the oscillation of $\langle \cos \theta \rangle$ are reduced, and that at $t = 0$ this state shows a significant orientation with $\langle \cos \theta \rangle = 0.547$.

For other ground states, such as $|2_{0,2}2\rangle_t$ and $|4_{0,4}4\rangle_t$, we have encountered similar phenomena, and their rotational dynamics is strongly dominated by avoided cross-

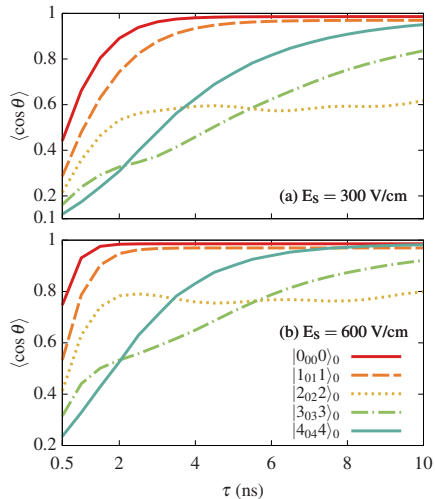


FIG. 7. (Color online) For the ground states of several irreducible representations, we plot the expectation value $\langle \cos \theta \rangle$ at $t = 0$ as a function of the FWHM of the Gaussian pulse for (a) $E_s = 300$ V/cm and (b) $E_s = 600$ V/cm. The peak intensity is fixed to $I_0 = 7 \times 10^{11}$ W/cm 2 .

ings.

1. Influence of FWHM of the Gaussian pulse

We consider now the ground states of the irreducible representations with $M \leq 4$, that is the states $|0_{0,0}0\rangle_t$, $|1_{0,1}1\rangle_t$, $|2_{0,2}2\rangle_t$, $|3_{0,3}3\rangle_t$ and $|4_{0,4}4\rangle_t$. In this section we investigate the impact of the temporal width of the Gaussian pulse in their rotational dynamics. Their orientation at the peak intensity, i.e., at $t = 0$, are plotted versus τ in Fig. 7(a) and Fig. 7(b) for $E_s = 300$ V/cm and $E_s = 600$ V/cm, respectively. The peak intensity is fixed to $I_0 = 7 \times 10^{11}$ W/cm 2 .

In contrast to the mixed-field orientation of a linear molecules [26], a smaller field-free rotational energy does not imply a larger orientation. For instance, using $E_s = 300$ V/cm, the state $|4_{0,4}4\rangle_0$ shows a larger orientation than $|2_{0,2}2\rangle_0$ and $|3_{0,3}3\rangle_0$ for $\tau \gtrsim 2$ ns and 3.5 ns, respectively. For $\tau \gtrsim 6$ ns, the state $|2_{0,2}2\rangle_0$ is the least oriented. As indicated above, the non-adiabatic features of field-dressed dynamics are due to the formation of the pendular doublets and to the avoided crossings. By increasing τ , we can ensure that less population is transferred from the oriented state to the antioriented one or vice-versa as the pendular doublet is formed. However, the characteristic time scale of the avoided crossings is different, and significantly larger FWHM are needed to pass them adiabatically. Each irreducible representation is characterized by a certain field-dressed level structure, and, therefore, by an amount of avoided crossings which contribute to the complexity of the rotational dynamics. The absence of avoided crossings close to the ground state gives rise to a monotonic increase of $\langle \cos \theta \rangle$ approaching

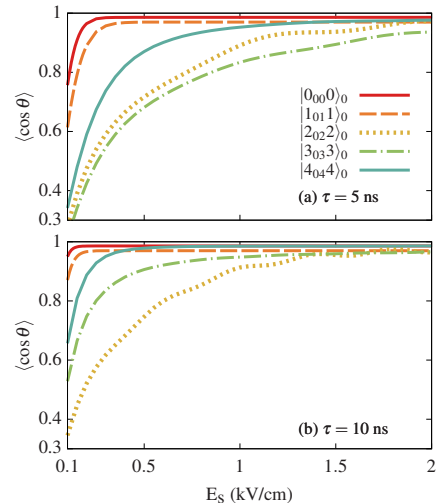


FIG. 8. (Color online) For the ground states of several irreducible representations, we present their expectation value $\langle \cos \theta \rangle$ once the peak intensity is reached at $t = 0$ as a function of the dc field strength E_s for (a) $\tau = 5$ ns and (b) $\tau = 10$ ns. The peak intensity is fixed to $I_0 = 7 \times 10^{11}$ W/cm 2 .

the adiabatic limit as τ is increased, this behavior is observed in the levels $|0_{0,0}0\rangle_t$ and $|1_{0,1}1\rangle_t$. In contrast, the influence of an avoided crossing in the corresponding dynamics implies that significantly longer pulses are needed to reach the adiabatic limit, e.g., the levels $|2_{0,2}2\rangle_t$ and $|3_{0,3}3\rangle_t$. In particular, for $\tau \gtrsim 2$ ns, the orientation $\langle \cos \theta \rangle$ of $|2_{0,2}2\rangle_t$ shows a smooth oscillatory behaviour as a function of τ .

2. Influence of electric-field strength

In this section, we consider the same set of ground states and analyze their orientation at $t = 0$ as a function of the dc field strength, see Fig. 8. For a given laser pulse, the largest is the energy gap between the two levels in a pendular pair, the less efficient is the population transfer when the doublet is formed [26]. This statement also holds for asymmetric top molecules. However, the impact of the electric field on the avoided crossings will influence the rotational dynamics. For both pulses, we encounter that the states $|2_{0,2}2\rangle_0$ and $|3_{0,3}3\rangle_0$ present a smaller orientation than $|4_{0,4}4\rangle_0$. The level $|3_{0,3}3\rangle_0$ is more (less) oriented than $|2_{0,2}2\rangle_0$ for the $\tau = 10$ ns ($\tau = 5$ ns) pulses. Our calculations show that for these ground states, the adiabatic pendular limit could be reached using a strong electric field and a 10 ns pulse, see Fig. 8 (b).

B. Field-dressed dynamics of excited states

In this section we analyze the mixed-field dynamics of two excited rotational states from different irreducible

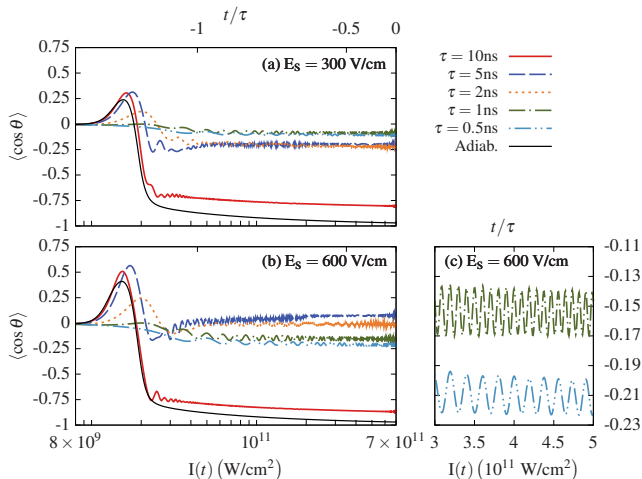


FIG. 9. (Color online) For the state $|4_{0,43}\rangle_t$, we present $\langle \cos \theta \rangle$ versus $I(t)$ for (a) $E_s = 300 \text{ V/cm}$ and (b) 600 V/cm . A detail of the oscillations of $\langle \cos \theta \rangle$ for 600 V/cm is shown in panel (c). The peak intensity of the pulses is $I_0 = 7 \times 10^{11} \text{ W/cm}^2$, and the FWHM are $\tau = 10 \text{ ns}$ (red solid line), 5 ns (dark blue long dashed line), 2 ns (orange dotted line), 1 ns (dark olive green dot-dashed line), 0.5 ns (light blue double-dot-dashed line). The adiabatic results is also plotted (black solid line).

representations. The field-dressed spectrum is characterized by a high density of adiabatic states and a large number of avoided crossings between neighboring levels. As a consequence, the rotational dynamics is more complex, and it is harder to achieve the diabatic limit.

1. Dynamics of the state $|4_{0,43}\rangle_t$

As a first example, we investigate the dynamics of the rotational state $|4_{0,43}\rangle_t$ which forms the pendular pair with $|3_{0,33}\rangle_t$. In Fig. 9(a) and Fig. 9(b) the orientation of $|4_{0,43}\rangle_t$ is plotted versus $I(t)$ for (a) $E_s = 300 \text{ V/cm}$ and (b) $E_s = 600 \text{ V/cm}$, respectively. In contrast to the case of a linear molecule in parallel dc and ac fields, this state does not show the same orientation but in opposite direction as its partner in the pendular doublet the level $|3_{0,33}\rangle_t$, except if the dynamics is adiabatic or very close to it. This can be explained in terms of the avoided crossings, which affect in different ways the rotational dynamics of $|3_{0,33}\rangle_t$ and $|4_{0,43}\rangle_t$. We present in Fig. 10(a) and Fig. 10(b) the contributions of adiabatic states to the rotational dynamics of $|4_{0,43}\rangle_t$ for a 5 ns pulse with $E_s = 300 \text{ V/cm}$ and 600 V/cm , respectively. For both dc field strengths, we observe that the population redistribution starts first to the adiabatic states $|3_{2,23}\rangle_p$ and $|3_{2,13}\rangle_p$. Due to the rotational constants of BN, the states $|3_{2,23}\rangle_p$ and $|3_{2,13}\rangle_p$ are quasi-degenerate in energy in the absence of the fields, and as $I(t)$ varies they possess a very close energy, see Fig. 6(a) and Fig. 6(b). As a consequence, population is initially transferred to both levels, but more to $|3_{2,23}\rangle_p$ which lies

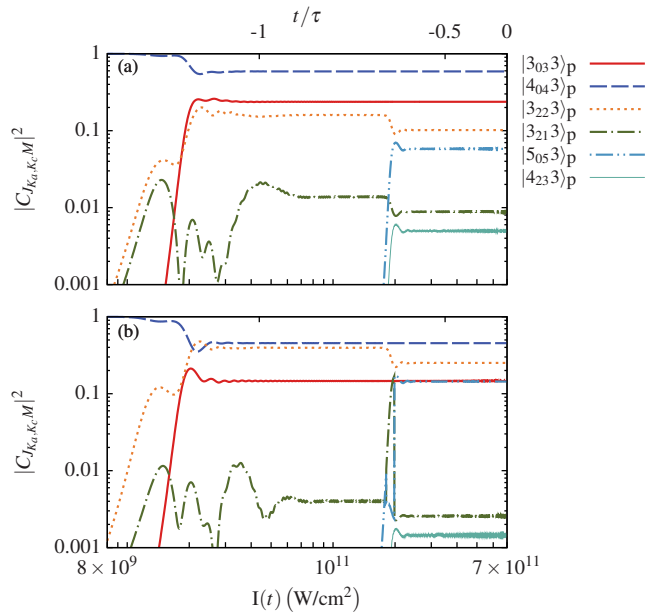


FIG. 10. (Color online) For the state $|4_{0,43}\rangle_t$, we present the squares of the projections of the time dependent wave function onto several adiabatic states versus the laser intensity $I(t)$ for dc field strengths (a) $E_s = 300 \text{ V/cm}$ and (b) $E_s = 600 \text{ V/cm}$. The Gaussian pulse has $I_0 = 7 \times 10^{11} \text{ W/cm}^2$ and $\tau = 5 \text{ ns}$. The notation and label of the adiabatic states is the same as in Fig. 5.

closer to $|4_{0,43}\rangle_p$. For a stronger laser intensity, the pendular pair $|3_{0,33}\rangle_p - |4_{0,43}\rangle_p$ starts to form and $|C_{3_{033}}(t)|^2$ increases. The main difference between both dc field strengths is that for $E_s = 300 \text{ V/cm}$, $|3_{0,33}\rangle_p$ acquires the largest population; whereas for $E_s = 600 \text{ V/cm}$ is $|3_{2,23}\rangle_p$. Indeed, at the largest dc field the avoided crossing is passed more diabatically, and more population is transferred to the $|3_{2,23}\rangle_p$, because the coupling between the states is larger. Whereas for $E_s = 600 \text{ V/cm}$, the pendular pair $|3_{0,33}\rangle_p - |4_{0,43}\rangle_p$ is formed more adiabatically because the energy splitting in the doublets is larger, and $|3_{0,33}\rangle_p$ is less populated than for $E_s = 300 \text{ V/cm}$. In these plots, we also observe how the second pendular doublet between $|3_{2,23}\rangle_p$ and $|3_{2,13}\rangle_p$ is formed around $I(t) \approx 2.3 \times 10^{10} \text{ W/cm}^2$. For stronger laser intensities, the next pendular pair $|5_{0,53}\rangle_p$ and $|4_{2,33}\rangle_p$ is also populated due to the avoided crossing that these levels suffer with those forming the second doublet, see Fig. 6(d). The couplings between these six pendular states provoke the oscillatory behavior of $\langle \cos \theta \rangle$. Let us mention that the first avoided crossing is not crossed adiabatically using a 10 ns pulse, but the population of the state $|3_{2,23}\rangle_p$ is smaller than 0.03 at $t = 0$ for both field strengths. Only these 10 ns pulses give rise to a significant antiorientation with values close to the adiabatic predictions.

We investigate now the rotational dynamics of this state as the dc field is increased. For four Gaussian

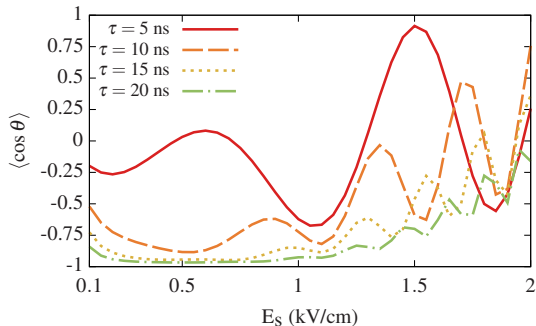


FIG. 11. (Color online) For the state $|4_{0,43}\rangle_0$, we show the orientation at $t = 0$ versus the electric field strength E_s , for a laser pulse with $I_0 = 7 \times 10^{11} \text{ W/cm}^2$ and several FWHM.

pulses with $I_0 = 7 \times 10^{11} \text{ W/cm}^2$, the orientation of $|4_{0,43}\rangle_0$ at $t = 0$ is plotted versus E_s in Fig. 11. For this state, the adiabatic prediction is $\langle \cos \theta \rangle = -0.970$, which is independent of E_s . Our time-dependent calculations show that the orientation oscillates as E_s is increased. This behavior can be explained in terms of the avoided crossings, and their evolution as E_s varies. At $E_s = 300 \text{ V/cm}$, the pendular states $|4_{0,43}\rangle_p$ and $|3_{2,23}\rangle_p$ suffer an avoided crossing for $I(t) \approx 1.53 \times 10^{10} \text{ W/cm}^2$, before the pendular doublet $|3_{0,33}\rangle_p - |4_{0,43}\rangle_p$ is formed, see Fig. 6(a). By increasing E_s , this avoided crossing is split into two, e.g., for $E_s = 2 \text{ kV/cm}$, the first and second one appear at $I(t) \approx 7.8 \times 10^9 \text{ W/cm}^2$ and $I(t) \approx 2.1 \times 10^{10} \text{ W/cm}^2$, respectively, and the minimal energy between the two states in the pendular doublet is reached at $I(t) \approx 2.47 \times 10^{10} \text{ W/cm}^2$, see Fig. 6(c). The rotational dynamics through these avoided crossings as $I(t)$ is varied strongly depends on the FWHM of the laser pulse. For instance, using a 10 ns pulse and $E_s = 2 \text{ kV/cm}$, these two avoided crossings are passed diabatically and the pendular level $|3_{2,23}\rangle_p$ is populated, and the formation of the two pendular doublets $|3_{0,33}\rangle_p - |4_{0,43}\rangle_p$ and $|3_{2,23}\rangle_p - |3_{2,13}\rangle_p$ is also diabatic. Furthermore, the next avoided crossing between the pendular states $|3_{2,13}\rangle_p$ and $|5_{0,53}\rangle_p$, see Fig. 6(d), is also crossed diabatically. Hence, the final orientation of $|4_{0,43}\rangle_0$ strongly depends on the rotational dynamics through these avoided crossings. Indeed, as E_s is increased the population redistribution through these avoided crossings is increased; whereas less population is transferred when the pendular doublets are formed as occurs in linear molecules. For this state, to reach an adiabatic dynamics through the avoided crossings, longer laser pulses are needed, but the dc field should be chosen properly. For instance, a 20 ns pulse ensures an adiabatic dynamics of this state with $300 \text{ V/cm} \lesssim E_s \lesssim 1 \text{ kV/cm}$, whereas for stronger dc fields, it is still diabatic.

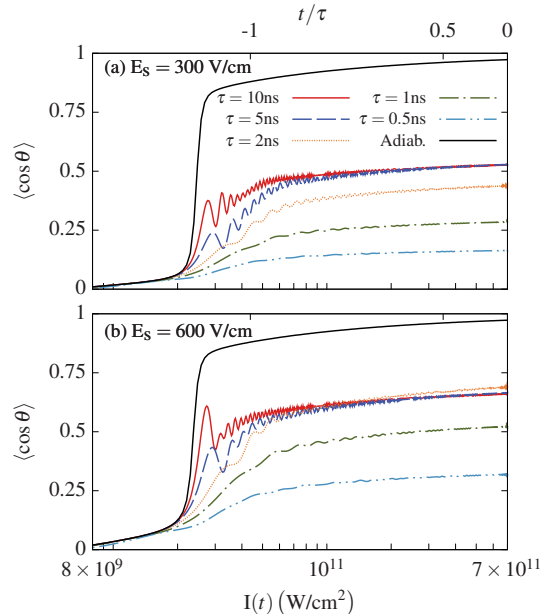


FIG. 12. (Color online) For the state $|3_{0,31}\rangle_t$, we plot $\langle \cos \theta \rangle$ versus $I(t)$ for (a) $E_s = 300 \text{ V/cm}$ and (b) $E_s = 600 \text{ V/cm}$. The peak intensity of the pulses is $I_0 = 7 \times 10^{11} \text{ W/cm}^2$, and the FWHM are $\tau = 10 \text{ ns}$ (red solid line), $\tau = 5 \text{ ns}$ (dark blue long dashed line), $\tau = 2 \text{ ns}$ (orange dotted line), $\tau = 1 \text{ ns}$ (dark olive green dot-dashed line), $\tau = 0.5 \text{ ns}$ (light blue double-dot-dashed line). The adiabatic results are also shown (black solid line).

2. Dynamics of the state $|3_{0,31}\rangle_t$

As a second example, we have chosen the state $|3_{0,31}\rangle_t$, which in the field-free spectrum is the third one with $M = 1$ and even symmetry in the reflection of the XZ -plane. The orientation cosine of $|3_{0,31}\rangle_t$ is presented in Fig. 12 for several Gaussian pulses. For $E_s = 300 \text{ V/cm}$, doubling the FWHM from 5 ns to 10 ns does not provoke an enhancement on the orientation. Analogously, using $E_s = 600 \text{ V/cm}$, the pulses with $\tau = 2 \text{ ns}$, 5 ns and 10 ns give rise a similar orientation at $t = 0$. The dynamics of $|3_{0,31}\rangle_t$ is strongly affected by the adiabatic states $|2_{2,1}\rangle_p$ and $|2_{2,01}\rangle_p$. The adiabatic state $|3_{0,31}\rangle_p$ undergoes an avoided crossing with $|2_{2,1}\rangle_p$, see Fig. 13, just before they form the second pendular pair in this irreducible representation. The field-free states $|2_{2,1}\rangle$ and $|2_{2,01}\rangle$ are quasi-degenerate in energy, and in the presence of the fields, their energies remain very close as $I(t)$ is varied if the electric field is weak. For $E_s = 300 \text{ V/cm}$, when the pendular doublet between $|3_{0,31}\rangle_p$ and $|2_{2,1}\rangle_p$ is formed, $|2_{2,01}\rangle_p$ is energetically very close and the levels $|2_{2,1}\rangle_p$ and $|2_{2,01}\rangle_p$ suffer an avoided crossing, see Fig. 13. The population redistribution is illustrated in Fig. 14 for the Gaussian pulse with $\tau = 10 \text{ ns}$ and the two dc field strengths. Due to the avoided crossing between $|3_{0,31}\rangle_p$ and $|2_{2,1}\rangle_p$, $|C_{2221}(t)|^2$ achieves a

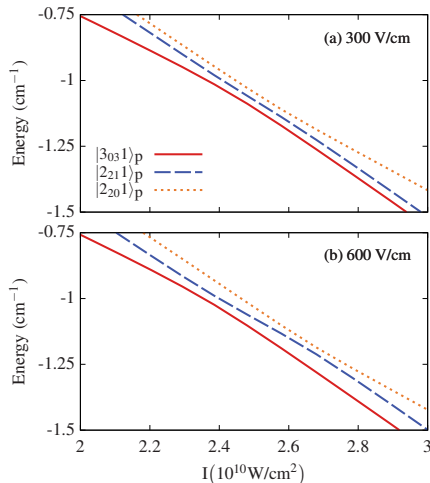


FIG. 13. We show the adiabatic level structure when the pendular doublet between the states $|3_{0,31}\rangle_p$ and $|2_{2,11}\rangle_p$ is formed for (a) $E_s = 300$ V/cm and (b) $E_s = 600$ V/cm.

first maximum as a function of $I(t)$, and afterwards it reaches a constant value once the pendular doublet is formed. As $I(t)$ is increased, the second avoided crossing $|2_{2,11}\rangle_p$ and $|2_{2,01}\rangle_p$ is encountered, and the adiabatic level $|2_{2,01}\rangle_p$ acquires a similar population as $|2_{2,11}\rangle_p$, and they get their population almost simultaneously for $E_s = 300$ V/cm. The dynamics of $|3_{0,31}\rangle_t$ is dominated by the adiabatic states $|3_{0,31}\rangle_p$, $|2_{2,11}\rangle_p$ and $|2_{2,01}\rangle_p$. Since the last two states have similar population and they are oriented in opposite directions, the final orientation at $t = 0$ of $|3_{0,31}\rangle_0$ is significantly smaller than the adiabatic prediction. The oscillations of $\langle \cos \theta \rangle$ are due to the couplings between these three pendular states.

Finally, we investigate the rotational dynamics of this state $|3_{0,31}\rangle_t$ as the dc field strength is increased for several FWHM and $I_0 = 7 \times 10^{11}$ W/cm². The orientation cosine is presented in Fig. 15. For the four Gaussian pulses, $\langle \cos \theta \rangle$ monotonically increases as E_s is enhanced. However, even the field parameters $\tau = 20$ ns and $E_s = 2$ kV/cm do not give rise to a fully adiabatic dynamics; our time-dependent calculations provide $\langle \cos \theta \rangle = 0.956$, which is smaller than the adiabatic limit $\langle \cos \theta \rangle = 0.973$. Note that the adiabatic value is independent of E_s . An important feature of this state is that using weak dc fields, the dynamics is not adiabatic even if the FWHM is increased up to 20 ns. This lack of adiabaticity is again explained in terms of the rotational dynamics through the avoided crossings. The avoided crossing involving the adiabatic states $|3_{0,31}\rangle_p$ and $|2_{2,11}\rangle_p$ is crossed diabatically even for $\tau = 20$ ns and $E_s \leq 2$ kV/cm. The second avoided crossing among $|2_{2,11}\rangle_p$ and $|2_{2,01}\rangle_p$ is again passed diabatically for these field configurations, and $|2_{2,01}\rangle_p$ acquires population. By increasing the dc field strength, the population of the state $|2_{2,01}\rangle_p$ at $t = 0$ is also increased. For sufficiently

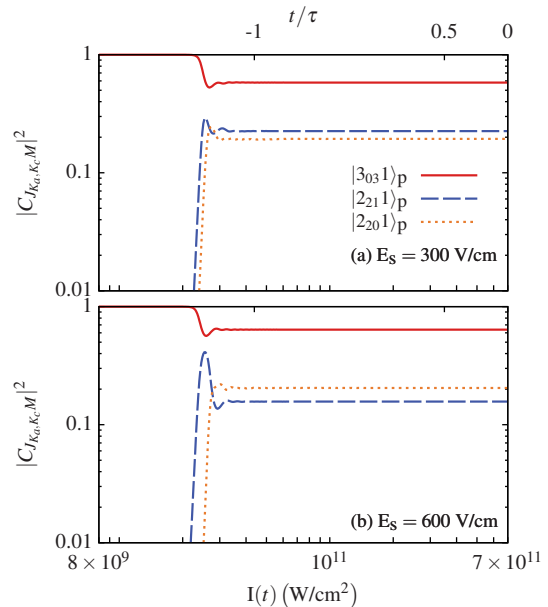


FIG. 14. (Color online) For the state $|3_{0,31}\rangle_t$, we show the squares of the projections of the time dependent wave function onto several adiabatic states versus the laser intensity $I(t)$ for dc field strengths (a) $E_s = 300$ V/cm and (b) $E_s = 600$ V/cm. The Gaussian pulse has $I_0 = 7 \times 10^{11}$ W/cm² and $\tau = 10$ ns.

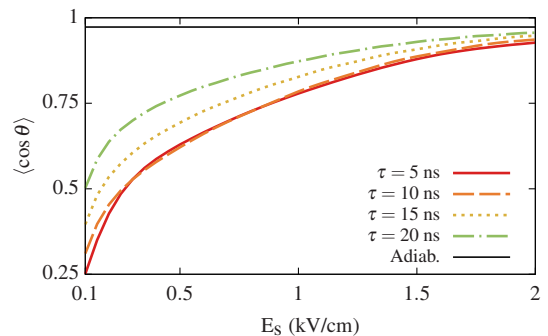


FIG. 15. (Color online) For the state $|3_{0,31}\rangle_0$, we show the orientation at $t = 0$ versus the electric field strength E_s , for a laser pulse with $I_0 = 7 \times 10^{11}$ W/cm² and several FWHM.

strong dc field, the dynamics of $|3_{0,31}\rangle_t$ is dominated by the adiabatic states $|3_{0,31}\rangle_p$ and $|2_{2,01}\rangle_p$, and the population of $|2_{2,11}\rangle_p$ is reduced. Since $|3_{0,31}\rangle_p$ and $|2_{2,01}\rangle_p$ are right-way oriented in the pendular regime, $\langle \cos \theta \rangle$ shows an smooth increasing behaviour as a function of E_s . For this state, the adiabatic dynamics is reached only if long enough Gaussian pulses are used, and increasing the dc field strengths will facilitate to reach of this adiabatic limit.

IV. CONCLUSIONS

In this work, we have investigated the impact of parallel dc fields and non-resonant laser pulses in an asymmetric top molecule. For several rotational levels, we have explored in detail their rotational dynamics as the intensity of the laser pulse is increased till its peak value. Such a study has allowed us to identify the sources of non-adiabatic effects and the regime when they appear. In addition, we have analyzed the degree of orientation as the FWHM of the Gaussian pulse and the electric field strength are varied.

We have encountered only a few rotational states, such as $|0_{0,0}\rangle_t$ and $|1_{0,1}\rangle_t$, for which the field-dressed dynamics is dominated by the formation of the pendular pairs. For other states, the dynamics is more complicated because the time evolution of their wave function is strongly affected by the avoided crossings. At the ac field regime where the pendular doublets are formed, the presence of additional avoided crossings provokes the interaction between three or even more adiabatic levels. In such a region, the complexity of these avoided crossings prevent us from using the Landau-Zener criteria or a two state model to analyze the rotational dynamics through them. The avoided crossings give rise to a highly non-adiabatic dynamics, and the final degree of orientation could be reduced. We have shown that dc fields with strengths up to 2 kV/cm do not ensure an adiabatic dynamics for low-lying rotational states. Thus, the path to the adiabaticity necessitates laser pulses with longer temporal widths. Due to the different time scales associated to both phenomena, the pendular doublet formation and avoided crossings, the field configuration required to achieve an adiabatic dynamics simultaneously for many rotational states becomes harder to produce experimentally. A laser pulse could be designed with a small slope of the intensity in the field regime where most of the avoided crossings appear and pendular doublet are formed, trying to minimize the population redistribution at that region. So that, the degree of adiabaticity could

be significantly enhanced.

In this work, we have analyzed the field-dressed dynamics of benzonitrile, but the above-observed physical phenomena are expected to occur in other polar asymmetric top molecules. Due to the complex structure of these systems, a similar theoretical study should be performed for each specific molecule. The field regime under which the adiabatic dynamics would be achieved strongly depends on the rotational constant, the polarizability tensor and the permanent dipole moment.

A natural extension to this work would consist on considering an asymmetric top molecule in a nonparallel field configuration, as those used in the mixed-field orientation experiments [21, 27]. For tilted fields, the complexity of the field-dressed level structure is enhanced due to the presence of avoided crossings between states having different field-free magnetic quantum numbers. Due to this new source of non-adiabatic effects, the degree of orientation in non-parallel dc and ac fields could be reduced. In this work, we have shown that for parallel fields, the avoided crossing among states with the same symmetry are passed, in general, diabatically for many field configurations. Thus, a time-dependent description will allow us to revise our prediction that in titled fields the avoided crossings among states with the same (different) field-free value of M are crossed adiabatically (diabatically) [24].

ACKNOWLEDGMENTS

We would like to thank Jochen Küpper and Henrik Stapelfeldt for fruitful discussions, and Hans-Dieter Meyer for providing us the code of the short iterative Lanczos algorithm. Financial support by the Spanish project FIS2011-24540 (MICINN), the Grants P11-FQM-7276 and FQM-4643 (Junta de Andalucía), and Andalusian research group FQM-207 is gratefully appreciated. J.J.O. acknowledges the support of ME under the program FPU.

-
- [1] P. R. Brooks, *Science* **193**, 11 (1976).
 - [2] P. R. Brooks and E. M. Jones, *J. Chem. Phys.* **45**, 3449 (1966).
 - [3] H. J. Loesch and J. Möller, *J. Chem. Phys.* **97**, 9016 (1992).
 - [4] F. J. Aoiz, B. Friedrich, V. J. Herrero, V. S. Rábanos, and J. E. Verdasco, *Chem. Phys. Lett.* **289**, 132 (1998).
 - [5] V. Aquilanti, M. Bartolomei, F. Pirani, D. Cappelletti, and F. Vecchiocattivi, *Phys. Chem. Chem. Phys.* **7**, 291 (2005).
 - [6] C. Z. Bisgaard, O. J. Clarkin, G. Wu, A. M. D. Lee, O. Gessner, C. C. Hayden, and A. Stolow, *Science* **323**, 1464 (2009).
 - [7] L. Holmegaard, J. L. Hansen, L. Kalhoj, S. L. Kragh, H. Stapelfeldt, F. Filsinger, J. Küpper, G. Meijer, D. Dimitrovski, M. Abu-samha, et al., *Nat. Phys.* **6**, 428 (2010).
 - [8] J. L. Hansen, H. Stapelfeldt, D. Dimitrovski, M. Abu-Samha, C. P. J. Martiny, and L. B. Madsen, *Phys. Rev. Lett.* **106**, 073001 (2011).
 - [9] E. Frumker, C. T. Hebeisen, N. Kajumba, J. B. Bertrand, H. J. Wörner, M. Spanner, D. M. Villeneuve, A. Naumov, and P. Corkum, *Phys. Rev. Lett.* **109**, 113901 (2012).
 - [10] P. M. Kraus, A. Rupenyan, and H. J. Wörner, *Phys. Rev. Lett.* **109**, 233903 (2012).
 - [11] L. S. Spector, M. Artamonov, S. Miyabe, T. Martinez, T. Seideman, M. Guehr, and P. H. Bucksbaum (2012), arXiv:1207.2517.
 - [12] S. Stolte, *Atomic and Molecular Beam Methods* (Oxford University Press, New York, 1988).

- [13] H. J. Loesch and A. Remscheid, *J. Chem. Phys.* **93**, 4779 (1990).
- [14] B. Friedrich and D. R. Herschbach, *Nature* **353**, 412 (1991).
- [15] B. Friedrich, D. P. Pullman, and D. R. Herschbach, *J. Phys. Chem.* **95**, 8118 (1991).
- [16] P. A. Block, E. J. Bohac, and R. E. Miller, *Phys. Rev. Lett.* **68**, 1303 (1992).
- [17] B. Friedrich, H. G. Rubahn, and N. Sathyamurthy, *Phys. Rev. Lett.* **69**, 2487 (1992).
- [18] A. Slenczka, B. Friedrich, and D. Herschbach, *Phys. Rev. Lett.* **72**, 1806 (1994).
- [19] B. Friedrich and D. R. Herschbach, *J. Chem. Phys.* **111**, 6157 (1999).
- [20] B. Friedrich and D. Herschbach, *J. Phys. Chem. A* **103**, 10280 (1999).
- [21] L. Holmegaard, J. H. Nielsen, I. Nevo, H. Stapelfeldt, F. Filsinger, J. Küpper, and G. Meijer, *Phys. Rev. Lett.* **102**, 023001 (2009).
- [22] I. Nevo, L. Holmegaard, J. Nielsen, J. L. Hansen, H. Stapelfeldt, F. Filsinger, G. Meijer, and J. Küpper, *Phys. Chem. Chem. Phys.* **11**, 9912 (2009).
- [23] T. Seideman and E. Hamilton, *Adv. Atom. Mol. Opt. Phys.* **52**, 289 (2006).
- [24] J. J. Omiste, M. Gärttner, P. Schmelcher, R. González-Férez, L. Holmegaard, J. H. Nielsen, H. Stapelfeldt, and J. Küpper, *Phys. Chem. Chem. Phys.* **13**, 18815 (2011).
- [25] J. H. Nielsen, H. Stapelfeldt, J. Küpper, B. Friedrich, J. J. Omiste, and R. González-Férez, *Phys. Rev. Lett.* **108**, 193001 (2012), enter text here.
- [26] J. J. Omiste and R. González-Férez, *Phys. Rev. A* **86**, 043437 (2012).
- [27] F. Filsinger, J. Küpper, G. Meijer, L. Holmegaard, J. H. Nielsen, I. Nevo, J. L. Hansen, and H. Stapelfeldt, *J. Chem. Phys.* **131**, 064309 (2009).
- [28] J. Bulthuis, J. Miller, and H. J. Loesch, *J. Phys. Chem. A* **101**, 7684 (1997).
- [29] R. Escribano, B. Maté, F. Ortigoso, and J. Ortigoso, *Phys. Rev. A* **62**, 023407 (2000).
- [30] A. Schwettman, J. Franklin, K. R. Overstreet, and J. P. Shaffer, *J. Chem. Phys.* **123**, 194305 (2005).
- [31] K. Wohlfart, F. Filsinger, F. Grätz, J. Küpper, and G. Meijer, *Phys. Rev. A* **78**, 033421 (2008).
- [32] M. Kirste, B. G. Sartakov, M. Schnell, and G. Meijer, *Phys. Rev. A* **79**, 051401 (2009).
- [33] S. A. Meek, H. Conrad, and G. Meijer, *Science* **324**, 1699 (2009).
- [34] T. E. Wall, S. K. Tokunaga, E. A. Hinds, and M. R. Tarbutt, *Phys. Rev. A* **81**, 033414 (2010).
- [35] R. N. Zare, *Angular Momentum: Understanding Spatial Aspects in Chemistry and Physics* (John Wiley and Sons, New York, 1988).
- [36] M. Beck, A. Jäckle, G. Worth, and H.-D. Meyer, *Physics Reports* **324**, 1 (2000).
- [37] J. J. Omiste, R. González-Férez, and P. Schmelcher, *J. Chem. Phys.* **135**, 064310 (2011).
- [38] G. W. King, R. M. Hainer, and P. C. Cross, *J. Chem. Phys.* **11**, 27 (1943).
- [39] L. B. Ballentine, *Quantum Mechanics: A Modern Development* (World Scientific, Singapore, 1998).
- [40] K. Wohlfart, M. Schnell, J.-U. Grabow, and J. Küpper, *J. Mol. Spectrosc* **247**, 119 (2007).
- [41] J. L. Hansen, L. Holmegaard, L. Kalhøj, S. L. Kragh, H. Stapelfeldt, F. Filsinger, G. Meijer, J. Küpper, D. Dimitrovski, M. Abu-samaha, et al., *Phys. Rev. A* **83**, 023406 (2011).
- [42] Y. Sugawara, A. Goban, S. Minemoto, and H. Sakai, *Phys. Rev. A* **77**, 031403(R) (2008).
- [43] M. Muramatsu, M. Hita, S. Minemoto, and H. Sakai, *Phys. Rev. A* **79**, 011403(R) (2009).

Mixed-field orientation of a thermal ensemble of linear polar molecules

Juan J. Omiste and Rosario González-Férez

Instituto Carlos I de Física Teórica y Computacional and Departamento de Física Atómica, Molecular y Nuclear, Universidad de Granada, 18071 Granada, Spain

E-mail: rogonzal@ugr.es

Abstract. We present a theoretical study of the impact of an electrostatic field combined with nonresonant linearly polarized laser pulses on the rotational dynamics of a thermal ensemble of linear molecules. We solve the time-dependent Schrödinger equation within the rigid rotor approximation for several rotational states. Using the carbonyl sulfide (OCS) molecule as a prototype, the mixed-field orientation of a thermal sample is analyzed in detail for experimentally accessible static field strengths and laser pulses. We demonstrate that for a characteristic field configuration used in current mixed-field orientation experiments, a significant orientation is obtained for rotational temperatures below 0.7 K as well as using stronger dc fields.

1. Introduction

The mixed-field orientation of polar molecules via the interaction with an electric field and a nonresonant laser field is a widespread technique to produce samples of oriented molecules. This method was proposed by Friedrich and Herschbach [1, 2], and is based on the dc-field induced coupling between the nearly degenerate pair of states with opposite parity forming the tunneling doublets in the strong laser field regime. A recent experimental and theoretical study has proven that under ns laser pulses the weak dc field orientation is not, in general, adiabatic, and that a time-dependent description of the mixed-field orientation process is required to explain the experimental results [3, 4]. Thus, depending on the field configuration, the orientation of a rotational state could be significantly smaller than the adiabatic prediction. In addition, not all the states present a right-way orientation, and some of them are antioriented.

In a thermal ensemble of molecules, the combination of these right- and wrong-way oriented states gives rise to a weakly oriented molecular beam [5, 6]. An enhancement of the orientation could be achieved by employing either lower rotational temperatures or quantum-state selected molecular beams. By using inhomogeneous electric fields, the amount of populated states is significantly reduced creating a quantum-state selected molecular beam, and achieving with this beam an unprecedented degree of orientation [7, 8, 9]. Cold molecular beams, with typical temperatures of the order of 1 K, are created in supersonic expansions of molecules seeded in an inert atomic carrier gas [10]. Depending on the rotational constant, the molecules could still be distributed over a large number of rotational states in these thermal ensembles. In the present work, we investigate the mixed-field orientation of a thermal sample of polar molecules as the rotational temperature is varied. Our aim is to find the temperature at which the thermal ensemble shows a similar orientation as the quantum-state selected molecular beam.

Herein, we consider a polar linear molecule exposed to an electric field combined with a nonresonant laser pulse, and provide a detailed theoretical analysis of the mixed-field orientation of a thermal sample of this molecule. To do so, we solve the time-dependent Schrödinger equation within the rigid rotor approximation for a large set of rotational states. Taking as prototype example the OCS molecule, we explore the mixed-field orientation as a function of the rotational temperature of the thermal sample for several experimental field configurations. We show that to achieve a significant orientation, rotational temperatures around 0.6 K and 1 K are required if either a weak or strong dc fields are applied, respectively. We also present the orientation of individual states and, for some of them, analyze the projections of the time-dependent wave functions on the corresponding adiabatic basis.

The paper is organized as follows: In Sec. 2 we describe the Hamiltonian of the system and the orientation of a molecular thermal ensemble. The mixed-field orientation of the thermal ensemble as a function of the rotational temperature is analyzed in Sec. 3. The conclusions are given in Sec. 4.

2. The Hamiltonian and the orientation of a thermal ensemble

We consider a polar linear molecule exposed to a homogeneous static electric field and a nonresonant linearly polarized laser pulse. In the framework of the rigid rotor approximation, the Hamiltonian of this system reads

$$H(t) = H_r + H_s(t) + H_L(t), \quad (1)$$

where H_r is the field-free Hamiltonian

$$H_r = B\mathbf{J}^2, \quad (2)$$

with \mathbf{J} being the total angular momentum operator and B the rotational constant. The interactions with the electric and laser fields are $H_s(t)$ and $H_L(t)$, respectively.

The dc field $\mathbf{E}_s(t)$ forms an angle β with the Z -axis and is contained in the XZ -plane of the laboratory fixed frame (LFF) (X, Y, Z) . The dipole coupling with this field reads

$$H_s(t) = -\boldsymbol{\mu} \cdot \mathbf{E}_s(t) = -\mu E_s(t) \cos \theta_s \quad (3)$$

with $\mathbf{E}_s(t) = E_s(t)(\sin \beta \hat{X} + \cos \beta \hat{Z})$, and $E_s(t)$ being the electric field strength. The angle between the dipole moment $\boldsymbol{\mu}$ and $\mathbf{E}_s(t)$ is θ_s , and $\cos \theta_s = \cos \beta \cos \theta + \sin \beta \sin \theta \cos \phi$. The angles $\Omega = (\theta, \phi)$ are the Euler angles, which relate the laboratory and molecular fixed frames. The molecule fixed frame (MFF) (X_M, Y_M, Z_M) is defined so that the molecular permanent dipole moment $\boldsymbol{\mu}$ is parallel to the Z_M -axis. Based on the mixed-field orientation experiments [8, 9, 3], the dc field is switched on first increasing its strength linearly with time. We ensure that this turning-on process is adiabatic, and once the maximum strength E_s is achieved, it is kept constant.

The polarization of the nonresonant laser field is taken parallel to the Z -axis. Thus, the interaction of the nonresonant laser field with the molecule can be written as [11]

$$H_L(t) = -\frac{I(t)}{2c\epsilon_0} \Delta\alpha \cos^2 \theta, \quad (4)$$

where $\Delta\alpha$ is the polarizability anisotropy, $I(t)$ is the intensity of the laser, c is the speed of light and ϵ_0 is the dielectric constant. Note that in Eq. (4) the term $-\alpha_{\perp} I(t)/2c\epsilon_0$ has been neglected because it represents only a shift in the energy. The laser is a Gaussian pulse with intensity $I(t) = I_0 \exp(-t^2/2\sigma^2)$, I_0 is the peak intensity, and σ is related with the full width

half maximum (FWHM) $\tau = 2\sqrt{2\ln 2}\sigma$. When the nonresonant laser field is turned on the interaction due to this field is much weaker than the coupling with the dc field.

The time-dependent Schrödinger equation associated to the Hamiltonian (1) is solved by means of a second-order split-operator technique [12], combined with the discrete-variable and finite-basis representation methods for the angular coordinates [13, 14, 15, 16]. The basis is formed by the spherical harmonics $Y_{JM}(\Omega)$, which are the eigenstates of the field-free Hamiltonian (2). J and M are the rotational and magnetic quantum numbers, respectively. At time t , the time-dependent states will be labelled as $|J, M, l\rangle_t^\beta$ with $l = e$ and o indicating even or odd parity with respect to the XZ -plane, respectively. The labels J , M and l refer to the field-free quantum numbers to which they are adiabatically connected and they depend on the way the fields are turned on [17].

We consider a thermal sample of molecules and investigate its mixed-field orientation at $t = 0$ once the peak intensity I_0 has been achieved. For a rotational temperature T , the orientation of a thermal distribution is given by

$$\langle\langle \cos \theta \rangle\rangle_T = \sum_{J=0}^{\infty} \sum_{M=-J}^J W_J^T \langle \cos \theta \rangle_{JM}$$

where the orientation of the field-dressed state $|J, M, l\rangle_0^\beta$ is $\langle \cos \theta \rangle_{JML} = {}_0^\beta \langle J, M, l | \cos \theta | J, M, l \rangle_0^\beta$. The thermal weight of the field-free state $|J, M, l\rangle$ is

$$W_J^T = \frac{e^{-\frac{J(J+1)B}{k_B T}}}{W^T} \quad W^T = \sum_{J=0}^{\infty} (2J+1) e^{-\frac{J(J+1)B}{k_B T}} \quad (5)$$

with k_B being the Boltzman constant.

In many mixed-field orientation experiments, the degree of orientation is measured by the ion imaging method [8, 9]. The up/down symmetry of the 2D-images of the ionic fragments is experimentally quantified by the ratio $N_{\text{up}}/N_{\text{tot}}$, with N_{up} being the amount of ions in the upper part of the screen plane, and N_{tot} the total number of detected ions. In order to compare with the experimental results [3], we also compute the orientation ratio $N_{\text{up}}/N_{\text{tot}}$, of this thermal sample on a 2D screen perpendicular to the electric field axis. This is defined as

$$\frac{N_{\text{up}}}{N_{\text{tot}}} = \sum_J \sum_{M=-J}^J W_J^T \frac{N_{\text{up}}^{JM}}{N_{\text{tot}}^{JM}}$$

where

$$N_{\text{up}}^{JM} = \int_{y^2+z^2 \leq 1} \int_{z \geq 0} P_{JM}(y, z) dydz,$$

and

$$N_{\text{tot}}^{JM} = \int_{y^2+z^2 \leq 1} P_{JM}(y, z) dydz$$

with $P_{JM}(y, z)$ being the projection on a 2D screen perpendicular to the electric field axis of the probability density associated to the state $|J, M, l\rangle_0^\beta$ [18], which includes the alignment selectivity of the probe laser. y and z are the abscissa and ordinate of a 2D coordinate system centered on the screen, due to their relation with the Euler angles (θ, ϕ) their values are restricted to $y^2 + z^2 \leq 1$ [18].

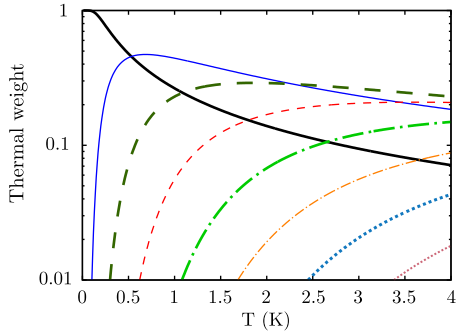


Figure 1. For OCS, thermal weights as a function of the temperature for several J -manifolds: $J = 0$ (thick solid line), $J = 1$ (thin solid line), $J = 2$ (thick dashed line), $J = 3$ (thin dashed line), $J = 4$ (thick dot-dashed line), $J = 5$ (thin dot-dashed line), $J = 6$ (thick dotted line) and $J = 7$ (thin dotted line).

To rationalize the mixed-field orientation results and illustrate the adiabaticity of this process, the time-dependent wave function is projected on the field-dressed adiabatic states

$$|J, M, l\rangle_t^\beta = \sum_{j=0}^N \sum_{m_j=-j}^j C_{jm_j l'}(t) |j, m_j, l'\rangle_p^\beta \quad (6)$$

with $C_{jm_j l'}(t) = \beta_p \langle j, m_j, l' | J M l \rangle_t^\beta$. This adiabatic basis is formed by the eigenstates $|j, m_j, l\rangle_p^\beta$ of the adiabatic Hamiltonian, i. e., the Hamiltonian (1) with constant electrostatic field E_s and constant laser intensity $I = I(t)$. For each time t , the time-independent Schrödinger equation is solved by expanding the wave function in a basis formed by linear combinations of spherical harmonics that respects the symmetries of the system. Note that for $|J, M, l\rangle_0^\beta$, the closer $|C_{J M l}|^2$ to one the more adiabatic is the mixed-field orientation process.

3. Results

In this work, we use the OCS molecule as prototype. The rotational constant of OCS is $B = 0.20286 \text{ cm}^{-1}$, the permanent dipole moment $\mu = 0.71 \text{ D}$ and the polarizability anisotropy $\Delta\alpha = 4.04 \text{ \AA}^3$. In Fig. 1, we present the thermal weights of several rotational manifolds $(2J + 1)W_J$, see Eq. (5). Due to the large rotational constant of OCS, the field-free energy splittings are large, and then, the thermal samples with $T \lesssim 1 \text{ K}$ are dominated by the $J = 0$ and $J = 1$ manifolds. Indeed, the relative weights of the states with $J = 0$ and $J = 1$ are $W_0 = 47.8\%$ and $W_1 = 44.7\%$ at $T = 0.5 \text{ K}$, and $W_0 = 99.1\%$ and $W_1 = 0.9\%$ at $T = 0.1 \text{ K}$. In our calculations, the thermal sample includes rotational states with $J \leq 9$, and we have ensured that the contribution of higher excitations can be neglected.

We first consider the OCS molecules exposed to an electric field and linearly polarized laser pulse, with both fields parallel to the LFF Z -axis. For several field configurations, we present in Fig. 2 the orientation cosine of the thermal ensemble as a function of the temperature for $E_s = 300 \text{ V/cm}$. Note the different scales used in each panel.

For this weak dc field, a significant orientation is only achieved if the rotational temperature is below 0.5 K , and the Gaussian pulse has $\tau = 10 \text{ ns}$, e. g., for the peak intensities $I_0 = 10^{12} \text{ W/cm}^2$ and $5 \times 10^{11} \text{ W/cm}^2$ we obtain $\langle\langle \cos\theta \rangle\rangle_T \gtrsim 0.5$. Using 1 ns Gaussian pulse, the orientation of the thermal sample is very small because the rotational states are weakly oriented, for instance, they satisfy $|\langle \cos\theta \rangle_{J M l}| < 0.13$ for $I_0 = 10^{12} \text{ W/cm}^2$ and $I_0 = 5 \times 10^{11} \text{ W/cm}^2$; whereas for $I_0 = 10^{11} \text{ W/cm}^2$, we obtain $\langle \cos\theta \rangle_{00e} = 0.24$ for the ground state. For these three FWHM, we encounter that a pulse with peak intensity $I_0 = 5 \times 10^{11} \text{ W/cm}^2$ gives rise to a larger orientation than one with $I_0 = 10^{12} \text{ W/cm}^2$, this is counterintuitive to what is expected in the adiabatic limit. This phenomenon can be explain by the non-adiabaticity of the mixed-field orientation process [3, 4], and can be rationalized in terms of the orientation of the individual

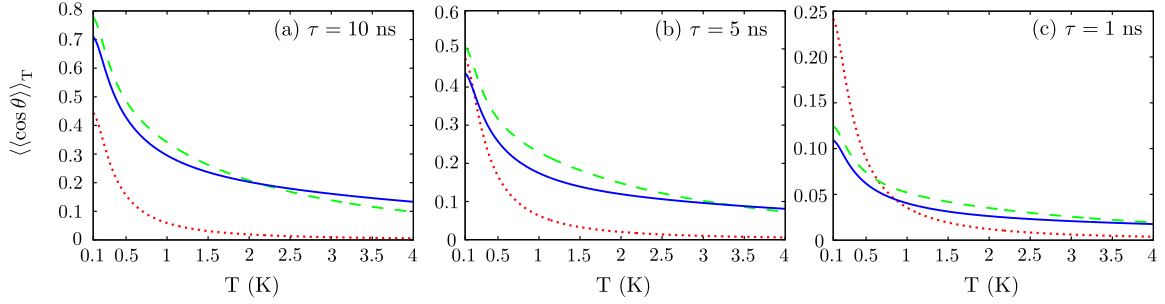


Figure 2. Orientation of a OCS thermal sample $\langle\langle \cos \theta \rangle\rangle_T$ as a function of the temperature for Gaussian pulses with $\tau = 10$ ns, $\tau = 5$ ns, and $\tau = 1$ ns and peak intensities $I_0 = 10^{12}$ W/cm 2 (thick solid line), $I_0 = 5 \times 10^{11}$ W/cm 2 (dashed line) and $I_0 = 10^{11}$ W/cm 2 (dotted line). The field configuration is $E_s = 300$ V/cm and $\beta = 0^\circ$.

levels. In Fig. 3, we present the orientation cosine of the field-dressed states $|J, |M|, e\rangle_0^0$ at $t = 0$ for two 10 ns Gaussian pulses with $I_0 = 10^{12}$ W/cm 2 and $I_0 = 5 \times 10^{11}$ W/cm 2 . In these plots, we observe that the levels $|J, M, e\rangle_0^0 - |J + 1, M, e\rangle_0^0$, which form a pendular doublet, are oriented and antioriented, respectively. The 5×10^{11} W/cm 2 pulse is not strong enough to affect the rotational dynamics in the excited rotational states with $J \geq 5$. The pulse with the strongest intensity $I_0 = 10^{12}$ W/cm 2 provokes a large orientation on highly excited states with $J \leq 7$. However, for the levels with $J \leq 3$, i.e., those that are important on the cold regime, the 5×10^{11} W/cm 2 pulse gives rise to a larger orientation compared to the 10^{12} W/cm 2 one. In the parallel field configuration, the population transfer between the two levels forming the doublets in the pendular regime is the only source of nonadiabatic effects in the field-dressed dynamics [3, 4]. For these levels, the population transfer to the neighboring state as the pendular pair is formed is the largest for the strongest laser. For the ground state, at $t = 0$ we obtain that the population of the adiabatic state $|0, 0, e\rangle_p^0$ is $|C_{00e}|^2 = 0.87$ and 0.91 with $I_0 = 10^{12}$ W/cm 2 and $I_0 = 5 \times 10^{11}$ W/cm 2 , respectively. As a consequence, the orientation is smallest for $I_0 = 10^{12}$ W/cm 2 , and, therefore, the thermal ensemble is less oriented. By increasing the temperature, the contribution of excited rotational states becomes important, and the thermal ensemble in a $I_0 = 10^{12}$ W/cm 2 pulse shows the largest orientation.

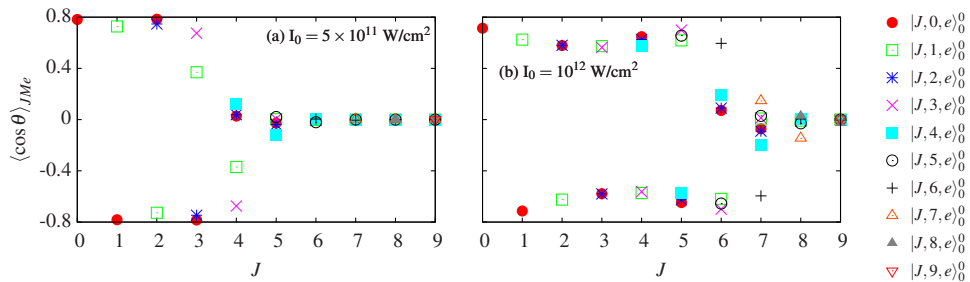


Figure 3. Orientation cosines $\langle \cos \theta \rangle_{JMe}$ at $t = 0$ of the states $|J, |M|, e\rangle_0^0$ versus the field-free rotational quantum number J . The Gaussian pulses have $\tau = 10$ ns, and peak intensities (a) $I_0 = 5 \times 10^{11}$ W/cm 2 and (b) $I_0 = 10^{12}$ W/cm 2 . The field configuration is $E_s = 300$ V/cm and $\beta = 0^\circ$.

Now, we consider that the electric field is tilted an angle $\beta = 30^\circ$ with respect to the polarization axis of the laser pulse, that is the LFF Z -axis. For several field configurations, we present in Fig. 4 the orientation cosine of the thermal ensemble as a function of the temperature

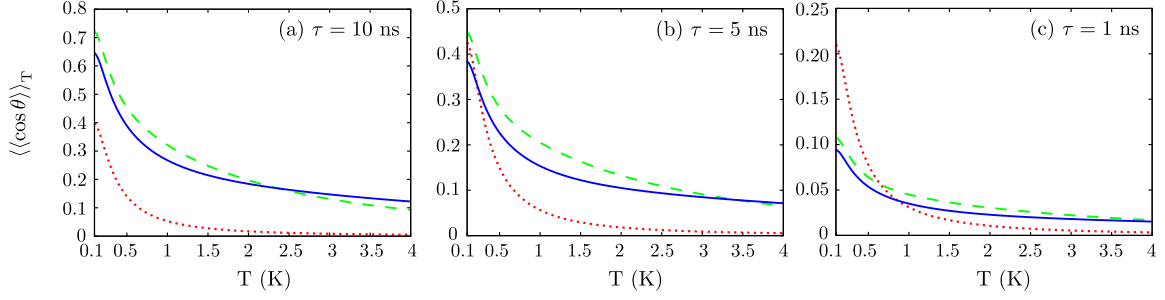


Figure 4. Same as Fig. 2 but for $\beta = 30^\circ$.

for $E_s = 300$ V/cm. Compared to the parallel field case, the orientation is reduced. For tilted fields, there are two main sources of nonadiabatic effects in the field-dressed dynamics: i) the transfer of population taking place when the quasidegenerate pendular doublets are formed as the laser intensity is increased; ii) at weak laser intensities, there is also population transfer due to the splitting of the states within a J -manifold now having the same symmetry. In addition, avoided crossings might be encountered as $I(t)$ is enhanced. The diabatic or adiabatic character of these avoided crossings depends on the field configuration and on the state. Hence, for a certain field configuration, the orientation of the individual states is smaller for $\beta = 30^\circ$ than for $\beta = 0^\circ$. This reduction of the orientation is illustrated for the rotational states $|J, M, e\rangle_0^0$ in Fig. 5 for two 10 ns Gaussian pulses. For $I_0 = 5 \times 10^{11}$ W/cm 2 , only the states $|0, 0, e\rangle_0^0$ and $|3, 1, e\rangle_0^0$ present a strong orientation with $|\langle \cos \theta \rangle_{JML}| > 0.6$, whereas for $I_0 = 10^{12}$ W/cm 2 only the ground state is strongly oriented. The other levels present a moderate or even small orientation. Due to the population redistribution within a J -manifold at weak intensities, the two levels forming a pendular doublet do not possess the same orientation $|\langle \cos \theta \rangle_{JML}|$ but in opposite directions as occurs in the parallel field configuration.

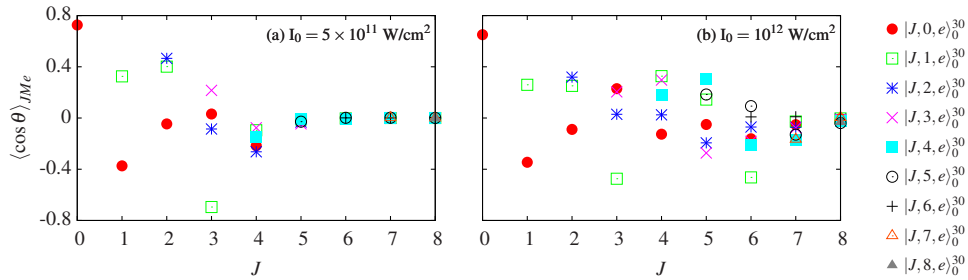


Figure 5. For the states $|J, |M|, e\rangle_0^{30}$, orientation cosines $\langle \cos \theta \rangle_{JML}$ at $t = 0$ versus the field-free rotational quantum number J . The Gaussian pulses have $\tau = 10$ ns and peak intensities (a) $I_0 = 5 \times 10^{11}$ W/cm 2 and (b) $I_0 = 10^{12}$ W/cm 2 . The field configuration is $E_s = 300$ V/cm and $\beta = 30^\circ$.

For the state $|2, 0, e\rangle_t^{30}$, we illustrate its rotational dynamics by presenting the projections of the time-dependent wave function in terms of the adiabatic states in Fig. 6(a) for a 10 ns pulse with $I_0 = 10^{12}$ W/cm 2 . The switching on of the electric field has been adiabatic and the level $|2, 0, e\rangle_p^{30}$ is the only one populated when the laser pulse is turned on. At weak laser intensities, the three states with the same symmetry in the $J = 2$ manifold, that is $|2, 0, e\rangle_p^{30}$, $|2, 1, e\rangle_p^{30}$ and $|2, 2, e\rangle_p^{30}$, are driven apart: $|C_{20e}(t)|^2$ decreases as $I(t)$ is increased, whereas $|C_{21e}(t)|^2$ and $|C_{22e}(t)|^2$ increase. For a wide range of laser intensities, these three coefficients keep their values constant. Around $I(t) \approx 2.84 \times 10^{10}$ W/cm 2 , the states $|2, 1, e\rangle_p^{30}$

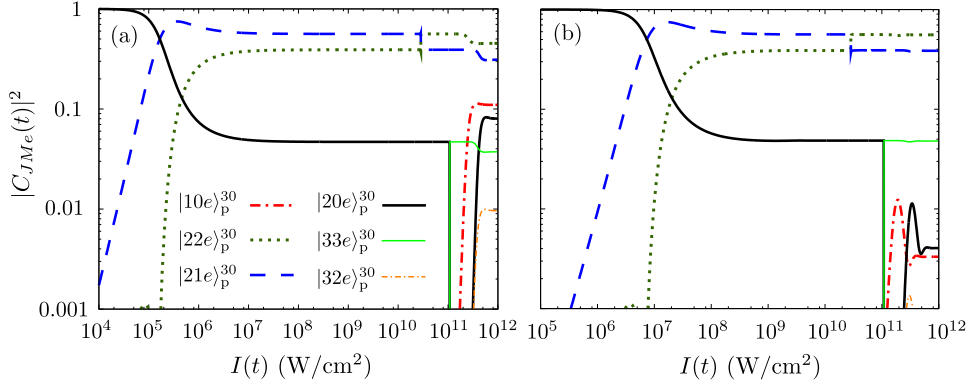


Figure 6. For the state $|2, 0, e\rangle_t^{30}$, we present the squares of the projections of the time dependent wave function onto the adiabatic pendular states versus the laser intensity $I(t)$, for dc field strengths (a) $E_s = 300$ V/cm and (b) $E_s = 2$ kV/cm. The Gaussian pulse has $\tau = 10$ ns and peak intensity $I_0 = 10^{12}$ W/cm², and the fields are tilted an angle $\beta = 30^\circ$.

and $|2, 2, e\rangle_p^{30}$ suffer an avoided crossings, which is crossed diabatically and the population of these two adiabatic levels is interchanged. Another diabatic avoided crossing is encountered around $I(t) \approx 1.09 \times 10^{11}$ W/cm², and the involved states $|2, 0, e\rangle_p^{30}$ and $|3, 3, e\rangle_p^{30}$ interchanged their population. Upon further increasing $I(t)$, the pendular doublets start to form, the coupling between the two involved states increases, and there is a new population redistribution. In this figure, it is appreciated how the different pendular doublets are formed sequentially according to their energy. The first one involves the states $|1, 0, e\rangle_p^{30}$ and $|2, 2, e\rangle_p^{30}$, the next one $|2, 1, e\rangle_p^{30}$ and $|2, 0, e\rangle_p^{30}$, and the third one in this figure $|3, 3, e\rangle_p^{30}$ and $|3, 2, e\rangle_p^{30}$. At $t = 0$, the contribution of the adiabatic states to the field-dressed wave function is $|C_{22e}(0)|^2 = 0.11$, $|C_{20e}(0)|^2 = 0.45$, $|C_{21e}(0)|^2 = 0.31$, $|C_{20e}(0)|^2 = 0.08$, $|C_{33e}(0)|^2 = 0.04$ and $|C_{32e}(0)|^2 = 0.01$. As a consequence of this population redistribution, at $t = 0$ the state $|2, 0, e\rangle_0^{30}$ is weakly antioriented ($\langle \cos \theta \rangle_{20e} = -0.089$), whereas in the adiabatic prediction present a strong anti-orientation ($\langle \cos \theta \rangle_{20e} = -0.886$). Analogously, other features of the system such as the energy, alignment, and hybridization of the angular motion are also affected by this population redistribution and do not resemble the adiabatic results.

For $\beta = 30^\circ$, the orientation ratio $N_{\text{up}}/N_{\text{tot}}$ is presented in Fig. 7. To compute $N_{\text{up}}/N_{\text{tot}}$ we have used a probe laser linearly polarized along the vertical axis of the screen detector as in the experiments [3]. In these results, we have neglected the volume effect [18], we should mention that by including it the value of $N_{\text{up}}/N_{\text{tot}}$ will be reduced.

In recent experiments [3], for a state selected molecular beam of OCS, 92% in $|0, 0, e\rangle_0^0$, 4% in $|1, 1, e\rangle_0^0$ and 4% in $|1, 1, o\rangle_0^0$, an orientation ratio of $N_{\text{up}}/N_{\text{tot}} = 0.73$ was achieved using a 8 ns YAG laser with $I_0 = 9.1 \times 10^{11}$ W/cm², $E_s = 286$ V/cm and $\beta = 30^\circ$. Using a 10 ns pulse, similar results for the orientation ratio of the thermal ensemble are reached if the rotational temperature is sufficiently low. For instance, $N_{\text{up}}/N_{\text{tot}} \gtrsim 0.73$ for $T \lesssim 0.65$ K and 0.46 K with peak intensities $I_0 = 5 \times 10^{11}$ W/cm² and $I_0 = 10^{12}$ W/cm², respectively. At $T = 0.65$ K, the field-free thermal ensemble is formed by 38.56% OCS in its ground state, 47.19% in $J = 1$ and 13% in $J = 2$; whereas for $T = 0.46$ K, 51.08% have $J = 0$, 43.07% $J = 1$, and 5.7% $J = 2$. For $\tau = 5$ ns, only when more than 95% of OCS molecules are in the ground state and $I_0 = 5 \times 10^{11}$ W/cm² we obtain a similar orientation ratio as in the experiment. By reducing the FWHM to 1 ns, the orientation ratio is significantly reduced.

An important ingredient to obtain realistic screen images and orientation ratios is the alignment selectivity of the probe laser, which depends on its polarization [18]. Here, we consider

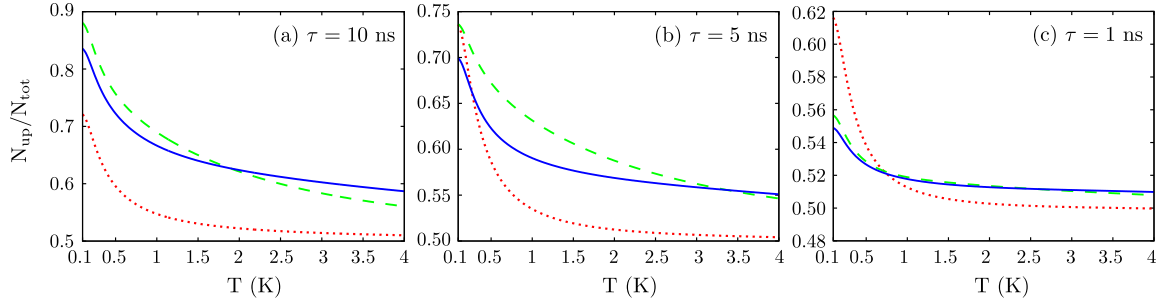


Figure 7. For the OCS thermal sample, we present the orientation ratio $N_{\text{up}}/N_{\text{tot}}$ as a function of the temperature for Gaussian pulses with FWHM $\tau = 10$ ns, $\tau = 5$ ns, and $\tau = 1$ ns and peak intensities $I_0 = 10^{12}$ W/cm² (thick solid line), $I_0 = 5 \times 10^{11}$ W/cm² (dashed line) and $I_0 = 10^{11}$ W/cm² (dotted line). The field configuration is $E_s = 300$ V/cm and $\beta = 30^\circ$.

a thermal sample in a laser pulse with $\tau = 10$ ns and $I_0 = 10^{12}$ W/cm², and electric field $E_s = 300$ V/cm and $\beta = 30^\circ$. In Fig. 8, we present its orientation ratio using the probe pulse with three possible polarizations. For a probe pulse linearly polarized parallel to the vertical axis of the screen, $N_{\text{up}}/N_{\text{tot}}$ is the largest because such a pulse favors the Coulomb explosion of the oriented molecules. In contrast, if the probe pulse is linearly polarized perpendicular to screen, the probability of the Coulomb explosion for the oriented molecules is reduced, and, therefore, $N_{\text{up}}/N_{\text{tot}}$ presents the smallest values. The circularly polarized probe laser ensures that any molecule is ionized and detected with the same probability independently of the angle β , and provides the intermediate values of $N_{\text{up}}/N_{\text{tot}}$ for any temperature. For a given state, there is no analytical relation between its orientation $\langle\langle\cos\theta\rangle\rangle_T$ and the orientation ratio $N_{\text{up}}/N_{\text{tot}}$ of the 2D projection of its wave function, although the approximation $N_{\text{up}}/N_{\text{tot}} \approx (1 + \langle\langle\cos\theta\rangle\rangle_T)/2$ could be used to obtain an estimation. For instance, a 0.29 K thermal sample presents an orientation of $\langle\langle\cos\theta\rangle\rangle_T = 0.506$, and orientation ratios $N_{\text{up}}/N_{\text{tot}} = 0.757$ and 0.774 for a probe laser linearly polarized perpendicular and parallel to the screen detector, respectively, and $N_{\text{up}}/N_{\text{tot}} = 0.761$ for a circularly polarized one. These results should be compared with the value 0.753 given by this approach, which provides a lower bound for the $N_{\text{up}}/N_{\text{tot}}$ of these three polarizations.

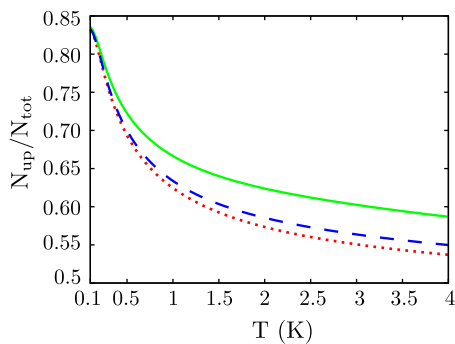


Figure 8. For a OCS thermal sample, we present the orientation ratio $N_{\text{up}}/N_{\text{tot}}$ using a probe pulse linearly polarized along the vertical axis of the screen (thick solid line), along the perpendicular axis to the screen (dashed line) and circularly polarized in a plane perpendicular to the screen (dotted line). The field parameters are $\tau = 10$ ns, $I_0 = 10^{12}$ W/cm², $E_s = 300$ V/cm and $\beta = 30^\circ$.

For parallel fields, if the electric field strength is increased, the energy splitting in a pendular doublet is increased, and as a consequence, the degree of adiabaticity in the molecular mixed-field orientation is also enhanced. However, this statement only holds for the ground state of the two irreducible representations if the fields are tilted. For an excited rotational state, a strong

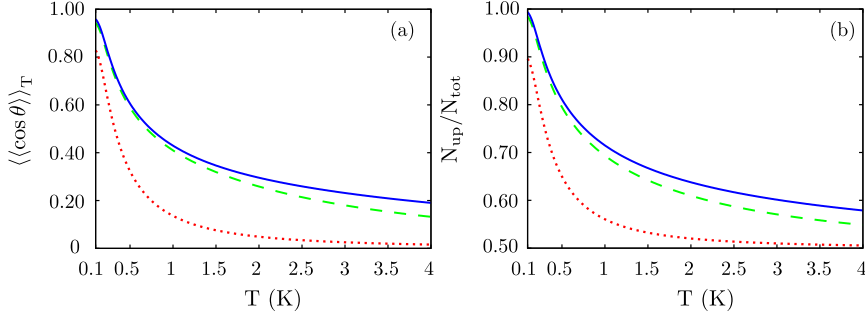


Figure 9. For a OCS thermal sample, we present (a) $\langle\langle\cos\theta\rangle\rangle_T$ and (b) $N_{\text{up}}/N_{\text{tot}}$ as a function of the temperature for a 10 ns Gaussian pulse with peak intensities $I_0 = 10^{12}$ W/cm² (thick solid line), $I_0 = 5 \times 10^{11}$ W/cm² (dashed line) and $I_0 = 10^{11}$ W/cm² (dotted line). The field configuration is $E_s = 2$ kV/cm and $\beta = 30^\circ$.

dc field does not ensure a large orientation because the coupling between levels with different field-free M values becomes important, and this affects the molecular dynamics. In contrast, for a weak dc field, the mixing between these states is so small that M can be considered as conserved.

In Fig. 9, we plot $\langle\langle\cos\theta\rangle\rangle_T$ and $N_{\text{up}}/N_{\text{tot}}$ for a thermal sample exposed to a 10 ns pulse combined with a dc field of $E_s = 2$ kV/cm tilted an angle $\beta = 30^\circ$. For cold samples with $T \lesssim 0.74$ K and $T \lesssim 0.69$ K, we obtain $\langle\langle\cos\theta\rangle\rangle_T \gtrsim 0.5$ with $I_0 = 10^{12}$ W/cm² and 5×10^{11} W/cm², respectively. For $I_0 = 5 \times 10^{11}$ W/cm² and 10^{12} W/cm², we obtain $N_{\text{up}}/N_{\text{tot}} \gtrsim 0.73$ if the rotational temperature is $T \lesssim 1.1$ K. Thus, using this strong dc field the orientation of a thermal ensemble becomes comparable to the experimental value for a quantum-state selected molecular beam in a very weak electric field. For this strong electric field, the orientation of the quantum-state selected beam is $N_{\text{up}}/N_{\text{tot}} = 0.99$ using a probe pulse linearly polarized along the vertical axis of the detector.

In Fig. 10, we present the expectation value $\langle\cos\theta\rangle_{JMe}$ at $t = 0$ for several rotational states in 10 ns Gaussian pulses with $I_0 = 5 \times 10^{11}$ W/cm² and 10^{12} W/cm², $E_s = 2$ kV/cm and $\beta = 30^\circ$. For both field configurations, the $|0, 0, e\rangle_0^{30}$ and $|3, 1, e\rangle_0^{30}$ states are strongly oriented and antioriented, respectively. The remaining states show a moderate or weak orientation. The effect of doubling the peak intensity is not noticeable for the levels with field-free rotational quantum number $J \leq 3$, and, in addition, for a certain peak intensity, we encounter similar

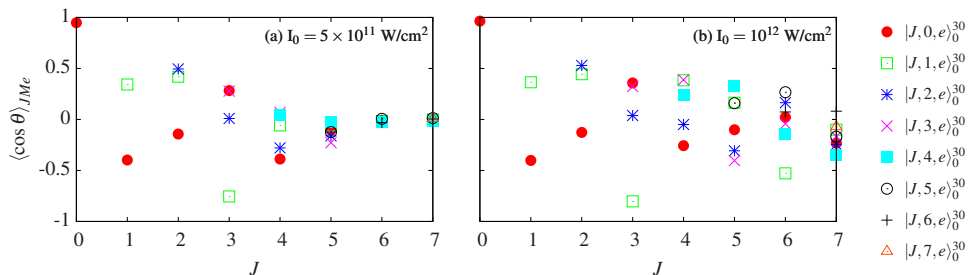


Figure 10. For the states $|J, M, e\rangle_0^{30}$, we present the orientation cosines $\langle\cos\theta\rangle_{JMe}$ at $t = 0$ versus the field-free rotational quantum number. The FWHM of the Gaussian pulses is $\tau = 10$ ns and the peak intensities (a) $I_0 = 5 \times 10^{11}$ W/cm² and (b) $I_0 = 10^{12}$ W/cm². The field configuration is $E_s = 2$ kV/cm and $\beta = 30^\circ$.

orientation using a Gaussian pulse of 10 ns or 5 ns. The rotational dynamics of the ground state is adiabatic for both pulses; whereas for the excited state, this phenomenon can be explained by the non adiabatic effects taking place at weak laser intensities. When the levels in a certain J manifold are driven apart by the laser field, the process is nonadiabatic and there is a population transfer between them, already at weak laser intensities. Thus, the wave function of any excited level has contributions from adiabatic states which correspond to different pendular doublets. By further increasing the laser intensity, the molecular dynamics is affected by the avoided crossings with adjacent levels having different field-free magnetic quantum numbers M and by the formation of these pendular doublets. The rotational dynamics in most of these crossings will be nonadiabatic and has to be analyzed for each specific state. When the electric field is strong, the energy splitting within the states in the pendular pair is sufficiently large, and, as a consequence, the population transfer when the doublets are formed is not significant.

For completeness, in Fig. 6(b) we present the field-dressed rotational dynamics of the state $|2, 0, e\rangle_t^{30}$ in a 10 ns pulse with $I_0 = 10^{12}$ W/cm² and a strong dc field of $E_s = 2$ kV/cm. After an adiabatic switching on of the electric field, the states in the $J = 2$ manifold are driven apart, $|C_{20e}(t)|^2$ decreases as $I(t)$ is increased, whereas $|C_{21e}(t)|^2$ and $|C_{22e}(t)|^2$ increase. Compared to the weak dc field case in Fig. 6(a), this J -manifold splitting takes place at a stronger laser intensity, because the energy gap between the adiabatic states $|2, 2, e\rangle_p^{30}$, $|2, 1, e\rangle_p^{30}$ and $|2, 0, e\rangle_p^{30}$ is larger for $E_s = 2$ kV/cm than for $E_s = 300$ V/cm. Let us mention that if E_s is increased, the energy splitting within this J -manifold is increased, and, therefore, the population redistribution will be reduced [4]. The avoided crossing between the states $|2, 1, e\rangle_p^{30}$ and $|2, 2, e\rangle_p^{30}$ occurs at $I(t) \approx 2.96 \times 10^{10}$ W/cm², whereas the one involving the levels $|2, 0, e\rangle_p^{30}$ and $|3, 3, e\rangle_p^{30}$ around $I(t) \approx 1.09 \times 10^{11}$ W/cm². Again, both of them are crossed diabatically, and the population of the adiabatic states is interchanged. By further increasing $I(t)$, the pendular doublets start to form. In this case, the dc field is stronger and the energy gap is larger but the coupling due to the ac field is the same, then the population transfer is reduced. Indeed, the adiabatic states $|1, 0, e\rangle_p^{30}$, $|2, 0, e\rangle_p^{30}$ and $|3, 2, e\rangle_p^{30}$, the partners in the pendular doublets of $|2, 2, e\rangle_p^{30}$, $|2, 1, e\rangle_p^{30}$ and $|3, 3, e\rangle_p^{30}$, respectively, show a small population, which is below 0.01 once the peak intensity at $t = 0$ is achieved. Thus, the population at $t = 0$ for the field-dressed state $|2, 0, e\rangle_0^{30}$ is $|C_{22e}(0)|^2 = 0.56$, $|C_{21e}(0)|^2 = 0.39$, and $|C_{33e}(0)|^2 = 0.05$. These results are similar for the four pulses formed by combining $\tau = 5$ ns and 10 ns with $I_0 = 5 \times 10^{11}$ W/cm² and 10^{12} W/cm².

4. Conclusions

In this work, we investigate the mixed-field orientation dynamics of a thermal sample of linear molecules. We solve the time-dependent Schrödinger equation within the rigid rotor approximation for a large set of rotational states. As prototype example, we use the OCS molecule. However, we stress that the above results could be used to describe the mixed-field orientation of a thermal ensemble of other polar linear molecules by rescaling the Hamiltonian (1) in terms of the rotational constant.

By considering prototypical field configurations with weak dc fields, as in current mixed-field orientation experiments, we have proven that the rotational temperature of the molecular beam should be smaller than 0.7 K to achieve a significant orientation. Using a weak electric field, if the aim is a strongly oriented molecular ensemble, this should be as pure as possible in the ground state. Thus, it is required a quantum-state-selected molecular beam, unless the rotational temperature could be efficiently reduced below 1 K. It is found that a significant orientation is achieved for 1 K molecular samples when the electric field strength is increased.

Acknowledgments

Financial support by the Spanish project FIS2011-24540 (MICINN), the Grants P11-FQM-7276 and FQM-4643 (Junta de Andalucía), and the Andalusian research group FQM-207 is gratefully appreciated. J.J.O. acknowledges the support of ME under the program FPU.

References

- [1] Friedrich B and Herschbach D R 1999 *J. Chem. Phys.* **111** 6157
- [2] Friedrich B and Herschbach D 1999 *J. Phys. Chem. A* **103** 10280
- [3] Nielsen J H, Stapelfeldt H, Küpper J, Friedrich B, Omiste J J and González-Férez R 2012 *Phys. Rev. Lett.* **108** 193001
- [4] Omiste J J and González-Férez R 2012 *Phys. Rev. A* **86** 043437
- [5] Sakai H, Minemoto S, Nanjo H, Tanji H and Suzuki T 2003 *Phys. Rev. Lett.* **90** 083001
- [6] Buck U and Fárník M 2006 *Int. Rev. Phys. Chem.* **25** 583
- [7] Ghafur O, Rouzee A, Gijsbertsen A, Siu W K, Stolte S and Vrakking M J J 2009 *Nat Phys* **5** 289–293
- [8] Holmegaard L, Nielsen J H, Nevo I, Stapelfeldt H, Filsinger F, Küpper J and Meijer G 2009 *Phys. Rev. Lett.* **102** 023001
- [9] Filsinger F, Küpper J, Meijer G, Holmegaard L, Nielsen J H, Nevo I, Hansen J L and Stapelfeldt H 2009 *J. Chem. Phys.* **131** 064309
- [10] Even U, Jortner J, Noy D, Lavie N and Cossart-Magos C 2000 *J. Chem. Phys.* **112** 8068
- [11] Seideman T and Hamilton E 2006 *Adv. Atom. Mol. Opt. Phys.* **52** 289
- [12] Feit M D, Fleck Jr J A and Steiger A 1982 *J. Comp. Phys.* **47** 412
- [13] Bačič Z and Light J C 1989 *Annu. Rev. Phys. Chem.* **40** 469
- [14] Corey G C and Lemoine D 1992 *J. Chem. Phys.* **97** 4115
- [15] Offer A R and Balint-Kurti G G 1994 *J. Chem. Phys.* **101** 10416–10428
- [16] Sánchez-Moreno P, González-Férez R and Schmelcher P 2007 *Phys. Rev. A* **76** 053413
- [17] Härtelt M and Friedrich B 2008 *J. Chem. Phys.* **128** 224313
- [18] Omiste J J, Gärttner M, Schmelcher P, González-Férez R, Holmegaard L, Nielsen J H, Stapelfeldt H and Küpper J 2011 *Phys. Chem. Chem. Phys.* **13** 18815–18824

Chapter 7

Conclusions and outlook

Let us finish by summing up our findings and providing a short outlook on the future research in the field of control of molecules by means of external fields.

In this thesis, we have investigated the impact of external fields on polar linear and asymmetric top molecules. We have worked within the Born-Oppenheimer approximation and assumed that the impact of the fields on the vibrational and electronic dynamics is small and could be described by first-order perturbation theory. Furthermore, we neglect relativistic effects, fine, and hyperfine interactions as well as couplings of different electronic states. We have worked with off-resonance conditions for the laser, and assumed that its frequency is larger than the inverse of both the pulse duration and the rotational period. This allows us to apply a two-photon rotating-wave approximation averaging over the rapid oscillations of the nonresonant field, so that only the interaction of this field with the molecular polarizability is taken into account. In addition, we have considered the weak or moderate dc-field regime, and neglected the coupling of this field with the polarizability and higher order terms.

Asymmetric top molecules

In the framework of the rigid rotor approximation, we have investigated the impact of combined nonresonant laser and a homogenous static electric fields on asymmetric top molecules. We have carried out a complete analysis of the symmetry features of the rigid rotor Hamiltonian, and numerically each irreducible representation has been treated independently, so that in the field-dressed spectrum the real crossings could be distinguished from the avoided ones. Within the adiabatic approximation, we have investigated the energy shifts, alignment, orientation and hybridization of the angular motion as the field parameters are varied. This study has pointed out the high complexity of the field-dressed level structure of these systems. We have explored not only the strong laser and weak electric field regimes, but the intermediate field regime, where the Stark and ac-field interactions compete or cooperate to orient and align the molecule. For instance, we have proposed the use of a strong static field perpendicular to the polarization of a laser field to achieve 3D orientation.

Based on our knowledge of asymmetric top molecules in external fields, we have performed a theoretical description of the mixed-field experiments on alignment and orientation of benzonitrile. We have carried out a time-independent study using the widely accepted idea of the adiabaticity of these processes. Our calculations have reproduced the measurements of the alignment, but predicted no orientation for the molecular beam, which did not agree with the experimental results. The field-dressed spectrum is characterized by the large amount of avoided crossings between neighboring levels, and using a diabatic criterion we could not ensure that all of them were passed adiabatically. As a consequence, the adiabatic approximation could not be used to describe this process. Hence, we have proposed a diabatic

model to classify the avoided crossing for the tilted-field configuration according to the field-free magnetic quantum number M of the involved states. The avoided crossings are passed adiabatically or diabatically if the two states have the same or different field-free M , respectively. Using such a model we found a better agreement with the experimental degree of orientation. However, there are two important features of the experimental results that our adiabatic model could not reproduce. The first one is the smooth dependence of the experimental orientation ratio on the angle between the electric field and the polarization of the alignment laser. The second one is that the orientation ratio increases as the dc field strength is increased.

As well, we have performed a time-dependent description of the impact of combined dc and ac fields on an asymmetric top molecule. Although our computational approach is prepared to investigate any field configuration, due to the complexity of the rotational dynamics, we have only analyzed the parallel field case. Let us mention, that the orientation (antiorientation) in parallel fields provides an upper (lower) bound to the results in the tilted case, which is important for the experiments. We have investigated in detail the rotational dynamics of benzonitrile for several experimentally accessible field configurations. We have found that the field-dressed dynamics is driven by the formation of pendular doublets and by the presence of numerous avoided crossings in the adiabatic spectrum. Since both phenomena are characterized by different time scales, the seek of an adiabatic dynamics becomes a more difficult task. For the ground states of several irreducible representations, we encounter that sufficiently long laser pulses ensure an adiabatic process. For excited states, the avoided crossings dominate and even under a 20 ns pulse the dynamics is not adiabatic and the degree of orientation strongly depends on the field parameters. In contrast to the linear molecules, we have shown that the electric field strength could not be used to manipulate the adiabaticity of this process.

Finally, we have studied the CPC molecule in external fields under the adiabatic approximation. Its most interesting feature is that the permanent dipole moment is not parallel to any axis of the polarizability or inertia. In the presence of an electric field, we have showed that the brute force orientation depends strongly not only on the components of the dipole moment, but also on the rotational constants and, therefore, on the level structure and the Stark interaction couplings. Our calculations have showed that an elliptically polarized laser field combined with a weak static field are able to fix the molecular plane to the polarization one, and at the same time to orient the two components of the dipole moment along the two polarization axes of the laser. In addition, we have found that the 3D orientation of this molecule could be achieved by using a strong dc field tilted an angle $0^\circ < \beta < 90^\circ$ with respect to a linearly polarized laser.

Linear molecules

We have performed the first time-dependent description of the mixed-field orientation of a linear molecule by taking into account the temporal profile of the electric field and laser pulse. Our numerical results show a good agreement with the experimental ones. In particular, they were able to explain the smooth dependence of the orientation ratio with the angle between both fields, and its variation with the dc field strength. Furthermore, we have found that under ns laser pulses the weak dc field orientation is not, in general, adiabatic, and that a time-dependent description of the mixed-field orientation process is required to explain the

experimental results. We have performed an extensive study of the field-dressed dynamics of OCS in several field configuration, which has allowed us to identify the field-induced couplings among the adiabatic states that cause the loss of adiabaticity. For parallel fields, we have shown that the coupling of the levels forming quasidegenerate pendular doublets as the laser intensity is increased gives rise to a transfer of population between them. When the fields are tilted, an additional nonadiabatic effect appears at weak laser fields: The strongly coupled states from a J manifold are driven apart as the laser intensity is increased and as a consequence, there is a population redistribution among them. Furthermore, we have seen that the time evolution of excited states is influenced by avoided crossings among the adiabatic levels, which enhances the difficulties to reach the adiabatic limit. Our theoretical study has found that the electric field strength and the temporal width of the laser pulse are the control knobs that could be exploited to tailor the interactions seeking for the adiabatic limit. Finally, we have considered a thermal ensemble of polar molecules, and investigated the mixed field orientation as a function of the temperature. We have shown that using weak electric fields, the thermal sample is significantly oriented if the rotational temperature is reduced to $T = 0.65$ K. For $T = 1$ K, a similar degree of orientation could be reached by increasing dc field strength to a few kV/cm.

Outlook

A rather natural continuation of our work is the study of the rotational dynamics of asymmetric tops in tilted dc fields and laser pulses. A time-dependent description of this system will allow us to revise our diabatic model about the avoided crossings, and confirm that those involving states with different field-free values of M are diabatic. In this thesis, we have found that the avoided crossings for parallel fields are, in general, passed diabatically. Note that these avoided crossings are equivalent to those between levels with the same $\langle J_Z^2 \rangle$ in tilted fields. For benzonitrile, we want to perform the time propagation of the quantum states of the molecular beam under the experimental field configurations. Such an exhaustive study will allow us to understand and interpret the mixed-field orientation experiments for asymmetric top molecules [20, 51]. The computational code needed for this study has been developed during this thesis and the calculation are being performed.

Our description of the impact of external fields on the CPC molecule is done under the adiabatic approximation. However, the results obtained during this thesis have pointed out that this approach is correct only under very specific field configurations, but unfortunately not for most of the configurations used in current experiments. A time-dependent description of these systems is highly demanding from a computational point of view; the large size of the Hamiltonian matrices implies an enhancement of the CPU time required for the propagation of a wave function. In particular, for elliptically polarized lasers, the number of symmetries are drastically reduced and new coupling terms appear in the Hamiltonian.

From a theoretical point of view, there is a lack of studies about the mixed-field orientation of fully unsymmetric molecules. For these systems, the relevant molecular-frame coordinate associated to inertial frame, dipole moment and polarizability do not coincide. Thus, a description within the rigid rotor approximation implies a large degree of complexity due to the non-diagonal coupling from the polarizability tensor. The theoretical study performed for asymmetric tops in this thesis provides an ideal platform to start the investigation of these more complicated molecules.

In a recent work [78], we have analyzed the impact of electric and magnetic fields on open shell molecules in their electronic ground state $^2\Pi$. We have found that a combination of magnetic and electric fields leads to aligned and orientated states under the adiabatic approach. We have also explored the influence of the Λ -doubling on the coupling of states and their orientation. It would be interesting to perform a time-dependent description of this system. To do so, the time-variation of the field strengths should be modeled to reproduce the experimental setup. This time-dependent study will determine the validity of the adiabatic approximation, and the field regimes where it could be applied.

Chapter 8

Conclusiones y perspectivas futuras

Terminamos resumiendo las conclusiones de esta tesis doctoral y exponiendo brevemente las posibles líneas futuras de investigación en el control de moléculas mediante campos externos.

En esta tesis hemos investigado el impacto de campos externos en moléculas lineales y asimétricas. Este trabajo se ha llevado a cabo dentro de la aproximación de Born-Oppenheimer y asumiendo que la influencia de los campos externos en la dinámica vibracional y electrónica es pequeña y puede ser descrita por medio de teoría de perturbaciones de primer orden. Más aún, hemos despreciado los efectos relativistas y la estructura fina e hiperfina, así como los acoplamientos entre diferentes estados electrónicos. Hemos trabajado fuera de resonancia para el láser, asumiendo que su frecuencia es mayor que el inverso tanto de la duración del pulso como del período rotacional. Esto nos ha permitido aplicar una aproximación de onda rotatoria a dos fotones (two-photon rotating-wave), y promediar sobre las rápidas oscilaciones del campo no resonante; de este modo, sólo contribuye la interacción del láser con la polarizabilidad molecular. Además, hemos considerado el régimen de campos eléctricos débiles y moderados, despreciando el acoplamiento de este campo con la polarizabilidad de la molécula y órdenes superiores.

Moléculas asimétricas

En el marco de la aproximación de sólido rígido, hemos investigado el impacto de un campo láser no resonante y uno eléctrico estático y homogéneo en una molécula asimétrica. Hemos llevado a cabo un análisis completo de las simetrías del Hamiltoniano del sólido rígido. Numéricamente, cada representación irreducible ha sido tratada de independientemente, de forma que los cruces reales pueden ser distinguidos de los evitados en el espectro en campos externos. Dentro de la aproximación adiabática, hemos investigado la variación de la energía, alineación, orientación e hibridación del movimiento angular al modificar los parámetros de la configuración de campos. Este estudio ha puesto de manifiesto la gran complejidad de la estructura de niveles de estos sistemas en presencia del campo. Hemos explorado no sólo el régimen de campo láser intenso y eléctrico débil, sino también intensidades a las que las interacciones Stark y del láser compiten o cooperan para orientar y alinear la molécula. Por ejemplo, hemos propuesto el uso de un campo estático intenso perpendicular a la polarización de un láser para alcanzar orientación 3D.

Basado en este estudio sobre las moléculas asimétricas en campos externos, hemos realizado una descripción teórica de los experimentos de alineación y orientación del benzonitrilo [20,51]. Hemos llevado a cabo un estudio independiente del tiempo, valiéndonos de la idea comúnmente aceptada de la adiabaticidad de estos procesos. Nuestros cálculos han reproducido las medidas de la alineación, pero predicen que el haz molecular no estaría orientado, lo que contradice las observaciones experimentales. El espectro en presencia de campos está caracterizado por

una gran cantidad de cruces evitados entre niveles vecinos. Nuestros cálculos muestran que un criterio adiabático no puede asegurar que todos ellos fuesen cruzados adiabáticamente. Esto implica que la aproximación adiabática no describiría adecuadamente este proceso. Así, hemos propuesto un modelo adiabático para clasificar los cruces evitados para la configuración de campos inclinados de acuerdo al número cuántico magnético en ausencia de campo M de los estados involucrados. Los cruces evitados se cruzan adiabática o diabáticamente si los dos estados tienen el mismo o diferente valor de M en ausencia de campo, respectivamente. Usando este modelo, se ha logrado un mejor acuerdo entre los resultados experimentales y teóricos del grado de orientación. Sin embargo, este modelo diabático no es capaz de reproducir dos características importantes de las observaciones experimentales. La primera es la dependencia suave de la orientación con el ángulo entre el campo eléctrico y la polarización del láser de alineación. La segunda es que la orientación crece al aumentar la intensidad del campo eléctrico.

En uno de los últimos proyectos de esta tesis, hemos realizado un análisis dependiente del tiempo del impacto de un campo estático y uno láser en las moléculas asimétricas. Nuestra descripción y el código computacional están preparados para estudiar cualquier configuración de los campos externos, pero debido a la complejidad de la dinámica rotacional, en esta tesis nos hemos centrado en el caso de campos paralelos. Nótese que la orientación (antiorientación) en campos paralelos proporciona una cota superior (inferior) de los resultados en campos inclinados. De modo que este primer estudio tiene una enorme relevancia para estos experimentos. Hemos analizado en detalle la dinámica rotacional del benzonitrilo para varias configuraciones experimentalmente accesibles. Hemos encontrado que la formación de los dobletes pendulares y los numerosos cruces evitados en el espectro adiabático contribuyen a la no-adiabaticidad de la dinámica en presencia de campos. Ambos fenómenos están caracterizados por diferentes escalas temporales; por tanto, la búsqueda de una dinámica adiabática se torna una tarea más complicada que para moléculas lineales. Para los estados fundamentales de varias representaciones irreducibles, hemos encontrado que pulsos láser suficientemente largos asegurarían una propagación adiabática. Para estados excitados, los cruces evitados dominan la dinámica e incluso bajo un pulso de 20 ns no se alcanza la adiabaticidad y el grado de orientación depende fuertemente de los parámetros del campo. En contraposición con las moléculas lineales, hemos mostrado que incrementar el campo eléctrico no permite aumentar de forma inmediata el grado de adiabaticidad de este proceso debido a los cruces evitados.

Finalmente, hemos estudiado la molécula de CPC en campos externos bajo la aproximación adiabática, cuyo momento dipolar permanente no es paralelo a ningún eje de polarizabilidad o inercia. En presencia de sólo un campo eléctrico, hemos mostrado que la orientación depende fuertemente no sólo de las componentes del momento dipolar sino también de las constantes rotacionales y, más aún, del espectro y los acoplamientos debidos a esta interacción. Nuestros cálculos han mostrado que un campo láser elípticamente polarizado junto con uno eléctrico débil son capaces de fijar el plano molecular al de polarización del láser, y al mismo tiempo orientar las dos componentes del momento dipolar a lo largo de los dos ejes de polarización. Además, hemos encontrado que la orientación 3D de esta molécula podría alcanzarse por medio de un campo estático intenso inclinado un ángulo $0^\circ < \beta < 90^\circ$ con respecto a un láser linealmente polarizado.

Moléculas lineales

Hemos llevado a cabo la primera descripción dependiente del tiempo de la orientación de una molécula lineal en una combinación de campos teniendo en cuenta el perfil temporal del campo eléctrico y el pulso láser. Nuestros resultados numéricos muestran un buen acuerdo con los experimentales. En concreto, hemos sido capaces de explicar la dependencia de la orientación con el ángulo formado por los campos, y su variación con la intensidad del campo eléctrico. Más aún, hemos mostrado que bajo pulsos láser de nanosegundos la orientación con campos estáticos débiles no es, en general, adiabática, y que se requiere una descripción dependiente del tiempo de este proceso para explicar e interpretar las observaciones experimentales. Se ha realizado un extenso estudio de la dinámica en presencia de campos externos para la molécula de OCS en varias configuraciones. Este análisis nos ha permitido identificar los acoplamientos inducidos por los campos entre estados adiabáticos que causan la pérdida de adiabaticidad. Para campos paralelos, hemos encontrado que el acoplamiento entre los dos niveles que forman un doblete pendular al aumentar la intensidad del láser da lugar a una transferencia de población entre ellos. Para campos inclinados, un fenómeno no adiabático adicional aparece a intensidades bajas del láser: los estados con el mismo número cuántico rotacional J en ausencia de campos ahora están fuertemente acoplados; a medida que la intensidad se incrementa se van separando energéticamente y como consecuencia se produce una redistribución de población entre ellos. Además, hemos visto que los cruces evitados tienen un gran impacto en la dinámica rotacional de estados excitados, y esto dificulta las condiciones necesarias para alcanzar el límite adiabático. Nuestro estudio teórico ha puesto claramente de manifiesto que la intensidad del campo eléctrico y la anchura temporal del pulso láser son los interruptores que permiten manipular las interacciones buscando el límite adiabático. Finalmente, hemos considerado una colectividad térmica de moléculas polares, e investigado la orientación en una combinación de campos al variar la temperatura. Hemos encontrado que con campos eléctricos débiles, la muestra térmica está muy orientada si la temperatura rotacional se reduce a $T = 0.65$ K. Para $T = 1$ K, un grado similar de orientación podría alcanzarse con campos estáticos de varios kV/cm.

Perspectivas futuras

Una continuación natural de este trabajo es el estudio de la dinámica rotacional de moléculas asimétricas en campos eléctricos y pulsos láser inclinados. Una descripción dependiente del tiempo de este sistema nos permitirá comprobar nuestro modelo diabático sobre los cruces evitados, y confirmar si aquellos entre estados con diferentes valores de M en ausencia de campos son diabáticos. En esta tesis hemos puesto de manifiesto que los cruces evitados en campos paralelos son, en general, cruzados diabáticamente. Nótese que estos cruces evitados son equivalentes a aquellos entre niveles con un valor similar de $\langle J_Z^2 \rangle$ en campos inclinados. Para el benzonitrilo, queremos realizar la propagación temporal de los estados cuánticos que forman haz molecular del experimento que ya hemos descrito de forma adiabática [20, 51]. Es plausible que estos cálculos nos permitan comprender e interpretar los resultados experimentales de orientación en una combinación de campos para moléculas asimétricas [20, 51]. El código computacional necesario para este estudio ha sido desarrollado durante esta tesis, y en la actualidad se están llevando a cabo los correspondientes cálculos.

Nuestra descripción del impacto de los campos externos en la molécula de CPC se hace

bajo la aproximación adiabática. Sin embargo, los resultados obtenidos en esta tesis ponen fehacientemente de manifiesto que esta hipótesis es correcta sólo bajo configuraciones de campo muy específicas, pero, desgraciadamente, no para la mayoría de las configuraciones usadas en los experimentos actuales. Una descripción dependiente del tiempo de estos sistemas es muy exigente desde un punto de vista computacional, debido al gran tamaño de las matrices del Hamiltoniano que conlleva un aumento significativo del tiempo de CPU necesario para la propagación de la función de onda. En concreto, para láseres elípticamente polarizados el número de simetrías es menor y nuevos términos de acoplamiento aparecen en el Hamiltoniano.

Desde un punto de vista teórico, no se han llevado a cabo estudios sobre el impacto de campos externos en moléculas totalmente asimétricas. Para estas moléculas los sistemas de referencia moleculares asociados a los ejes de inercia, el momento dipolar, y la polarizabilidad no coinciden. Por consiguiente, una descripción dentro de la aproximación de sólido rígido implica un alto grado de complejidad computacional debido a los acoplamientos no diagonales del tensor de polarizabilidad. El estudio teórico realizado para moléculas asimétricas en esta tesis constituye una base sólida para la investigación de estas moléculas más complicadas.

En un reciente estudio [78], hemos analizado el impacto de campos eléctricos y magnéticos en moléculas de capa abierta en su estado electrónico fundamental $^2\Pi$. Hemos encontrado que una combinación de campos magnéticos y eléctricos conduce a estados alineados y orientados bajo la aproximación adiabática. Hemos explorado también la influencia del desdoblamiento Λ en el acoplamiento de estados y su orientación. Sería interesante realizar una descripción dependiente del tiempo para este sistema. Para ello, la dependencia temporal de las intensidades de estos campos debería ser modelada según los datos experimentales. Este estudio dependiente del tiempo nos permitirá determinar la validez de la aproximación adiabática así como sus condiciones de aplicabilidad.

Chapter 9

Author's publications

From this list, the results of publications 3, 4, 5, 6, 8, 9 and 10 are included in this thesis.

1. **J.J. Omiste**, R.J. Yáñez and J.S. Dehesa
Information-theoretic properties of the half-line Coulomb potential
Journal of Mathematical Chemistry **47**, 911 (2009)
2. P. Sánchez-Moreno, **J.J. Omiste** and J.S. Dehesa
Entropic functionals of Laguerre polynomials and complexity properties of the half-line Coulomb potential
International Journal of Quantum Chemistry **111**, 2283 (2011)
3. **J.J. Omiste**, M. Gärttner, R. González-Férez, P. Schmelcher, L. Holmegaard, J.H. Nielsen, H. Stapelfeldt and J. Küpper
Theoretical description of adiabatic laser alignment and mixed field orientation: the need for a non-adiabatic model
Physical Chemistry Chemical Physics **13**, 18815 (2011)
4. **J.J. Omiste**, R. González-Férez and P. Schmelcher
Rotational spectrum of asymmetric top in combined static and laser field
Journal of Chemical Physics **135**, 064310 (2011)
5. J. H. Nielsen, H. Stapelfeldt, J. Küpper, B. Friedrich, **J.J. Omiste** and R. González-Férez
Making the best of mixed-field orientation of polar molecules: A recipe for achieving adiabatic dynamics in an electrostatic field combined with laser pulses
Physical Review Letters **108**, 193001 (2012)
6. **J.J. Omiste** and R. González-Férez
Non-adiabatic effects in long-pulse mixed-field orientation of a linear polar molecule
Physical Review A **86**, 043437 (2012)
7. M. Gärttner, **J.J. Omiste**, P. Schmelcher and R. González-Férez
Fine Structure of Open Shell Diatomic Molecules in Combined Electric and Magnetic Fields
Accepted in Molecular Physics (2013)
8. **J.J. Omiste** and R. González-Férez
Rotational dynamics of an asymmetric top molecule in parallel electric and non-resonant laser fields
arXiv:1306.1429v1 (2013)
9. J.L. Hansen, **J.J. Omiste**, J.H. Nielsen, D. Pentlehner, J. Küpper, R. González-Férez and H. Stapelfeldt
Mixed-field orientation of non-symmetric molecules
Preprint (2013)

10. **J.J. Omiste** and R. González-Férez

Mixed-field orientation of a thermal ensemble of polar molecules

arXiv:1306.1251v1 (2013)

Appendix A

The Molecular and the Laboratory Fixed Frames: the Euler Angles

In our approach, we investigate the rotational degree of freedom of the molecules, our approximation is to treat them as rigid rotors. Physically, the rigid rotor is an object that has no deformation, that is, the distance between any two point of the rigid solid is always constant. An asymmetric top molecule can be modeled as a rigid frame, that we call the Molecular Fixed Frame (MFF) with the axes (x, y, z) . Any property of the molecule such as permanent dipole moment or polarizability, are referred to this frame. Then, the description of the dynamics of the molecule to know the relative position of the MFF with respect to a frame fixed in the free space, that is, the Laboratory Fixed Frame (LFF) with the axes (X, Y, Z) . Since we work in the center of mass, this two frames are related by a rotation, which is described by the Euler angles (ϕ, θ, χ) [59, 79]. To derive the MFF from the FWW, we perform the following finite rotations

- Counterclockwise rotation of ϕ around the Z axis, $R_Z(\phi)$. As a result the Y axis becomes the node line N

$$R_Z(\phi) = \begin{pmatrix} \cos \phi & \sin \phi & 0 \\ -\sin \phi & \cos \phi & 0 \\ 0 & 0 & 1 \end{pmatrix} \quad (\text{A.1})$$

- Counterclockwise rotation of θ around the line N , $R_N(\theta)$. This transform Z to the z axis

$$R_N(\theta) = \begin{pmatrix} \cos \theta & 0 & -\sin \theta \\ 0 & 1 & 0 \\ \sin \theta & 0 & \cos \theta \end{pmatrix} \quad (\text{A.2})$$

- Counterclockwise rotation of χ around z , then the line N becomes y

$$R_z(\chi) = \begin{pmatrix} \cos \chi & \sin \chi & 0 \\ -\sin \chi & \cos \chi & 0 \\ 0 & 0 & 1 \end{pmatrix}. \quad (\text{A.3})$$

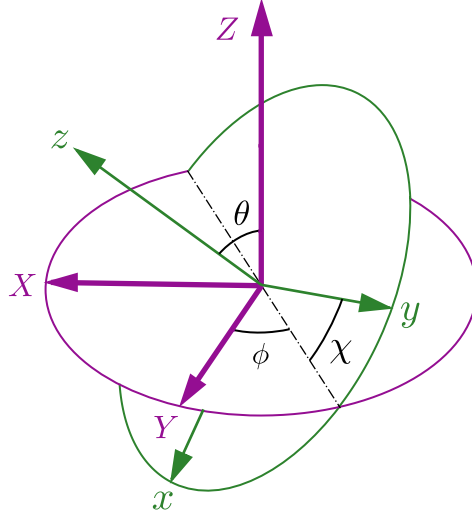


Figure A.1: Euler angles

Then, the relation of the MFF and the LFF is given by the rotation $R(\phi, \theta, \chi)$

$$\begin{aligned} \begin{pmatrix} x \\ y \\ z \end{pmatrix} &= R_z(\chi)R_N(\theta)R_Z(\phi) \begin{pmatrix} X \\ Y \\ Z \end{pmatrix} \\ &= R(\phi, \theta, \chi) \begin{pmatrix} X \\ Y \\ Z \end{pmatrix}. \end{aligned} \quad (\text{A.4})$$

The rotation $R(\phi, \theta, \chi)$ reads as

$$R(\phi, \theta, \chi) = \begin{pmatrix} \cos \theta_{Xx} & \cos \theta_{Yx} & \cos \theta_{Zx} \\ \cos \theta_{Xy} & \cos \theta_{Yy} & \cos \theta_{Zy} \\ \cos \theta_{Xz} & \cos \theta_{Yz} & \cos \theta_{Zz} \end{pmatrix}, \quad (\text{A.5})$$

where θ_{Pq} is the angle formed by the axis P of the LFF and the axis q of the MFF. These angles are related to the Euler angles as follows

$$\begin{aligned} \cos \theta_{Xx} &= \cos \phi \cos \theta \cos \chi - \sin \phi \sin \chi, \\ \cos \theta_{Yx} &= \sin \phi \cos \theta \cos \chi + \cos \phi \sin \chi, \\ \cos \theta_{Zx} &= -\sin \theta \cos \chi, \\ \cos \theta_{Xy} &= -\cos \phi \cos \theta \sin \chi - \sin \phi \cos \chi, \\ \cos \theta_{Yy} &= -\sin \phi \cos \theta \sin \chi + \cos \phi \cos \chi, \\ \cos \theta_{Zy} &= \sin \theta \sin \chi, \\ \cos \theta_{Xz} &= \cos \phi \sin \theta, \\ \cos \theta_{Yz} &= \sin \phi \sin \theta, \\ \cos \theta_{Zz} &= \cos \theta. \end{aligned}$$

In our system, the molecular state is represented by a wavefunction. To rotate a wavefunction, we use the rotation operator $R(\phi, \theta, \chi)$

$$\begin{aligned} R(\phi, \theta, \chi) &= \exp(-i\chi \vec{J} \cdot \vec{n}_\chi) \exp(-i\theta \cdot \vec{J} \cdot \vec{n}_\theta) \exp(-i\phi \vec{J} \cdot \vec{n}_\phi) \\ &= \exp(-i\chi J_z) \exp(-i\theta J_N) \exp(-i\phi J_Z), \end{aligned} \quad (\text{A.6})$$

where \vec{n}_i are unitary vectors defining the rotation axes, \vec{J} the angular momentum operator and J_i its projection along the i axis. Rewriting (A.6) as [59]

$$R(\phi, \theta, \chi) = \exp(-i\phi J_Z) \exp(-i\theta J_Y) \exp(-i\chi J_Z) \quad (\text{A.7})$$

where we have used that

$$\exp(-i\theta J_N) = \exp(-i\phi J_Z) \exp(-i\theta J_Y) \exp(i\phi J_Z), \quad (\text{A.8})$$

$$\exp(-i\chi J_z) = \exp(-i\theta J_N) \exp(-i\chi J_Z) \exp(i\theta J_N), \quad (\text{A.9})$$

$$\exp(-i\chi J_Z) = \exp(-i\phi J_Z) \exp(-i\chi J_Z) \exp(i\phi J_Z). \quad (\text{A.10})$$

By substituting (A.9)-(A.10) in expression (A.6). Applying the operator on the eigenstate of \vec{J}^2 J_Z , $|JM\rangle$, we get

$$R(\phi, \theta, \chi) |JM\rangle = \sum_{M'=-J}^J D_{M',M}^J(\phi, \theta, \chi) |JM'\rangle, \quad (\text{A.11})$$

where the expansion coefficients are the Wigner matrix elements [59],

$$D_{M',M}^J(\phi, \theta, \chi) = \langle JM' | R(\phi, \theta, \chi) | JM \rangle. \quad (\text{A.12})$$

The main properties of the Wigner matrix elements are collected in Appendix B.

Appendix B

Wigner matrix elements

The Wigner matrix elements show many and useful properties which have been helpful throughout this thesis. Below we list some of them [59].

- Complex conjugate

$$D_{M,K}^J(\phi, \theta, \chi)^* = (-1)^{M-K} D_{-M,-K}^J(\phi, \theta, \chi). \quad (\text{B.1})$$

- The reduced Wigner matrix elements, $d_{M',M}^J(\theta)$, are defined as

$$D_{M',M}^J(\phi, \theta, \chi) = e^{-i\phi M'} d_{M',M}^J(\theta) e^{-i\chi M}, \quad (\text{B.2})$$

- $d_{M',M}^J(\theta)$ is expressed as the series

$$d_{M',M}^J = \frac{\sqrt{(J+M)!(J-M)!(J+M')!(J-M')!}}{\sum_{\nu} \frac{(-1)^{\nu}}{(J-M'-\nu)!(J+M-\nu)!(\nu+M'-M)!\nu!}} \left[\cos\left(\frac{\theta}{2}\right) \right]^{2J+M-M'-2\nu} \left[\sin\left(\frac{\theta}{2}\right) \right]^{M'-M'+2\nu}$$

- Main properties of the reduce Wigner matrix elements of $d_{m',m}^J(\theta)$

$$d_{m',m}^j(\theta) = (-1)^{m-m'} d_{m,m'}^j(\theta), \quad (\text{B.3})$$

$$d_{m',m}^j(\theta) = d_{-m',-m}^j(\theta), \quad (\text{B.4})$$

$$d_{m',m}^j(\theta) = d_{m,m'}^j(-\theta). \quad (\text{B.5})$$

- Relevant values of $d_{m',m}^J(\theta)$:

$$d_{m',m}^j(0) = \delta_{m',m}, \quad (\text{B.6})$$

$$d_{m',m}^j(\pi) = (-1)^{j+m'} \delta_{m',-m}, \quad (\text{B.7})$$

where $\delta_{a,b}$ is the Kronecker delta.

- Completeness

$$\sum_{m'} [D_{m',m}^J(\Omega)]^\dagger D_{m',n}^J(\Omega) = \sum_{m'} [d_{m,m'}^J(\theta)]^\dagger d_{m',n}^J(\theta) = \delta_{m,n}, \quad (\text{B.8})$$

$$(\text{B.9})$$

$$\sum_m [D_{m',m}^J(\Omega)]^\dagger D_{n',m}^J(\Omega) = \sum_m [d_{m,m'}^J(\theta)]^\dagger d_{n',m}^J(\theta) = \delta_{m',n'}. \quad (\text{B.10})$$

- Orthogonality

$$\int_0^{2\pi} d\phi \int_0^\pi \sin\theta d\theta \int_0^{2\pi} d\chi \left[D_{K',M'}^{J'}(\phi, \theta, \chi) \right]^* D_{K,M}^J(\phi, \theta, \chi) = \frac{8\pi^2}{2J+1} \delta_{M',M} \delta_{K',K} \delta_{J',J}. \quad (\text{B.11})$$

- Three Wigner matrix elements integrals

$$\begin{aligned} & \int d\Omega D_{-K,-M}^J(\phi, \theta, \chi) D_{K_1,M_1}^{J_1}(\phi, \theta, \chi) D_{K_2,M_2}^{J_2}(\phi, \theta, \chi) = \\ & = (-1)^{M-K} \frac{8\pi^2}{2J+1} \langle J_1 M_1 J_2 M_2 | J M \rangle \langle J_1 K_1 J_2 K_2 | J K \rangle = \\ & = 8\pi^2 \begin{pmatrix} J_1 & J_2 & J \\ M_1 & M_2 & -M \end{pmatrix} \begin{pmatrix} J_1 & J_2 & J \\ K_1 & K_2 & -K \end{pmatrix}. \end{aligned} \quad (\text{B.12})$$

where $\begin{pmatrix} J_1 & J_2 & J \\ K_1 & K_2 & K \end{pmatrix}$ are the 3J Symbols

- They are related with the spherical harmonics and with the Legendre polynomials

$$D_{m,0}^l(\phi, \theta, 0) = \sqrt{\frac{4\pi}{2l+1}} Y_l^m(\theta, \phi). \quad (\text{B.13})$$

$$D_{0,0}^l(0, \theta, 0) = P_l(\cos\theta). \quad (\text{B.14})$$

Appendix C

Hamiltonian matrix elements

As we have seen in Chapter 3, the interaction terms in the Hamiltonian are given in terms of linear combinations of Wigner matrix elements, $D_{MK}^J(\Omega)$ [48, 59, 80]. This fact allows us to write the Hamiltonian matrix elements in the basis of eigenstates of the symmetric rotor, see expression (3.6), as a finite expression in terms of the 3J Symbols. Below we list the matrix elements which appear in each interaction term of the Hamiltonian:

Electric field interaction term

$$\begin{aligned} \langle J'K'M' | \cos \theta_{S_z} | JKM \rangle &= (-1)^{M-K} \sqrt{(2J+1)(2J'+1)} \\ &\quad \left\{ \frac{\sin \beta}{\sqrt{2}} \left[\begin{pmatrix} J & 1 & J' \\ -M & -1 & M' \end{pmatrix} + \begin{pmatrix} J & 1 & J' \\ -M & 1 & M' \end{pmatrix} \right] \right. \\ &\quad \left. + \cos \beta \begin{pmatrix} J & 1 & J' \\ -M & 0 & M' \end{pmatrix} \right\} \begin{pmatrix} J & 1 & J' \\ -K & 0 & K' \end{pmatrix}, \end{aligned}$$

$$\begin{aligned} \langle J'K'M' | \cos \theta_{S_x} | JKM \rangle &= (-1)^{M-K} \sqrt{(2J+1)(2J'+1)} \\ &\quad \left\{ \frac{\cos \beta}{\sqrt{2}} \left[\begin{pmatrix} J & 1 & J' \\ -K & 0 & K' \end{pmatrix} - \begin{pmatrix} J & 1 & J' \\ -K & 0 & K' \end{pmatrix} \right] \begin{pmatrix} J & 1 & J' \\ -M & 0 & M' \end{pmatrix} \right. \\ &\quad + \frac{\sin \beta}{2} \left[\begin{pmatrix} J & 1 & J' \\ -K & 1 & K' \end{pmatrix} - \begin{pmatrix} J & 1 & J' \\ -K & -1 & K' \end{pmatrix} \right] \\ &\quad \left. \times \left[\begin{pmatrix} J & 1 & J' \\ -M & 1 & M' \end{pmatrix} - \begin{pmatrix} J & 1 & J' \\ -M & -1 & M' \end{pmatrix} \right] \right\} \end{aligned}$$

Laser field interaction term

$$\begin{aligned} \langle J'K'M' | \cos^2 \theta_{Zz} | JKM \rangle &= \frac{1}{3} \delta_{J,J'} \delta_{K,K'} \delta_{M,M'} + (-1)^{M-K} \sqrt{(2J+1)(2J'+1)} \\ &\quad \begin{pmatrix} J & 2 & J' \\ -K & 0 & K' \end{pmatrix} \begin{pmatrix} J & 2 & J' \\ -M & 0 & M' \end{pmatrix}, \end{aligned}$$

$$\begin{aligned}
\langle J'K'M' | \cos^2 \theta_{Zy} | JK M \rangle &= (-1)^{M-K} \sqrt{(2J+1)(2J'+1)} \left\{ \left[\frac{1}{3} \begin{pmatrix} J & 2 & J' \\ -K & 0 & K' \end{pmatrix} \right. \right. \\
&- \left. \frac{1}{\sqrt{6}} \left(\begin{pmatrix} J & 2 & J' \\ -K & -2 & K' \end{pmatrix} + \begin{pmatrix} J & 2 & J' \\ -K & 2 & K' \end{pmatrix} \right) \right] \\
&\times \left. \begin{pmatrix} J & 2 & J' \\ -M & 0 & M' \end{pmatrix} \right\} + \frac{1}{3} \delta_{J,J'} \delta_{K,K'} \delta_{M,M'},
\end{aligned}$$

$$\begin{aligned}
\langle J'K'M' | \cos^2 \theta_{Xz} | JK M \rangle &= (-1)^{M-K} \sqrt{(2J+1)(2J'+1)} \begin{pmatrix} J & 2 & J' \\ -K & 0 & K' \end{pmatrix} \\
&\left\{ \frac{1}{\sqrt{6}} \left[\begin{pmatrix} J & 2 & J' \\ -M & 2 & M' \end{pmatrix} + \begin{pmatrix} J & 2 & J' \\ -M & -2 & M' \end{pmatrix} \right] \right. \\
&- \left. \frac{1}{3} \begin{pmatrix} J & 2 & J' \\ -M & 0 & M' \end{pmatrix} \right\} + \frac{1}{3} \delta_{J,J'} \delta_{K,K'} \delta_{M,M'},
\end{aligned}$$

$$\begin{aligned}
\langle J'K'M' | \cos^2 \theta_{Xy} | JK M \rangle &= \frac{1}{3} \delta_{J,J'} \delta_{K,K'} \delta_{M,M'} + (-1)^{M-K} \\
&\sqrt{(2J+1)(2J'+1)} \left\{ \frac{1}{2\sqrt{6}} \begin{pmatrix} J & 2 & J' \\ -M & 0 & M' \end{pmatrix} \right. \\
&\left[\begin{pmatrix} J & 2 & J' \\ -K & 2 & K' \end{pmatrix} + \begin{pmatrix} J & 2 & J' \\ -K & -2 & K' \end{pmatrix} \right] \\
&+ \frac{1}{6} \begin{pmatrix} J & 2 & J' \\ -K & 0 & K' \end{pmatrix} \left[\frac{1}{6} \begin{pmatrix} J & 2 & J' \\ -M & 0 & M' \end{pmatrix} \right. \\
&- \left. \frac{1}{2\sqrt{6}} \left[\begin{pmatrix} J & 2 & J' \\ -M & 2 & M' \end{pmatrix} + \begin{pmatrix} J & 2 & J' \\ -M & -2 & M' \end{pmatrix} \right] \right] \\
&- \frac{1}{4} \left[\begin{pmatrix} J & 2 & J' \\ -M & 2 & M' \end{pmatrix} + \begin{pmatrix} J & 2 & J' \\ -M & -2 & M' \end{pmatrix} \right] \\
&\left. \left[\begin{pmatrix} J & 2 & J' \\ -K & 2 & K' \end{pmatrix} + \begin{pmatrix} J & 2 & J' \\ -K & -2 & K' \end{pmatrix} \right] \right\},
\end{aligned}$$

where these cosines are given in terms of the inclination angle β and the Euler angles ϕ, θ, χ as

$$\begin{aligned}
\cos \theta_{Sz} &= \cos \beta \cos \theta + \sin \beta \cos \phi \sin \theta, \\
\cos \theta_{Sx} &= -\cos \beta \sin \theta \cos \chi + \sin \beta (\cos \phi \cos \theta \cos \chi - \sin \phi \sin \chi), \\
\cos^2 \theta_{Zz} &= \cos^2 \theta, \\
\cos^2 \theta_{Zy} &= \sin^2 \theta \cos^2 \chi, \\
\cos^2 \theta_{Xz} &= \cos^2 \phi \sin^2 \theta, \\
\cos^2 \theta_{Xy} &= (\sin \phi \cos \chi + \cos \phi \cos \theta \sin \chi)^2.
\end{aligned}$$

Let us note that the 3J Symbols satisfy that $\begin{pmatrix} J_1 & J_2 & J_3 \\ M_1 & M_2 & M_3 \end{pmatrix} \neq 0$ if $0 \leq |J_1 - J_2| \leq J_3$ and $M_1 + M_2 + M_3 = 0$.

Bibliography

- [1] V. Aquilanti, M. Bartolomei, F. Pirani, D. Cappelletti, and F. Vecchiocattivi, *Orienting and aligning molecules for stereochemistry and photodynamics*, Phys. Chem. Chem. Phys. **7**, 291 (2005).
- [2] F. J. Aoiz, B. Friedrich, V. J. Herrero, V. S. Rábanos, and J. E. Verdasco, *Effect of pendular orientation on the reactivity of $H + DCl$: a quasiclassical trajectory study*, Chem. Phys. Lett. **289**, 132 (1998).
- [3] R. Zare, *Laser control of chemical reactions*, Science **20**, 1875 (1998).
- [4] P. R. Brooks and E. M. Jones, *Reactive scattering of K atoms from oriented CH_3I molecules*, J. Chem. Phys. **45**, 3449 (1966).
- [5] D. H. Parker, K. K. Chakravorty, and R. B. Bernstein, *Crossed beam reaction of oriented methyl iodide with rubidium - steric factor and reactive asymmetry versus scattering angle*, Chem. Phys. Lett. **86**, 113 (1982).
- [6] S. Stolte, K. K. Chakravorty, R. B. Bernstein, and D. H. Parker, *Analysis of the steric dependence of the CH_3I+Rb reaction using a Legendre expansion technique*, Chem. Phys. **71**, 353 (1982).
- [7] R. J. Beuhler, R. B. Bernstein, and K. H. Kramer, *Observation of the reactive asymmetry of methyl iodide. Crossed beam study of the reaction of rubidium with oriented methyl iodide molecules*, J. Am. Chem. Soc. **88**, 5331 (1966).
- [8] R. Kanya and Y. Ohshima, *Pendular-state spectroscopy of the S_1-S_0 electronic transition of 9-cyanoanthracene*, J. Chem. Phys. **121**, 9489 (2004).
- [9] D. T. Moore, L. Oudejans, and R. E. Miller, *Pendular state spectroscopy of an asymmetric top: parallel and perpendicular bands of acetylene-HF*, J. Chem. Phys. **110**, 197 (1999).
- [10] P. Reckenthaeler, M. Centurion, W. Fuß, S. A. Trushin, F. Krausz, and E. E. Fill, *Time-resolved electron diffraction from selectively aligned molecules*, Phys. Rev. Lett. **102**, 213001 (2009).
- [11] A. Landers, T. Weber, I. Ali, A. Cassimi, M. Hattass, O. Jagutzki, A. Nauert, T. Osipov, A. Staudte, M. H. Prior, H. Schmidt-Böcking, C. L. Cocke, and R. Dörner, *Photoelectron diffraction mapping: molecules illuminated from within*, Phys. Rev. Lett. **87**, 013002 (2001).
- [12] L. Holmegaard, J. L. Hansen, L. Kalhoj, S. L. Kragh, H. Stapelfeldt, F. Filsinger, J. Küpper, G. Meijer, D. Dimitrovski, M. Abu-samha, C. P. J. Martiny, and L. B. Madsen, *Photoelectron angular distributions from strong-field ionization of oriented molecules*, Nat. Phys. **6**, 428 (2010).

- [13] C. Z. Bisgaard, O. J. Clarkin, G. Wu, A. M. D. Lee, O. Gessner, C. C. Hayden, and A. Stolow, *Time-resolved molecular frame dynamics of fixed-in-space CS₂ molecules*, *Science* **323**, 1464 (2009).
- [14] J. Levesque, Y. Mairesse, N. Dudovich, H. Pépin, J.-C. Kieffer, P. B. Corkum, and D. M. Villeneuve, *Polarization state of high-order harmonic emission from aligned molecules*, *Phys. Rev. Lett.* **99**, 243001 (2007).
- [15] R. Velotta, N. Hay, M. B. Mason, M. Castillejo, and J. P. Marangos, *High-order harmonic generation in aligned molecules*, *Phys. Rev. Lett.* **87**, 183901 (2001).
- [16] J. C. H. Spence and R. B. Doak, *Single molecule diffraction*, *Phys. Rev. Lett.* **92**, 198102 (2004).
- [17] F. Filsinger, G. Meijer, H. Stapelfeldt, H. N. Chapman, and J. Küpper, *State- and conformer-selected beams of aligned and oriented molecules for ultrafast diffraction studies*, *Phys. Chem. Chem. Phys.* **13**, 2076 (2011).
- [18] R. J. D. Miller, R. Ernstorfer, M. Harb, M. Gao, C. T. Hebeisen, H. Jean-Ruel, C. Lu, G. Moriena, and G. Sciaini, *'Making the molecular movie': first frames*, *Acta Crystallogr. A* **66**, 137 (2010).
- [19] H. Stapelfeldt and T. Seideman, *Colloquium: Aligning molecules with strong laser pulses*, *Rev. Mod. Phys.* **75**, 543 (2003).
- [20] L. Holmegaard, J. H. Nielsen, I. Nevo, H. Stapelfeldt, F. Filsinger, J. Küpper, and G. Meijer, *Laser-induced alignment and orientation of quantum-state-selected large molecules*, *Phys. Rev. Lett.* **102**, 023001 (2009).
- [21] O. Ghafur, A. Rouzee, A. Gijsbertsen, W. K. Siu, S. Stolte, and M. J. J. Vrakking, *Impulsive orientation and alignment of quantum-state-selected NO molecules*, *Nat Phys* **5**, 289 (2009).
- [22] A. Rouzée, A. Gijsbertsen, O. Ghafur, O. M. Shir, T. Bäck, S. Stolte, and M. J. J. Vrakking, *Optimization of laser field-free orientation of a state-selected no molecular sample*, *New J. Phys.* **11**, 105040 (2009).
- [23] K.-K. Ni, S. Ospelkaus, M. H. G. de Miranda, A. Pe'er, B. Neyenhuis, J. J. Zirbel, S. Kotochigova, P. S. Julienne, D. S. Jin, and J. Ye, *A high phase-space-density gas of ground-state polar molecules*, *Science* **322**, 231 (2008).
- [24] P. R. Brooks, J. S. McKillop, and H. G. Pippin, *Molecular-beam reaction of K-atoms with sideways oriented CF₃I*, *Chem. Phys. Lett.* **66**, 144 (1979).
- [25] D. H. Parker and R. B. Bernstein, *Oriented molecule beams via the electrostatic hexapole: preparation, characterization, and reactive scattering*, *Annu. Rev. Phys. Chem.* **40**, 561 (1989).
- [26] V. A. Cho and R. B. Bernstein, *Tight focusing of beams of polar polyatomic molecules via the electrostatic hexapole lens*, *J. Phys. Chem.* **95**, 8129 (1991).
- [27] P. R. Brooks, *Orientation effects in electron transfer collisions*, *International Reviews in Physical Chemistry* **14**, 327 (1995).

- [28] H. J. Loesch and A. Remscheid, *Brute force in molecular reaction dynamics: A novel technique for measuring steric effects*, J. Chem. Phys. **93**, 4779 (1990).
- [29] B. Friedrich and D. R. Herschbach, *Spatial orientation of molecules in strong electric fields and evidence for pendular states*, Nature **353**, 412 (1991).
- [30] B. Friedrich and D. R. Herschbach, *On the possibility of orienting rotationally cooled polar molecules in an electric field*, Z. Phys. D **18**, 153 (1991).
- [31] A. Gijsbertsen, W. Siu, M. F. Kling, P. Johnsson, P. Jansen, S. Stolte, and M. J. J. Vrakking, *Direct determination of the sign of the NO dipole moment*, Phys. Rev. Lett. **99**, 213003 (2007).
- [32] A. Slenczka, B. Friedrich, and D. Herschbach, *Determination of the electric-dipole moment of ICl ($B^3\Pi_0$) from pendular spectra*, Chem. Phys. Lett. **224**, 3 (1994).
- [33] B. Friedrich and D. Herschbach, *Polarizability interaction in molecules and double-well tunneling*, Z. Phys. D **36**, 221 (1995).
- [34] B. Friedrich and D. R. Herschbach, *Polarization of molecules induced by intense nonresonant laser fields*, J. Phys. Chem. **99**, 15686 (1995).
- [35] W. Kim and P. M. Felker, *Spectroscopy of pendular states in optical-field-aligned species*, J. Chem. Phys. **104**, 1147 (1996).
- [36] T. Seideman, *Rotational excitation and molecular alignment in intense laser fields*, J. Chem. Phys. **103**, 7887 (1995).
- [37] T. Seideman, *Manipulating external degrees of freedom with intense light: Laser focusing and trapping of molecules*, J. Chem. Phys. **106**, 2881 (1997).
- [38] T. Seideman, *Shaping molecular beams with intense light*, J. Chem. Phys. **107**, 10420 (1997).
- [39] T. Seideman, *Molecular optics in an intense laser field: A route to nanoscale material design*, Phys. Rev. A **56**, r17 (1997).
- [40] T. Seideman, *New means of spatially manipulating molecules with light*, J. Chem. Phys. **111**, 4397 (1999).
- [41] H. Sakai, C. P. Safvan, J. J. Larsen, K. M. Hilligsøe, K. Hald, and H. Stapelfeldt, *Controlling the alignment of neutral molecules by a strong laser field*, J. Chem. Phys. **110**, 10235 (1999).
- [42] J. J. Larsen, K. Hald, N. Bjerre, H. Stapelfeldt, and T. Seideman, *Three dimensional alignment of molecules using elliptically polarized laser fields*, Phys. Rev. Lett. **85**, 2470 (2000).
- [43] B. Friedrich and D. R. Herschbach, *On the possibility of aligning paramagnetic molecules or ions in a magnetic-field*, Z. Phys. D **24**, 25 (1992).
- [44] A. Slenczka, B. Friedrich, and D. Herschbach, *Pendular alignment of paramagnetic molecules in uniform magnetic fields*, Phys. Rev. Lett. **72**, 1806 (1994).

- [45] B. Friedrich and D. Herschbach, *Alignment and trapping of molecules in intense laser fields*, Phys. Rev. Lett. **74**, 4623 (1995).
- [46] B. Friedrich and D. R. Herschbach, *Enhanced orientation of polar molecules by combined electrostatic and nonresonant induced dipole forces*, J. Chem. Phys. **111**, 6157 (1999).
- [47] B. Friedrich and D. Herschbach, *Manipulating molecules via combined static and laser fields*, J. Phys. Chem. A **103**, 10280 (1999).
- [48] M. Härtelt and B. Friedrich, *Directional states of symmetric-top molecules produced by combined static and radiative electric fields*, J. Chem. Phys. **128**, 224313 (2008).
- [49] U. Buck and M. Fárník, *Oriented xenon hydride molecules in the gas phase*, Int. Rev. Phys. Chem. **25**, 583 (2006).
- [50] H. Sakai, S. Minemoto, H. Nanjo, H. Tanji, and T. Suzuki, *Controlling the orientation of polar molecules with combined electrostatic and pulsed, nonresonant laser fields*, Phys. Rev. Lett. **90**, 083001 (2003).
- [51] F. Filsinger, J. Küpper, G. Meijer, L. Holmegaard, J. H. Nielsen, I. Nevo, J. L. Hansen, and H. Stapelfeldt, *Quantum-state selection, alignment, and orientation of large molecules using static electric and laser fields*, J. Chem. Phys. **131**, 064309 (2009).
- [52] J. J. Omiste, M. Gärttner, P. Schmelcher, R. González-Férez, L. Holmegaard, J. H. Nielsen, H. Stapelfeldt, and J. Küpper, *Theoretical description of adiabatic laser alignment and mixed-field orientation: the need for a non-adiabatic model*, Phys. Chem. Chem. Phys. **13**, 18815 (2011).
- [53] J. H. Nielsen, H. Stapelfeldt, J. Küpper, B. Friedrich, J. J. Omiste, and R. González-Férez, *Making the best of mixed-field orientation of polar molecules: A recipe for achieving adiabatic dynamics in an electrostatic field combined with laser pulses*, Phys. Rev. Lett. **108**, 193001 (2012).
- [54] J. L. Hansen, J. J. Omiste, J. H. Nielsen, D. Pentlehner, J. Küpper, R. González-Férez, and H. Stapelfeldt, *Mixed-field orientation of non-symmetric molecules*, Preprint (2013).
- [55] J. J. Omiste, R. González-Férez, and P. Schmelcher, *Rotational spectrum of asymmetric top molecules in combined static and laser fields*, J. Chem. Phys. **135**, 064310 (2011).
- [56] J. J. Omiste and R. González-Férez, *Nonadiabatic effects in long-pulse mixed-field orientation of a linear polar molecule*, Phys. Rev. A **86**, 043437 (2012).
- [57] J. J. Omiste and R. González-Férez, *Rotational dynamics of an asymmetric top molecule in parallel electric and non-resonant laser fields*, (2013), arXiv:1306.1429v1.
- [58] J. J. Omiste and R. González-Férez, *Mixed-field orientation of a thermal ensemble of linear polar molecules*, Preprint (2013), arXiv:1306.1251v1.
- [59] R. N. Zare, *Angular Momentum: Understanding spatial Aspects in Chemistry and Physics*, John Wiley and Sons, New York, 1988.
- [60] G. W. King, R. M. Hainer, and P. C. Cross, *The asymmetric rotor I. Calculation and symmetry classification of energy levels*, J. Chem. Phys. **11**, 27 (1943).

- [61] T. Seideman and E. Hamilton, *Nonadiabatic Alignment by Intense Pulses. Concepts, Theory, and Directions*, volume 52 of *Advances In Atomic, Molecular, and Optical Physics*, Academic Press, 2005.
- [62] C. M. Dion, A. Keller, O. Atabek, and A. D. Bandrauk, *Laser-induced alignment dynamics of HCN: Roles of the permanent dipole moment and the polarizability*, Phys. Rev. A **59**, 1382 (1999).
- [63] N. E. Henriksen, *Molecular alignment and orientation in short pulse laser fields*, Chem. Phys. Lett. **312**, 196 (1999).
- [64] A. Rouzée, S. Guérin, O. Faucher, and B. Lavorel, *Field-free molecular alignment of asymmetric top molecules using elliptically polarized laser pulses*, Phys. Rev. A **77**, 043412 (2008).
- [65] D. M. Bishop, *Group Theory and Chemistry*, New York: Dover, 1993.
- [66] W. Ritz, *Über eine neue methode zur lösung gewisser Variationsprobleme der mathematischen physik*, J. f. Reine u. Angew. Math. **135**, 1 (1909).
- [67] J. K. L. MacDonald, *Successive approximations by the Rayleigh-Ritz Variation method*, Phys. Rev. **43**, 830 (1933).
- [68] D. C. Sorensen, *Implicit application of polynomial filters in a k-step Arnoldi method*, SIAM J. Matrix Analysis and Applications **13**, 357.
- [69] R. B. Lehoucq, D. C. Sorensen, and C. Yang, *Arpack Users' Guide*, Siam, 1998.
- [70] R. B. Lehoucq, K. Maschhoff, D. C. Sorensen, and C. Yang, ARPACK Software Package, <http://www.caam.rice.edu/software/ARPACK>, 1996.
- [71] L. N. Trefethen and D. Bau, *Numerical Linear Algebra*, Society for Industrial & Applied Mathematics, U.S., 1997.
- [72] M. D. Feit, J. A. Fleck Jr., and A. Steiger, *Solution of the Schrödinger equation by a spectral method*, J. Comp. Phys. **47**, 412 (1982).
- [73] C. Leforestier, R. H. Bisseling, C. Cerjan, M. D. Feit, R. Friesner, A. Guldborg, A. Hammerich, G. Jolicard, W. Karrlein, H.-D. Meyer, N. Lipkin, O. Roncero, and R. Kosloff, *A comparison of different propagation schemes for the time dependent Schrödinger equation*, J. Comp. Phys. **94**, 59 (1990).
- [74] M. Beck, A. Jäckle, G. Worth, and H.-D. Meyer, *The multiconfiguration time-dependent Hartree (MCTDH) method: a highly efficient algorithm for propagating wavepackets*, Physics Reports **324**, 1 (2000).
- [75] T. J. Park and J. C. Light, *Unitary quantum time evolution by iterative Lanczos reduction*, J. Chem. Phys. **85**, 5870 (1986).
- [76] W. H. Press, S. A. Teukolsky, W. T. Vetterling, and B. P. Flannery, *Numerical Recipes*, Cambridge University Press, 2007.
- [77] I. Nevo, L. Holmegaard, J. Nielsen, J. L. Hansen, H. Stapelfeldt, F. Filsinger, G. Meijer, and J. Küpper, *Laser-induced 3D alignment and orientation of quantum state-selected molecules*, Phys. Chem. Chem. Phys. **11**, 9912 (2009).

- [78] M. Gärttner, J. J. Omiste, P. Schmelcher, and R. González-Férez, *Fine structure of open shell diatomic molecules in combined electric and magnetic fields*, Accepted in special issue in honor of Bretislav Friedrich's 60th Birthday in Molecular Physics (2013).
- [79] H. Goldstein, *Classical Mechanics*, Addison-Wesley Publishing Company Inc., 1959.
- [80] M. Artamonov and T. Seideman, *Optimal-control approach to field-free three-dimensional alignment of polyatomic molecules*, Phys. Rev. A **82**, 023413 (2010).